UCLA
UCLA Electronic Theses and Dissertations

Title

Integrating developmental processes with leaf structure and function to clarify mechanisms of environmental adaptation of leaves

Permalink

https://escholarship.org/uc/item/3nn63627

Author

Baird, Alec Stephen

Publication Date

2023

Supplemental Material

https://escholarship.org/uc/item/3nn63627#supplemental

Peer reviewed|Thesis/dissertation

UNIVERSITY OF CALIFORNIA

Los Angeles

Integrating developmental processes with leaf structure and function to clarify mechanisms of

environmental adaptation of leaves

A dissertation submitted in partial satisfaction

of the requirements for the degree

Doctor of Philosophy in Biology

by

Alec Baird

2023

ABSTRACT OF THE DISSERTATION

Integrating developmental processes with leaf structure and function to clarify mechanisms of

environmental adaptation of leaves

by

Alec Baird

Doctor of Philosophy in Biology

University of California, Los Angeles, 2023

Professor Lawren Sack, Chair

Leaf structure and function is important in driving ecosystem fluxes, tolerance of environmental

stressors, species distributions and climate change responses, with applications for agricultural

breeding and engineering. Yet, the interface of leaf hydraulic structure and function with the

spatial and temporal aspects of developmental processes has largely been unexplored across

species. Such a pursuit has the power to provide deep insight into the drivers and constraints on

the evolution of physiological adaptation. In this dissertation, I leverage developmental processes

to gain insight into how diverse hydraulic mechanisms arise, how developmental constraints

influence environmental adaptation, how allometric relationships among cell and tissue anatomy

and leaf size arise, and how leaf economics are linked with leaf expansion processes. For three of

these chapters, I focus on diverse grasses, and demonstrate that grass leaf size is critical trait for

climate adaptation globally, due to developmental constraints between leaf growth and venation,

C_3 and C_4 grasses evolved some similar but also differential leaf cell, tissue and morphological allometries, and C_3 and C_4 grasses evolved contrasting hydraulic adaptations that underlie their differential climate adaptation. For two chapters, I focus on diverse eudicot species, and show the developmental bases for leaf trichome and stomatal densities for trichomous species and how their developmental processes allow for positive coordination across species, and the developmental determinants underlying leaf size and their integration with the leaf economics spectrum. This work highlights the importance of incorporating developmental processes to better understand the evolutionary ecology of leaf structure and function, and will provide critical avenues for predicting responses to climate change and applications for agriculture.

The dissertation of Alec Baird is approved.

Lachezar Atanasov Nikolov

Van Maurice Savage

Felipe Zapata Hoyos

Lawren Sack, Committee Chair

University of California, Los Angeles

2023

Table of Contents

List of Tables

Chapter 6

List of Boxes

List of Figures

Chapter 6

Acknowledgements

First and foremost, I thank my mentor, Dr. Lawren Sack, for his continual support and wisdom, for pushing me to keep asking questions and to grow as a scientist, and for always having confidence in my work and capabilities. I certainly would not have been able to complete all that is within this dissertation without his continual advice, discussion and support. I am also grateful to have had a mentor that has incredible enthusiasm for plant science and the natural world as this has allowed me to be integrative with my work and pursue novel questions. From Lawren's mentoring, I feel a tremendous amount of growth not just as a scientist, but as a friend, colleague and collaborator. I am grateful for the relationship we have built throughout my time at UCLA and I am happy to continue on knowing I will have a mentor that will always support me.

I thank my committee members: Lachezar Nikolov, Van Savage and Felipé Zapata for providing guidance, suggestions and support. Thank you for your enthusiasm with my work and for helping me grow.

I thank my mentors outside of UCLA, Drs. Elizabeth Van Volkenburgh, Janneke HilleRisLambers, Leander Anderegg, Melissa Lacey and Steve Kroiss for their time, guidance and support as I entered the field of plant science as an undergraduate. I am thankful that they championed my integrative thinking and pushed me to pursue more than I ever thought possible. Thank you for welcoming me into your lives like family. The many gatherings at many of your homes and the lab outings/trips will always have a place in my heart and I hope to instill a similar feeling to students within my own lab one day.

I thank the many members of the Sack lab, past and present. First, I am thankful to Marvin Browne, for our chats about plant growth and function, for your inspiring individuality, and for pursuing our PhDs together. I will always remember your humor and great capabilities as

a scientist, and I hope we can work together in the future. To Marissa Ochoa, I am thankful for the support you have provided both as a friend and scientists. I am so thankful for your humor and chillness, and also for watching Arya when I am away! To Leila Fletcher, I am thankful for your friendship as you have helped me through hard times, and your empathy is inspiring. I admire your quirkiness and individuality. To Camila Medeiros, I am thankful for the friendship we have forged over the years. We are similar in so many ways. Your work and willingness as a scientist are always inspiring to me. To Christian Henry, I am thankful for your welcoming friendship and our chats about our collections of house plants. To Anna Ongjoco, your humor and originality are inspiring! To Nidhi Vinod, thank you for your continual enthusiasm in plants and life in general! To Santiago Trueba, thank you for being an incredibly welcoming desk buddy when I first arrived. I will always remember your thoughtfulness. Jessica Smith, thank you for your enthusiasm to help and for your friendship. I am grateful that you care deeply about the wellbeing of me and everyone else in the lab. Lastly, I am grateful to the numerous undergraduates that have worked with me over the years: Thomas Condon, Jason Zhao, Sachin Reddi, Julia Bowers, John Liang, Michelle Hii, Josh Matsuda, Kirthana Pisipati, Benjamin Simon, Caroline Pohl and Silva Tagaryen.

I am thankful to the many collaborators that helped make the work in this dissertation possible, including: Thomas Buckley, Pascal-Antoine Christin, Erika Edwards, Congcong Liu, Zeqing Ma, Colin Osborne, Christine Scoffoni, Samuel Taylor and Teera Watcharamongkol.

I am also thankful to my friends and colleagues at Adaptive Symbiotic Technologies, and especially to Rusty Rodriguez and Regina Redman as your work and mentorship are inspiring. I am thankful for your welcoming me into your company as a research scientist.

I am indebted to my mother, who has provided for me my whole life and always supported my endeavors. Thank you for allowing me to grow and thrive in my own way. Your work-ethic and adventurous nature have always been so inspiring and I am happy to have inherited those traits. Thank you for your continual unconditional love and for always instilling in me that I can achieve what I want through hard work. To my sister Lindsay, thank you for your love and support.

I thank my little girl Arya, for bringing joy to my life in my hardest time. I have learned so much from taking care of you these past three years and I am excited to explore more of the world together. I love you so much. I am thankful to my best friend Nick Cutlip, for being the brother I never had but always wanted. You are inspiring, thoughtful and too smart for your own good. Thank you for your unconditional love. To my best friend Gigi Debortoli, thank you for your love and support for these past two decades. You have helped through so many hard times and I look forward to growing old with you!

Chapter Two is a reprint of:

Baird AS, Taylor SH, Pasquet-Kok J, Vuong C, Zhang Y, Watcharamongkol T, Scoffoni C, Edwards EJ, Christin P-A, Osborne CP, Sack L. 2021. Developmental and biophysical determinants of grass leaf size worldwide. *Nature* **592**: 242-247. doi:10.1038/s41586-021-03370-0. Author contribution statement: A.S.B., S.H.T., C.P.O. and L.S. conceptualized the project. A.S.B., S.H.T., J.P-K., C.V., Y.Z., T.W., C.S., E.J.E., and P-A. C collected data. A.S.B., S.H.T., J.P-K., C.V., Y.Z., T.W., C.S., P-A.C and L.S. performed the analysis of data. All authors reviewed and revised the manuscript.

Chapter Three is from:

Baird AS, Taylor SH, Reddi S, Pasquet-Kok J, Vuong C, Zhang Y, Watcharamongkol T, John GP, Scoffoni C, Osborne CP, Sack L. (*in revision at Plant, Cell & Environment*). Allometries of cell and tissue anatomy and photosynthetic rate across leaves of C_3 and C_4 grasses. Author contribution statement: A.S.B., S.H.T., C.P.O. and L.S. conceptualized the project. A.S.B., S.H.T., S.R., J.P-K., C.V., and Y.Z. collected data. A.S.B., S.H.T., and L.S. performed the analysis of data. All authors reviewed and revised the manuscript.

Chapter Four is from:

Baird AS, Taylor SH, Pasquet-Kok J, Vuong C, Zhang Y, Watcharamongkol T, Cochard H, Scoffoni C, Edwards EJ, Osborne CP, Sack L. (*in prepaparation for submission to Science*). Leaf hydraulic design of C_3 and C_4 grasses. Author contribution statement: A.S.B., S.H.T., C.P.O. and L.S. conceptualized the project. A.S.B., S.H.T., J.P-K., C.V., Y.Z., C.S. collected data. A.S.B., S.H.T., H.C., and L.S. performed the analysis of data. All authors reviewed and revised the manuscript.

Chapter Five is from:

Baird AS, Medeiros CD, Bowers J, Hii Michelle, Liang J, Matsuda J, Pisipati K, Pohl C, Simon B, Tagaryan S, Buckley TN, Sack L. (*in preparation for submission to American Journal of Botany)*. Disentangling the developmental associations of leaf trichome and stomatal densities across diverse angiosperm species. Author contribution statement: A.S.B., C.D.M., T.N.B. and L.S. conceptualized the project. A.S.B., C.D.M., J.B., M.H., J.L., J.M., K.P., C.P., B.S., S.T. collected data. A.S.B., T.N.B. and L.S. performed the analysis of data. All authors reviewed and revised the manuscript.

Chapter Six if from:

> Baird AS, Ma Z, Buckley TN, Sack L. (*in preparation for submission to Nature Plants*). Integrating leaf expansion kinematics into the leaf economic spectrum: a meta-analysis across species. Author contribution statement: A.S.B. and L.S. conceptualized the project. A.S.B. and L.S. collected data. A.S.B., T.N.B. and L.S. performed the analysis of data. All authors reviewed and revised the manuscript.

Vita

Professional Preparation
2016   B.S. in Biology (Plant), minor in French (University of Washington)

Publications
Baird AS, Taylor SH, Pasquet-Kok J, Vuong C, Zhang Y, Watcharamongkol T, Scoffoni C, Edwards EJ, Christin P-A, Osborne C, Sack L. (2021) Developmental and biophysical determinants of grass leaf size worldwide. *Nature*. **592**, 242-247
 doi: https://dx.doi.org/10.1038/s41586-021-03370-0

Liu C, Li Y, Zhang J, **Baird AS**, He N. (2020) Optimal community assembly related to leaf economic-hydraulic-anatomical traits. *Frontiers in Plant Science.* **11** doi: https://doi.org/10.3389/fpls.2020.00341

Rodriguez R, **Baird AS**, Cho S, Gray Z, Groover E, Harto R, Hsieh M, Malmberg K, Manglona R, Mercer M, Nasman N, Nicklason T, Rienstra M, Van Inwegen A, VanHooser A, Redman R. (2019) Mitigating climate impacts on crop production via symbiosis, in *Endophyte Biotechnology: potential for agriculture and pharmacology,* pp. 59-67. Cabi. doi: https:doi.org/ 10.1079/9781786399427.0059

Rodriguez R, **Baird AS**, Batson A, Cho S, Gray Z, Harto R, Hsieh M, Malmberg K, Manglona R, Mercer M, Nasman N, Nicklason T, Rienstra M, Van Inwegen A, VanHooser A, Redman R (2019) Programming plants for climate resilience through symbiogenics, in *Seed Endophytes,* pp. 127 – 137. Verma, S., White, Jr J. Springer, Cham. doi: https://doi.org/10.1007/978-3-030-10504-4_7

Selected Awards, Grants & Honors
2022 Conference travel award ($1,500), Dept. of Ecology $ Evolutionary Biology, UCLA
2022 Dissertation year fellowship (3 quarters funding), The Graduate Division, UCLA
2022 Excellence in research, PhD Candidate, Life Sciences, UCLA ($500)
2021 Conference award ($200), Dept. of Ecology & Evolutionary Biology, UCLA
2021 1ˢᵗ Place best graduate research poster ($250 amazon gift card), Dept. of Ecology & Evolutionary Biology, UCLA
2021 Quarter fellowship ($7,500 + fees/tuition), Dept. of Ecology & Evolutionary Biology, UCLA
2020 Conference award ($200), Dept. of Ecology & Evolutionary Biology, UCLA
2020 Research award ($400), Dept. of Ecology & Evolutionary Biology, UCLA
2019 Quarter fellowship ($7,000 + fees/tuition), Dept. of Ecology & Evolutionary Biology, UCLA
2018 Conference travel grant ($1,000), The Graduate Division, UCLA
2019 Conference travel award ($1,200), Dept. of Ecology & Evolutionary Biology, UCLA
2019 Research award ($2,000), Dept. of Ecology & Evolutionary Biology, UCLA
2019 Honorable mention, National Science Foundation Graduate Research Fellowship
2018 Conference travel award ($500), Dept. of Ecology & Evolutionary Biology, UCLA

2018 2nd Place best research poster ($150), Dept. of Ecology & Evolutionary Biology, UCLA
2017 University fellowship ($3,000), The Graduate Division, UCLA
2017 Edwin W. Pauley fellowship ($30,000), College of Letters and Science, UCLA

Selected presentations
Baird AS, Taylor SH, Pasquet-Kok J, Vuong C, Zhang T, Watcharamongkol T, Scoffoni C, Edwards EJ, Osborne CP, Sack L. The hydraulic adaptation of grasses with contrasting photosynthetic pathways. **Contributed Poster Presentation June 2022**: Gordon Research Conference: Multiscale Plant Vascular Biology, Sunday River, Maine

Baird AS, Medeiros C, Buckley T, Sack L. Developmental basis of leaf trichome density. **Contributed Poster Presentation, May 2021:** Department of Ecology and Evolutionary Biology Research Symposium, UCLA, CA, U.S.

Baird AS. Integrating leaf development, structure and physiology to unravel insights and mechanisms of eco-evolutionary adaptation of leaves. **Invited Guest Lecture, February 2021**: California State University Los Angeles (CSULA) Biol 4300: Fundamental Research in Plant Ecological Physiology.

Baird AS, Taylor SH, Pasquet-Kok J, Vuong C, Zhang T, Watcharamongkol T, Scoffoni C, Edwards EJ, Christin P-A, Osborne CP, Sack L. Developmental scaling of venation architecture in grasses underlies worldwide leaf size distribution. **Contributed Oral Presentation, May 2019**: UCLA Department of Ecology and Evolution Biology: EcoEvo Pub, UCLA, CA, U.S., **August 2019**: American Society of Plant Biologists: Plant Biology 2019, San Jose, CA, U.S., **January 2020**: UCLA Plant Biology Seminar Series

Activities

2021	**Podcast Interviewee**, Agriculture, GMOs and Plant physiology (https://anchor.fm/dragonfruit/episodes/Alec-Baird-Agriculture--GMOs--and-Plant-Physiology-epuo14)
Past and Present	**Society Member,** British Ecological Society (BES), Society of Plant Signaling and Behavior (PSB), Cactus and Succulent Society of America (CSSA), Ecological Society of America (ESA), American Society of Plant Biologists (ASPB), Union of Concerned Scientists (UCS)
Past and Present	**Peer Reviewer,** 15 publications reviewed total, Annals of Botany (1), AoB Plants (1), Ecography (1), Ecology and Evolution (1), Ecology Letters (1) Frontiers in Plant Science (1), Journal of Plant Ecology (1), Journal of Plant Physiology (1), Nature Scientific Reports (1), New Phytologist (4), Plant Biology (1), Plant Ecology (1), ScienceAsia (1)
Past and Present	**Mentor to UCLA undergraduate researchers,** Julia Bowers (2022 – 2023), John Liang (2022 – 2023), Josh Matsuda (2022 – 2023), Kirthana Pisipati (2022 – 2023), Benjamin Simon (2022 – 2023), Caroline Pohl (2022), Silva Tagaryen (2022), Sachin Reddi (2019 – 2021), Jason Zhao (2018 – 2019), Thomas Condon (2018-2019)

Chapter 1: Premise of the Dissertation

The global diversity of the characteristics of the leaf, the primary photosynthetic organ, highlights its importance in plant adaptation and ecosystem function (Wright et al., 2004, 2017; Sack & Scoffoni 2013). A universal trade-off exists in leaves of terrestrial plants that underlies the evolution of leaf functional diversity: for carbon dioxide to be exchanged from the atmosphere to the sites of photosynthesis in the leaf, water must be transpired in the opposite direction from the leaf to the atmosphere (Sack & Holbrook, 2006). Such a trade-off has led to the evolution of diverse leaf vascular architecture that drives variation in the capacity for leaves to maintain hydration and stomatal opening as water is continually transpired, thereby influencing leaf photosynthetic function, stress tolerance and plant productivity (Sack & Holbrook, 2006; Sack & Scoffoni, 2013). This theory is the basis of leaf hydraulics, a relatively novel sub-discipline that has seen exponential growth in the last decade within plant physiology that has expanded our knowledge of regulation of leaf photosynthesis, and leaf tolerance and survival of stressful conditions (Sack & Holbrook, 2006; Sack & Scoffoni, 2013).

Plant hydraulics extends a classical approach to plant physiological investigations, emphasizing the identification of the mechanistic linkages between structure and function, utilization of mathematical equations to understand physiological processes, and focusing on how structure-function linkages impact physiological transport and growth (Sinclair & Purcell, 2005; Nobel 2020). Indeed, structural-functional linkages are remarkably important because they allow for a direct mechanistic understanding of the structural consequences on physiological transport, function, and tolerance of environmental stressors, thus elevating our understanding of the adaptive consequences of variation in structure and function across species (Sack & Scoffoni,

2013). Such an approach has largely been neglected within plant physiology, relative to molecular processes, given the increasing technological advancements enabling a greater understanding of biochemistry and the genes underlying phenotypes and processes, and particularly within model species (Sinclair & Purcell, 2005). Yet, new concepts and synergies of structure-function research, in particular that related to hydraulics, has led to a surge in the field even as its findings become more important to predict and potentially mitigate climate change responses to vegetation.

One new source of synergy in plant structure-function research is the role of development, and particularly the conserved developmental programs that can provide tremendous insight into the constraints of adaptive trait diversification (Sack et al., 2012; John, Scoffoni & Sack, 2013; Cardoso, Randall, Jordan & McAdam, 2018). Linking physiology with the spatial and temporal aspects of development has the power to address unanswered questions in plant biology, i.e. because linking structure and physiological function addresses "why" plants vary in performance and tolerance, and the developmental processes can address "how" such variation arises, due to the influence of development on structure and composition.

Although the structural and compositional components of leaves are of key importance in driving variability in hydraulic transport across eudicotyledonous species, such physiological hydraulic adaptations, and their developmental drivers, have remained largely unexplored in monocotyledonous species, the other dominant lineage within flowering plants, which includes the grasses (Sack & Scoffoni, 2013). Extending this theory, as well as identifying other leaf level adaptations within lineages such as the grasses will elucidate their function with respect to climate adaptation. This exploration can provide implications and applications in ecology, agriculture and paleobiology as the grass family includes 12,000 species that dominate >40% of

the earth's terrestrial surface, contribute 33% of terrestrial primary productivity and from which the bulk of crops are derived (Beer et al., 2010; Soreng et al., 2017). Further, 41% of grass species function via the C_4 photosynthetic pathway which evolved 18 independent times within the Poaceae (Sage, Christin & Edwards, 2011). The artificial incorporation of this highly productive photosynthetic pathway into species exhibiting C_3 photosynthesis is a goal for ecology and agriculture, as C_4 species have elevated yields and stress tolerance (Langdale, 2011). Grass leaves show immense diversity in morphological and functional variation, with distinctive linearized leaves with parallel veins. Thus, the grasses provide an independent system to resolve both the generality and the adaptive basis for the association of leaf traits and climate.

My dissertation research integrates approaches to the developmental, anatomical and compositional basis of mechanistic hydraulic adaptation across species. In Chapter 2 I utilized many separate datasets to explore global adaptation of leaf size and climate in the grasses (Poaceae), and the mechanisms underlying such patterns, through a detailed study of grass leaf biophysics, development, anatomy and morphology. This work established that grass species with smaller leaves dominate both cold and dry climates globally, constraints imposed by a common leaf developmental program result in smaller grass leaves having vein traits that provide tolerance to cold and dry climates, thus explaining the global grass leaf size and climate patterns. I used biophysical modeling to assess whether thermal advantages associated with small leaves would provide further explanation for such patterns which showed that smaller leaves achieve higher photosynthetic rates in both cold or dry conditions, and under warm and moist conditions, thus also contributing to climate adaptation. Lastly, I provided a new method to estimate grass leaf size based on grass leaf fragments that improves reconstructions of grass evolutionary history and paleo-analyses. In Chapter 3 I established allometric relationships, that

is, the constrained associations of the dimensions and physical properties of leaves and their developmental drivers, for the grasses, using experimental data for 27 common garden grown grass species. I show that grass leaf cells exhibit distinct development and functional modules that drive differential allometries, such that across species: 1) photosynthetic and epidermal cell sizes scale together, though independent of vascular cells, 2) vascular cell sizes scale across vein orders, 3) thicker leaves have larger photosynthetic and epidermal cells, longer leaves have smaller photosynthetic cells but larger vascular cells, wider leaves have larger photosynthetic, epidermal, and bundle sheath cells, and taller plants have larger vascular conduits and 4) allometries of cell size converge to maximize photosynthetic function. This was the first study to test leaf allometric relationships for grass leaves, and emphasizes the leaf design rules driven by developmental coordination that constrains leaf structure and function. In Chapter 4 I established the anatomical basis for leaf water transport of C_3 and C_4 photosynthesis in the grasses, as well as resolving a paradox of grass leaf physiology, using experimental data for 27 common garden grown grass species and modeling. I show that C_3 grasses conform similarly to C_3 eudicots with tight coordination of leaf hydraulics and gas exchange, and gas exchange and climate. The higher minor vein density of C_4 plants does not elevate their capacity for leaf hydraulic flow, as the major veins constitute the bulk of flow, and because pathways outside the xylem principally determine hydraulic flow for the grasses. Lastly, I show that C_4 grasses evolved higher rates of leaf hydraulic supply to demand (i.e. hyper-efficient water transport), which enables the higher photosynthetic rates of C_4 grasses compared to C_3 grasses, in both moist and drying soils, but leads to decoupling of C_4 gas exchange from aridity. This is the first study to establish the differential role of leaf hydraulics for C_3 and C_4 grasses, and highlights the importance of leaf hydraulic design in grass leaf physiology.

In Chapter 5 I disentangled the developmental drivers of leaf trichome density, and its association with stomatal density across diverse species by deriving mathematical expressions of trichome density and stomatal density as functions of their underlying anatomical variables more proximal to development, testing the validity of the expressions, examining the sensitivity of trichome and stomatal densities to underlying variables. I show that positive coordination in leaf trichome and stomatal densities arises because they have similar developmental determinants, which contrasts with their proposed trade-off in model species. This study highlights the power of analyzing a functional trait in terms of its underlying traits, clarifying the evolutionary mechanisms of functional diversity and coordination, and potentially targeting specific traits for agricultural breeding. In Chapter 6 I performed a meta-analysis and collected data for leaf area with time for developing leaves to examine the developmental determinants of leaf size across diverse eudicot species and their potential coordination with the leaf economics spectrum. I show that maximum leaf size variation arises from variation in the maximum growth rate, and not by expansion duration, and that the developmental processes underlying leaf size are tightly linked with leaf economics traits across species.

Overall, by integrating developmental processes with leaf structure and function my dissertation work clarifies the evolutionary adaptation of leaf functional diversity for C_3 and C_4 grasses and diverse eudicots. Such work highlights the importance of developmental constraints to physiological adaptation across different taxonomic scales.

References

1. Beer, C., M. Reichstein, E. Tomelleri, P. Ciais, M. Jung, N. Carvalhais, C. Rödenbeck, et al. 2010. Terrestrial Gross Carbon Dioxide Uptake: Global Distribution and Covariation with Climate. *Science* 329: 834–838.

2. Cardoso, A. A., J. M. Randall, G. J. Jordan, and S. A. M. McAdam. 2018. Extended differentiation of veins and stomata is essential for the expansion of large leaves in Rheum rhabarbarum. *American Journal of Botany* 105: 1967–1974.

3. John, G. P., C. Scoffoni, and L. Sack. 2013. Allometry of cells and tissues within leaves. *American Journal of Botany* 100: 1936–1948.

4. Langdale, J. A. 2011. C4 cycles: past, present, and future research on C_4 photosynthesis. *The Plant Cell* 23: 3879–3892.

5. Nobel, P. S. 2020. Physicochemical and environmental plant physiology. 5th ed. Academic Press, San Diego, CA.

6. Sack, L., and N. M. Holbrook. 2006. Leaf Hydraulics. *Annual Review of Plant Biology* 57: 361–381.

7. Sack, L., and C. Scoffoni. 2013. Leaf venation: structure, function, development, evolution, ecology and applications in the past, present and future. *New Phytologist* 198: 983–1000.

8. Sack, L., C. Scoffoni, A. D. McKown, K. Frole, M. Rawls, J. C. Havran, H. Tran, and T. Tran. 2012. Developmentally based scaling of leaf venation architecture explains global ecological patterns. *Nature Communications* 3: 837.

9. Sage, R. F., P.-A. Christin, and E. J. Edwards. 2011. The C_4 plant lineages of planet Earth. *Journal of Experimental Botany* 62: 3155–3169.

10. Sinclair, T. R., and L. C. Purcell. 2005. Is a physiological perspective relevant in a 'genocentric' age?*. *Journal of Experimental Botany* 56: 2777–2782.

11. Soreng, R. J., P. M. Peterson, K. Romaschenko, G. Davidse, J. K. Teisher, L. G. Clark, P. Barberá, et al. 2017. A worldwide phylogenetic classification of the Poaceae (Gramineae) II: An update and a comparison of two 2015 classifications. *Journal of Systematics and Evolution* 55: 259–290.

12. Wright, I.J., N. Dong, V. Maire, I.C. Prentice, M. Westoby, S. Díaz, et al. 2017. Global climatic drivers of leaf size. *Science* 357: 917–921.

13. Wright, I.J., P.B. Reich, M. Westoby, D.D. Ackerly, Z. Baruch, F. Bongers, et al. 2004. The worldwide leaf economics spectrum. *Nature* 428: 821–827.

Article

Developmental and biophysical determinants of grass leaf size worldwide

Alec S. Baird[1✉], Samuel H. Taylor[2,3], Jessica Pasquet-Kok[1], Christine Vuong[1], Yu Zhang[1], Teera Watcharamongkol[3,4], Christine Scoffoni[1,5], Erika J. Edwards[6], Pascal-Antoine Christin[3], Colin P. Osborne[3] & Lawren Sack[1✉]

One of the most notable ecological trends—described more than 2,300 years ago by Theophrastus—is the association of small leaves with dry and cold climates, which has recently been recognized for eudicotyledonous plants at a global scale[1–3]. For eudicotyledons, this pattern has been attributed to the fact that small leaves have a thinner boundary layer that helps to avoid extreme leaf temperatures[4] and their leaf development results in vein traits that improve water transport under cold or dry climates[5,6]. However, the global distribution of leaf size and its adaptive basis have not been tested in the grasses, which represent a diverse lineage that is distinct in leaf morphology and that contributes 33% of terrestrial primary productivity (including the bulk of crop production)[7]. Here we demonstrate that grasses have shorter and narrower leaves under colder and drier climates worldwide. We show that small grass leaves have thermal advantages and vein development that contrast with those of eudicotyledons, but that also explain the abundance of small leaves in cold and dry climates. The worldwide distribution of leaf size in grasses exemplifies how biophysical and developmental processes result in convergence across major lineages in adaptation to climate globally, and highlights the importance of leaf size and venation architecture for grass performance in past, present and future ecosystems.

The grasses (Poaceae), which originated at least 55 million years ago[8], comprise about 11,500 species in 750 genera[9] and dominate up to 43% of the land surface of the Earth[7] (Fig. 1). Small leaves have previously been linked with arid climates in specific grass lineages and communities (see Supplementary Table 1 for a summary of the relevant publications). A worldwide climatic association could be an important influence on the distributions of grass species and their tolerance of climate change, as well as on crop breeding. We tested relationships of leaf size with climate across 1,752 grass species from 373 genera in a global database, and for 27 diverse and globally distributed species in a common garden (Extended Data Fig. 1, Supplementary Tables 2, 3).

We also tested for an adaptive basis for the association of grass leaf size with climate (Fig. 1). Because smaller leaves couple more tightly with air temperature (owing to their thinner boundary layer), small-leafed eudicotyledons avoid damage from night-time chilling and daytime overheating[4]; smaller leaves may also achieve a higher photosynthetic rate and water-use efficiency, and compensate for shorter growing periods[4,10–12]. We evaluated these potential advantages for small-leafed grasses using energy balance modelling.

Smaller leaves may also develop vein traits that confer stress tolerance[5]. In typical eudicotyledons the large ('major') veins are patterned before the bulk of leaf expansion[5]; leaves that expand less have narrower major veins and xylem conduits, and major veins that are more closely spaced, which results in a higher vein length per leaf area (VLA)

of their major veins[5,6]. Across eudicotyledons, major vein traits scale allometrically with mature leaf size: $trait = a \times leaf\,area^b$ (in which a is a scaling coefficient and b is the scaling exponent)[13]. The major vein traits in small leaves of eudicotyledons can provide greater water transport and lower vulnerability to freezing and dehydration[6] (Fig. 1a, Supplementary Table 4). However, grass leaves are highly distinct from those of eudicotyledons, far smaller on average, and characterized by parallel longitudinal veins connected by transverse veins[14]. To determine vein scaling and its adaptive consequences for small leaves in grasses, we synthesized a model of leaf development for C_3 and C_4 grasses (Table 1, Box 1).

Developmental scaling of grass venation

Our synthetic model of leaf development in grasses (Box 1) is conserved across grass species, and therefore scaling predictions can be derived for species that vary in leaf size (Supplementary Tables 5, 6). Some of these scaling relationships arise intrinsically from the sequence of development: for example, major VLA is lower in wider leaves, as their major veins are spaced further apart. In the model, VLA for first-order veins declines geometrically as the inverse of leaf width, whereas the VLA for second-order veins declines less steeply than geometrically (because the formation of more second-order veins partially counteracts their greater spacing). Other scaling trends are not intrinsic,

[1]Department of Ecology and Evolutionary Biology, University of California Los Angeles, Los Angeles, CA, USA. [2]Lancaster Environment Centre, University of Lancaster, Lancaster, UK. [3]Department of Animal and Plant Sciences, University of Sheffield, Sheffield, UK. [4]Faculty of Science and Technology, Kanchanaburi Rajabhat University, Kanchanaburi, Thailand. [5]Department of Biological Sciences, California State University Los Angeles, Los Angeles, CA, USA. [6]Department of Ecology and Evolutionary Biology, Yale University, New Haven, CT, USA. ✉e-mail: alecsbaird@gmail.com; lawrensack@ucla.edu
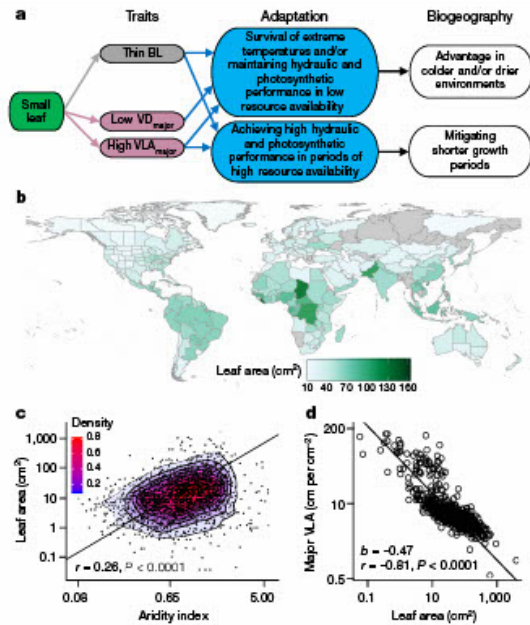
Fig. 1 | Relationship of grass leaf size, traits and climatic distribution of species worldwide. a, Links between small leaf size and traits, adaptation to cold and dry climates, and biogeography, as established for eudicotyledons (Supplementary Table 4) and hypothesized for grasses. Small leaves have thin boundary layers (BL), develop lower major vein diameters (VD_{major}) and have higher major VLA (VLA_{major}), which provide advantages in cold or dry climates (Supplementary Table 4). Large leaves would be disadvantaged in such climates (relative to warm and moist climates). **b,** Grass leaf area averaged per country in the global database (across-species mean of leaf area for 21 to 547 species per country; grey denotes that <20 species are represented). **c,** Grass leaf area in relation to the aridity index (a low index reflects a drier climate). Each point represents a species ($n = 912$ C_3 and 840 C_4 species). Contour lines and colours represent the 2D kernel density of points. **d,** The association of VLA_{major} with leaf area across grass species ($n = 600$ species). Statistics represent the fits for $\log(y) = \log(a) + b\log(x)$ from ordinary least squares in **c, d.** $P = 2.3 \times 10^{-27}$ (**c**), 1.6×10^{-139} (**d**) (both two-tailed).

but are instead 'enabled' by the developmental program[15]. The diameters of first- and second-order veins are expected to scale positively with leaf length and area, because a greater rate or duration of leaf length expansion enables a greater growth of vein diameters. Similarly, a positive scaling of the diameters of first- and second-order vein xylem conduits with vein diameter is enabled by the greater vein expansion in larger leaves.

Minor veins differ from major veins in their predicted scaling with leaf size across species. As minor veins are initiated at the tip of the developing leaf, greater length expansion provides more space and time for initiating additional minor veins. Minor VLA therefore scales positively with final leaf length. However, as minor veins are initiated later during leaf-width expansion and their diameter growth and spacing is more limited than that of major veins, their vein traits are independent of final width. The positive scaling of minor VLA with leaf length, and its decoupling from leaf width, would result in weak scaling of minor VLA with leaf area. Total VLA (that is, summing major and minor veins) is decoupled from leaf area, owing to the negative scaling of major VLA with leaf width and the positive scaling of minor VLA with leaf length. Additional scaling predictions arise from the relationships of

vein diameters and lengths with leaf size (Supplementary Table 6). As with the diameters of major veins, the major vein surface area, vein projected area and vein volume per unit leaf area (VSA, VPA and VVA, respectively) scale positively with leaf length and—similar to major VLA—negatively with leaf width. These counteracting trends lead to predictions that VSA, VPA and VVA are decoupled from leaf area.

Our developmental model predicts that grass species with smaller leaf dimensions will develop vein traits that confer stress tolerance; these traits include narrower major veins and higher major VLA, VSA, VPA and VVA, which contribute to water transport efficiency and a lower vulnerability to cold and drought[5,6] (Fig. 1a, Supplementary Table 4). By contrast, large grass leaves can attain high minor and total VLA, VSA, VPA and VVA independently of leaf size, which enables high transport efficiency for competition in sunny, moist climates. The model also predicts that C_3 and C_4 species will converge in their vein scaling. C_4 grasses have a higher total VLA, providing a large vein bundle-sheath compartment for concentrating CO_2 to enable high rates of photosynthetic assimilation[15–17]. We hypothesized that the high total VLA of C_4 grasses arises from minor VLA, and is therefore independent of leaf area.

To test these predictions, we compared the measured scaling relationships of 27 grass species in a common garden against null expectations from the developmental model and against geometric scaling[5,13] (Extended Data Fig. 1, Supplementary Table 3), and assessed whether developmental scaling would confer small leaves with potential climatic advantages.

Relationship of leaf size with climate

Globally, grasses vary by more than 625-fold, 275-fold and 160,000-fold in leaf length, width and area, respectively[8,18], and smaller leaves are associated with cooler and drier climates (Fig. 1b, c, Supplementary Tables 1, 2, 7). We found that, across species, leaf length, width and area were interrelated and that all of these were positively correlated with mean annual temperature, mean annual precipitation and the aridity index (for leaf area, $r = 0.24–0.31$, $P < 0.001$; phylogenetic $r = 0.08–0.17$, $P < 0.001$) (Fig. 1c, Extended Data Fig. 2, Supplementary Table 7). We found similar relationships with growing season temperature, growing season precipitation and growing season length (Supplementary Table 7). The climatic associations of smaller leaves were independent of plant stature, and statistically similar for C_3 and C_4 species (Supplementary Tables 7, 8). The size of grass leaves was associated interactively with climatic temperature and precipitation, whether considered annually or for the growing season (Extended Data Fig. 3, Supplementary Table 8). The climatic distribution of grass leaf size arises at least in part from the exclusion of large-leafed species from dry and cold climates (Extended Data Fig. 4, Supplementary Table 8).

Thermal benefits of small leaf size

We tested three hypotheses for the thermal advantages of small grass leaves in cold and dry climates using heuristic energy-budget modelling[19,20]. First, small leaves may avoid chilling or overheating damage (a mechanism that explains the global biogeographical trend in eudicotyledon leaf size[3]). However, 98% of grass species in the global database had leaves smaller than the modelled width thresholds for such damage (8.16 and 4.47 cm for chilling and overheating, respectively[3]) and among these species leaf size remained associated with climate (Extended Data Fig. 5), which indicates that this mechanism cannot explain the global trend. Second, small leaves—which are better coupled with air temperature—may achieve a higher light-saturated photosynthetic rate or leaf water-use efficiency under cold or dry climates[20] (Extended Data Fig. 5, Supplementary Table 9). These benefits were supported by model simulations (especially at slower wind speeds): in comparisons between the 5th and 95th percentile of leaf sizes in our

9

Article

Table 1 | Parameters for the scaling of vein diameters and VLA with mature leaf dimensions

Trait and vein order[a]	Scaling with leaf length				Scaling with leaf width				Scaling with leaf area			
	Expected b	r (P)	a	b (95% CI[b])	Expected b	r (P)	a	b (95% CI)	Expected b	r (P)	a	b (95% CI)
VD[c] 1°[d]	$0<b<1$; e*	0.61 (0.0007)	−1.64	0.368 (0.267, 0.508)	$b\sim0$*	0.25 (0.21)			$0<b<0.5$; e*	0.71 (3.0×10⁻⁵)	−1.52	0.319 (0.24, 0.424)
2°[d]	$0<b<1$; e*	0.76 (3.9×10⁻⁶)	−1.69	0.363 (0.279, 0.473)	$b\sim0$*	0.003 (0.99)			$0<b<0.5$; e*	0.65 (0.0003)	−1.58	0.32 (0.224, 0.44)
VLA[f] 1°[g]	$b\sim0$*	0.36 (0.065)			$b\sim-1.0$; i*	−1.0 (1.2×10⁻³⁴)	0.009	−1.01 (−1.03, −0.99)	$b\sim-0.5$; i*	−0.61 (7.0×10⁻⁴)	0.943	−0.558 (−0.845, −0.27)
2°[g]	$b\sim0$*	0.36 (0.062)			$-1.0\le b<0$; i*	−0.82 (1.4×10⁻⁷)	0.951	−0.616 (−0.769, −0.462)	$-0.5\le b<0$; i*	−0.46 (0.017)	1.51	−0.313 (−0.555, −0.072)
Total major[g]	$b\sim0$*	0.37 (0.058)			$-1\le b<0$; i*	−0.87 (3.6×10⁻⁹)	0.999	−0.67 (−0.805, −0.534)	$-0.5\le b<0$; i*	−0.49 (0.0090)	1.61	−0.346 (−0.589, −0.104)
3°[h]	$0<b<1$; e	0.34 (0.085)			$b\sim0$*	−0.29 (0.137)			$0<b<0.5$; e	0.02 (0.94)		
4°[h]	$0<b<1$; e	0.3 (0.51)			$b\sim0$*	−0.13 (0.774)			$0<b<0.5$; e	0.02 (0.97)		
5°[h]	$b\sim0$*	−0.33 (0.095)			$b\sim0$	0.57 (0.0020)	0.858	0.273 (0.138, 0.408)	$b\sim0$*	0.32 (0.10)		
Total minor[h]	$0<b<1$; e*	0.56 (0.0023)	1.13	0.664 (0.489, 1.05)	$b\sim0$*	−0.36 (0.068)			$0<b<0.5$; e	0.20 (0.33)		
Overall total[h]	$0<b<1$; e*	0.57 (0.0018)	1.27	0.619 (0.425, 0.878)	$-1\le b<0$; i*	−0.56 (0.0025)	1.75	−0.317 (−0.496, −0.138)	$b\sim0$*	0.01 (0.95)		

[a]1° to 5° denote first- to fifth-order veins.

[b]CI, confidence interval.

[c]VD, vein diameter (in mm)

[d]Smaller leaves are predicted to have smaller major vein diameters, which tend to contain narrower xylem conduits (providing tolerance of embolism in cold and dry climates).

[e]The b values predicted from the developmental model are supported in the experimental data (that is, the scaling relationship across species is either absent when expected, or significant, and the predicted b value is within the 95% confidence intervals of the observed b value).

[f]VLA in cm of vein per cm² of leaf area.

[g]Smaller leaves are predicted to have higher major VLA, which contributes to high maximum hydraulic and photosynthetic function (potentially mitigating a short growing period, and additionally reducing vulnerability to hydraulic decline in dry conditions).

[h]Minor and total VLA are predicted to be decoupled from final leaf size. As these contribute to high maximum hydraulic and photosynthetic function, this independence enables potential adaptation to high resource conditions in both small and large leaves.

Parameters are shown across 27 grass species ($n=11$ C₃ and 16 C₄ grass species) grown in a common garden. Tolerance of cold or dry climates can be conferred by these vein traits (among others, such as VSA, VPA and VVA (Supplementary Table 10)), as they influence hydraulic capacity and safety, and vascular cost (Supplementary Table 4). Expectations for these across-species scaling relationships were derived from a developmental model that predicts the allometric slope b in the equation log(trait) = log(a) + b log(mature leaf length, width or area), owing to intrinsic (i) and enabling (e) effects (Supplementary Table 6). Expectations from the alternative, geometric scaling model were also derived and tested (Supplementary Tables 6, 10). Allometric equations were fitted using two-tailed phylogenetic reduced major axis (PRMA) or phylogenetic generalized least squares for the scaling of vein diameter and VLA, respectively, yielding r values and P values, as well as parameters a and b (including 95% confidence intervals for b values).

---

global database, the smaller leaves had 9–27% higher light-saturated photosynthetic rates and/or water-use efficiencies under cold or dry climates (Supplementary Table 9). Third, smaller leaves may mitigate the short daily and/or seasonal growth period that is associated with cold and dry regions with a higher light-saturated photosynthetic rate under warm and moist conditions[4]. This benefit was supported by our simulations (which also showed that smaller leaves had higher transpiration rates) (Supplementary Table 9).

Developmental scaling of grass venation

Developmental vein scaling results in a strong association between vein traits and grass leaf size. As predicted, at a global scale, smaller-leafed species had higher major VLA ($r=-0.84$ to -0.75, $P<0.001$) (Fig. 1d, Extended Data Fig. 6). For the 27 grass species that were grown in our common garden, developmental scaling was supported over the null hypothesis of geometric scaling for numerous vein traits (91 versus 27 of the 111 scaling predictions; $P<0.001$, proportion test) (Table 1, Fig. 2, Extended Data Figs. 6, 7, Supplementary Tables 10, 11). The diameters

of first-order and second-order veins scaled positively with leaf length and area ($b=0.32–0.37$, $r=0.61–0.76$, $P<0.001$) (Fig. 2, Extended Data Fig. 6), and the diameters of xylem conduits scaled with their vein diameters ($b=1.3–1.5$, $r=0.48–0.65$, $P<0.05–0.001$) (Extended Data Fig. 6). The VLA of the first-order vein decreased geometrically with increasing leaf width and area ($b=-1.0$ and -0.56, and $r=-1.00$ and -0.61, respectively, $P<0.001$), whereas the VLA of second-order veins decreased less steeply ($b=-0.62$ and -0.31, and $r=-0.82$ and -0.46, respectively, $P<0.05$) (Fig. 2, Extended Data Fig. 6), and the major and total VLA scaled negatively with leaf width ($b=-0.67$ and -0.32, and $r=-0.87$ and -0.56, respectively, $P<0.01$). The diameters of minor veins were independent of leaf length, width and area. The trends of the VLA of third-order and fourth-order veins with leaf length were not significant, but their sum (the total minor VLA) scaled positively with leaf length ($b=0.35–0.56$, $r=0.56–0.57$, $P<0.01$) and was independent of leaf width and area. The VSA, VPA and VVA also scaled positively with leaf length, and negatively with leaf width (with the exception of the VVA of third-order veins), and all were independent of leaf area (Extended Data Fig. 7). We found trends for the fifth-order veins not anticipated

10

Synthetic model of vein development in grass leaves

This model is based on published data for 20 species of grass (Supplementary Tables, 5, 6), and shows how traits that are advantageous under cold and dry climates develop in small leaves. The development of leaves in grasses includes five phases that are based on developmental zones.

Formation and expansion of the primordium (phase P)
'Founder cells' in the periphery of the shoot apical meristem generate the leaf primordium. Cell divisions drive the growth of a hood-like structure, in which the central first-order vein (midvein) and the large second-order veins are initiated early and extend acropetally, which enables their prolonged diameter growth (Box 1 Fig. a, c, e). After this, discrete spatial growth zones develop at the leaf base and drive leaf expansion laterally and longitudinally.

Formation of the cell division zone (phase D)
The basal cell division zone expands slightly, driving minimal growth (Box 1 Fig. a, b). The first- and parallel second-order vein (major veins) complete their patterning basipetally along the leaf blade and increase in diameter (Box 1 Fig. c, e). Meanwhile, beginning at the lamina tip, C_3 species form a single order of small parallel longitudinal minor veins (that is, third-order veins) as do most C_4 species (which we refer to as C_{4-3L} species). Some

C_4 species of the subfamily Panicoideae additionally form smaller parallel fourth-order veins (which we refer to as C_{4-4L} species[15]) (Box 1 Fig. c).

Division zone, and formation of the expansion zone (phase D–E)
Cells from the division zone transition to a distinct, distal expansion zone. In the expansion zone, cell expansion in width and length spaces apart the first- and second-order veins, resulting in the declines in their VLA (Box 1 Fig. a, b, d). Additional third-order veins (and in some species, fourth-order veins) continue to initiate at the leaf tip between major vein orders and extend basipetally (Box 1 Fig. c–e). The transverse fifth-order veins form last, connecting the longitudinal veins.

Division zone, expansion zone and maturation zone (phase D–E–M)
Cells from the expansion zone mature distally to generate the maturation zone, which increases in size as cells move through the developmental zones (Box 1 Fig. a). The xylem, phloem and bundle sheath of the veins mature.

All of the leaf is in the maturation zone (phase M)
Leaf development is complete, and all cells are differentiated and expanded (Box 1 Fig. a, b).
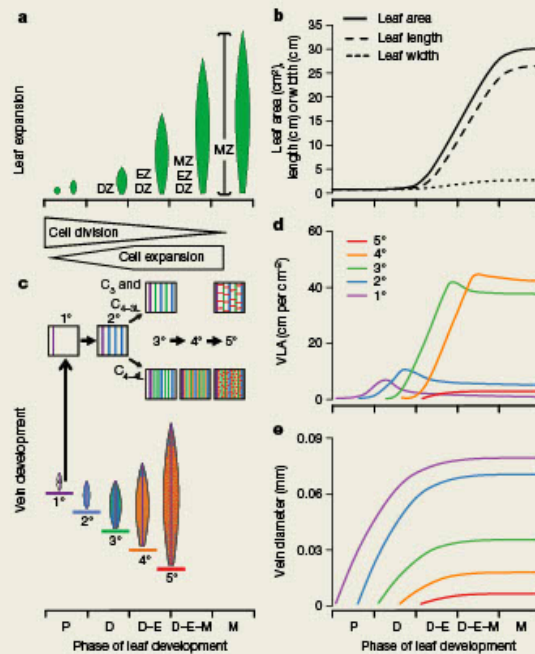
Box 1 Fig. | Synthetic model for grass leaf ontogeny that predicts developmentally based scaling of vein traits with final leaf size across species. Processes are plotted against developmental phases: phases P and D refer to the formation of the leaf primordium and the cell division zone (DZ) at the base of the leaf, respectively; phases D–E and D–E–M describe additions of the expansion zone (EZ) and the maturation zone (MZ), respectively; and phase M denotes the maturation of the whole leaf blade. **a,** Leaf expansion and the formation of zones. **b,** Increases in leaf length, width and area. **c,** Patterning of leaf vein orders from first-order veins to fifth-order transverse veins for C_3 and C_4 species; some C_4 species develop fourth-order longitudinal veins (C_{4-4L} species), whereas C_3 species and C_{4-3L} species do not. **d, e,** Increases in VLA (**d**) and vein diameter (**e**) for each vein order.

Article

by the developmental model, being positive scaling of their VLA, VSA and VPA with leaf width ($r = 0.46$–0.57, $P < 0.05$).

C_3 and C_4 grasses converged in vein scaling (Fig. 2, Extended Data Fig. 8, Supplementary Table 3). C_4 species had more numerous, narrower third-order veins with higher VLA, VSA and VPA, and 7 out of 16 C_4 species had fourth-order veins; this resulted in the C_4 species having, on average, almost double the total VLA of the C_3 species. The C_4 species also had narrower fifth-order veins with lower VSA, VPA and VVA ($P = 0.001$–0.05).

Hydraulic benefits of small leaf size

Across the 27 grass species that we grew experimentally, a number of key vein traits were related to the native climates of the species. Small leaf size and higher major VLA, VSA, VPA and VVA were associated with lower mean annual and growing season precipitation, a lower aridity index and a shorter growing season (Supplementary Table 7). Furthermore, our tests supported assumptions based on the published literature (which is collated in Supplementary Table 4) that C_3 grasses adapted to colder or drier climates have higher light-saturated photosynthetic rates in moist soil, which are associated with their major vein traits (Extended Data Fig. 9)

Developmental scaling contributes mechanistically to climate adaptation globally. Vein scaling can explain the absence of leaves larger than 51.4 cm² in areas in which the mean annual temperatures are below 0 °C (Extended Data Fig. 5), as the midrib conduits of leaves larger than this would be wider than 35 μm (Extended Data Fig. 6) and thus vulnerable to freeze–thaw embolism[21]. Additionally, the narrow xylem conduits of small leaves resist embolism during drought, and their higher major VLA provides a high capacity flow around blockages, which further reduces hydraulic vulnerability to dehydration[6,22–25] (Supplementary Table 4). The higher major VLA of smaller leaves also contributes to mitigating the shorter growing periods that are associated with colder, drier climates[11,12] by providing higher hydraulic conductance, which enables the maintenance of open stomata for higher photosynthetic rates despite the higher transpiration loads expected from their thinner boundary layer[6,26] (Extended Data Fig. 9).

Discussion

The worldwide association of small leaf size in grasses with cold and arid climates arises from millions of years of grass migration and evolution, from the tropics to colder, drier climates and from forest understoreys to open grasslands[8] (Supplementary Table 1). The biophysical and developmental advantages of small leaves can explain this pattern. The thinner boundary layer of small grass leaves confers a moderately higher photosynthetic rate and water-use efficiency in cold and dry climates, and can partially mitigate shorter growing days and seasons (especially under the very low wind speeds that are expected for closed, dense stands)[27–30]. The higher major VLA and narrower xylem conduits of these smaller leaves directly contribute to cold and drought tolerance. The strong climatic association of leaf size and vein traits indicates their substantial importance to plant adaptation against a background of other features—including leaf hairs, leaf rolling and mesophyll desiccation tolerance, and (beyond leaves) annual versus perennial life history, stem and root hydraulic adaptation, and root morphology—that help plants to cope with climatic pressures[31–33].

Developmentally based vein scaling relationships held strongly across diverse grass species—even including those species (such as bamboos) that possess a pseudopetiole. These relationships may also apply to nongrass species from other families within the Poales. Developmental vein scaling relationships in grass leaves are distinct from, though analogous to, those of typical eudicotyledon leaves (Figs. 1, 2, Box 1). In eudicotyledons (as expected from their diffuse lamina growth), major vein traits scale negatively with final leaf area (Supplementary
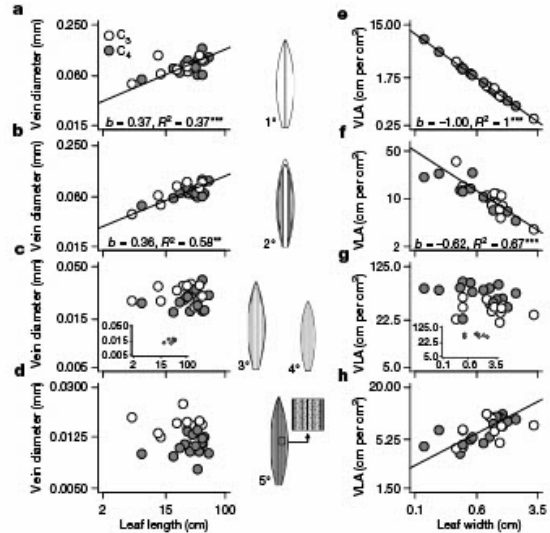
Fig. 2 | The scaling of vein traits with leaf dimensions for 27 species of grass grown in a common garden. $n = 11$ C_3 (shown as white points) and 16 C_4 (shown as grey points) grass species. a–d, Relationship of vein diameters with leaf length. e–h, Relationship of VLA with leaf width. In a, e, relationships are shown for first-order veins; in b, f, for second-order veins; in c, g, for third-order veins (inset panels show fourth-order veins for the species that possess them); and in d, h, fifth-order transverse veins. Each point represents the mean value of a species. PRMA or phylogenetic generalized least square regressions were fitted for log(vein diameter or VLA) = log(a) + b log(leaf length or width), respectively. Parameters and the goodness of fit are given in Table 1, Supplementary Table 10. **$P < 0.01$, ***$P < 0.001$. $P = 0.0007$ (a), 3.9×10^{-6} (b), 1.2×10^{-34} (e), 1.4×10^{-7} (f) and 0.0020 (h) (all two-tailed). Significant trends are plotted with PRMA. Supplementary Table 3 gives the s.e. for species trait values.

Table 4), whereas in grasses vein traits scale more directly with length or width (Table 1, Fig. 2, Box 1). However, for both grasses and eudicotyledons, total VLA—which is a key determinant of hydraulic capacity and photosynthetic rate[6]—was independent of final leaf area. This lack of constraint on total VLA would enable grass diversification in leaf size across environments, as for eudicotyledons[5,26,34]: large-leafed grasses, despite their low major VLA, can achieve sufficient hydraulic capacity with their minor vein length to occupy wet, sunny habitats[6,34,35]. The decoupling of total VLA from leaf size also enables C_4 species to achieve, on average, a higher VLA than that of C_3 species, irrespective of leaf size (Fig. 2, Box 1). Unlike in eudicotyledons[5], larger leaves in grasses did not have a higher VVA (which contributes substantially to the cost of leaf construction[36]); this indicates that there is less restriction on the evolution of grass leaf size in resource-rich environments, in which larger leaves may confer advantages in light-use efficiency and by shading other species[37,38]. Although the common developmental program across grass species explains many vein scaling relationships, these relationships may also arise from selection on the basis of function. In longer leaves, larger-diameter veins may provide necessary structural and hydraulic support[6,39] In wider leaves, more numerous fifth-order transverse veins may reinforce the grass leaves against bending[40] and provide hydraulic pathways that mitigate their lower major VLA[6]. Similarly, the greater diameters of fifth-order veins in C_3 species than in C_4 species may compensate for their lower minor VLA (Fig. 2).

The relationships among grass leaf size, vein traits and climate have diverse potential applications. In eudicotyledons, these traits

are frequently included for estimating the adaptation of species to climate[6], an approach that can now be extended to grasses. For grasses (as shown for eudicotyledons[5,41]), vein scaling can enable the reconstruction of leaf size from fossilized leaf fragments, to improve palaeoclimate reconstructions (Extended Data Fig. 10). Anticipating future climate change, leaf size and vein traits represent key targets for the design of grass crops, which are central to food and biofuel security[42,43]. A current grand challenge is the engineering of C_4 metabolism into C_3 crops such as rice[43], and introducing a higher total VLA has been targeted as a promising step[44,45]. Global trends indicate that C_4 species with narrow leaves and high major VLA would be especially advantaged under the increased temperature and irregular precipitation that are expected for grasslands in scenarios of global climate change[25,46,47].

Online content

Any methods, additional references, Nature Research reporting summaries, source data, extended data, supplementary information, acknowledgements, peer review information; details of author contributions and competing interests; and statements of data and code availability are available at https://doi.org/10.1038/s41586-021-03370-0.

1. Hort, A. *Enquiry into Plants, Vol. I, by Theophrastus* (Harvard Univ. Press, 1948).
2. Peppe, D. J. et al. Sensitivity of leaf size and shape to climate: global patterns and paleoclimatic applications. *New Phytol.* 190, 724–739 (2011).
3. Wright, I. J. et al. Global climatic drivers of leaf size. *Science* 357, 917–921 (2017).
4. Gates, D. M. Transpiration and leaf temperature. *Annu. Rev. Plant Physiol.* 19, 211–238 (1968).
5. Sack, L. et al. Developmentally based scaling of leaf venation architecture explains global ecological patterns. *Nat. Commun.* 3, 837 (2012).
6. Sack, L. & Scoffoni, C. Leaf venation: structure, function, development, evolution, ecology and applications in the past, present and future. *New Phytol.* 198, 983–1000 (2013).
7. Beer, C. et al. Terrestrial gross carbon dioxide uptake: global distribution and covariation with climate. *Science* 329, 834–838 (2010).
8. Gallaher, T. J. et al. Leaf shape and size track habitat transitions across forest-grassland boundaries in the grass family (Poaceae). *Evolution* 73, 927–946 (2019).
9. Soreng, R. J. et al. A worldwide phylogenetic classification of the Poaceae (Gramineae) II: an update and a comparison of two 2015 classifications. *J. Syst. Evol.* 55, 259–290 (2017).
10. Schuepp, P. H. Tansley review no. 59 leaf boundary layers. *New Phytol.* 125, 477–507 (1993).
11. Orians, G. H. & Solbrig, O. T. A cost–income model of leaves and roots with special reference to arid and semiarid areas. *Am. Nat.* 111, 677–690 (1977).
12. Körner, C. Plant adaptation to cold climates. *F1000Res.* 5, 2769 (2016).
13. Niklas, K. J. *Plant Allometry: The Scaling of Form and Process* (Univ. Chicago Press, 1994).
14. Nelson, T. & Dengler, N. Leaf vascular pattern formation. *Plant Cell* 9, 1121–1135 (1997).
15. Christin, P. A. et al. Anatomical enablers and the evolution of C_4 photosynthesis in grasses. *Proc. Natl Acad. Sci. USA* 110, 1381–1386 (2013).
16. Ueno, O., Kawano, Y., Wakayama, M. & Takeda, T. Leaf vascular systems in C_3 and C_4 grasses: a two-dimensional analysis. *Ann. Bot.* 97, 611–621 (2006).
17. Sage, R. F. The evolution of C_4 photosynthesis. *New Phytol.* 161, 341–370 (2004).
18. Clayton, W. D., Vorontsova, M. S., Harman, K. T. & Williamson, H. GrassBase–The Online World Grass Flora http://www.kew.org/data/grasses-db.html (2006).
19. Parkhurst, D. F. & Loucks, O. L. Optimal leaf size in relation to environment. *J. Ecol.* 60, 505–537 (1972).
20. Okajima, Y., Taneda, H., Noguchi, K. & Terashima, I. Optimum leaf size predicted by a novel leaf energy balance model incorporating dependencies of photosynthesis on light and temperature. *Ecol. Res.* 27, 333–346 (2012).
21. Davis, S. D., Sperry, J. S. & Hacke, U. G. The relationship between xylem conduit diameter and cavitation caused by freezing. *Am. J. Bot.* 86, 1367–1372 (1999).
22. Blackman, C. J., Brodribb, T. J. & Jordan, G. J. Leaf hydraulic vulnerability is related to conduit dimensions and drought resistance across a diverse range of woody angiosperms. *New Phytol.* 188, 1113–1123 (2010).
23. Scoffoni, C., Rawls, M., McKown, A., Cochard, H. & Sack, L. Decline of leaf hydraulic conductance with dehydration: relationship to leaf size and venation architecture. *Plant Physiol.* 156, 832–843 (2011).
24. Scoffoni, C. et al. Leaf vein xylem conduit diameter influences susceptibility to embolism and hydraulic decline. *New Phytol.* 213, 1076–1092 (2017).
25. Craine, J. M. et al. Global diversity of drought tolerance and grassland climate-change resilience. *Nat. Clim. Chang.* 3, 63–67 (2013).
26. Scoffoni, C. et al. Hydraulic basis for the evolution of photosynthetic productivity. *Nat. Plants* 2, 16072 (2016).
27. Jones, H. G. *Plants and Microclimate: A Quantitative Approach to Environmental Plant Physiology* 3rd edn (Cambridge Univ. Press, 2014).
28. Grace, J. *Plant-Atmosphere Relationships* 1st edn (Chapman and Hall, 1983).
29. Weiser, R. L., Asrar, G., Miller, G. P. & Kanemasu, E. T. Assessing grassland biophysical characteristics from spectral measurements. *Remote Sens. Environ.* 20, 141–152 (1986).
30. Meinzer, F. C. & Grantz, D. A. Stomatal control of transpiration from a developing sugarcane canopy. *Plant Cell Environ.* 12, 635–642 (1989).
31. Liu, H. et al. Life history is a key factor explaining functional trait diversity among subtropical grasses, and its influence differs between C_3 and C_4 species. *J. Exp. Bot.* 70, 1567–1580 (2019).
32. Fort, F., Jouany, C. & Cruz, P. Root and leaf functional trait relations in Poaceae species: Implications of differing resource-acquisition strategies. *J. Plant Ecol.* 6, 211–219 (2013).
33. Holloway-Phillips, M. M. & Brodribb, T. J. Contrasting hydraulic regulation in closely related forage grasses: implications for plant water use. *Funct. Plant Biol.* 38, 594–605 (2011).
34. Brodribb, T. J., Feild, T. S. & Sack, L. Viewing leaf structure and evolution from a hydraulic perspective. *Funct. Plant Biol.* 37, 488–498 (2010).
35. Linacre, E. T. Further notes on a feature of leaf and air temperatures. *Archiv Meteorol. Geophys. Bioklimatol. B* 15, 422–436 (1967).
36. John, G. P. et al. The anatomical and compositional basis of leaf mass per area. *Ecol. Lett.* 20, 412–425 (2017).
37. Givnish, T. J. Comparative studies of leaf form: assessing the relative roles of selective pressures and phylogenetic constraints. *New Phytol.* 106, 131–160 (1987).
38. Lusk, C. H., Grierson, E. R. P. & Laughlin, D. C. Large leaves in warm, moist environments confer an advantage in seedling light interception efficiency. *New Phytol.* 223, 1319–1327 (2019).
39. Olson, M. E. et al. Plant height and hydraulic vulnerability to drought and cold. *Proc. Natl Acad. Sci. USA* 115, 7551–7556 (2018).
40. Niklas, K. J. A mechanical perspective on foliage leaf form and function. *New Phytol.* 143, 19–31 (1999).
41. Merkhofer, L. et al. Resolving Australian analogs for an Eocene Patagonian paleorainforest using leaf size and floristics. *Am. J. Bot.* 102, 1160–1173 (2015).
42. Somerville, C. The billion-ton biofuels vision. *Science* 312, 1277 (2006).
43. Sedelnikova, O. V., Hughes, T. E. & Langdale, J. A. Understanding the genetic basis of C_4 kranz anatomy with a view to engineering C_3 crops. *Annu. Rev. Genet.* 52, 249–270 (2018).
44. Sage, R. F. & Zhu, X. G. Exploiting the engine of C_4 photosynthesis. *J. Exp. Bot.* 62, 2989–3000 (2011).
45. Feldman, A. B. et al. Increasing leaf vein density via mutagenesis in rice results in an enhanced rate of photosynthesis, smaller cell sizes and can reduce interveinal mesophyll cell number. *Front. Plant Sci.* 8, 1883 (2017).
46. Edwards, E. J. et al. The origins of C_4 grasslands: integrating evolutionary and ecosystem science. *Science* 328, 587–591 (2010).
47. Linder, H. P., Lehmann, C. E. R., Archibald, S., Osborne, C. P. & Richardson, D. M. Global grass (Poaceae) success underpinned by traits facilitating colonization, persistence and habitat transformation. *Biol. Rev. Camb. Philos. Soc.* 93, 1125–1144 (2018).

13

Article

Methods

No statistical methods were used to predetermine sample size. Investigators were not blinded to allocation during experiments and outcome assessment.

Testing for the linkage of leaf size and vein traits with climate across grass species worldwide

We extracted data from the Kew Royal Botanic Garden Grassbase, which was compiled from a combination of floristic accounts and publications[18]. We extracted all available data for maximum leaf length, maximum leaf width, maximum second-order vein number and maximum culm height data, which included values for up to 1,752 species depending on the trait (that is, up to 912 C_3 and 840 C_4 species from 373 genera)[18]. We calculated leaf area by multiplying maximum leaf length by maximum leaf width. We divided the maximum leaf length and maximum second-order vein number, respectively, by maximum leaf width to determine the VLA of first- and second-order veins, and summed these to calculate the major VLA, resulting in values for 616 species for these traits. To test associations of leaf morphological and venation traits with the native climates of the species, we extracted geographical records from the Global Biodiversity Information Facility web portal (http://www.gbif.org). The names of species were checked against the Kew grass synonymy database[18] via the software package Taxonome[48] and The Plant List (http://www.theplantlist.org) using the package Taxostand in R[49]. We discarded records if these were duplicates, the names were not recognized in any databases, the country did not match the coordinates, the coordinates contained fewer than three decimals or species had fewer than five occurrences. For each location, values for mean annual temperature (MAT), mean annual precipitation (MAP) and mean monthly temperature and precipitation were extracted from WorldClim 2.5-arc minute resolution[50]; values for the aridity index[51] were from CRU TS4.01 01[52]. We also estimated growing season variables, considering growing season months as those with mean temperature ≥4 °C and precipitation ≥2× the mean monthly temperature; growing season length was calculated as the number of months that fulfilled these criteria, growing season temperature was calculated by averaging the mean temperatures of these months, and growing season precipitation was calculated by summing their mean precipitation[53]. Climate variables were averaged from all given locations for each species. We focused on the relationships of traits with mean climate variables based on the hypothesis that, if gene flow occurs among populations of a given species across its native range, then the mean phenotypic trait values of this species will be related to their mean climate variables[54].

Construction of a synthetic model for grass leaf development, and derivation of allometric predictions based on developmental and geometric scaling

To determine whether leaf development constrains specific vein traits in smaller leaves, we formulated a synthetic grass leaf developmental model and derived expectations for the relationship of vein traits with final leaf dimensions across species (Box 1, Supplementary Tables 5, 6). To construct this model, we conducted searches for previously published studies that included developmental data and/or images of grass leaf development using the keywords 'grass leaf development', 'grass vein development', 'grass histogenesis', 'grass morphogenesis', 'Poaceae', 'leaf ontogeny', 'leaf histology', 'leaf growth', 'leaf anatomy', 'vascular development' and 'vasculature development' in the Web of Science database and Google Scholar search engine, resulting in a compilation of 61 studies of 20 grass species[14,55–114]. From these studies, we extracted the key steps in leaf and vein development that were general across species into a synthetic model. Then, given the spatial and temporal constraints arising from development according to this model, we derived expectations for the scaling across species of vein traits with mature leaf size. For instance, the VLA of first-order veins declines

geometrically with final leaf width (1° VLA = 1/leaf width) as veins are separated by greater numbers of cell divisions and/or by larger cells. By contrast, the VLA of second-order veins declines less steeply than geometrically with final leaf width, as wider leaves may form greater numbers of second-order veins (though these will be spaced further apart by subsequent leaf expansion); Box 1 and Supplementary Table 6 provide additional derivations.

Further, as a null hypothesis against which to test developmentally based scaling predictions, we derived expectations for the relationships of vein traits to leaf dimensions on the basis of geometric scaling[5,13]. Geometric scaling represents the relationships expected among the dimensions of an object given increases in size, while maintaining constant proportions and composition. Thus, dimensions such as length (L), area (A) and volume (V) would be inter-related as $A \propto L^2$ and $V \propto L^3$. Predictions can then be derived for any other traits on the basis of their dimensions. For instance, given geometric scaling, VLA would be expected to scale with leaf width as $\text{VLA} \propto LW^{-1}$, because VLA (as a linear dimension divided by an area (that is, L/A)) would be related to $L/L^2 = L^{-1}$, whereas LW would scale directly with L. In total, we compared 111 predictions derived from the developmental model to respective predictions from geometric scaling. These 111 predictions included the scaling relationships of five vein diameters (that is, for each of five vein orders) versus three leaf dimensions (that is, leaf length, width and area), amounting to 15 predictions, plus the scaling relationships for VLA, VSA, VPA and VVA for each of the five vein orders, for the major veins, minor veins, and the total vein systems, versus the three leaf dimensions (amounting to $4 \times 8 \times 3 = 96$ predictions). The developmental model predictions for relationships generally differed strongly from those of geometric scaling (that is, 75% of predictions differed), although—for a few relationships, such as that of the VLA of first-order veins with final leaf size—the expectations from developmental scaling and geometric scaling were the same. Overall, developmental scaling predicted that 51 vein traits would scale with leaf size and 60 traits would be independent of leaf dimensions, whereas geometric scaling predicted 63 and 48, respectively (Supplementary Tables 6, 10).

Plant material

To test vein scaling relationships, we grew grasses of 27 diverse species in a common garden to reduce the environmentally induced plasticity that would occur in wild plants in their native ranges (Extended Data Fig. 2, Supplementary Table 3). Although experimental species were selected to encompass large phylogenetic and functional variation (including 11 C_3 species and 16 C_4 species that represented 11 independent C_4 origins), the species necessarily included a only subset of the phylogenetic distribution of the 1,752 species in the database analyses of global trait–climate relationships. Seeds were acquired from seed banks and commercial sources (Supplementary Table 3). Before germination, seeds were surface-sterilized with 10% NaClO and 0.1% Triton X-100 detergent, rinsed three times with sterile water and finally sown on plates of 0.8% agar sealed with Micropore surgical tape (3M). Seeds were germinated in chambers maintained at 26 °C, under moderate-intensity cool white fluorescent lighting with a 12-h photoperiod. When roots were 2–3 cm long, seedlings were transplanted to 3.6-l pots with potting soil (1:1:1.5:1.5:3 of coarse vermiculite:perlite:washed plaster sand:sandy loam:peat moss).

Plants were grown at the UCLA Plant Growth Center (minimum, mean and maximum daily values for temperature, 20.1, 23.4 and 34.0 °C; for relative humidity, 28, 50 and 65%; and mean and maximum photosynthetically active radiation during daylight period, 107 and 1,988 μmol photons m^{-2} s^{-1} (HOBO Micro Station with Smart Sensors, Onset)), arranged in 6 randomized blocks spread over 3 benches, with 1 individual per species per block and 2 blocks per bench ($n = 6$, except $n = 4$ for *Alloteropsis semialata*). Plants were irrigated daily with water containing fertilizer (200–250 ppm of 20:20:20 N:P:K, Scotts Peters Professional water soluble fertilizer, Everris International B.V.). All species were grown until flowering to confirm the identities of the species.

14

Sample anatomical preparation

Leaves were collected when plants had numerous mature leaves, after 2.5–7 months of growth, depending on species (given variation in growth rates). Leaves from each of 6 individuals per species were fixed and stored in FAA solution (37% formaldehyde–glacial acidic acid, 95% ethanol in deionized water). Transverse sections were made for one leaf from each of three individuals. Rectangular samples were cut from the centre of leaves halfway along the length of the blade and gradually infiltrated under vacuum with low viscosity acrylic resin for one week (L. R. White; London Resin), and set in resin in gelatin capsules to dry at 55 °C overnight. Transverse cross-sections of 1 μm in thickness were prepared using glass knives (LKB 7800 KnifeMaker, LKB Produkter) in a rotary microtome (Leica Ultracut E, Reichert-Jung), placed on slides, and stained with 0.01% toluidine blue in 1% sodium borate (w/v). Slides were imaged with a light microscope using 5×, 20× and 40× objectives (Leica Lietz DMRB; Leica Microsystems) and a camera with imaging software (SPOT Imaging Solution, Diagnostic Instruments). Additionally, one leaf from each of three individuals was used to prepare chemically cleared leaf sections to visualize veins. Square sections of 1 cm × 1 cm were cut from the centre of the leaf at the widest point, cleared with 5% NaOH in ethanol, stained with safranin and counterstained with fast-green[115]. Sections were mounted with water in transparency film (CG5000; 3M Visual Systems Division) and scanned (flatbed scanner; Canon Scan Lide 90; 1,200 dots per inch), and further imaged with a light microscope using 5× and 10× objectives.

Quantification of leaf dimensions and vein traits

The leaf dimensions tested were leaf width, leaf length and leaf area, with leaf width and leaf length measured at the widest and longest regions of the leaf, respectively. Leaf area was calculated as leaf length × leaf width[116–118]. Estimates of leaf area from length and width can be improved by multiplying by a constant correction factor, which has been proposed as 0.7–0.9 for grasses[116–118]; however, as there is no standard value we did not apply such a correction factor. Applying a constant correction factor would have no influence on correlations or regression fits or their statistical significance for trait–climate relationships. Further, applying a constant correction factor would not influence the tests of scaling of vein traits with leaf area, which focused on power-law scaling exponents; multiplying estimates of leaf area by a constant would result only in a change to the power-law scaling intercept, and not the exponent. Thus, applying a correction factor to leaf area or not would have no influence on any of the findings of our study.

We measured and analysed cross-sections of one leaf for each of three individuals per species, to quantify the diameters and numbers of veins in the transverse plane for all vein orders (excluding fifth-order veins, which generally were not visible in transverse sections and for which we used the chemically cleared and stained leaf sections). Vein orders were established for each species on the basis of vein size, presence or absence of enlarged metaxylem and presence or absence of fibrous tissue above or below the vein[119,120]. The first-order vein (midvein) was the large central vein containing the largest metaxylem and fibrous tissue, and the second-order veins were the 'large' veins that were substantially smaller than the midvein and of similar structure. We identified the minor veins as the smaller veins (that is, the third-order 'intermediate' and fourth-order 'small' veins, and perpendicular fifth-order transverse veins)[120]. Notably, fourth-order veins occur only in NADP-ME C_4 grasses of the subfamily Panicoideae (7 out of the 16 of the C_4 species we grew)[15], and can be distinguished on the basis of their smaller overall size than third-order veins and their absence of sclerenchyma strands. For the species *Lasiacis sorghoidea*, second-order veins were too few to be counted in our prepared transverse sections, and we established vein orders and quantified associated traits using the chemically cleared and stained leaves.

For each vein order, VLA was quantified as the vein number per leaf width (per cm or per mm), which is equivalent to VLA (same units), assuming an approximately rectangular leaf. Cross-sectional vein diameters (VD) were measured excluding the bundle and mestome sheath cell layers, and averaging horizontal and vertical axes. Cross-sectional diameters were measured for all xylem conduits in each vein order by considering the lumen cross-sections as ellipses and averaging the major and minor axes. We categorized two metaxylem types within major veins on the basis of their highly distinct sizes (that is, large and small metaxylem), and one metaxylem type for minor veins (that is, small metaxylem). We focused on the large metaxylem conduits within major veins in calculating average conduit diameter values, as these would contribute the bulk of maximum flow[121,122]. For *L. sorghoidea*, as second-order veins were too few to be counted from our prepared transverse sections, we could not quantify the conduits within these veins and thus analyses of second-order vein conduit dimensions excluded this species.

For all vein orders, we estimated VSA, VPA and VVA as VSA = VLA × π × VD; VPA = VLA × VD; and VVA = VLA × π × (VD/2)^2.

Determining vein allometries and testing against predictions from developmental and geometric scaling

We determined trait scaling relationships by fitting lines to log-transformed data. The relationship of each vein trait (y) to a given leaf dimension (x) was considered as an allometric power law: $y = ax^b$, $\log(y) = \log(a) + b\log(x)$, in which b is the scaling exponent.

We tested these relationships against the predictions from developmentally based scaling derived from the synthetic leaf developmental model (as described in 'Construction of a synthetic model for grass leaf development, and derivation of allometric predictions based on developmental and geometric scaling' (Table 1, Box 1, Supplementary Table 6). A scaling relationship was considered to be consistent with a prediction if its 95% confidence intervals included the predicted slope. We tested whether a greater proportion of predictions were explained by developmental scaling than by geometric scaling using a proportion test (Minitab 16).

Testing assumptions for the linkages of photosynthetic rate with climate and vein traits

For the grass species grown experimentally, light-saturated rates of photosynthesis were measured for plants in moist soil, enabling a test of the assumptions that C_3 grass species from arid or cold environments have high photosynthetic rates, and that photosynthetic rate would be related to VLA and VSA. Light-saturated rates of photosynthesis were measured from 17 February 2010 to 28 June 2010, between 09:00 h and 15:00 h, on a mature leaf on each plant for 6 plants per species. Measurements were taken of steady-state net light-saturated photosynthetic rate per leaf area (<2% change over six minutes) using a LI-6400 XT portable photosynthesis system (LI-COR). Conditions within the leaf chamber were set to 25 °C, with reference CO_2 400 ppm, photosynthetic photon flux density 2,000 μmol m^{-2} s^{-1}, and relative humidity 60–80%, resulting in vapour pressure deficits of 0.80–1.6 kPa. Measurements were made on 1 or 2 leaves from each of 4–6 plants (except *L. sorghoidea* for which 3 leaves from each of 2 plants were used).

In addition, we tested for stronger general support of the relationships of photosynthetic rate with climate variables by combining our data for 8 C_3 terrestrial species with data for 13 Northern Hemisphere temperate terrestrial C_3 grass species from the Global Plant Trait Network (GLO-PNET) database[123], for which photosynthesis, latitude and longitude data for their field site were available (Supplementary Table 12). We extracted the climate variables MAT, MAP and monthly temperature and precipitation to calculate growing season length (methods of calculation are described in 'Testing for the linkage of leaf size and vein traits with climate across grass species worldwide'), on the basis of the latitude and longitude from which each species was measured.

15

Article

Phylogenetic reconstruction

A phylogenetic hypothesis for the 27 experimentally grown species considered in this study was inferred from three markers from the chloroplast genome (*rbcL*, *ndhF* and *trnK matK*), available for the exact same accessions in published datasets[124,125]. Each marker was aligned individually using MUSCLE[126], and the alignments were manually refined. The total dataset was 6,179-bp long. The program BEAST[127] was used to obtain a time-calibrated phylogeny under a relaxed clock model with uncorrelated evolutionary rates that follow a log-normal distribution. The substitution model was set to a general time reversible model with a gamma-shape parameter and a proportion of invariants. The root of the tree (split of BOP and PACMAD clades) was forced to follow a normal distribution with a mean of 51.2 million years ago (Ma) and a standard deviation of 0.0001 Ma, on the basis of previous estimates[128]. The addition of phytolith fossils would alter the absolute ages estimated by molecular dating[129], but the relative ages would remain unchanged and the comparative analyses consequently would be unaffected. Two parallel analyses were run for 10,000,000 generations, sampling a tree every 1,000 generations. Median ages across the 18,000 trees samples of a burn-in period of 1,000,000 generations were mapped on the maximum credibility tree. The burn-in period was largely sufficient for the analysis to reach stability, as verified with the program Tracer (http://beast.community/tracer).

Using the R Language and Environment version 3.4.1[130] with the ape R package[131] a phylogenetic hypothesis for 1,752 of the Grassbase species was extracted from a published phylogeny available through Dryad[132]. The source phylogeny assessed relationships among 3,595 species using a set of 14 subtrees using various genetic datasets in combination with three core plastid markers *rbcL*, *ndhF* and *matK*, with dating based on macrofossil evidence[9].

Testing trait–climate associations

To test trait–climate associations, we quantified the strength of correlations using Pearson's *r* rather than fitting specific predictive regression equations with R^2 values. For trait–climate associations, we calculated both ahistorical correlations and relationships accounting for phylogenetic relatedness (phylogenetic generalized least squares (PGLS) or PRMA, as described in 'Comparative analyses'). Although the phylogenetic analyses more robustly test our evolutionary hypotheses, the ahistorical Pearson's *r* values better resolve the strengths of existing relationships across species—especially when trends arise from variation among groups that split in evolution deep in the phylogeny[133]. In both types of analysis, the *r* values provide a conservative estimate of trait–climate relationships. As in previous biogeographical trait–climate analyses[134,135], we related the average trait values of a species from a database or experimental measurements to modelled native climates on the basis of natural occurrences; relationships would be stronger if traits and climate were matched for individual plants[136]. Additionally, the modelled native climates do not account for variation in temperature, irradiance and water availability (owing to microclimates associated with topography and canopy cover, or soil characteristics) to which species would be adapted in the field; accounting for this variation would probably improve the strength of trait–climate relationships[136]. Overall, global associations of traits with climate that are supported by substantial, statistically significant ahistorical *r* values indicate robust, biologically important relationships, and significant phylogenetic correlations additionally indicate support for the evolutionary hypotheses[137,138].

We implemented several further analyses to resolve the associations of traits with climate in the worldwide grass trait database. We conducted phylogenetic multiple regression to test for significant interactive effects of temperature and precipitation on leaf traits. Models including MAT and MAP (or growing season temperature and growing season precipitation) alone or in combination, and including an interaction, were compared using the Akaike information criterion[139]. Before phylogenetic multiple regression analyses, MAP values were divided by 50 to achieve a similar scale of values as those for MAT, and growing season precipitation values were divided by 100 to achieve a similar scale of values as for growing season temperature. Plant traits, MAP and MAT were then log-transformed, and MAT and MAP (and growing season temperature and growing season precipitation) were centred by subtracting the mean to render coefficients of main effects and interaction terms biologically interpretable[140].

The parametric correlation and regression statistics calculated in this study are subject to assumptions (that is, the independence of observations, and the normal distribution and homoscedasticity of residuals)[141]. Evolutionary nonindependence among species was adjusted for using phylogenetic statistics[133]. To check that the assumptions of normality and heteroscedasticity did not influence statistical significance of univariate analyses, we checked for significance of Spearman's rank correlations, which are not subject to these assumptions, and confirmed as significant ($P < 0.05$) the relationships presented in the Article. For the multiple regression of leaf area versus MAT and MAP in the 1,752-species global database, the 29 species with MAT <0 °C resulted in a left-skew of log-transformed MAT and a notable heteroscedasticity of residuals (Supplementary Fig. 1). To confirm that this skew did not influence the findings of the multiple regressions, we repeated the analysis excluding the 29 species, which alleviated the skew and heteroscedasticity (Supplementary Fig. 2); the key finding of the multiple regression analysis (that is, the interactive effect of MAT and MAP) was unaffected (Supplementary Table 8). Notably, the multiple regression analysis of leaf area versus growing season temperature and growing season precipitation also confirmed the trend, with greater normality and homoscedasticity of residuals, both when including all 1,752 species and when excluding the 29 species with MAT <0 °C (Supplementary Tables 7, 8, Supplementary Figs. 3, 4).

We conducted hierarchical partitioning analyses on log-transformed data to resolve the independent statistical associations of leaf size with individual climate variables[142]. Finally, we distinguished whether trait–climate correlations can be partially explained owing to 'triangular relationships' (that is, when data are missing in one or more corners of the plot, an analysis that can provide special insights)[143,144]. For example, a positive trait–climate correlation would arise at least in part from a triangular relationship if high trait values are few or absent at lower values of the climate variable, or if low trait values are few or absent at high values of the climate variable. To test for the presence of triangular relationships, we implemented quantile regression analyses, determining regression slopes fitted through the 5%, 50% and 95% quantiles of log-transformed data[145–147]. A triangular relationship was supported when the regressions through the 95% and 5% quantiles differed according to *t*-tests.

Comparative analyses

Comparative phylogenetic statistical analyses accounting for the effects of phylogenetic covariance on trait–climate and trait–trait relationships were conducted using the R Language and Environment version 3.4.1[130].

Regression coefficients were estimated using PGLS and/or PRMA, in each case basing the phylogenetic correction on Pagel's λ[148,149] estimated by maximum likelihood[150]. For PGLS, corPagel[151] was used in combination with gls[150] and optimized[131] to establish maximum likelihood estimates of λ in the 0–1 range; for PRMA, phyl.RMA[151] was used. Confidence intervals for *b* estimated using PRMA were determined following previous work[152]:

$$\pm \hat{b}(\sqrt{B+1} \pm \sqrt{B}), \text{ in which } B = \frac{1-r^2}{N-2}f_{1-\alpha,1,n-2}$$

in which $\hat{b}$ is the fitted value for *b*; *r* is a correlation coefficient, for which we used a phylogenetically corrected estimate based on the

16

variance–covariance matrix output by phyl.RMA; n is the number of pairs of observations; and $f_{1-\alpha,n-2}$ is the critical value from the f distribution.

Differences in species-level trait means between C_3 and C_4 species were tested using a phylogenetically corrected analysis of variance (ANOVA), both parametric (based on PGLS) and nonparametric[153] using the phyloANOVA R package[151].

The effect of phylogenetic corrections was evaluated by comparing PGLS or PRMA with Pagel's λ estimated by maximum likelihood, to equivalent models in which Pagel's λ was set to 0. When using Pagel's λ, to assess normality and homoscedasticity assumptions we first extracted phylogenetic residuals. For PGLS, the function 'residuals' was used to extract normalized residuals; for PRMA, a custom code derived from an original provided by R. P. Freckleton was used to produce an equivalent transformation of raw residuals obtained from phyl.RMA. Normality was tested using Anderson Darling tests[154] and heteroscedasticity using Bartlett's test[130]. Additionally, PGLS was used to estimate Pagel's λ for phylogenetic residuals, which should be 0.

The PGLS and PRMA approaches used to test for scaling relationships of vein traits with leaf dimensions and to estimate the slopes of linearized power law relationships are phylogenetic approaches equivalent to ordinary least squares and reduced major axis regressions, respectively. The decision of which of the two to use depended on the specific relationship tested. The least squares approach is preferable in cases when a dependent Y variable is related to an independent X variable, specifically when (1) there is much less error (that is, natural variation and/or measurement error) in X than Y and/or when (2) conceptually, Y is causally determined by or to be predicted from X, but never X from Y[155,156]. By contrast, the reduced major axis approach is preferable in cases in which (1) X and Y have similar error and/or in which (2) X or Y are codetermined, or their relationship arises from an underlying functional coordination or either could reasonably be predicted using the other; this approach is typically used in studies of allometric scaling relationships among functional traits or organ dimensions[155,156]. An exception to the use of reduced major axis for allometry is when testing whether the allometric slope of a relationship is consistent with an expected slope that was derived algebraically from other equations, as only least-squares slopes are robust to algebraic manipulation[156]. For example, PGLS would be selected over PRMA to test an expectation for the scaling slope of VSA with leaf length that was derived algebraically by multiplying the expected scaling slopes of VLA and VD with leaf length, given that VSA is determined from VLA and VD (as described in 'Quantification of leaf dimensions and vein traits'). Further, although the least squares approach is appropriate for testing relationships of a dependent versus an independent trait, the reduced major axis approach can be preferable for illustrating the relationship in a plot, as it captures more closely the central trend among two variables with high and/or similar error[155,156].

Thus, we selected PGLS or PRMA for the tested relationships according to which was most appropriate given the above principles; the application of any single approach globally would not affect the findings of the study, but would reduce the accuracy of the specific slope estimates. We used PRMA to test relationships of traits with climate variables, as the magnitude of variation in modelled climate variables globally was similar to that for species means for leaf traits. We also used PRMA for testing scaling relationships of vein diameters with leaf length and width, and of xylem conduit diameters with vein diameters, given the preference of this approach for testing allometric relationships, and the similar error in the X and Y variables. We used PGLS for testing relationships of VLA, VSA, VPA and VVA with leaf dimensions, given the higher variability in the vein traits than leaf dimensions arising owing to their determination from one or more vein traits as well as leaf dimensions (for example, VLA = vein number/leaf width). Further, PGLS was most appropriate for testing allometric slopes for the relationships of vein traits to leaf area, because the expectations for these slopes from the developmental model were derived algebraically from expected slopes of vein traits in relation to leaf length and leaf width[155]. Finally, we used PRMA in all figure plots to most clearly illustrate the central trends accounting for phylogeny[155,156].

Finally, we evaluated whether the scaling of vein traits with leaf dimensions differed between C_3 and C_4 species. C_3 and C_4 species were considered to differ significantly in trait–trait or trait–climate associations if significant relationships were found independently for both groups, and if there was no overlap in scaling slope 95% confidence intervals using the selected regression approach (PGLS or PRMA).

Modelling the effects of leaf energy budget and testing hypotheses for the benefits of smaller leaves under different climates

We considered three hypotheses for the advantage of small leaf sizes in cold or dry climates on the basis of their thinner boundary layer. Smaller leaves have been hypothesized to (1) experience less damage under extreme temperatures (that is, chilling on colds nights and overheating on hot days)[3,157,158], (2) maintain higher rates of photosynthesis and/or higher leaf water-use efficiency in cold and/or dry conditions[19,20] and (3) achieve higher gas exchange in favourable, warm and wet climates[4], which would provide an advantage in mitigating the shorter diurnal and/or seasonal growing periods of cold or dry climates.

To test hypothesis (1) (that is, that small grass leaves are typical in cold or dry climates because they avoid extreme temperatures), we calculated the minimum threshold of leaf size for chilling or overheating. We used the 100-cm^2 leaf size threshold for damage by night-time chilling and 30 cm^2 for damage by daytime overheating (that is, the lowest thresholds that were modelled for eudicotyledons globally, given in figure 3 of ref.[3]). These leaf size thresholds for eudicotyledons were derived from estimated damage thresholds based on the 'characteristic dimension' of the leaf (d) (that is, the diameter of the largest circle that can be delimited within a leaf) of 8.16 cm and 4.47 cm, according to equation (4) in the supplementary information of ref.[3] ($LA = 1.5 d^2$). Thus, we used these threshold values to exclude species with leaf width >8.16 cm and >4.47 cm, and then tested whether the observed trends of leaf dimensions with MAT and MAP globally remained. Significant trends for this restricted species set would indicate that thresholds for leaf damage under extreme temperatures cannot explain trends for grasses with leaves smaller than those thresholds. By testing trends against these very low thresholds, we provided a very conservative test to establish that avoidance of extreme temperatures would not explain the global climatic distribution of grass leaf size.

To test hypotheses (2) and (3), we used heuristic leaf energy balance modelling to simulate the consequences for gas exchange of leaf sizes varying in size[159]. Using the Tealeaves R package[159], given inputs of leaf width, wind speed, stomatal conductance and air temperature, we simulated boundary layer conductance, leaf temperature and transpiration rate. To represent the bulk of the global range of grass leaf size, we focused on comparing the global 5th and 95th quantiles of leaf width (0.1 cm and 2.7 cm). We simulated leaves in wet and dry conditions by setting stomatal conductance values at 0.4 mol m^{-2} s^{-1} and 0.2 mol m^{-2} s^{-1}, respectively[160]; our tests showed that selecting other values would yield similar qualitative results. To represent warm and cold climates we simulated gas exchange under air temperatures of 315 K and 280 K (41.85 °C and 6.85 °C, respectively)[161]. All other physical and environmental inputs were maintained constant at typical values[159]. We used the output values of leaf temperature and boundary layer conductance to simulate C_3 photosynthetic rate for leaves of different widths using the Farquhar model[162,163]. We tested these effects at the two wind speeds, 0.1 m s^{-1} and 2 m s^{-1}. Finally, we tested simulations for both amphistomatous and hypostomatous leaves, and we present results for amphistomatous leaves given that most grasses are amphistomatous[164]. To test for the potential benefit of smaller leaves, we calculated the ratios of photosynthetic rate, transpiration and leaf water-use efficiency for

Article

a small relative to large leaf; values >1 indicate an advantage for the small leaf in cold or dry conditions. To test for the potential benefit of smaller leaves in mitigating a shorter period with favourable climate, we calculated the ratios of photosynthetic rate, transpiration and leaf water-use efficiency under warm and wet conditions for a small versus a large leaf; again, values >1 reflect a small leaf advantage.

Reporting summary

Further information on research design is available in the Nature Research Reporting Summary linked to this paper.

Data availability

All data are available in the Article and its Supplementary Information. Leaf trait data for the 1,752 grass species was provided by the published Kew Grassbase Database (http://www.kew.org/data/grassbase/). Climate data for species were extracted from WorldClim 2 5-arc minute resolution (https://www.worldclim.org/) and from CRU TS4.01 01 (https://crudata.uea.ac.uk/cru/data/hrg/cru_ts_4.01/) on the basis of the geographical records for each species (http://www.gbif.org). Photosynthetic trait data and field locations were extracted for the 13 C_3 grass species for which this was available in GLOPNET (http://bio.mq.edu.au/~iwright/glopian.htm). Source data are provided with this paper.

Code availability

Custom-written R code is available on GitHub (https://github.com/smuel-tylor/grass-leaf-size-).

48. Kluyver, T. A. & Osborne, C. P. Taxonome: a software package for linking biological species data. *Ecol. Evol.* 3, 1262–1265 (2013).
49. Cayuela, L., Granzow-de la Cerda, I., Albuquerque, F. S. & Golicher, D. J. TAXONSTAND: an R package for species names standardisation in vegetation databases. *Methods Ecol. Evol.* 3, 1078–1083 (2012).
50. Fick, S. E. & Hijmans, R. J. WorldClim 2: new 1-km spatial resolution climate surfaces for global land areas. *Int. J. Climatol.* 37, 4302–4315 (2017).
51. Cherlet, M. H. C., Reynolds, J., Hill, J., Sommer, S. & von Maltitz, G. *World Atlas of Desertification* 3rd edn (Publication Office of the European Union, 2018).
52. Harris, I., Jones, P. D., Osborn, T. J. & Lister, D. H. Updated high-resolution grids of monthly climatic observations – the CRU TS3.10 dataset. *Int. J. Climatol.* 34, 623–642 (2014).
53. Lasky, J. R. et al. Characterizing genomic variation of *Arabidopsis thaliana*: the roles of geography and climate. *Mol. Ecol.* 21, 5512–5529 (2012).
54. Sexton, J. P., McIntyre, P. J., Angert, A. L. & Rice, K. J. Evolution and ecology of species range limits. *Annu. Rev. Ecol. Evol. Syst.* 40, 415–436 (2009).
55. Dengler, N. G., Dengler, R. E. & Hattersley, P. W. Differing ontogenetic origins of PCR (Kranz) sheaths in leaf blades of C_4 grasses (Poaceae). *Am. J. Bot.* 72, 284–302 (1985).
56. Dengler, N. G., Woodvine, M. A., Donnelly, P. M. & Dengler, R. E. Formation of vascular pattern in developing leaves of the C_4 grass *Arundinella hirta*. *Int. J. Plant Sci.* 158, 1–12 (1997).
57. Ikenberry, G.-J. J. *Developmental Vegetative Morphology of Avena sativa*. PhD thesis, Iowa State Univ. (1959).
58. Kaufman, P. B. & Brock, T. G. in *Oat Science and Technology* (eds Marshall, H. G. & Sorrells, M. E.) 53–75 (American Society of Agronomy, 1992).
59. Hitch, P. A. & Sharman, B. C. Initiation of procambial strands in leaf primordia of *Dactylis glomerata* L as an example of a temperate herbage grass. *Ann. Bot.* 32, 153–164 (1968).
60. Davidson, J. L. & Milthorpe, F. L. Leaf growth in *Dactylis glomerata* following defoliation. *Ann. Bot.* 30, 173–184 (1966).
61. Volenec, J. J. & Nelson, C. J. Cell dynamics in leaf meristems of contrasting tall fescue genotypes. *Crop Sci.* 21, 381–385 (1981).
62. Macadam, J. W. & Nelson, C. J. Specific leaf weight in zones of cell division, elongation and maturation in tall fescue leaf blades. *Ann. Bot.* 59, 369–376 (1987).
63. MacAdam, J. W., Volenec, J. J. & Nelson, C. J. Effects of nitrogen on mesophyll cell division and epidermal cell elongation in tall fescue leaf blades. *Plant Physiol.* 89, 549–556 (1989).
64. Skinner, R. H. & Nelson, C. J. Elongation of the grass leaf and its relationship to the phyllochron. *Crop Sci.* 35, 4–10 (1995).
65. Skinner, R. H. & Nelson, C. J. Epidermal cell division and the coordination of leaf and tiller development. *Ann. Bot.* 74, 9–15 (1994).
66. Maurice, I., Gastal, F. & Durand, J. L. Generation of form and associated mass deposition during leaf development in grasses: a kinematic approach for non-steady growth. *Ann. Bot.* 80, 673–683 (1997).
67. Durand, J. L., Schaufele, R. & Gastal, F. Grass leaf elongation rate as a function of developmental stage and temperature: morphological analysis and modelling. *Ann. Bot.* 83, 577–588 (1999).
68. Martre, P., Durand, J. L. & Cochard, H. Changes in axial hydraulic conductivity along elongating leaf blades in relation to xylem maturation in tall fescue. *New Phytol.* 146, 235–247 (2000).
69. Martre, P. & Durand, J. L. Quantitative analysis of vasculature in the leaves of *Festuca arundinacea* (Poaceae): Implications for axial water transport. *Int. J. Plant Sci.* 162, 755–766 (2001).
70. Gallagher, J. N. Field studies of cereal leaf growth 1. Initiation and expansion in relation to temperature and ontogeny. *J. Exp. Bot.* 30, 625–636 (1979).
71. Gallagher, J. N. & Biscoe, P. V. Field studies of cereal leaf growth 3. Barley leaf extension in relation to temperature, orradiance, and water potential. *J. Exp. Bot.* 30, 645–655 (1979).
72. Dannenhoffer, J. M., Ebert, W. & Evert, R. F. Leaf vasculature in barley, *Hordeum vulgare* (Poaceae). *Am. J. Bot.* 77, 636–652 (1990).
73. Dannenhoffer, J. M. & Evert, R. F. Development of the vascular system in the leaf of barley (*Hordeum vulgare* L). *Int. J. Plant Sci.* 155, 143–157 (1994).
74. Trivett, C. L. & Evert, R. F. Ontogeny of the vascular bundles and contiguous tissues in the barley leaf blade. *Int. J. Plant Sci.* 159, 716–723 (1998).
75. Soper, K. & Mitchell, K. J. The developmental anatomy of perennial ryegrass (*Lolium perenne* L.). *N. Z. J. Sci. Technol.* 37, 484–504 (1956).
76. Schnyder, H., Nelson, C. J. & Coutts, J. H. Assessment of spatial distribution of growth in the elongation zone of grass leaf blades. *Plant Physiol.* 85, 290–293 (1987).
77. Arredondo, J. T. & Schnyder, H. Components of leaf elongation rate and their relationship to specific leaf area in contrasting grasses. *New Phytol.* 158, 305–314 (2003).
78. Kaufman, P. B. Development of the shoot of *Oryza sativa* L. – II. Leaf histogenesis. *Phytomorphology* 9, 277–311 (1959).
79. Yamazaki, K. Studies on the leaf formation in rice plants I. Observation on the successive development of the leaf. *Jpn. J. Crop. Sci.* 31, 371–379 (1963).
80. Chonan, N. K. H. & Matsuda, T. Morphology on vascular bundles of leaves in gramineous crops: I. Observations on vascular bundles of leaf blades, sheaths and internodes in rice plants. *Jpn. J. Crop. Sci.* 43, 425–432 (1974).
81. Hoshikawa, K. *The Growing Rice Plant: An Anatomical Monograph* (Nobunkyo, 1989).
82. Matsukura, C. et al. Transverse vein differentiation associated with gas space formation – fate of the middle cell layer in leaf sheath development of rice. *Ann. Bot.* 85, 19–27 (2000).
83. Itoh, J. et al. Rice plant development: from zygote to spikelet. *Plant Cell Physiol.* 46, 23–47 (2005).
84. Sakaguchi, J. & Fukuda, H. Cell differentiation in the longitudinal veins and formation of commissural veins in rice (*Oryza sativa*) and maize (*Zea mays*). *J. Plant Res.* 121, 593–602 (2008).
85. Parent, B., Conejero, G. & Tardieu, F. Spatial and temporal analysis of non-steady elongation of rice leaves. *Plant Cell Environ.* 32, 1561–1572 (2009).
86. Begg, J. E. & Wright, M. J. Growth and development of leaves from intercalary meristems in *Phalaris arundinacea* L. *Nature* 194, 1097–1098 (1962).
87. Colbert, J. T. & Evert, R. F. Leaf vasculature in sugarcane (*Saccharum officinarum* L.). *Planta* 156, 136–151 (1982).
88. Bernstein, N., Silk, W. K. & Lauchli, A. Growth and development of sorghum leaves under conditions of NaCl stress – spatial and temporal aspects of leaf growth inhibition. *Planta* 191, 433–439 (1993).
89. Sud, R. M. & Dengler, N. G. Cell lineage of vein formation in variegated leaves of the C_4 grass *Stenotaphrum secundatum*. *Ann. Bot.* 86, 99–112 (2000).
90. Sharman, B. C. & Hitch, P. A. Initiation of procambial strands in leaf primordia of bread wheat *Triticum aestivum* L. *Ann. Bot.* 31, 229–243 (1967).
91. Blackman, E. The morphology and development of cross veins in the leaves of bread wheat (*Triticum aestivum* L.). *Ann. Bot.* 35, 653–665 (1971).
92. Kemp, D. R. The location and size of the extension zone of emerging wheat leaves. *New Phytol.* 84, 729–737 (1980).
93. Paolillo, D. J. Protoxylem maturation in the seedling leaf of wheat. *Am. J. Bot.* 82, 337–345 (1995).
94. Beemster, G. T. S. & Masle, J. The role of apical development around the time of leaf initiation in determining leaf width at maturity in wheat seedlings (*Triticum aestivum* L.) with impeded roots. *J. Exp. Bot.* 47, 1679–1688 (1996).
95. Sharman, B. C. Developmental anatomy of the shoot of *Zea mays* L. *Ann. Bot.* 6, 245–282 (1942).
96. Esau, K. Ontogeny of the vascular bundle in *Zea mays*. *Hilgardia* 15, 325–368 (1943).
97. Bosabalidis, A. M., Evert, R. F. & Russin, W. A. Ontogeny of the vascular bundles and contiguous tissues in the maize leaf blade. *Am. J. Bot.* 81, 745–752 (1994).
98. Poethig, S. in *Contemporary Problems in Plant Anatomy* (eds Dickison R. A. & White, W. C.) 235–259 (Academic, 1984).
99. Russell, S. H. & Evert, R. F. Leaf vasculature in *Zea mays* L. *Planta* 164, 448–458 (1985).
100. Smith, L. G., Greene, B., Veit, B. & Hake, S. A dominant mutation in the maize homeobox gene, Knotted-1, causes its ectopic expression in leaf cells with altered fates. *Development* 116, 21–30 (1992).
101. Fournier, C. & Andrieu, B. A 3D architectural and process-based model of maize development. *Ann. Bot.* 81, 233–250 (1998).
102. Muller, B., Reymond, M. & Tardieu, F. The elongation rate at the base of a maize leaf shows an invariant pattern during both the steady-state elongation and the establishment of the elongation zone. *J. Exp. Bot.* 52, 1259–1268 (2001).
103. Muller, B. et al. Association of specific expansins with growth in maize leaves is maintained under environmental, genetic, and developmental sources of variation. *Plant Physiol.* 143, 278–290 (2007).
104. Johnston, R., Leiboff, S. & Scanlon, M. J. Ontogeny of the sheathing leaf base in maize (*Zea mays*). *New Phytol.* 205, 306–315 (2015).
105. Ben-Haj-Salah, H. & Tardieu, F. Temperature affects expansion rate of maize leaves without change in spatial distribution of cell length – analysis of the coordination between cell division and cell expansion. *Plant Physiol.* 109, 861–870 (1995).
106. Tardieu, F., Reymond, M., Hamard, P., Granier, C. & Muller, B. Spatial distributions of expansion rate, cell division rate and cell size in maize leaves: a synthesis of the effects of soil water status, evaporative demand and temperature. *J. Exp. Bot.* 51, 1505–1514 (2000).
107. Runions, A. et al. Modeling and visualization of leaf venation patterns. *ACM Trans. Graphic.* 24, 702–711 (2005).

108. Scarpella, E. & Meijer, A. H. Pattern formation in the vascular system of monocot and dicot plant species. *New Phytol.* 164, 209–242 (2004).

109. Baskin, T. I. Anisotropic expansion of the plant cell wall. *Annu. Rev. Cell. Dev.* 21, 203–222 (2005).

110. Fujita, H. & Mochizuki, A. The origin of the diversity of leaf venation pattern. *Dev. Dyn.* 235, 2710–2721 (2006).

111. Granier, C. & Tardieu, F. Multi-scale phenotyping of leaf expansion in response to environmental changes: the whole is more than the sum of parts. *Plant Cell Environ.* 32, 1175–1184 (2009).

112. Scarpella, E., Barkoulas, M. & Tsiantis, M. Control of leaf and vein development by auxin. *Cold Spring Harb. Perspect. Biol.* 2, a001511 (2010).

113. Gázquez, A. & Beemster, G. T. S. What determines organ size differences between species? A meta-analysis of the cellular basis. *New Phytol.* 215, 299–308 (2017).

114. Scarpella, E. The logic of plant vascular patterning. Polarity, continuity and plasticity in the formation of the veins and of their networks. *Curr. Opin. Genet. Dev.* 45, 34–43 (2017).

115. Berlyn, G. P. M. J. P. *Botanical Microtechnique and Cytochemistry* (Iowa State Univ. Press, 1976).

116. Kemp, C. D. Methods of estimating leaf area of grasses from linear measurements. *Ann. Bot.* 24, 491–499 (1960).

117. Stickler, F. C., Wearden, S. & Pauli, A. W. Leaf area determination in grain sorghum. *Agronomy* 53, 187–188 (1961).

118. Shi, P. et al. Leaf area-length allometry and its implications in leaf shape evolution. *Trees* 33, 1073–1085 (2019).

119. Ellis, R. P. A procedure for standardizing comparative leaf anatomy in the Poaceae. I. The leaf blade as viewed in transverse section. *Bothalia* 12, 65–109 (1976).

120. Evert, R. F. *Esau's Plant Anatomy: Meristems, Cells, and Tissues of the Plant Body: Their Structure, Function, and Development* (John Wiley, 2006).

121. Neufeld, H. S. et al. Genotypic variability in vulnerability of leaf xylem to cavitation in water-stressed and well-irrigated sugarcane. *Plant Physiol.* 100, 1020–1028 (1992).

122. Tyree, M. T., Zimmermann, M. H. & Zimmermann, M. H. *Xylem Structure and the Ascent of Sap* 2nd edn (Springer, 2002).

123. Wright, I. J. et al. The worldwide leaf economics spectrum. *Nature* 428, 821–827 (2004).

124. Grass Phylogeny Working Group II. New grass phylogeny resolves deep evolutionary relationships and discovers C_4 origins. *New Phytol.* 193, 304–312 (2012).

125. Taylor, S. H. et al. Photosynthetic pathway and ecological adaptation explain stomatal trait diversity amongst grasses. *New Phytol.* 193, 387–396 (2012).

126. Edgar, R. C. MUSCLE: multiple sequence alignment with high accuracy and high throughput. *Nucleic Acids Res.* 32, 1792–1797 (2004).

127. Drummond, A. J. & Rambaut, A. BEAST: Bayesian evolutionary analysis by sampling trees. *BMC Evol. Biol.* 7, 214 (2007).

128. Christin, P. A. et al. Molecular dating, evolutionary rates, and the age of the grasses. *Syst. Biol.* 63, 153–165 (2014).

129. Prasad, V. et al. Late Cretaceous origin of the rice tribe provides evidence for early diversification in Poaceae. *Nat. Commun.* 2, 480 (2011).

130. R Core Team. *R: A Language and Environment for Statistical Computing*, http://www.R-project.org/ (R Foundation for Statistical Computing, 2019).

131. Paradis, E. & Schliep, K. ape 5.0: an environment for modern phylogenetics and evolutionary analyses in R. *Bioinformatics* 35, 526–528 (2019).

132. Spriggs, E. L., Christin, P.-A. & Edwards, E. J. Data from: C_4 photosynthesis promoted species diversification during the Miocene grassland expansion, https://doi.org/10.5061/dryad.74b5d (2015).

133. Felsenstein, J. Phylogenies and the comparative method. *Am. Nat.* 125, 1–15 (1985).

134. Schmerler, S. B. et al. Evolution of leaf form correlates with tropical-temperate transitions in *Viburnum* (Adoxaceae). *Proc. R. Soc. B.* 279, 3905–3913 (2012).

135. Fletcher, L. R. et al. Evolution of leaf structure and drought tolerance in species of Californian Ceanothus. *Am. J. Bot.* 105, 1672–1687 (2018).

136. Bramer, I. et al. in *Next Generation Biomonitoring: Part 1 (Advances in Ecological Research, volume 58)* (eds. Bohan, D. A. et al.) 101–161 (Academic, 2018).

137. Zanne, A. E. et al. Three keys to the radiation of angiosperms into freezing environments. *Nature* 506, 89–92 (2014).

138. Watcharamongkol, T., Christin, P. A. & Osborne, C. P. C_4 photosynthesis evolved in warm climates but promoted migration to cooler ones. *Ecol. Lett.* 21, 376–383 (2018).

139. Burnham, K. P. & Anderson, D. R. *Model Selection and Multimodel Inference* 2nd edn (Springer, 2002).

140. Gelman, A. & Hill, J. *Data Analysis Using Regression and Multilevel/Hierarchical Models* (Cambridge Univ. Press, 2006).

141. Faraway, J. J. *Linear Models with R* (Chapman & Hall, 2009).

142. Murray, K. & Conner, M. M. Methods to quantify variable importance: implications for the analysis of noisy ecological data. *Ecology* 90, 348–355 (2009).

143. Westoby, M. & Wright, I. J. Land-plant ecology on the basis of functional traits. *Trends Ecol. Evol.* 21, 261–268 (2006).

144. Grubb, P. J. Trade-offs in interspecific comparisons in plant ecology and how plants overcome proposed constraints. *Plant Ecol. Divers.* 9, 3–33 (2016).

145. Cade, B. S. & Noon, B. R. A gentle introduction to quantile regression for ecologists. *Front. Ecol. Environ.* 1, 412–420 (2003).

146. Grubb, P. J., Coomes, D. A. & Metcalfe, D. J. Comment on "A brief history of seed size". *Science* 310, 783 (2005).

147. Moles, A. T. et al. Global patterns in plant height. *J. Ecol.* 97, 923–932 (2009).

148. Pagel, M. Inferring the historical patterns of biological evolution. *Nature* 401, 877–884 (1999).

149. Freckleton, R. P., Harvey, P. H. & Pagel, M. Phylogenetic analysis and comparative data: a test and review of evidence. *Am. Nat.* 160, 712–726 (2002).

150. Pinheiro, J. et al. nlme: linear and nonlinear mixed effect models. R package version 3.1-140, https://CRAN.R-project.org/package=nlme (2019).

151. Revell, L. J. phytools: an R package for phylogenetic comparative biology (and other things). *Methods Ecol. Evol.* 3, 217–223 (2012).

152. Warton, D. I., Wright, I. J., Falster, D. S. & Westoby, M. Bivariate line-fitting methods for allometry. *Biol. Rev. Camb. Philos. Soc.* 81, 259–291 (2006).

153. Garland, T., Dickerman, A. W., Janis, C. M. & Jones, J. A. Phylogenetic analysis of covariance by computer simulation. *Syst. Biol.* 42, 265–292 (1993).

154. Gross, J. & Ligges, U. nortest: tests for normality. R package version 1.0-4, https://cran.r-project.org/package=nortest (2015).

155. Poorter, H. & Sack, L. Pitfalls and possibilities in the analysis of biomass allocation patterns in plants. *Front. Plant Sci.* 3, 259 (2012).

156. Smith, R. J. Use and misuse of the reduced major axis for line-fitting. *Am. J. Phys. Anthropol.* 140, 476–486 (2009).

157. Gates, D. M. Energy, plants, and ecology. *Ecology* 46, 1–13 (1965).

158. Lusk, C. H. et al. Frost and leaf-size gradients in forests: global patterns and experimental evidence. *New Phytol.* 219, 565–573 (2018).

159. Muir, C. D. tealeaves: an R package for modelling leaf temperature using energy budgets. *AoB Plants* 11, plz054 (2019).

160. Taylor, S. H. et al. Ecophysiological traits in C_3 and C_4 grasses: a phylogenetically controlled screening experiment. *New Phytol.* 185, 780–791 (2010).

161. Huang, M. et al. Air temperature optima of vegetation productivity across global biomes. *Nat. Ecol. Evol.* 3, 772–779 (2019).

162. Farquhar, G. D., von Caemmerer, S. & Berry, J. A. A biochemical model of photosynthetic CO_2 assimilation in leaves of C_3 species. *Planta* 149, 78–90 (1980).

163. Bernacchi, C. J., Pimentel, C. & Long, S. P. In vivo temperature response functions of parameters required to model RuBP-limited photosynthesis. *Plant Cell Environ.* 26, 1419–1430 (2003).

164. Muir, C. D. Making pore choices: repeated regime shifts in stomatal ratio. *Proc. R. Soc. B.* 282, 1–9 (2012).

165. Brummitt, R. K. *World Geographical Scheme for Recording Plant Distributions* (Hunt Institute for Botanical Documentation, 2001).

a

Ch

Pa

Da

Mi
Aru

Ari

Or

Ba

Po

C₃
C₄

— 10 Ma

Subfamily key:
Ari = Aristidoideae, Aru = Arundinoideae, Mi = Micrairoideae,
Da = Danthonioideae, Ch = Chloridoideae, Pa = Panicoideae,
Or = Oryzoideae, Ba = Bambusoideae, Po = Pooideae

b

Alloteropsis semialata
Alloteropsis cimicina
Echinochloa crus-galli
Lasiacis sorghoidea
Oplismenus hirtellus
Sacciolepis africana
Cenchrus setaceus
Panicum virgatum
Digitaria eriantha
Digitaria ciliaris
Andropogon gerardii
Paspalum dilatatum
Chasmanthium latifolium
Phragmites australis
Eriachne aristidea
Danthonia decumbens
Danthonia californica
Eragrostis cilianensis
Chloris elata
Chloris gayana
Stipagrostis zeyheri
Aristida purpurea
Aristida ternipes
Ehrharta calycina
Oryza sativa
Triticum aestivum
Nassella viridula

50   40   30   20   10   0 Ma

c

d

Extended Data Fig. 1 | Time-calibrated phylogenetic trees for 1,752 worldwide grass species and for 27 grass species grown in a greenhouse common garden. a, Phylogeny for 1,752 species, trimmed from a previous publication[132], used for analyses of global scaling of leaf size with climate. C_3 and C_4 species are in black and red, respectively ($n = 840$ and $n = 912$, respectively). **b**, Phylogeny for 27 species used for analyses of leaf vein scaling (black branches, 11 C_3 grasses; red branches, 16 C_4 grasses), emphasizing the inclusion of 11 independent C_4 origins. **c**, **d**, Map of the distributions of the 11 C_3 species (**c**) and 16 C_4 species (**d**).
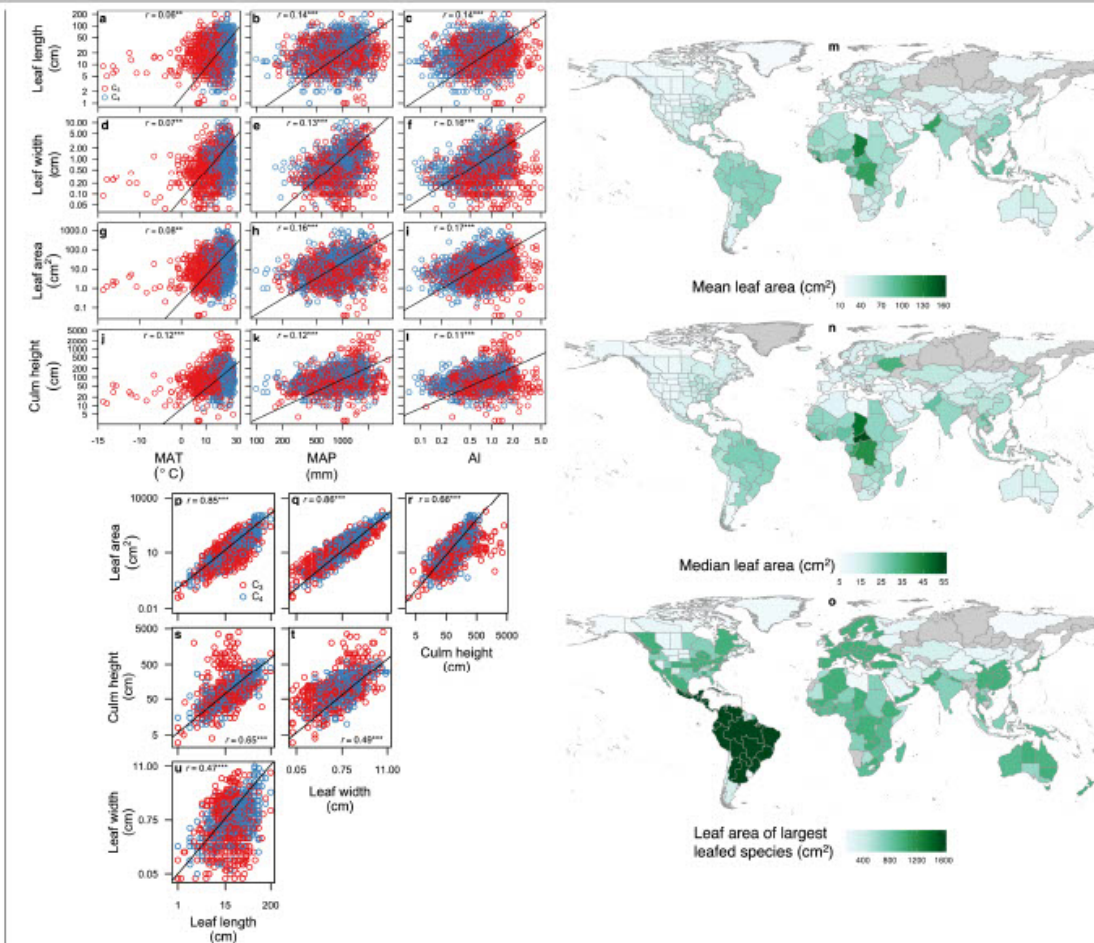
Extended Data Fig. 2 | Worldwide relationships of grass leaf and plant dimensions with the native climate of species, the global distribution of grass leaf size, and the scaling of grass leaf and plant dimensions. a–l, Relationship of leaf length (a–c), leaf width (d–f), leaf area (leaf width × leaf length) (g–i) and culm height (j–l) with MAT, MAP and the aridity index (AI). m–o, Average across species of leaf area for each country in the global database (International Working Group on Taxonomic Databases for Plant Sciences, TDWG level-3 spatial units[165]), including countries for which >20 species occur in the global database (21–547 species for each country; grey for countries with <20 species represented); that is, mean leaf area (m), median leaf area (n) and leaf area for the largest leafed species (o). p–u, The scaling of leaf area with leaf length (p) and leaf width (q), leaf area with culm height (r), culm height with leaf length (s) and leaf width (t), and leaf width with leaf length (u). Leaf trait and climate data are provided in Supplementary Table 2. $n = 1,752$ globally distributed grass species in a–i, p, q, u, and 1,729 in j–l, r–t. Corresponding regression coefficients for a historical analyses of relationships in a–l: 0.14, 0.17, 0.14, 0.26, 0.34, 0.28, 0.24, 0.31, 0.26, 0.24, 0.29 and 0.3. Two-tailed PRMA regressions were fitted for log(trait) = log(a) + b log(trait) in a–l, p–u. ***$P < 0.001$, **$P < 0.01$. $P = 0.0099$ (a), 7.8×10^{-9} (b), 4.2×10^{-9} (c), 0.004 (d), 1.8×10^{-6} (e), 2.4×10^{-11} (f), 0.0014 (g), 2.9×10^{-11} (h), 2.2×10^{-13} (i), 1.7×10^{-6} (j), 4.0×10^{-7} (k), 1.1×10^{-5} (l), about 0 (p), about 0 (q), 3.17×10^{-39} (r), 1.92×10^{-205} (s), 7.92×10^{-106} (t), 2.7×10^{-96} (u). C_3 and C_4 species are shown in red and blue, respectively.
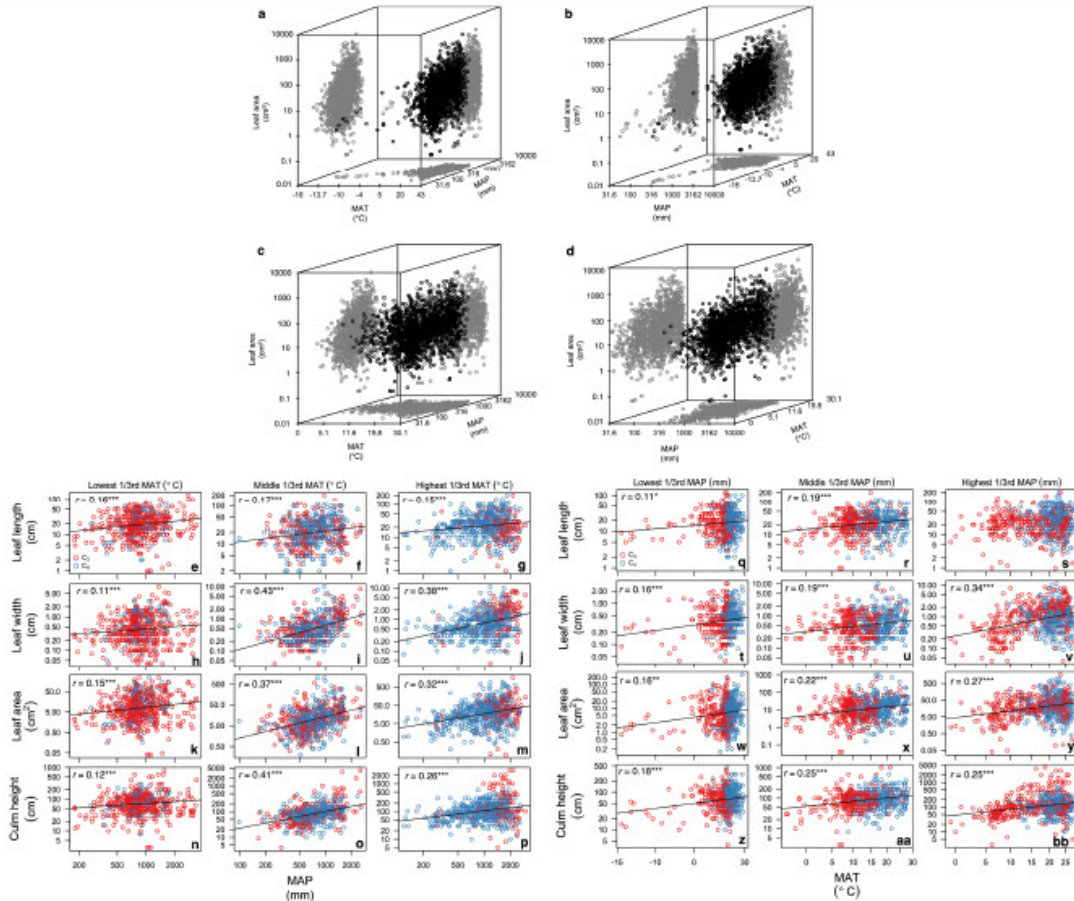
Extended Data Fig. 3 | Worldwide association of grass leaf size with the native climate of the species in 3D, and binned by 1/3rd lowest, middle and highest MAT or MAP in 2D. a–d, Leaf area versus climate variables (that is, *x* − MAT and *y* − MAP) (**a, c**); horizontal axes are flipped (that is, leaf area versus *x* − MAP and *y* − MAT) in **b, d. e–p**, Relationship of leaf length (**e–g**), leaf width (**h–j**), leaf area (**k–m**) and culm height (**n–p**) to MAP. *n* − 584 globally distributed grass species in **e–m**, and 576 in **n–p. q–z, aa, bb**, Relationships of leaf length (**q–s**), leaf width (**t–v**), leaf area (**w–y**) and culm height (**z, aa, bb**) with MAT. *n* − 584 globally distributed grass species in **e–m, q–y**, and 576 for **n–p, z, aa, bb**. In **a, b**, data for all species in the global database (*n* − 1,752) are presented; in

c, d, 29 species with MAT < 0 °C are excluded, for a clearer view of the bulk of the species. Projected grey shadows in **a–d** represent the bivariate relationships. Parameters from multiple regression analysis are presented in Supplementary Table 8. Two-tailed ordinary least square regressions were fitted for $\log(\text{trait}) - \log(a) + b \log(\text{climate variable})$ in **e–z, aa, bb**. ***$P < 0.001$, **$P < 0.01$. $P - 8.1 \times 10^{-5}$ (**e**), 2.2×10^{-5} (**f**), 0.0002 (**g**), 0.0094 (**h**), 8.4×10^{-20} (**i**), 1.7×10^{-18} (**j**), 0.0002 (**k**), 1.1×10^{-20} (**l**), 1.8×10^{-15} (**m**), 0.0028 (**n**), 4.7×10^{-22} (**o**), 2.2×10^{-10} (**p**), 0.0106 (**q**), 2.9×10^{-6} (**r**), 7.0×10^{-5} (**t**), 6.7×10^{-6} (**u**), 1.5×10^{-17} (**v**), 0.0001 (**w**), 7.9×10^{-8} (**x**), 2.6×10^{-11} (**y**), 1.3×10^{-5} (**z**), 1.7×10^{-9} (**aa**), 8.5×10^{-10} (**bb**). C_3 and C_4 species are shown in red and blue, respectively.
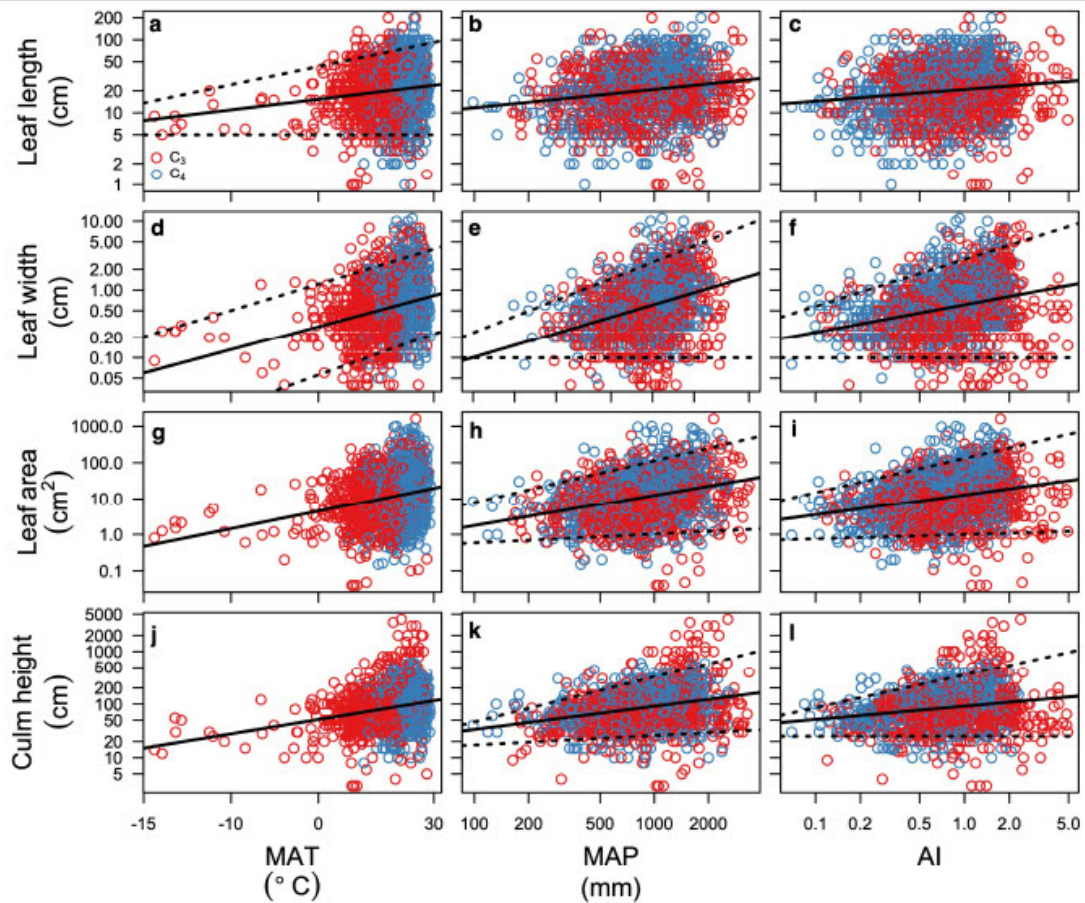
Extended Data Fig. 4 | Quantile regression analyses of worldwide associations of grass leaf traits with the native climate of species. a–l, Relationship of leaf length (a–c), leaf width (d–f), leaf area (g–i) and culm height (j–l) with MAT, MAP and the aridity index. n =1,752 globally distributed grass species in a–i, and 1,729 in j–l. Two-tailed ordinary least square (solid lines) and 95% and 5% quantile regressions (dotted lines) were fitted for $\log(\text{trait}) = \log(a) + b\log(\text{climate variable})$; quantile lines are drawn if significantly different in slope at $P < 0.05$. C_3 and C_4 species are in red and blue, respectively.

23
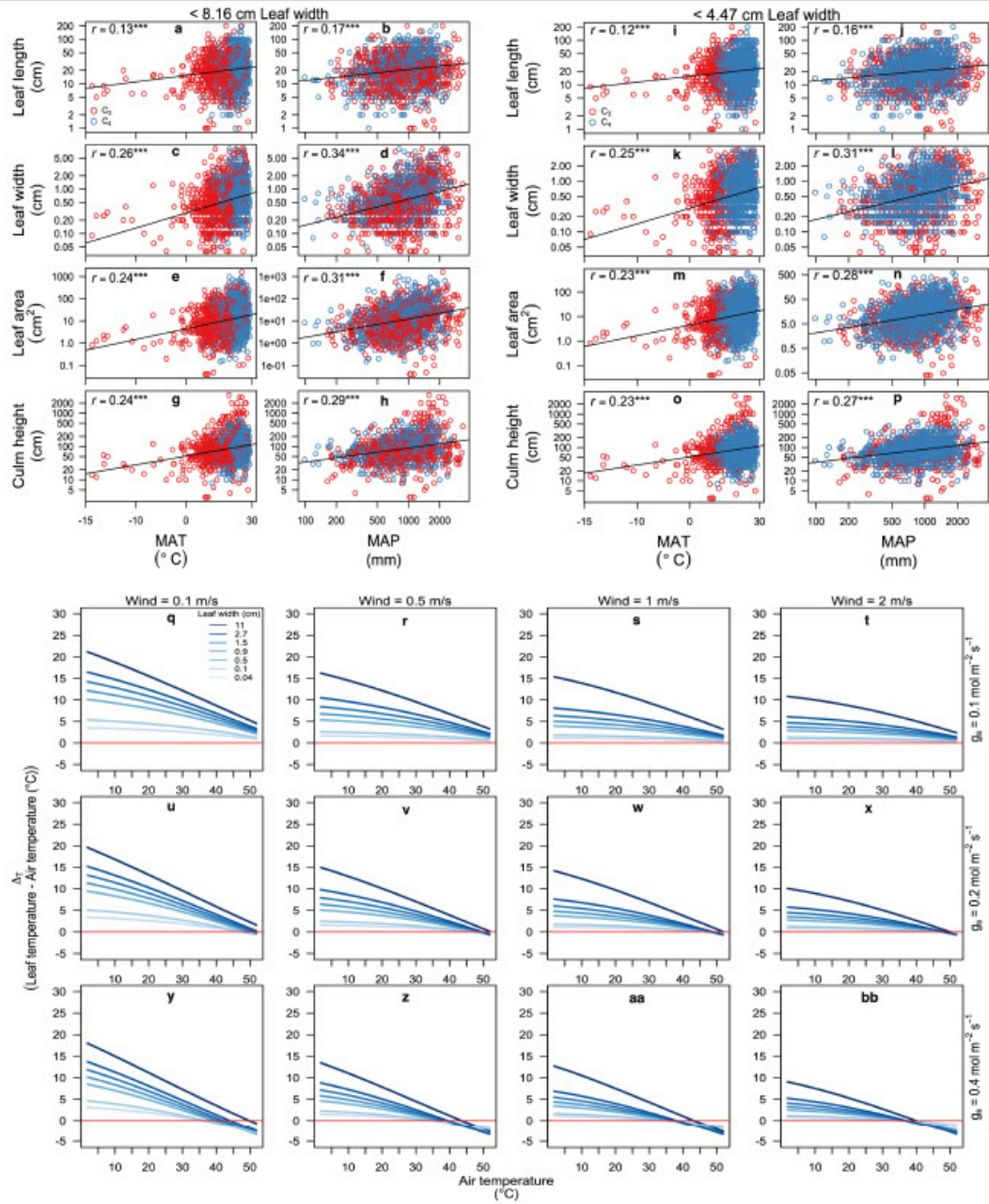
Extended Data Fig. 5 | See next page for caption.

Extended Data Fig. 5 | Worldwide associations of grass leaf and plant dimensions with the native climate of species for species with leaf width <8.16 cm or <4.47 cm (below the modelled threshold for damage owing to night-time chilling or overheating) and modelled leaf temperature difference from air temperature for amiphistomatous grass leaves under different air temperatures. a–h, Relationship of leaf length (a, b), leaf width (c, d), leaf area (e, f) and culm height (g, h) to MAT and MAP for species with leaf width <8.16 cm. i–p, Relationships of leaf length (i, j), leaf width (k, l), leaf area (m, n) and culm height (o, p) to MAT and MAP for species with leaf width <4.47 cm. $n = 1{,}748$ globally distributed grass species for a–f, 1,725 for g, h, 1,716 for i–n and 1,694 for o, p. q–z, aa, bb, Simulations were run with stomatal conductance (mol m^{-2} s^{-1}) 0.1 (q–t), 0.2 (u–x) and 0.4 (y, z, aa, bb), and wind speed (m s^{-1}), at 0.1 (q, u, y), 0.5 (r, v, z), 1 (s, w, aa) and 2 (t, x, bb), with leaf width (cm) of 0.04, 0.1, 0.5, 0.9, 1.5, 2.7 and 11 shown as increasing darker blue lines. No difference in leaf temperature from air temperature line in red. Two-tailed ordinary least square regressions were fitted for log(trait) = log(a) + b log(climate variable) in a–p. ***$P < 0.001$, **$P < 0.01$, *$P < 0.05$. $P = 2.1 \times 10^{-4}$ (a), 6.2×10^{-13} (b), 4.7×10^{-29} (c), 6.2×10^{-48} (d), 2.0×10^{-24} (e), 6.8×10^{-40} (f), 1.9×10^{-24} (g), 1.3×10^{-33} (h), 2.4×10^{-7} (i), 7.4×10^{-11} (j), 1.0×10^{-26} (k), 3.4×10^{-39} (l), 5.4×10^{-22} (m), 9.8×10^{-33} (n), 4.4×10^{-22} (o), 3.8×10^{-29} (p). C_3 and C_4 species are shown in red and blue, respectively.

25
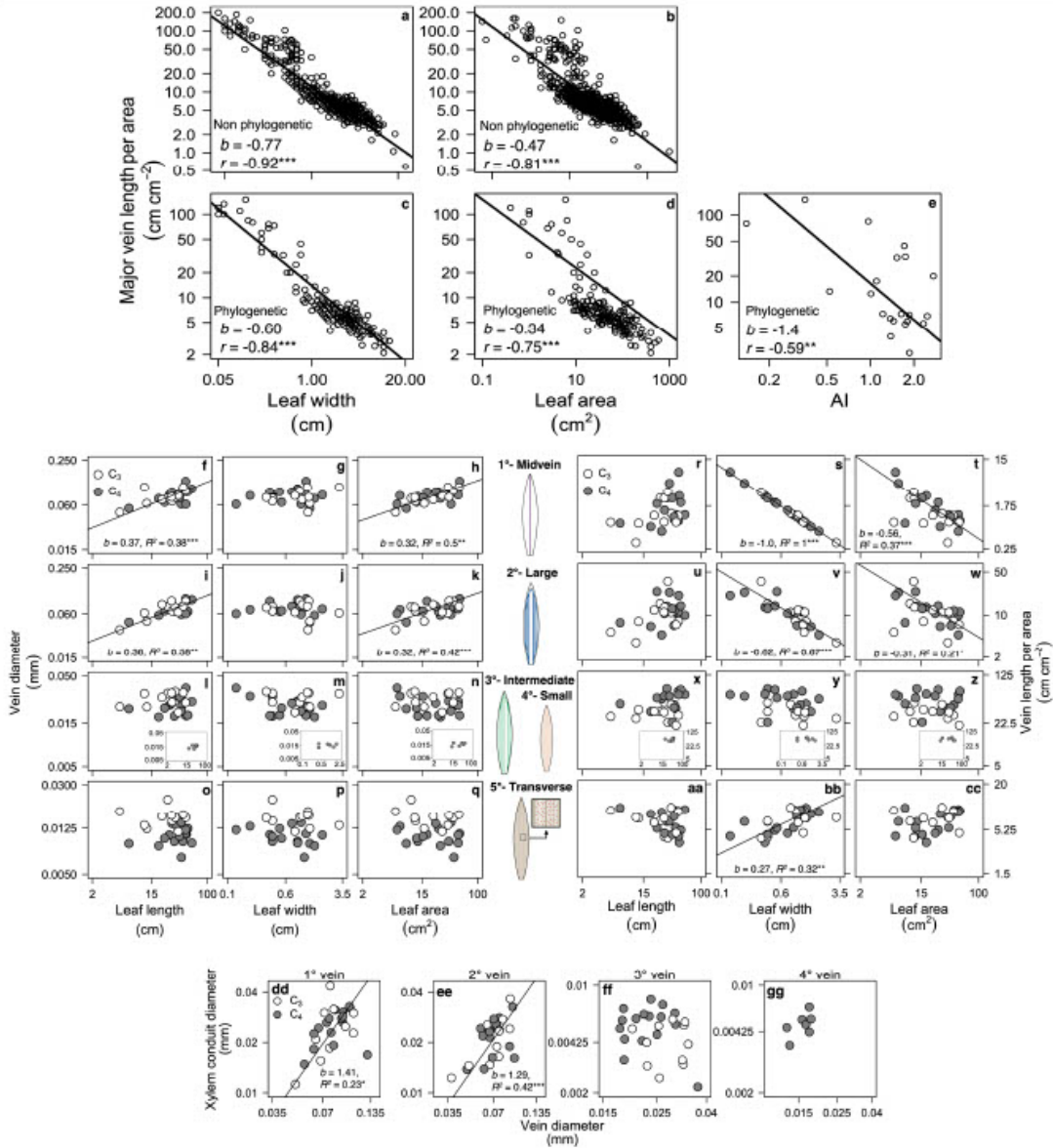
Extended Data Fig. 6 | Worldwide scaling of grass VLA and vein diameter with leaf size and aridity of the native climate of the species, and of vein xylem conduit diameter with vein diameter. a–d, Relationship of major VLA to leaf width (a, c), leaf area (b, d) and the aridity index (e) (in which lower values correspond to greater climatic aridity). f–q, Relationship of vein diameters to leaf length (f, i, l, o), leaf width (g, j, m, p) and leaf area (h, k, n, q). r–z, aa, bb, cc, Relationship of VLA to leaf length (r, u, x, aa), leaf width (s, v, y, bb) and leaf area (t, w, z, cc). dd, ee, ff, gg, Relationships of vein xylem conduit diameters with vein diameter of first-order veins (dd), second-order veins (ee), third-order veins (ff) and fourth-order veins (gg). n = 616 species in a, 600 in b, 170 in c, 166 in d, 21 in e, 27 in f–z, aa, bb, cc, dd, ee, ff and 7 in gg. Two-tailed ordinary least square regressions, PGLS or PRMA regressions were fitted for log(trait) = log(a) + b log(trait or climate variable) in a and b, c and d or e, respectively. PRMA or

PGLS regressions were fitted for log(vein diameter or VLA) = log(a) + b log(leaf length, width or leaf area) in f–q and r–z, aa, bb, cc, respectively. PRMA regressions were fitted for log(xylem conduit diameter) = log(a) + b log(vein diameter) in dd, ee, ff, gg. *$P < 0.05$, **$P < 0.01$, ***$P < 0.001$. $P = 9.4 \times 10^{-250}$ (a), 1.6×10^{-139} (b), 7.0×10^{-46} (c), 1.0×10^{-31} (d), 0.0051 (e), 0.0007 (f), 3.0×10^{-5} (h), 3.9×10^{-6} (i), 0.0003 (k), 1.2×10^{-34} (s), 7.0×10^{-4} (t), 1.4×10^{-7} (v), 0.0167 (w), 0.0020 (bb), 0.0110 (dd) and 0.0004 (ee). Line parameters for f–z, aa, bb, cc are given in Table 1, Supplementary Table 10; line parameters for dd, ee, ff, gg are given in Supplementary Table 11. Significant relationships are plotted with PRMA to illustrate the central trends (Methods). C$_3$ and C$_4$ species are shown in white and grey, respectively. The s.e. for species trait values are given in Supplementary Table 3.
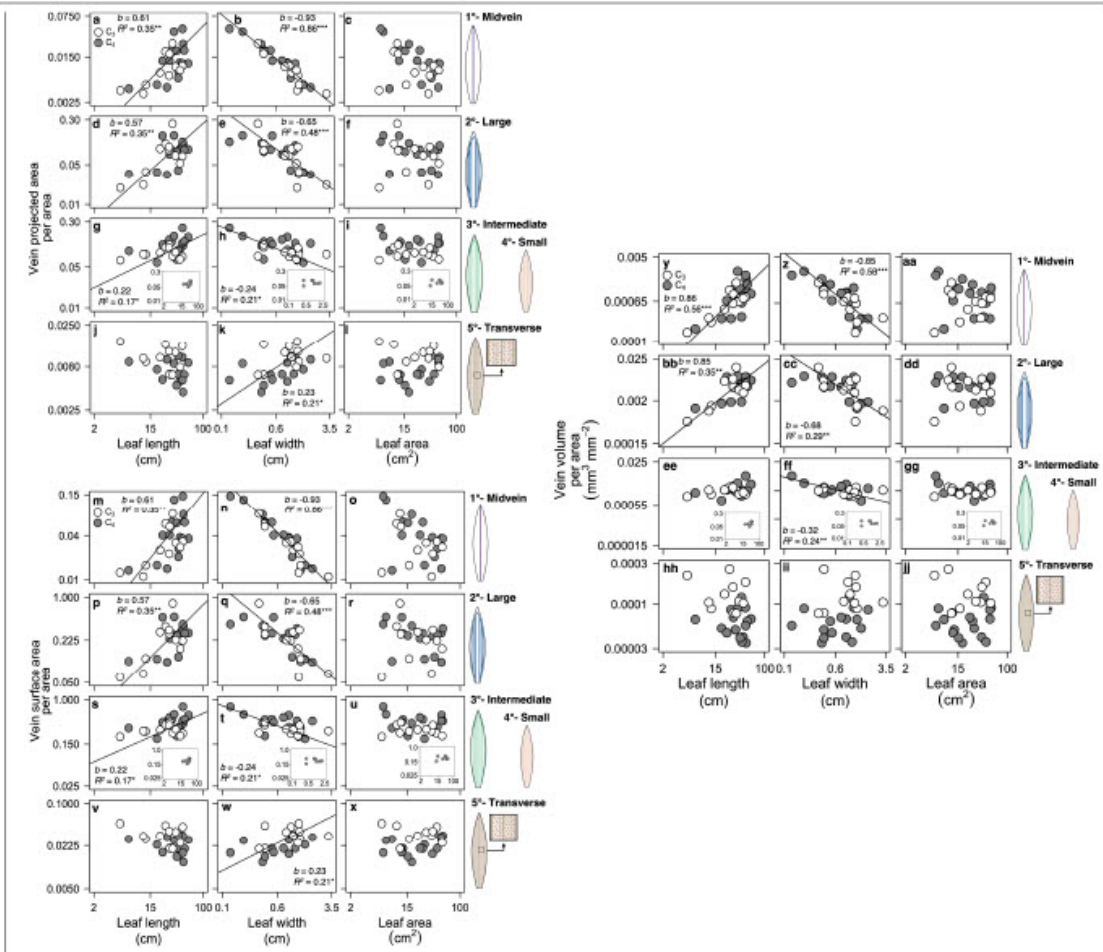
Extended Data Fig. 7 | Scaling of leaf vein projected area, vein surface area and vein volume of given vein orders with leaf dimensions across 27 grass species grown experimentally. a–l, Relationship of VPA to leaf length (**a, d, g, j**), leaf width (**b, e, h, k**) and leaf area (**c, f, i, l**). **m–x**, Relationship of VSA to leaf length (**m, p, s, v**), leaf width (**n, q, t, w**) and leaf area (**o, r, u, x**). **y, z, aa, bb, cc, dd, ee, ff, gg, ii**, Relationship of VVA to leaf length (**y, bb, ee, hh**), leaf width (**z, cc, ff, ii**) and leaf area (**aa, dd, gg, jj**). Two-tailed PGLS regressions were fitted for log(VPA, VSA or VVA) ~ log(a) + b log(leaf length, width or area) and drawn when significant. *$P < 0.05$, **$P < 0.01$, ***$P < 0.001$; line parameters are given in Supplementary Table 10. $P = 0.0011$ (**a**), 1.2×10^{-12} (**b**), 0.0011 (**d**), 7.0×10^{-5} (**e**), 0.0335 (**g**), 0.0161 (**h**), 0.0167 (**k**), 0.0011 (**m**), 1.2×10^{-12} (**n**), 0.0011 (**p**), 7.0×10^{-5} (**q**), 0.0335 (**s**), 0.0161 (**t**), 0.0167 (**w**), 8.2×10^{-6} (**y**), 5.4×10^{-6} (**z**), 5.2×10^{-5} (**bb**), 0.0037 (**cc**), 0.0093 (**ff**). Significant trends are plotted with PRMA to illustrate the central trends (Methods). The s.e. for species trait values are given in Supplementary Table 3. C_3 and C_4 species are in white and grey, respectively.

27
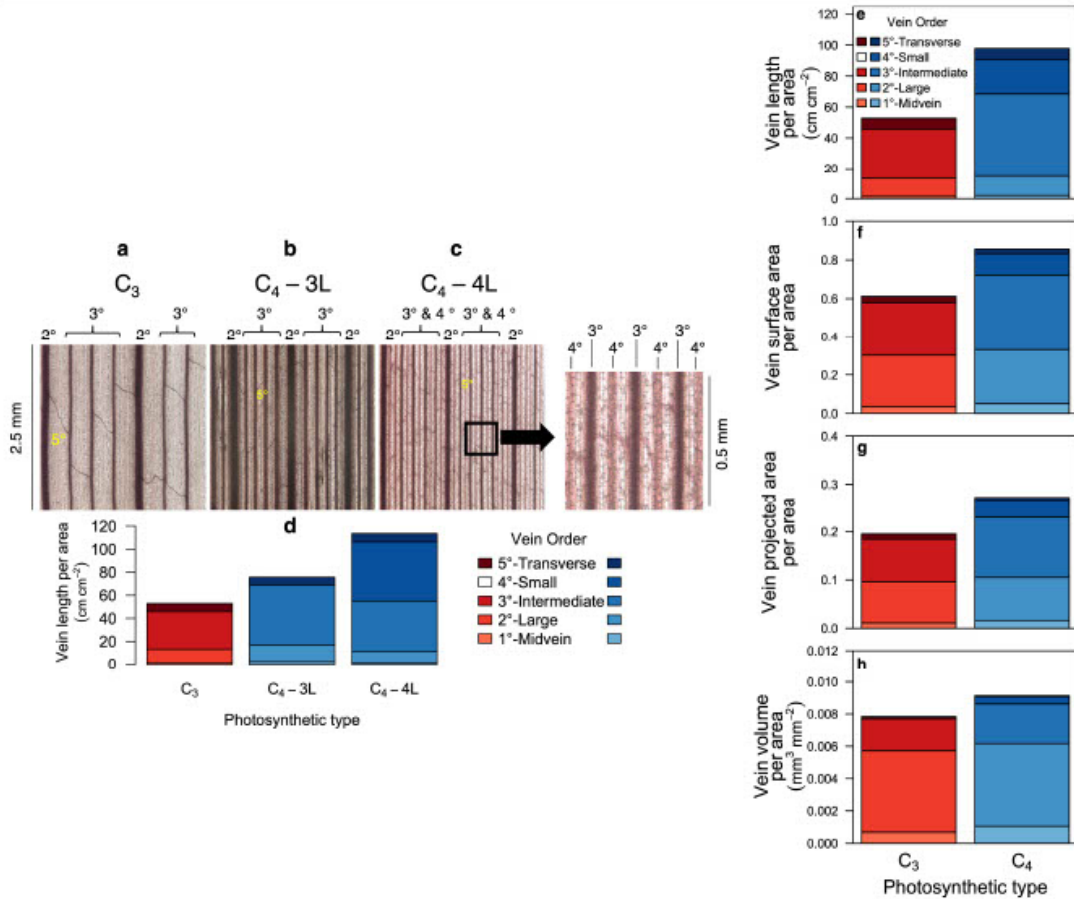
Extended Data Fig. 8 | Partitioning of the contributions of given vein orders of the venation architecture of C₃ and C₄ grasses, with minor veins accounting for the differences in VLA. a, *Triticum aestivum*, a C₃ species. **b**, *Aristida ternipes*, a C₄ species without fourth-order veins (C₄-₃ₗ) (that is, third-order veins are the highest longitudinal vein order). **c**, *Paspalum dilatatum*, a C₄ species with fourth-order veins (C₄-₄ₗ) (that is, fourth-order veins are the highest longitudinal vein order). **d**, VLA (cm per cm²) distribution across vein orders for each type (C₃, *n* =11, C₄-₃ₗ =9, C₄-₄ₗ = 7). **e–h**, VLA (**e**), VSA (**f**), VPA (**g**) and VVA (**h**) distribution across vein orders for each type (C₃, *n* =11; C₄, *n* =16). Statistical comparisons by phylogenetic ANOVA are given in Supplementary Table 3.

28
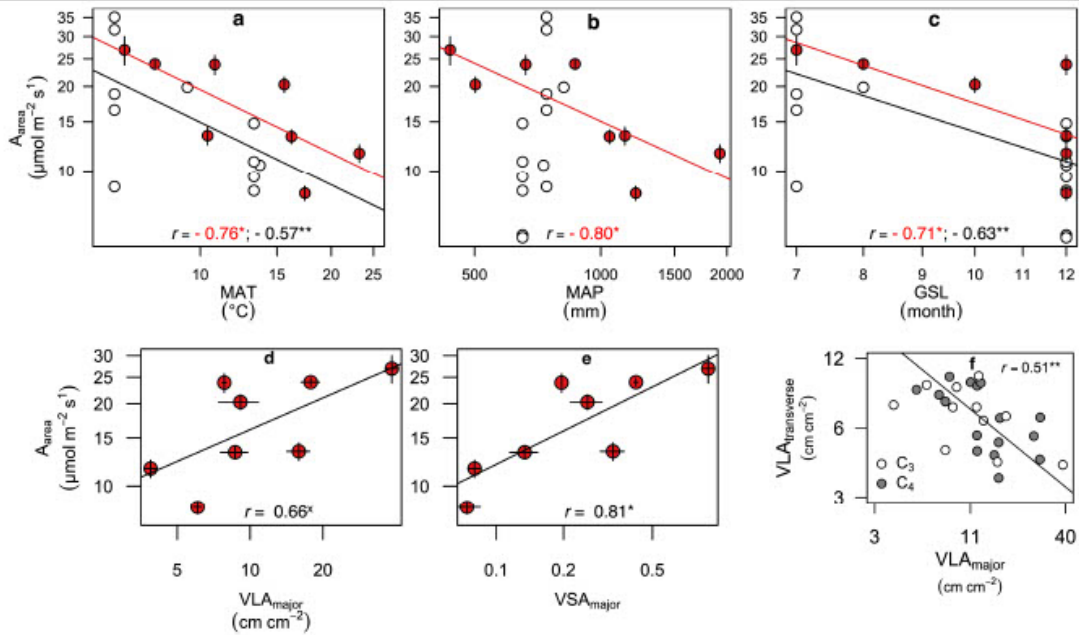
Extended Data Fig. 9 | Associations between light-saturated leaf photosynthetic rate and native climate and vein traits for terrestrial C₃ species, and the scaling of VLA of transverse fifth-order veins with major VLA in 27 C₃ and C₄ grass species grown experimentally. a–c, Relationship of area-based light-saturated photosynthetic rate (A_{area}) measured with photosynthesis systems and MAT (a), MAP (b) and growing season length (GSL) (c). d–f, Relationship of light-saturated photosynthetic rate per area and VLA_{major} (cm per cm²) (d) and major VSA (VSA_{major}, unitless) (e), and transverse VLA ($VLA_{transverse}$) (cm per cm²) with VLA_{major}. Points and lines in red represent eight terrestrial C₃ grasses (from this study) grown in a greenhouse common garden related to the mean climate of their native distribution, supporting the assumption of a higher photosynthetic rate in colder and drier climates with shorter growing seasons. Open points represent 13 Northern Hemisphere temperate terrestrial C₃ grass species from the global plant trait network (GLOPNET[126]) measured in the field, as related to the mean climate at their field site. Black lines represent the significant trend through all the points in a, c, which—given the disparate data sources combined here (and the consideration of field site rather than native range climate for the GLOPNET species)—provides strong support for the generality of the relationships of

A_{area} to MAT and growing season length. Notably, these are conservative tests of the relationships of photosynthetic rate with native climate, as measurements of A_{area} that use the photosynthesis system chamber do not include the effect of the boundary layer conductance (which is made very high and invariant)[27]. Under natural conditions (and especially under slow wind speeds), smaller leaves would have a boundary layer conductance higher than that of larger leaves (as shown in the simulation in Extended Data Fig. 5), and thus—under natural conditions that included the effects of boundary layer—a stronger trend would be expected for small-leafed species in colder and drier climates to have higher photosynthetic rates than larger-leafed species of warm, moist climates. Two-tailed ordinary least square regressions or PRMA were fitted for log(trait) = log(a) + b log(trait or climate variable) in a–e and f, respectively. *$P < 0.05$, **$P < 0.01$, ˣ$P = 0.04$ in a one-tailed test of the hypothesized positive correlation. $P = 0.0301$ (red line in a), 0.0071 (black line in a), 0.0183 (b), 0.0474 (red line in c), 0.0021 (black line in c), 0.0794 (d), 0.0138 (e), 0.0061 (f). Error bars represent s.e. in a–e. The s.e. for species trait values in f are given in Supplementary Table 3. C₃ and C₄ species are shown in white and grey, respectively, in e.
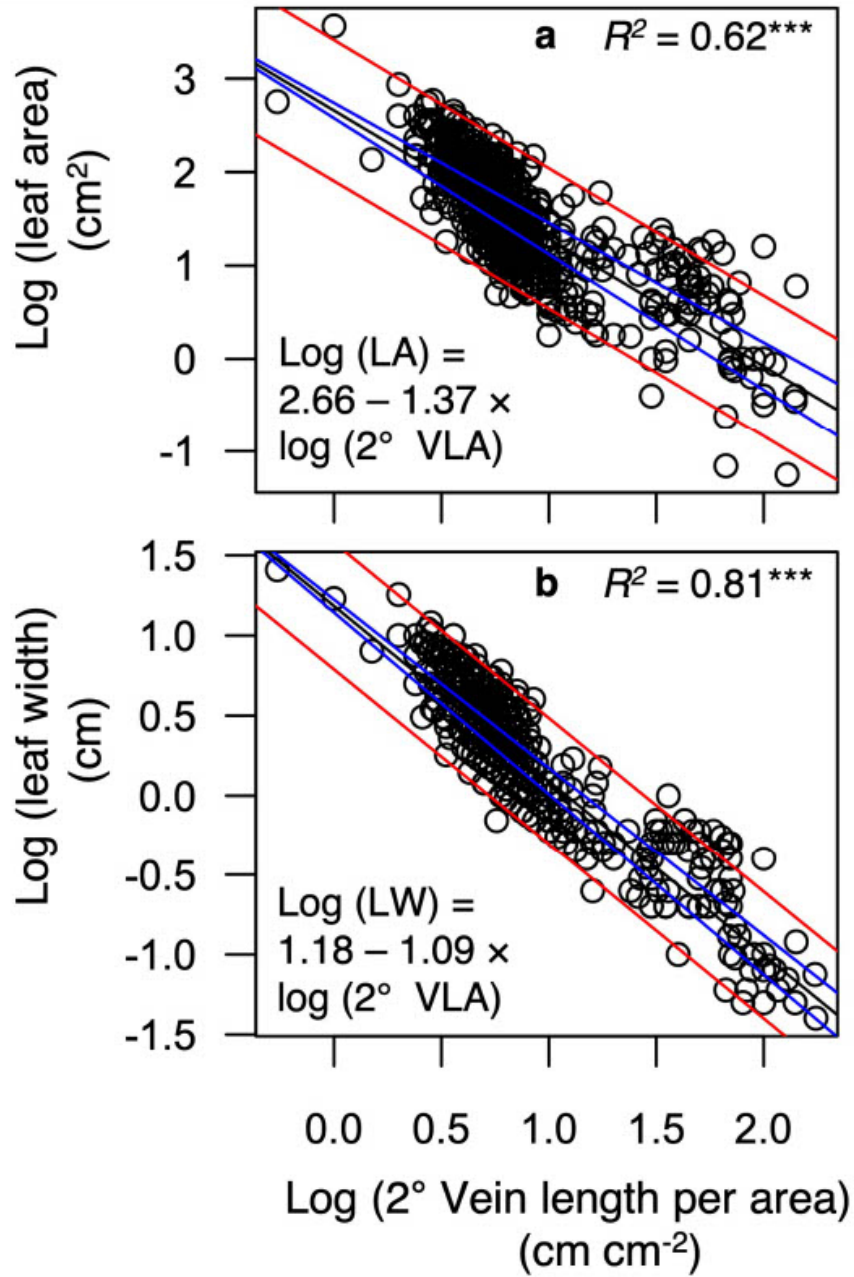
Extended Data Fig. 10 | Estimating leaf size from venation traits that can be measured on small samples or fragments of grass leaves. a, b, Leaf area (a) and leaf width (b) predicted from VLA of second-order veins. $n = 600$ and 616 species in **a** and **b**, respectively (Grassbase dataset, Supplementary Table 2). The relationships were fitted with two-tailed ordinary least square regressions. These relationships enable the determination of intact leaf size from fragments that include at least two second-order veins (including fragmentary fossil remains). The 95% confidence intervals are in blue and 95% prediction intervals in red. ***$P < 0.001$. $P = 1.4 \times 10^{-127}$ (**a**), 7.6×10^{-227} (**b**).

Supplementary Materials

Supplementary Data Captions (see attached Excel Workbook)

Table S2.1. Published studies of the relationship of grass leaf size to climate or hydrological variables. Previous studies focused on specific lineages, communities or biogeographic ranges, limited in scope relative to this study of worldwide trends. For each study, I report the number of species and genera of grasses tested, and the significant correlations of leaf traits and climate variables (key provided below the Table), and the range of leaf trait values tested. "≈" signifies approximate values as data were extracted from published figures.

Table S2.2. Database for globally distributed grass species, with phylogenetic statistics testing for differences between photosynthetic types. We present for each species the photosynthetic type (C_3 or C_4), mean climate variables for the native range, and (a) leaf dimensions for 1752 species and (b) leaf vein trait values for 616 species from the RGB Kew: GrassBase. Statistics from parametric and non parametric phylogenetic analysis of variance comparing C_3 and C_4 traits are presented below for table (a). For the data in table (b) these tests were omitted given the far greater representation of C_3 species in this smaller dataset (ratio of C_4 to C_3 species = 17:593). The global diversity of grass leaf size would be yet greater if it included the species with the largest leafed species (i.e., bamboos *Chusquea spectabilis* and *C. nobili*, data not available); their inclusion would have further strengthened the global trends, given their distribution in warm, wet climates. Significance: *$P < 0.05$, **$P < 0.01$, ***$P < 0.001$.

Table S2.3. Experimental data for 27 C$_3$ and C$_4$ grass species grown in a greenhouse common garden and measured for the scaling of vein traits with leaf size. We present grass subfamily and tribe (Soreng et al., 2017), photosynthetic type (C$_3$ or C$_4$) and C$_4$ subtype, seed source, accession number, seed treatment for germination, habitat preference (terrestrial/aquatic), climate data for species' native ranges, mean values for measured traits (with key below the table), and calculated statistics (in rows below). Cells with NA signify that the given species did not possess a trait or that data were not available. Notably, the three shade adapted species, associated with forest/woodland habitats, have some of the widest leaves and lowest values for major vein lengths per area across the species.

Table S2.4. Published studies for eudicotyledons on the scaling of vein traits and leaf size (a)-(c), and on the contribution of vein traits to hydraulic and photosynthetic performance and its maintenance under cold or dry conditions, (d)-(g). For each study, we report the species numbers and taxonomic information; growing conditions; and confirmation of trends supported across species, as presented in the study or by our analyses of their data, i.e., those supporting the arrows linking small leaf size to vein traits, and traits to tolerance of cold and dry conditions in Figure 2.1. Legend is provided below Table. References ordered from largest and most diverse species sampling to smallest and least diverse sampling.

Table S2.5. Grass species from which the synthetic grass developmental model was derived, based on previously published data and literature reviews.

Table S2.6. Expectations for the slopes of leaf size-scaling relationships across species derived from the synthetic developmental model, and, alternatively, from geometric scaling. Expectations are provided for *b* in log (*y*) = log (*a*) + *b* log(*x*), where *y* is a vein trait, and *x* is a mature leaf dimension. Predicted scaling relationships are designated as "intrinsic" or "enabling" (e or i, respectively) (see Box 2.1).

Table S2.7. Statistics and parameters describing the relationships of grass leaf traits with climate variables. We present, for each trait and climate variable (see key below), the statistical method (ordinary least squares, OLS; standard major axis, SMA; or phylogenetic reduced major axis, PRMA; all two-tailed), *r*- and *p*-values, *a*- and *b*- values from the equation log (trait) = log (*a*) + *b* log (climate variable) for (a) 1752 and 1729 species from RGBKew: GrassBase for leaf traits and culm height, respectively (b) 27 species grown in a common garden at UCLA . *r*- and *p*-values are provided for each test, and *a*- and *b*-values provided when significant at *$P < 0.05$, **$P < 0.01$, ***$P < 0.001$.

Table S2.8. Analyses of the relationship of grass traits with climate variables for species of globally distributed grasses, including multiple regression, hierarchical partitioning, and quantile regression. (a) - (d) Multiple regression analysis of the relationships of leaf size dimensions and culm height with climate (see legend below) considering single and multiple climate variables, with interactions, for (a) and (c) 1752 species and (b) and (d) 1723 species, i.e. excluding species with MAT < 0 °C; statistical method, model parameter coefficients and intercepts and AIC values are provided for each model; (e) Hierarchical partitioning analysis of the relationship of leaf dimensions and culm height with climate variables, resolving the

independent effects of individual climate variables; the total R^2, independent % contribution, and actual R^2 for each variable, joint R^2 contribution, and total R^2 contribution are provided; (f) Quantile regression analysis of the relationship of leaf dimensions with given climate variables, for 5% and 95% quantiles; b-values (i.e., the model slope) are provided for associations tested across all data, and 5%, 50% and 95% quantiles, and P-value for significance of the test for different slopes between the 5% and 95% quantiles. Significance: *$P < 0.05$, **$P < 0.01$ ***$P < 0.001$.

Table S2.9. Testing hypotheses for the advantages of small leaf size in gas exchange (photosynthetic rate, transpiration rate and leaf water use efficiency) under cold and/or dry climates, including for mitigating short warm and wet growing periods. In our simulations we estimated leaf temperatures, rates of transpiration per leaf area (E) and boundary layer conductance from inputs of leaf width values (0.04, 0.1, 0.5, 0.875, 1.5, 2.7 and 11 cm), at low and moderately high wind speeds (0.1 and 2 m/s), and across a range of air temperatures (1.85, 6.85, 11.85, 16.85, 21.85, 26.85, 31.85, 36.85, 41.85, 46.85, 51.85 °C) for amphistomatous leaves, using the R package Tealeaves, using constants for other physical and environmental inputs (see Table 1 of Muir (2019)). We simulated both wet and dry conditions by halving stomatal conductance from the C_3 input value (from 0.4 to 0.2 mol m^{-2} s^{-1}). We then used the boundary layer conductance and leaf temperature to estimate C_3 leaf photosynthetic rate (A) using the Farquhar model (Farquhar, von Caemmerer & Berry 1980), including temperature responses of Farquhar parameters (Bernacchi, Pimentel & Long 2003). We calculated leaf water use efficiency as A/E. We then tested hypotheses for the advantage of small leaves relative to large leaves, considering leaf widths of 0.1 and 2.7 cm, the 5% to 95% quantile of the global

database, under cold and/or dry climates, or under moist and warm climates (thus considering the ability to mitigate short moist and warm growing periods). In the comparisons below, we consider cold and warm temperatures of respectively 6.85 and 41.85 °C, and wet and dry climates represented by g_s of 0.4 and 0.2 mol m^{-2} s^{-1}. Data simulated for hyperstomatous leaves under the same conditions for each trait and compared to amphistomatous values were highly similar ($R^2 = 0.71 - 0.99$). Simulations that confirmed hypotheses for the advantages of small relative to large leaves under cold or dry climates are bold-faced. Comparisons of small relative to large leaves using other specific simulated conditions resulted in qualitatively similar conclusions.

Table S2.10. Parameters for the scaling of vein traits with leaf dimensions across 27 C$_3$ and C$_4$ grass species grown in a greenhouse common garden (*n*=11 and 16 respectively). Results are presented for vein diameters; and vein lengths, surface areas, projected areas, and vein volumes per unit leaf area for each vein order. Predictions were derived from the developmental model for the allometric slope of each relationship across species, i.e., the variable b in the equation log (trait) = log (*a*) + b log (leaf dimension for mature leaves) (Table S2.6); Allometric equations were fitted using two-tailed phylogenetic reduced major axis (PRMA) or phylogenetic generalized least squares (PGLS) for the scaling of vein diameter or vein length per area, respectively, and *r*- and *p*-values are provided for each test, and parameters parameters a and b are provided including 95% confidence intervals (CIs) for *b*-values (see Methods). Bold type indicates that the *b*-values predicted from the developmental model were supported by the experimental data, i.e., the scaling relationship across species was significant, and the predicted *b*-value was within the 95% CIs for the observed *b*-value. Significance: *P < 0.05, **P < 0.01,

***$P < 0.001$. Intrinsic versus enabling scaling: i or e, respectively (see Box 2.1). NS: Not significant. The scaling of major and minor vein traits with leaf dimensions were consistent with developmentally based predictions in 91/111 cases compared to geometric scaling, which was supported for 27/111 cases; these proportions differed at $P < 0.001$ (proportion test).

Table S2.11. Scaling of xylem conduit diameter with vein and leaf dimensions leaf dimensions across 27 C$_3$ and C$_4$ grass species grown in a greenhouse common garden (n=11 and 16 respectively). We present the parameters for the fitted lines for two-tailed tests of log (conduit diameter) = log (a) + b log (vein diameter or leaf length). Key for vein traits provided below. Columns include the line-fitting method used (two-tailed), r- and p-values, and parameters a- and b- are provided including 95% confidence intervals (CIs) for b-values when significant at *$P < 0.05$, **$P < 0.01$, ***$P < 0.001$.

Table S2.12. Data for 13 C$_3$ grasses from the global plant trait network (GLOPNET) database and extracted for testing assumptions of photosynthetic rate and climate. We present climate data for the latitude and longitude where the species was measured, and light-saturated photosynthetic rate.

Chapter 3: Allometries of cell and tissue anatomy and photosynthetic rate across leaves of C$_3$ and C$_4$ grasses

Abstract

Allometric relationships among the dimensions of leaves and their cells hold across diverse eudicotyledons, but have remained untested in the leaves of grasses. We hypothesized that geometric (proportional) allometries of cell sizes across tissues and of leaf dimensions would arise due to the coordination of cell development and that of cell functions such as water, nutrient and energy transport, and that cell sizes across tissues would be associated with light-saturated photosynthetic rate. We tested predictions across 27 globally distributed C$_3$ and C$_4$ grass species grown in a common garden. We found positive relationships among average cell sizes within and across tissues, and of cell sizes with leaf dimensions. Grass leaf anatomical allometries were similar to those of eudicots, with exceptions consistent with the fewer cell layers and narrower form of grass leaves, and the specialized roles of epidermis and bundle sheath in storage and leaf movement. Across species, mean cell sizes in each tissue were associated with light-saturated photosynthetic rate per leaf mass, supporting the functional coordination of cell sizes. These findings highlight the generality of evolutionary allometries within the grass lineage and their interlinkage with coordinated development and function.

Introduction

Relationships among the quantitative properties of cells, organs and organisms, i.e., allometries, provide insights into evolution, development and function (Huxley, 1932; Niklas, 1994; Meinzer, James, Goldstein & Woodruff, 2003; Sperry, Hacke & Wheeler, 2005; Sack et al., 2012; John, Scoffoni & Sack, 2013; Smith & Sperry, 2014; Zhong, Cerabolini, Castro-Díez, Puyravaud & Cornelissen, 2020; Baird et al., 2021). Across diverse eudicotyledons, cell sizes in the leaf epidermis and mesophyll are positively correlated, but independent from xylem cell sizes; further, cell dimensions increase with leaf thickness (John et al., 2013). Such allometries would arise from coordinated development during leaf expansion, and may be reinforced by selection as coordination in cell sizes leads to efficient transport of water, nutrients and sugars between cells of different types (Cadart & Heald, 2022). Further, allometric analyses of cell properties provide important insights into physiological functions, including rates of exchange of carbon and water, and environmental stress tolerance (Meinzer, James, Goldstein & Woodruff, 2003; Sperry, Hacke & Wheeler, 2005; Brodribb, Jordan & Carpenter, 2013; Smith & Sperry, 2014; Olson et al., 2018; Nobel, 2020; Zhong, Cerabolini, Castro-Díez, Puyravaud & Cornelissen, 2020).

Leaf anatomical allometries have not been tested for grasses, a family (Poaceae) of 12,000 species diverse in morphology (Table S3.1), that dominates 43% of the terrestrial surface, and accounts for the majority of crop production (Beer et al., 2010; McSteen & Kellogg, 2022). The optimization of grass anatomy is part of Grand Challenge efforts to improve the physiology of stress tolerance and productivity, including the engineering of novel C_4 crops from C_3 precursors (Lowry et al., 2019; Ermakova, Danila, Furbank & von Caemmerer, 2020; Eckardt et al., 2023). Grasses differ from typical eudicotyledons in leaf development and form. Grass leaves arise from an intercalary meristem, in which cells file through distinct zones of division, expansion and

differentiation at the leaf base (Table 3.1; Figure 3.1; Skinner & Nelson, 1994; Fournier et al., 2005; Evert, 2006) resulting in linearized forms with parallel longitudinal veins connected by transverse veins (Ellis, 1976; Evert, 2006). Like eudicots, grasses possess a parenchymatous bundle sheath surrounding all veins, derived from dividing lamina cells, yet grass leaves typically also possess a mestome sheath interior to the vein bundle sheath, which is derived from procambium precursors, like the xylem and phloem (Dengler, Dengler & Hattersley, 1985; Evert, 2006). Further, 41% of grasses have C_4 photosynthesis, and these possess specialized "Kranz" anatomy, including higher vein length per area, enlarged sheath cells, and much more extensive plasmodesmata connecting mesophyll with sheath cells, relative to C_3 grasses (Dengler et al., 1985; Sage, 2004; Christin et al., 2013; Danila, Quick, White, Furbank & von Caemmerer, 2016), all of which contribute to their C_4 syndrome that confers higher rates of CO_2 uptake and tolerance to aridity and extreme temperatures (Sage, 2004; Watcharamongkol, Christin & Osborne, 2018).

Across species, I hypothesized a framework of inter-related anatomical allometries ("scaling relationships") of the form

$$y = ax^b \text{ or } \log y = \log a + b \log x, \quad \text{eqn 3.1}$$

where y and x are dimensions, and *a* and *b* the allometric intercept and slope (Table 3.2). First, I hypothesized *allometries among cell dimensions* due to proportional development, and, additionally, due to cell size coordination for integrated function (Table 3.2; Granier & Tardieu, 1998; Van Volkenburgh, 1999; Brodribb et al., 2013; Cadart & Heald, 2022; see Appendix, "*Relationship of leaf developmental and evolutionary allometries, and insights into development and function*"). Second, I hypothesized that *leaf dimensions would be related to those of their constituent cells* (Table 3.2; John et al., 2013). Third, I hypothesized that *xylem cell areas would increase with leaf size and plant height*, such that xylem water transport capacity would at least in

part compensate for the longer transport pathlengths in longer leaves of taller grasses (Table 3.2; Olson et al., 2018; Baird et al., 2021). Fourth, I hypothesized that grasses would show *similar leaf anatomical scaling as eudicots*, with exceptions arising from their different leaf morphology (Table 3.2; Appendix). I expected that grasses would differ from eudicots in some leaf allometries, given their fewer cell layers, highly elongated shape and specialized roles of the epidermis and bundle sheath, including high shrinkage and expansion capacity allowing for leaf movements (including rolling), and/or water storage enabling buffering of low-resource availability. I thus expected grasses to differ from eudicots in allometries for cell cross-sectional areas of epidermis and bundle sheath vs. overall leaf dimensions. Lastly, I hypothesized that across grass species, light-saturated photosynthetic rate per leaf mass (A_{mass}) would scale positively with cell sizes in multiple tissues due to the integrated impact of cell size on leaf structure and function (Table 3.2). A_{mass} is equivalent to light-saturated photosynthetic rate per leaf area (A_{area}) / leaf mass per area (*LMA*) (Sack et al., 2013). Given that leaves with large cells would tend to be thicker (John et al., 2013, 2017), I hypothesized they would have higher A_{area}, as previously found in studies of grasses and eudicotyledonous species (Wilson & Cooper, 1967; Charles-Edwards, Charles-Edwards & Sant, 1974; Koike, 1988; Garnier, Salager, Laurent & Sonié, 1999), and that they would be wider, with lower major vein length per area (Baird et al., 2021), contributing to a lower *LMA* (John et al., 2017). Further, larger xylem drive higher hydraulic supply which would enable higher A_{area} and would also be reflected in a high A_{mass}. A parallel coordination of A_{mass} with cell sizes in multiple tissues, including photosynthetic mesophyll and xylem transport tissue, would further support our first hypothesis of functional coordination of cell sizes throughout the leaf for metabolism and transport.

For the majority of relationships among cell and leaf dimensions, I expected that proportional development would result in *geometric allometries*, which would be reinforced by selection for coordinated and integrated function. Thus, areas (A) would scale together isometrically as $A \propto A^1$ and with lengths (L) as $L \propto A^{1/2}$ (Table 3.1; Appendix; Niklas, 1994; Sack et al., 2012; John et al., 2013; Baird et al., 2021). I expected divergences from geometric scaling, i.e., decoupling of proportional development, for certain functionally specialized tissues (Table 3.3). Thus, relative to other cell types, I expected disproportional increases in cell size for the upper epidermis, reflecting a greater investment in supporting functions including large specialized bulliform cells that provide water storage and enable leaf rolling (Ellis, 1976; Evert, 2006). Further, I expected divergence from geometric scaling for allometries among xylem cell types that would be coordinated for optimal hydraulic design; for the major and minor vein systems to maintain matched transport efficiency across leaves of different size, the size of type I xylem conduits (which occur only in major veins) would increase disproportionately relative to type II xylem (which occur in both major and minor veins) to compensate for the declining density of major veins that are spaced out further in larger leaves (Baird et al., 2021). I expected leaf dimensions to increase disproportionately with cell cross-sectional areas, as dimensions also depend on the additional role of cell number, which in larger leaves increases disproportionately relative to cell areas (Gázquez & Beemster, 2017; John et al., 2017). I expected leaf length and culm height would increase disproportionately relative to vein xylem cell sizes; increases in xylem cell size that would mitigate of impacts of increasing path length need not be proportionate, because hydraulic conductance through xylem increases as the radius to the fourth power (Sack & Scoffoni, 2013). Finally, I expected that C_3 and C_4 grasses would differ in allometries, with more generalized across all cell types across C_3 species. because specialized C_4 cell functions associated

41

with Kranz anatomy and carbon concentrating mechanism, including higher densities of plasmodesmata (Danila et al., 2016), may disrupt cell size-function relationships. I expected that for C_4 species, selection for enlarged sheath cells (Christin et al., 2013) would decouple the cell cross-sectional areas of bundle and mestome sheaths, mesophyll and xylem.

To test this framework of hypothesized general relationships, I used a common garden, glasshouse experiment to measure leaf anatomy and photosynthetic rate in a phylogenetically structured sample of 27 grass species.

Material and Methods

Study species and sampling

I selected 27 grass species to represent high functional and phylogenetic diversity, encompassing 11 C_4 origins (16 C_4 species; 11 C_3 species), and including terrestrial and aquatic species and important crops (Figure 3.2; Figures S3.1-S3.3; Table S3.1). Plants were grown in a common garden to minimize environmentally-driven plasticity. The individuals sampled for anatomical measurements in this study (see "***Anatomical sample preparation and measurements***") were the same individuals and leaves sampled for leaf venation traits in a previous publication (Baird et al., 2021).

Seeds were acquired from seed banks and commercial sources (Table S3.1), and prior to germination were surface-sterilized with 10% NaClO and 0.1% Triton X-100 detergent, rinsed with sterile water, and sown on plates of 0.8% agar sealed with Micropore surgical tape (3M, St. Paul, MN). Seeds were germinated in chambers maintained at 26˚C, under moderate intensity cool white fluorescent lighting with a 12-hour photoperiod. When roots ranged from 2-3 cm long, seedlings were transplanted to 3.6 L pots with potting soil (1:1:1.5:1.5:3 of coarse vermiculite:

perlite: washed plater sand: sandy loam: peat moss). Plants were grown in a common garden at the UCLA Plant Growth Center (minimum, mean and maximum daily values for temperature: 20.1, 23.4 and 34.0 °C; for relative humidity: 28, 50 and 65%; and mean and maximum photosynthetically active radiation during daylight period: 107 and 1988 μmol photons m^{-2} s^{-1}; HOBO Micro Station with Smart Sensors; Onset, Bourne, MA). To reduce the impacts of variation in light and temperature on plant growth and traits, plants were arranged in six randomized blocks across three benches, with one individual per species per block (n = 6 except *Alloteropsis semialata*, n = 4) and two blocks per bench. Plants were irrigated daily with water containing fertilizer (200-250 ppm of 20:20:20 N:P:K; Scotts Peters Professional water soluble fertilizer; Everris International B.V., Geldermalsen, The Netherlands). I grew all 27 species in potting soil, including the three species classified as aquatic (*Oryza sativa*, *Phragmites australis*, *Sacciolepis africana*), to maximize similarities in growth conditions across species; as in previous studies these aquatic grasses grew to maturity under non-aquatic conditions (Clevering, 1999; Kato & Okami, 2010). All species were grown until flowering to verify species identities.

Anatomical sample preparation and measurements

For three individuals per species that possessed many mature leaves, one leaf was fixed and stored, and 1 μm thick transverse cross sections were prepared, stained, and imaged by light microscopy (Nobel, Zaragoza & Smith, 1975; Nobel, 1976; John et al., 2013; Fletcher et al., 2018) (Leica Leitz DMRB; Leica Microsystems with SPOT Imaging Solution camera; Diagnostic Instruments, Sterling Heights, Michigan USA). Leaves were fixed and stored in FAA solution (37% formaldehyde-glacial acidic acid-95% ethanol in deionized water). Central rectangular samples were cut from each leaf halfway along the length of the blade and gradually infiltrated under

vacuum with low viscosity acrylic resin (L.R. White; London Resin Co., UK). Infiltrated samples were set in resin in gelatin capsules to dry at 55 °C overnight. Transverse cross sections of 1 μm thickness and of varying width (species dependent) were prepared using glass knives (LKB 7800 KnifeMaker;LKB Produkter; Bromma, Sweden) in a rotary microtome (Leica Ultracut E, Reichert-Jung California, USA), placed on slides and stained with 0.01% toluidine blue in 1% sodium borate (w/v). Slides were then imaged at 5×, 20×, and 40× objective using a light microscope (Leica Lietz DMRB; Leica Microsystems) and camera with imaging software (SPOT Imaging Solution; Diagnostic Instruments, Sterling Heights, Michigan USA).

I quantified leaf thickness and cell cross-sectional areas of the mesophyll, upper and lower epidermis, parenchymatous bundle and mestome sheaths and xylem using the program ImageJ (Nobel et al., 1975; Nobel, 1976; John et al., 2013; Fletcher et al., 2018) (ImageJ version 1.42q; National Institutes of Health, Bethesda, Maryland, USA). Cell cross-sectional area was used as an index of cell size (Nobel, 2020), which would reflect cell volumes in the case of mesophyll cells, which are symmetrical in shape, but not for epidermal, vascular sheath and xylem cells, which differ in shape between transverse and paradermal planes (Nobel et al., 1975; Nobel, 1976). Measurements of cells of the mesophyll and the lower and upper epidermis were replicated three times for each cross section. In the middle of the left, center and right thirds of the cross section, mesophyll cells were selected for determination of cell area and, given their irregular shapes, were traced. I measured leaf thickness three times at the left, center and right thirds of the cross section that excluded leaf furrows (Table 3.1; Ellis, 1976). Epidermal cells were similarly selected, but their areas were determined as the area of an ellipse, area = $\pi \times a \times b$, where a and b are the radii of the major and minor axes, i.e., the lengths and widths of the

cells. Dimensions of parenchymatous bundle and mestome sheath cells and xylem conduits were quantified for each specific vein order, and their areas determined as for epidermal cells. Cells were measured for vein xylem and parenchymatous bundle and mestome sheaths in the major veins, i.e., the 1° "midvein" and 2° "large" veins, and in the minor veins, i.e., the 3° "intermediate" veins, and, for the species that possessed them, the 4° "small" veins; these 4° "small" veins occur in one C_4 clade (the NADP-ME of Panicodeae), represented by seven species in this study, for which the mestome sheath functions for carbon reduction and is the only vein sheath, excluding *Alloteropsis semialata* which possesses 4° veins, and has both sheaths (Dengler et al., 1985). To reduce biases in calculating average xylem cell sizes, I differentiated two metaxylem conduit types within the major veins, which is consistent with previous studies noting that these conduit types are clearly developmentally and functionally distinct (Russell & Evert, 1985; Dannenhoffer, Ebert Jr. & Evert, 1990). The major veins contain large "type I xylem" conduits, and both major and minor veins contain the distinctively smaller "type II xylem" conduits (Baird et al., 2021). For each vein order, I selected one small, one medium and one large parenchymatous bundle sheath cell (same for mestome sheath cells), and determined their average area, and I quantified all xylem cell areas within each vein order, and averaged these for type I and for type II xylem. I also calculated average parenchymatous bundle and mestome sheath and type I and II xylem cell areas across all vein orders. I did not quantify second-order vein or sheath traits for the species *Lasiacis sorghoidea*, as I lacked high magnification images that included their very widely spaced second-order veins. I did not quantify phloem cell dimensions due to the inability to competently distinguish sieve cells from parenchyma in the images.

45

I also utilized published values for maximum leaf length and width, and leaf area as their product, and published values for culm height data as a measure of plant height, to test relationships with leaf and plant morphology with cross-sectional cell areas (Clayton, Vorontsova, Harman & Williamson, 2006; Baird et al., 2021). The product of maximum length and width overestimates leaf area for grasses; however no standard correction value exists for grasses (Kemp, 1960; Stickler et al., 1961; Shi et al., 2019). Considering the diverse set of leaf shapes included in our experiment, and noting that a correction factor is unlikely to impact differences on the log scales used to establish correlation coefficients, scaling exponents and their statistical significance, I did not apply a correction factor and our estimates of leaf area should be taken as approximate. I utilized published data for major vein length per leaf area (VLA_{major}; Baird et al., 2021) to test relationships of cell cross-sectional areas with VLA_{major} .

Quantification of leaf gas exchange

Leaf gas exchange data for the eight C_3 terrestrial grasses was previously published (Baird et al., 2021). For all 27 grass species, including the eight C_3 terrestrial grasses, I measured light-saturated rates of gas exchange from 17 Feb to 28 June 2010, between 0900 and 1500 each day, for a mature leaf on each plant for six plants per species. I measured steady state gas exchange (<2% change over 6 minutes) using a LI-6400XT portable photosynthesis system (LI-COR, Lincoln, Nebraska, USA). The leaf chamber was maintained at 25°C, with reference CO_2 400 ppm, and PPFD 2000 $\mu mol\ m^{-2}\ s^{-1}$, which was assumed to be saturating irradiance for these species (Taylor et al., 2010). The ranges of relative humidity and vapor pressure deficit (VPD) were respectively 60-80% and 0.80-1.6 kPa (overall mean 1.1 kPa). Measurements were made for 1-2 leaves from each of 6 plants (except from 5, 4 and 7 plants for *A. purpurea*, *A. semialata* and *P. australis* respectively, and for

3 leaves from each of two plants for *L. sorghoidea*); overall, 5-9 leaves (mean of 6) were measured per species. Leaf-area normalized values were determined for net photosynthetic rate per leaf area (A_{area}). Leaves were harvested, scanned for leaf area (Canon Scan Lide 90, Canon USA, Lake Success, NY), dried at 70 °C for at least 48h and weighed to determine the leaf dry mass per unit area (LMA). Net CO_2 assimilation rate per unit leaf dry mass (A_{mass}) values were determined as A_{area} / LMA.

Data analysis

Before testing cross-species relationships, I evaluated whether species differed meaningfully in mean trait values, using a nonphylogenetic analysis of variance (ANOVA) on all traits, and tested for the influence of species identity, such that residual error was associated with replicate individuals of a species, enabling estimation of the percent of variation in each trait arising across species relative to that arising among individuals of the same species (Table S3.2).

Using a published phylogeny, I tested trait-trait relationships across all species and within particular groups: C_3 grasses; C_4 grasses; C_3 terrestrial, i.e., removing the C_3 aquatic species (which were in several cases outliers); and $C_4 + C_3$ terrestrial (Figure 3.2; Baird et al., 2021). For comprehensiveness, I tested relationships among cell sizes for the seven tissue types (i.e., 21 pairwise combinations). For vein type I and II xylem, and parenchymatous bundle and mestome sheath cells, relationships were tested within each vein order (six pairwise combinations each for 1° and 2° veins; three for 3° veins, lacking type I xylem; and 1 for 4° veins, lacking type I xylem and parenchymatous bundle sheath = 16 combinations). Analyses were performed using the R Language and Environment, modifying published code with phylogenetic functions (Baird et al., 2021). I fitted lines to log-transformed data, the typical approach in allometric analyses (Niklas,

1994; Warton, Wright, Falster & Westoby, 2006; Poorter & Sack, 2012; Baird et al., 2021). I used the phytools package (Revell, 2012) to fit phylogenetic reduced major axes regressions (PRMA) for the majority of scaling relationships. Because only seven species had fourth order veins, I used non-phylogenetic standard major axis (SMA; a synonym of reduced major axis, i.e., RMA; Warton et al., 2006) regression to evaluate scaling of fourth order vein cell area traits with other cell areas (Niklas, 1994; Warton et al., 2006; Poorter & Sack, 2012; Baird et al., 2021).

Typically, allometric relationships arise as two-parameter power laws with zero intercepts when considered with untransformed data (eqn 1). As is typical of allometric studies, I considered a slope to be consistent with geometric scaling when its 95% confidence interval included the test value (Poorter & Sack, 2012; Baird et al., 2021). I tested for differences in trait means between C_3 and C_4 species using a phylogenetically corrected analysis of variance, both parametric and nonparametric (Garland, Dickerman, Janis & Jones, 1993; Revell, 2012).

For several relationships in our study, data were inconsistent with a power-law, because they had a clear nonzero intercept. In these cases, linear relationships fitted well:

$$y = b\text{x} + a, \qquad \text{eqn 2}$$

where y and x are dimensions, and a and b are the intercept and slope. When y and x have the same dimensionality (i.e., two areas, or two lengths), a positive linear relationship would support geometric (proportional) scaling, given the smallness of the b-value. Thus, when hypothesized relationships were not significant as power law relationships, I tested linear regressions, and report these when significant; this was the case for the scaling of the parenchymatous bundle sheath and the lower epidermis, and, for C_3 species only, the scaling of the mestome sheath and the upper epidermis (Figure 3.3).

I utilized a trimmed phylogeny to test relationships with the parenchymatous bundle sheath, which was possessed by only 21 of the grass species (Figure S3.1; i.e., all C_3 and C_4 species with three longitudinal vein orders). Finally, analyses including second order vein or sheath traits excluded the species *Lasiacis sorghoidea*, and trimmed phylogenies excluding this species were also implemented.

Results

Diversity in grass leaf cell and tissue anatomy

Grass species varied strongly in the mean cell cross-sectional areas of all tissues, from fourfold for type II xylem conduits to 17-fold for parenchymatous bundle sheath cells, and in leaf dimensions, from threefold for thickness to 24-fold for leaf width (Table S3.1). On average, 76% of trait variation was explained by differences among species rather than among individuals in each species (ANOVA; Table S3.2, Figures S3.2-S3.3). C_4 species had larger cell areas on average than C_3 for the upper epidermis, mestome sheath, and 3° vein xylem (phylogenetic ANOVAs; Table S3.2).

Anatomical allometries of cell sizes across tissues

I found allometries among cell sizes across tissues for fifteen of the twenty-one pairwise combinations of tissues, i.e., the lower and upper epidermis, mesophyll, parenchymatous bundle and mestome sheaths, and type I and type II xylem (phylogenetic reduced major axis; Figure 3). The allometries between epidermises, for epidermises vs. mesophyll, for parenchymatous bundle sheath vs. mesophyll, between xylem types, and for xylem vs. mestome sheath were significant

across all species. However, several relationships involving xylem, epidermises and vein sheaths, were significant only for the terrestrial grasses or the terrestrial C_3 grasses (Figure 3.3; Figure S3.5, Tables S3.3-S3.4). Xylem cell sizes were statistically independent of those in mesophyll and epidermises. Within vein orders, significant relationships arose for fourteen of the sixteen allometries, i.e., among parenchymatous bundle and mestome sheaths and type I and II xylem (Figure 3.4 and S3.4-S3.5; Table S3.4).

Cell size allometries were geometric for ten of the fifteen significant across-tissue relationships and for eight of the fourteen significant within-vein relationships ($b = 1$). Non-geometric allometries across-tissues were those of mesophyll vs. upper epidermis, mesophyll vs. parenchymatous bundle sheath, type I vs type II xylem, parenchymatous bundle sheath vs. mestome sheath and parenchymatous bundle sheath vs. type II xylem. Non-geometric relationships within-veins were those of type I vs. type II xylem, mestome sheath vs. type I xylem, and parenchymatous bundle sheath vs. type II xylem (all within the 1° vein), and mestome sheath vs parenchymatous bundle sheath (within the 1°, 2°, and 3° veins; Tables S3.3-S3.4).

Allometries among cell, leaf and plant dimensions

Across species, leaf dimensions and plant height were positively related to leaf cell sizes in all tissues (Figure 3.5-3.6; Table S3.5; Figure S3.6). Thus, leaf thickness was allometrically linked with cell areas in the mesophyll and epidermises; leaf width was allometrically linked with cell areas in the mesophyll, parenchymatous bundle sheath and type I xylem (Figure 3.5); and leaf area was allometrically linked with cell area in the lower epidermis. Further, leaf length, leaf area and plant size (culm height) were allometrically linked with cell areas in the type I and II xylem; leaf length and leaf area with cell areas in the mestome sheath; and culm height with cell areas of the

parenchymatous bundle sheath (Figure 3.6). The majority of allometries held across all species, but several relationships involving the epidermises and vein tissues were significant only for the terrestrial grasses or the terrestrial C_3 grasses (Figures 3.5-3.6). The allometries of leaf thickness vs cell areas were geometric, whereas the majority of the relationships of leaf width, leaf length, leaf area and culm height vs cell areas were greater than geometric (Figures 3.5-3.6; Table S3.5).

Contrasting anatomical allometries of grasses and eudicots

Grasses showed similar allometries between cell sizes for lower epidermis vs. upper epidermis and the parenchymatous bundle sheath as previously found for diverse eudicots (Figure 3.2; John et al., 2013) However, grasses differed from eudicots for allometries between cell sizes for the mesophyll vs. the parenchymatous bundle sheath ($b < 1$ for grasses; $b = 1$ for eudicots), and for mesophyll vs. epidermises ($b < 1$ and $b = 1$ with the lower and upper epidermis respectively in grasses; $b > 1$ for both in eudicots; Figure 3.3), and for leaf thickness vs. cell areas of the upper epidermis ($b = 0.5$ for grasses; $b > 0.5$ for eudicots; Figure 3.5).

Coordination of allometries and functional traits

Across species, cell sizes were associated with mass-based light-saturated photosynthetic rates (A_{mass}) and its determinants, the area-based light-saturated photosynthetic rate (A_{area}) and the leaf mass per area (LMA). Cell sizes were also associated with the major vein length per area (VLA_{major}) (Figure 3.7; Figure S3.7; Table S3.6). A_{mass} was generally positively coordinated with the mean cross-sectional areas of cells in all tissues; however, the association with mesophyll cell size was significant only for C_4 species, and marginally nonsignificant for C_3 species alone or for all species pooled (Table S3.6). Compared with the majority of C_3 grasses included in this study C_4 grasses

achieved higher A_{mass} for a given mesophyll cell size (Figure 3.7). C_4 species had significantly

higher $A_{area,}$ and the similar investment in *LMA* between C_3 and C_4 species resulted in C_4 species

also having higher A_{mass} (Table S3.2). A_{area} was correlated with fewer cell cross-sectional areas

than A_{mass}, showing significant associations with those of the upper epidermis (terrestrial species

only), mestome sheath, and type I and II xylem (Figure S3.7). *LMA* was negatively related to the

cross-sectional areas of the mesophyll, bundle sheath, and lower epidermis across all species, and

additionally to cell areas in the upper epidermis when considering only C_4 species, but was not

linked with cell areas in the mestome sheath and xylem. Finally, VLA_{major} was negatively related

to the cross-sectional areas of just the mesophyll and bundle sheath (Figure S3.7).

Discussion

Allometries across the morphological and anatomical diversity of C_3 and C_4 grass leaves suggest

conserved developmental processes and functional coordination of cell sizes and organ and plant

dimensions, with implications for leaf and plant design and function (Figures 3.3-3.7).

Allometries of cell sizes: patterns across tissues, and contrasts between C_3 and C_4 grasses

While Kranz anatomy of C_4 species meant that C_3 and C_4 species differed strongly in their

anatomy, many allometries were conserved across the two photosynthetic types (Figures 3.3-3.7;

Table 3.2). Across-species allometries between cell areas within and among tissues would emerge

from conserved coordinated cell expansion within organs (Granier & Tardieu, 1998; Van

Volkenburgh, 1999), reinforced by selection for proportional cell sizes (and possibly cell numbers)

that would facilitate coordination of metabolic and transport functions within and across tissues

(Brodribb et al., 2013; John et al., 2013; Cadart & Heald, 2022). Generally, cell area allometries

occurred among cells derived from the same developmental precursors (Table 3.1). Thus, I found cell size allometries for cells arising from lamina precursor cells, including epidermises, mesophyll and the parenchymatous bundle sheath (Figure 3.3). Separately, I found independent cell size allometries for cells arising from the procambium, including xylem and mestome sheath (Figure 3.3).

I note that our study did not include a focus on phloem cells, which also arise from procambium precursors. Elucidating potential allometries of phloem with other cell types and whole plant design remains an urgent avenue for future research linking sugar transport with leaf and whole plant function (Hölttä, Kurppa & Nikinmaa, 2013; Ronellenfitsch et al., 2015).

Beyond the allometries that could be explained by shared developmental precursor cells, I found that C_3 species showed more generalized scaling of cell areas across tissues than C_4 species (Figure 3.3 and S3.4-S3.5; Table 3.2). For C_3 species, I found allometries between cells that arose from different precursors, i.e., cells of mestome sheath vs. mesophyll, epidermis and parenchymatous bundle sheath, and xylem vs. parenchymatous bundle sheath cells (Figure 3.3). Allometries among cells arising from different developmental precursors in C_3 species suggest selection for coordination of metabolism and transport (Brodribb et al., 2013). In the C_4 species, the independence of cell sizes of the parenchymatous bundle sheath from xylem, and mestome sheath from mesophyll, is consistent with the additional constraints imposed by their Kranz anatomy, including the necessity for large sheath cells, irrespective of mesophyll cell sizes (Christin et al., 2013). The large C_4 sheath cells, with specialized metabolism and transport, have much more extensive plasmodesmatal connections with the mesophyll than sheath cells of C_3 species, which presumably act as an alternative to coordination of cell size and interfacing cell

surface areas for transport function (Christin et al., 2013; Danila et al., 2016; Cadart & Heald, 2022).

I found several allometries that occurred only among terrestrial grasses, including the relationships of cell sizes in the parenchymatous bundle sheath vs. upper and lower epidermises. Overall, the aquatic species had consistently smaller epidermal cells than terrestrial grasses, potentially reflecting their generally less pronounced water storage and potentially a lower requirement for large bulliform cells that enables leaves to roll and thereby better avoid overheating and dehydrating under dry conditions (Ellis, 1976; Evert, 2006).

Allometries among cell, leaf and plant dimensions: cells as building blocks and hydraulic design

I found strong allometries between leaf dimensions and the sizes of their constituent cells (Figure 3.5; Table 3.2). Cell sizes (in addition to cell numbers) may make especially important contributions to leaf dimensions especially given the low airspace porosity of grass leaves (Figures S3.2-S3.3; Gázquez & Beemster, 2017). Thus, thicker grass leaves are associated with larger cells in the mesophyll and epidermises, and wider leaves with larger mesophyll and parenchymatous bundle sheath cells (Figures 3.5 and S3.6). Notably, the scaling of leaf width with the cell sizes in the mesophyll and the parenchymatous bundle sheath provides an anatomical mechanism for the global relationship of lower VLA_{major} in wider grass leaves (Baird et al., 2021). The major veins are patterned early by the procambium and thus greater mesophyll and parenchymatous bundle sheath cell expansion would space major veins further apart in wider leaves (Baird et al., 2021), a pattern supported by the negative relationship of VLA_{major} with cell sizes in those tissues (Figure S3.7). Thus, the allometric linkages of cell size and leaf dimensions enables stress tolerance traits to be

selected across levels of organization as smaller cells and narrower leaves, both linked with higher vein densities, would contribute to tolerance of drought (Cutler, Rains & Loomis, 1977; Baird et al., 2021).

I found strong allometries of xylem cell sizes with leaf length, leaf area and plant height (Figure 3.6; Table 3.2). These relationships are consistent with selection of larger xylem cells for greater biomechanical support, and hydraulic capacity to mitigate both the greater pathlength in longer leaves and the potentially higher evaporative loads in larger plants. Indeed, these trends are consistent with global trends for the scaling of plant height with xylem conduit sizes in the stems of taller plants, including trees (Figure 3.5; Sack et al., 2013; Olson et al., 2018; Baird et al., 2021). Likewise, the larger parenchymatous bundle sheath cells in leaves of taller grasses may provide greater storage and outside-xylem hydraulic conductance that would contribute to mitigating the hydraulic stresses associated with both larger plant size and greater exposure and thus, higher evaporative demand (Figure 3.5; Buckley, John, Scoffoni & Sack, 2015).

Geometric scaling was typical for the allometric relationships of cell sizes across grass species. Geometric scaling is consistent with both proportional cell expansion, and coordination of cell sizes for matched flows of water, nutrients and sugars (Granier & Tardieu, 1998; Van Volkenburgh, 1999; Brodribb et al., 2013; John et al., 2013; Cadart & Heald, 2022). The cases in which specific allometries departed from geometric scaling could be explained based on specific developmental causes and functional benefits for the disproportionate size of one cell type over another (Table 3.3). For example, the greater increase in cell sizes in the parenchymatous bundle sheath and upper epidermis relative to the mesophyll ($b > 1$) is consistent with a disproportionate investment in support functions including water storage in epidermises, and bundle sheath (Griffiths, Weller, Toy & Dennis, 2013) and for epidermal bulliform cells influencing mechanical

protection and leaf rolling during dehydration (Ellis, 1976; Evert, 2006) which would protect leaves with larger mesophyll cells (Figure 3.3). Further, the less-than-geometric scaling in the cell size of type II relative to type I xylem ($b < 1$) is consistent with the optimization of vascular system design, as type I xylem are present only in major vein orders, which decline in vein length per area in wider leaves (Figure 3.3; Table 3.3; Baird et al., 2021). Thus, a disproportionate increase in type I relative to type II xylem cell size would compensate at least in part for the effect of declining vein length per area of major veins on vein transport efficiency and also provide greater mechanical rigidity (Table 3.3). Several of the allometries of leaf and plant dimensions with cell areas exhibited greater-than-geometric scaling, which would arise for several reasons. First, the greater than geometric scaling of leaf width with the cell areas of mesophyll and the parenchymatous bundle sheath ($b > 0.5$) is consistent with wider leaves being determined by greater cell numbers even more than by larger cells, with a particular role of the larger diameter veins in wider leaves (Figure 3.5; Table 3.3; Pantin, Simonneau & Muller, 2012; Gázquez & Beemster, 2017; John et al., 2017). This contrasts with the geometric scaling of leaf thickness with the cell areas of mesophyll and the epidermises, which indicates a greater role for cell size than cell number in driving thickness differences. Further, the greater-than-geometric scaling of leaf length, leaf area and culm height with xylem cell areas ($b > 0.5$ for leaf length and culm height, $b > 1$ for leaf area) is consistent with optimization of the vascular system design, as hydraulic conductance through xylem conduits increases as a function of the radius to the fourth power, so xylem would not need to increase proportionally in size to counteract the impact of increasing path length in longer leaves and taller grass shoots (Nobel 2020).

Contrasting leaf allometries align with key morphological divergences between grasses and eudicots

Grasses and eudicots were similar in several anatomical allometries, including geometric scaling of cell areas of the epidermises, and of the lower epidermis vs. the parenchymatous bundle sheath, consistent with coordinated development and function (Figure 3.3, 3.5-3.6; Table 3.2). However, several trends differed for grasses. The scaling of xylem cell sizes with leaf dimensions in grasses, not observed for eudicots, is consistent with the specific importance of cell sizes for biomechanical support and axial hydraulic transport in longer grass leaves (Figure 3.6). The less than geometric scaling of cell areas of mesophyll vs. upper epidermis in grasses, but geometric scaling in eudicots, is consistent with many grass leaves investing in large bulliform cells for storage and leaf rolling movements, a specialization typically not observed in eudicots (Figure 3.1; Table 3.3). The geometric scaling of leaf thickness vs. cell area of the upper epidermis in grasses, but greater than geometric scaling in eudicots, indicates coordinated contribution of cell size to leaf thickness in grasses and a greater contribution of cell layers to thickness in eudicots. This is consistent with eudicot leaves having many palisade layers and the lower proportion of airspace in grass leaves relative to eudicots (Figure 3.5, Figures S3.2-S3.3). While these differences between grasses and eudicots are consistent with their contrasting structure, sampling additional diversity will improve our ability to generalize; for example, I do not know whether the trends I report here for grasses are generalizable more broadly to monocots. Similarly, it may be possible to resolve similar allometries in some eudicot lineages, depending on taxonomic scale.

Allometric scaling of photosynthetic rate with cell size in grasses

Across grass species, light-saturated photosynthetic rate was strongly related to cell sizes. Our data provide a novel resolution of the relationship across grass species of A_{mass} with coordinated changes in cell cross-sectional size across the mesophyll, epidermises, parenchymatous bundle sheath, mestome sheath, and type I and II xylem (Figure 3.7; Table 3.2). That photosynthetic rate coordinates with cell size across cell types indicates that the separate allometries between procambium and nonprocambium derived cell types converge to maximize photosynthetic function (Figure 3.7; Figure S3.7).

Notably, light-saturated photosynthetic rate can be limited by many factors (Niinemets, Díaz-Espejo, Flexas, Galmés & Warren, 2009; Salvi, Smith, Adams, McCulloh & Givnish, 2021), and A_{mass} in particular is influenced by structural relative to photosynthetic allocation. Leaves with high A_{mass} allocate more mass to photosynthetic structure relative to structural components that increase leaf longevity (Wright et al., 2004); thus, a higher A_{mass} can arise from a higher A_{area} and/or lower *LMA* (Sack et al., 2013). I expected that smaller-celled leaves would have higher A_{mass}, not due to direct causality but from several structural effects. First, larger cells, and particularly larger cells in the mesophyll (Figure 3.5), were associated with thicker leaves, as found for eudicots (John et al., 2013, 2017) and would correspond to a higher number of chloroplasts (Ellis & Leech, 1985) and a higher concentration of photosynthetic machinery per leaf area (Koike, 1988; Garnier et al., 1999) and thus, a higher A_{area} (Niinemets, 1999). Second, I expected that small cells would be related to higher *LMA* through a higher concentration of cell wall material per leaf area (John et al., 2017), and, as $A_{mass} = A_{area}/LMA$, this higher *LMA* would correspond to a lower A_{mass} for small-celled species. Indeed, I found that higher *LMA* was related to smaller cell size in several tissues, including the mesophyll, epidermises and parenchymatous

bundle sheath (Figure S3.7). Third, VLA_{major} may also contribute substantially to higher LMA (Sack et al., 2013; John et al., 2017), and small mesophyll and bundle sheath cells were associated with more closely-spaced veins and thus higher VLA_{major}. While a higher VLA_{major} is implicated in hydraulic function and contributes to higher A_{area} in grasses (Baird et al., 2021), across species, the contribution of high VLA_{major} to a higher LMA in small-celled species would contribute to a low A_{mass} in small-celled species, and higher A_{mass} in large-celled species. Finally, the association of higher A_{area} with larger type I and type II xylem conduits (Figure S3.7) is consistent with these larger conduits providing greater hydraulic supply that enables greater stomatal opening and higher photosynthetic gas exchange (Sack & Scoffoni, 2013). Thus, the association between A_{mass} and cell sizes in all tissues are consistent with multiple expected impacts of cell size on A_{area} and/or LMA (Figure S3.7). The possibility that cell size is a relatively simple predictor of mass normalized photosynthetic productivity in grasses is a finding with potential applications both in understanding the ecology of diverse grass species and for improving crop productivity.

Tables

Table 3.1. Glossary of terminology related to allometry, leaf anatomy and grass development.

Term	Definition
Allometry	Study of size related properties, i.e. dimensions, mass, and/or metabolic processes and consequences for biological function (Huxley, 1932; Niklas, 1994).
Bulliform cell	Specialized enlarged upper epidermal cells that regulate leaf rolling and unrolling via changes in cell turgor (Ellis, 1976; Evert, 2006).
C_4 photosynthesis	Photosynthesis that occurs through compartmentalizing and concentrating CO_2 at sites of carbon reduction within bundle sheath, leading to elevated rates of carbon accumulation and minimized photorespiratory losses (Dengler et al., 1985; Sage, 2004; Christin et al., 2013).
Cell size	The cross-sectional area of the specified cell type.
Culm height	The height of the central grass shoot, typically quantified after flowering, and preceded by shoot elongation (Clayton et al., 2006; Evert, 2006).
Epidermal cell	Cells that form the outer layer of the plant, i.e. upper and lower surface of leaves, regulating gas exchange and providing protection of internal cells (Evert, 2006).
Furrow	The intercostal zone between vascular bundles that is often much thinner than the leaf section where vascular bundles and mesophyll occur (Ellis, 1976, e.g. Figure S3.3).
Geometric scaling	Proportional changes in dimensional size across species, individuals or organs; indicated by $b = 1$ (i.e., isometry) for relationships among dimensions of the same scale, i.e., for lengths with lengths or areas with area, and $b = 0.5$ for relationships of areas with lengths (Huxley, 1932; Niklas, 1994; John et al., 2013).
Intercalary meristem	The growing region at the base of grass leaves, where cells divide, expand and differentiate; surrounded by the grass sheath (Skinner & Nelson, 1994; Fournier et al., 2005; Evert, 2006).
Kranz anatomy	Specialized conformation of leaf cells and tissues, with mesophyll cells arranged closely to parenchymatous bundle sheath, facilitating CO_2 concentration from mesophyll to bundle sheath, and CO_2 assimilation in bundle sheath (Dengler et al., 1985; Sage, 2004; Christin et al., 2013).
Mesophyll cell	Cells that contain chloroplasts and generate sugars via photosynthesis (Evert, 2006).
Mestome sheath cell	Inner layer of thick-walled cells that surround vascular bundles, interior to the bundle sheath in most grasses, and is the only sheath in some C_4 grasses, i.e. location for carbon reduction; hypothesized to function for regulating water, sugar and hormonal transport in C_3 and C_4 grasses with both sheaths. Arises from procambium (Dengler et al., 1985; Evert, 2006).
Parenchymatous bundle sheath cell	Outer layer of thin-walled parenchymatous cells that surrounds vascular bundles and functions for water and nutrient storage, and regulating water, sugar and hormonal transport; in C_4 plants, location of carbon reduction (Dengler et al., 1985; Evert, 2006; Griffiths et al., 2013).
Plasmodesmata	Channels connecting plasma membranes of adjacent cells that function for symplastic transport, i.e. exchange of cytoplasmic materials, including proteins and sugars (Evert, 2006; Danila et al., 2016).
Precursor cell	Undifferentiated but often identifiable cells distinct in properties that indicate their mature cell type, e.g. procambium (Evert, 2006)
Procambium	Precursor cells to vascular cell types, i.e. xylem, phloem and mestome cells, during leaf development, distinct in cytoplasm density, degree of vacuolation and cell elongation (Dengler et al., 1985; Nelson & Dengler, 1997; Evert, 2006).
Type I xylem cell	Enlarged xylem present in major vein orders; much larger but less numerous than type II xylem. Arises from procambium (Nelson & Dengler, 1997; Fournier et al., 2005; Baird et al., 2021).
Type II xylem cell	Smaller xylem present in all vein orders; much smaller but more numerous than type I. Arises from procambium (Nelson & Dengler, 1997; Evert, 2006; Baird et al., 2021).

Table 3.2. Framework of hypotheses tested in this study, rationale for hypotheses, traits measured and if the hypothesis was supported. See Table 3.1 for definitions of terminology.

	Hypothesis	Rationale	Relationships measured (y vs. x)	Hypothesis supported
1.	Positive allometries among cell cross-sectional areas	Cells may have proportional development, reinforced by integrated function by cell size coordination.	The cross-sectional areas of: Epidermises vs. mesophyll; Epidermises vs. parenchymatous bundle sheath; Epidermises vs. mestome sheath; Epidermises vs. type I xylem; Epidermises vs. type II xylem; Mesophyll vs. parenchymatous bundle sheath; Mesophyll vs. mestome sheath; Mesophyll vs. type I xylem; Mesophyll vs. type II xylem; Parenchymatous bundle sheath vs. mestome sheath; Parenchymatous bundle sheath vs. type I xylem; Parenchymatous bundle sheath vs. type II xylem; Mestome sheath vs. type I xylem; Mestome sheath vs. type II xylem; Type I vs. type II xylem.	yes
2.	Positive allometries of leaf dimensions and the cell cross-sectional areas of constituent cells	Cells are building blocks of dimensions of the whole organ, particularly that of leaf thickness and width.	Leaf thickness and leaf width vs. the cross-sectional areas of epidermises; Leaf thickness and leaf width vs. the cross-sectional area of mesophyll; Leaf thickness and leaf width vs. the cross-sectional area of parenchymatous bundle sheath; Leaf thickness and leaf width vs. the cross-sectional area of mestome sheath; Leaf thickness and leaf width vs. the cross-sectional area of type I xylem; Leaf thickness and leaf width vs. the cross-sectional area of type II xylem.	yes
3.	Positive allometries of leaf size and plant height with cross-sectional areas of procambium derived cell types	Longer leaves and taller plants would require larger xylem for optimal hydraulic design/delivery. Mestome sheath cells may also show scaling, from being derived from the procambium.	Leaf length, leaf area and culm height vs. the cross-sectional area of mestome sheath; Leaf length, leaf area and culm height vs. the cross-sectional area of type I xylem; Leaf length, leaf area and culm height vs. the cross-sectional area of type II xylem.	yes
4.	Grasses would show similar leaf anatomical scaling as eudicots, with exceptions arising from their different leaf morphology	In grasses, the fewer cell layers, highly elongated leaf blade and specialized roles of bundle sheath and bulliform epidermal cells drives different allometries	Leaf length, leaf area and culm height vs. the cross-sectional areas of epidermises; Leaf length, leaf area and culm height vs. the cross-sectional area of mesophyll; Leaf length, leaf area and culm height vs. the cross-sectional area of parenchymatous bundle sheath.	yes
5.	Positive allometries of light-saturated photosynthetic rate per leaf mass (A_{mass}) and cell cross-sectional areas	Allometries of cell dimensions in hypothesis one would arise from the coordination of cell function (transport, metabolism and/or photosynthesis)	A_{mass} vs. the cross-sectional areas of epidermises; A_{mass} vs. the cross-sectional area of mesophyll; A_{mass} vs. the cross-sectional area of parenchymatous bundle sheath; A_{mass} vs. the cross-sectional area of mestome sheath; A_{mass} vs. the cross-sectional area of type I xylem; A_{mass} vs. the cross-sectional area of type II xylem.	yes

Table 3.3. Explanations for allometries of grass leaf cells that differed from expectations based on geometric scaling. Expectations for *b* may depart from geometric scaling when 1) developmental processes for cells differ in the timing or rates of growth as would apply to scaling with type II xylem or mestome sheath which both form relatively late in the sequence of leaf and vein development, and leads to disproportionate scaling of non-procambium derived tissue with mestome sheath cells in C_3 species, and of type II xylem and bundle sheath in C_3 species, and of type II xylem with type I xylem across all species, 2) due to selection on function of a specific tissue, as would apply to the scaling with the upper epidermis or bundle sheath, which would increase in size greater than mesophyll, leading to greater storage and support in upper epidermis and bundle sheath and departed scaling of mesophyll vs. upper epidermis, mesophyll vs. bundle sheath, 3) due to constraints imposed by coordinated optimal vascular design, as would apply to the disproportionate scaling of type II xylem with type I xylem, as type II xylem occur only in major veins, and thus need to increase in size to compensate for the declining density of major veins and 4) for relations of cell areas and whole leaf dimensions, as different cell types differ in number, which would impact the contribution of one cell type scaling with a whole leaf dimension.

[a] = Our analysis of data from (John et al., 2013).

Allometry	y vs. x relationship	Allometric slope b observed	Explanation for expected slope b
1. Scaling of cell areas within and across tissues§	mesophyll vs. upper epidermis	< 1	Disproportionately large increase of upper epidermis required for storage and support relative to increase of mesophyll cell size
	mesophyll vs. bundle sheath	< 1	Disproportionately large increase of bundle sheath required for storage and support relative to mesophyll cell size
	type II xylem vs. type I xylem	< 1	For the major and minor vein systems to maintain matched transport efficiency across leaves of different size, type I xylem conduit sizes must increase disproportionately relative to type II xylem to compensate for the declining vein density of major veins.
	type II xylem vs. mestome sheath	> 1	Shorter development time for mestome sheath cells than type I xylem would result in diminishing scaling as mestome sheath cells form relatively late in the sequence of leaf and vein development.
	mestome sheath vs. bundle sheath	< 1	Longer development time for bundle sheath than mestome sheath enables departed scaling, as mestome sheath cells forms relatively late in the sequence of leaf and vein development, reinforced by functional coordination of sheath sizes, to match radial transport capacity through both sheaths.
	type II xylem vs. bundle sheath	< 1	Longer development time for bundle sheath than type II xylem enables departed scaling, as type II xylem forms relatively late in the sequence of leaf and vein development, reinforced by functional coordination, to match radial transport capacity out of the xylem with axial (longitudinal) transport capacity.
	mestome sheath vs. upper epidermis	> 1	Longer development time for mesophyll than mestome sheath enables disproportionate scaling, as mestome sheath forms relatively late in the sequence of leaf and vein development, reinforced by functional coordination of sheath and epidermal cell sizes, to match transport capacity with demand.
	mestome sheath vs. lower epidermis	> 1	"
2. Scaling of leaf and plant dimensions with nonxylem cell areas	leaf width vs. mesophyll	> 0.5	Cell size in a given tissue is one of a series of contributors to whole leaf dimensions, including also numbers of cells or cell layers, and cells of other tissues.
	leaf width vs. bundle sheath	> 0.5	"
	culm height vs. bundle sheath	> 0.5	Less than proportionate increases of bundle sheath cell size relative to culm height (and thus disproportionate increases in culm height relative to bundle sheath) would be sufficient to limit path length constraints to flow, as the bulk of path length is through xylem.
3. Scaling of leaf and plant dimensions with xylem cell areas	leaf length vs. type I xylem	> 0.5	Less than proportionate increases of xylem cell size relative to organ length or plant size (and thus disproportionate increases in organ length and plant size relative to xylem) would be sufficient to limit path length constraints to flow, as flow rate through xylem increases as the radius to the fourth power, and thus would not need to increase proportionally.
	leaf length vs. type II xylem	> 0.5	"
	culm height vs. type I xylem	> 0.5	"
	culm height vs. type II xylem	> 0.5	
Eudicot scaling[a] 4. Similar scaling of grasses and eudicots, except for those of mesophyll vs. upper epidermis	mesophyll vs. upper epidermis	< 1	Scaling would be lower in grasses due to disproportionately large increase of upper epidermis required for mechanical support, storage and leaf movements relative to increase of mesophyll cell size
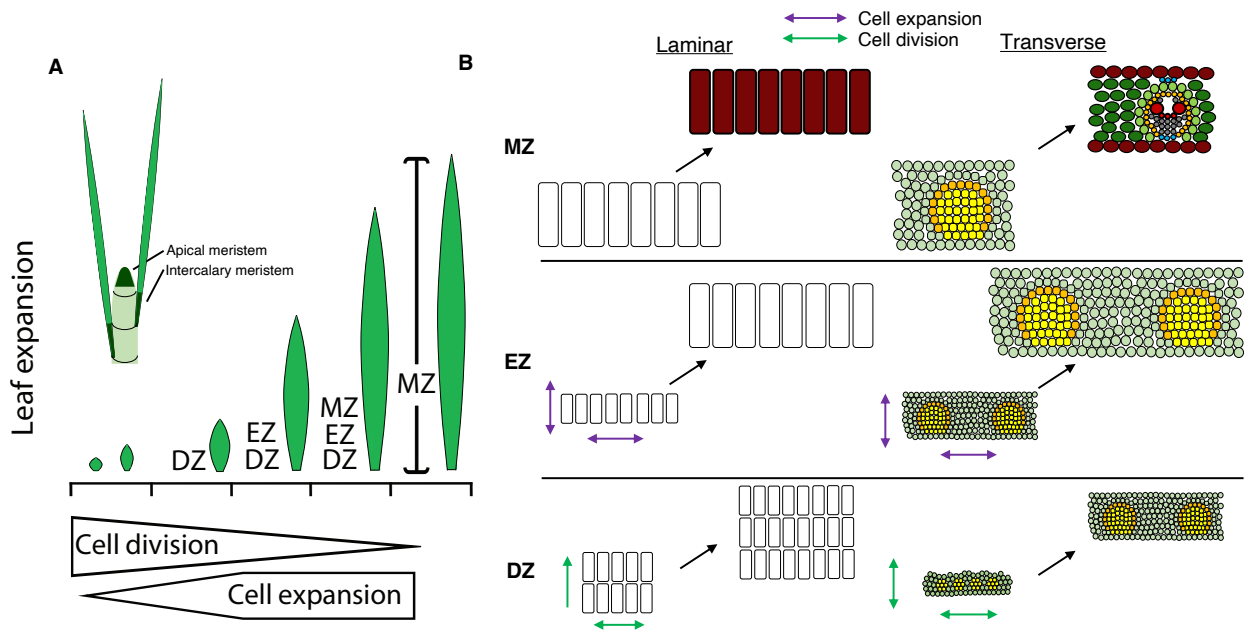
Figures

Figure 3.1. Grass leaf development. (A) In grasses, leaf expansion is restricted to distinct

developmental zones driven by the generation of the leaf primordium via the apical meristem.

Although growth initially begins via the apical meristem, leaf growth becomes restricted to the

intercalary meristem at the base of the growing leaf in which cells proliferate in the division zone

(DZ), expand laterally and longitudinally in the expansion zone (EZ), and complete their

differentiation in the maturation zone (MZ). Thus, growth occurs as cells continuously

proliferate in the DZ and then expand in the EZ. **(B)** Laminar, or projected viewpoint, and

transverse visualizations of the different growing zones of a typical C_3 grass, with epidermal

cells in the laminar column, and all cell types depicted in the transverse column, with

procambium cells shown in orange and yellow (mestome cells shown in orange) and non

procambium cells shown in light green. Bundle sheath precursors are the cells surrounding the

orange mestome sheath cells. The intercalary meristem is typically covered by the grass sheath,

64

and thus protected, but this was omitted from panel **(A)** so as to illustrate the location of the intercalary meristem with respect to the shoot apical meristem. Panel **(A)** was originally published in Baird et al., 2021 and modified to include a visualization of the two grass shoot meristems for this study, and panel **(B)** was created based on findings from (Dengler et al., 1985; Skinner & Nelson, 1994; Van Volkenburgh, 1999; Fournier et al., 2005; Evert, 2006; Granier & Tardieu, 2009; Baird et al., 2021).
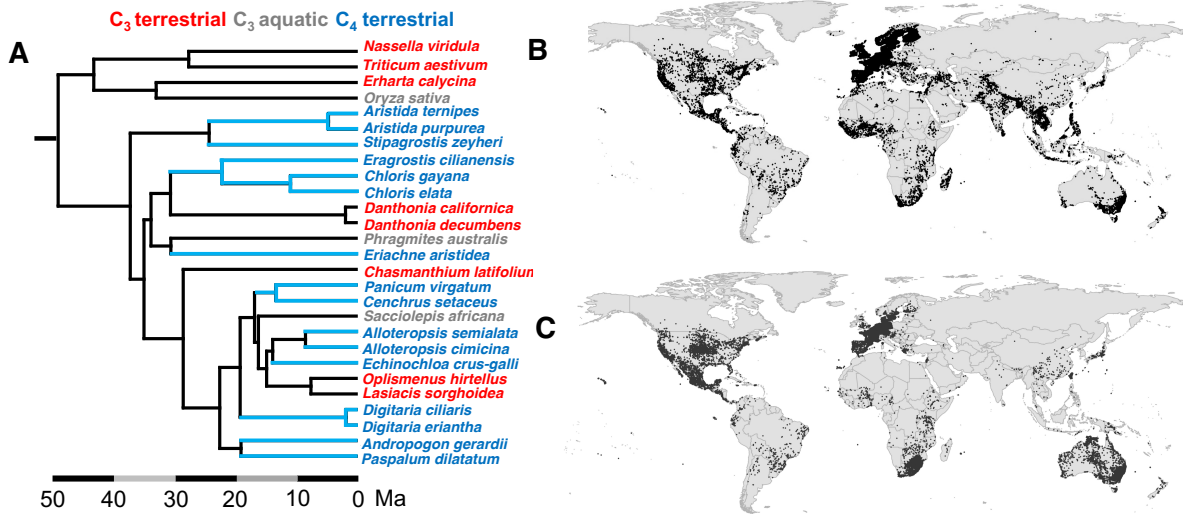
Figure 2. Phylogenetic tree used to account for the influence of species relatedness on scaling relationships, and species distribution maps. (A) All grass species included in the study, colored as (B) C3 grass species and (C) C4 grass species. Blue branches in (A) indicate C4 taxa. (B) and (C) reflect independent evolutions...
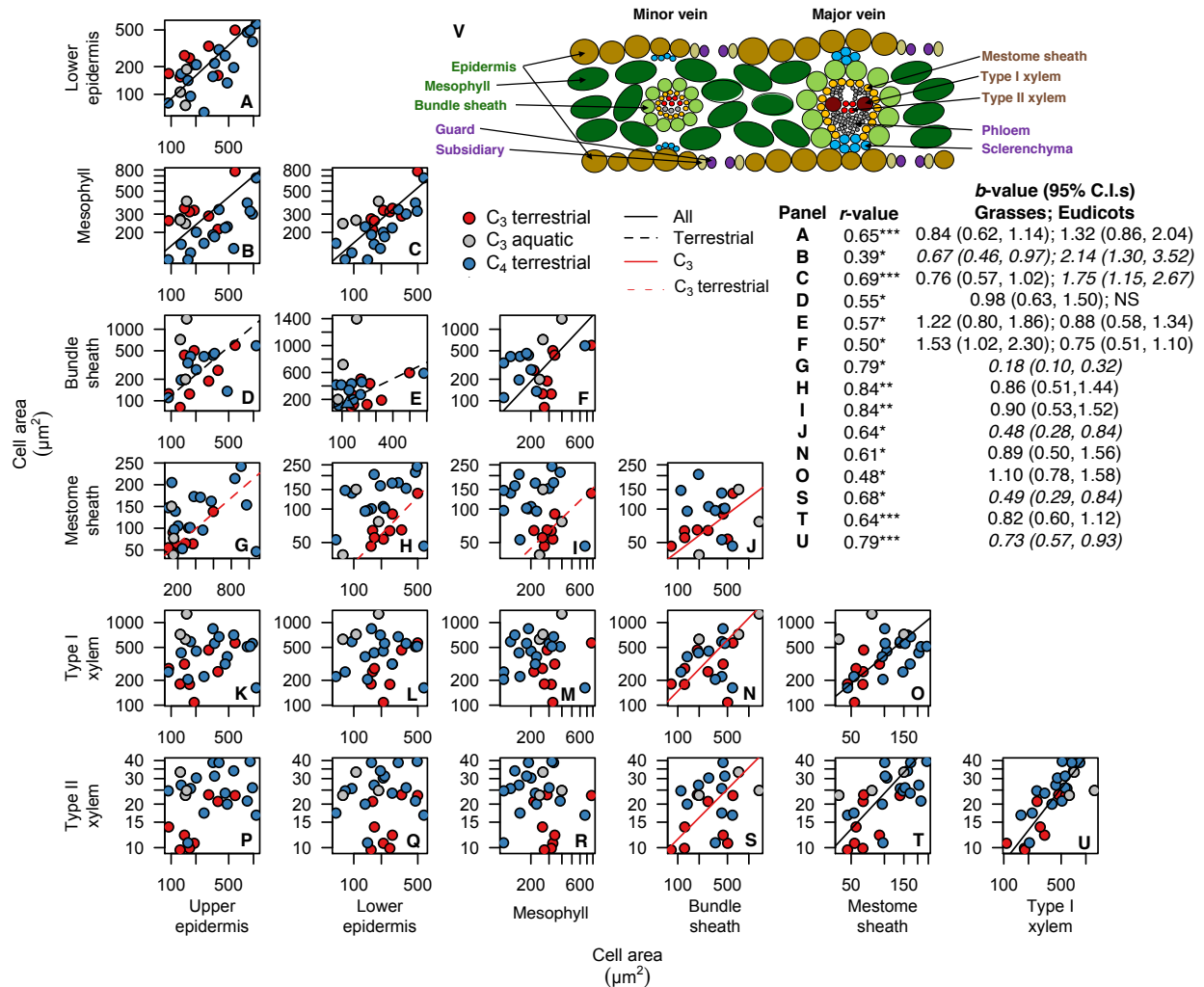
Figure 3.3. Grass cell size allometries and anatomy. **(A)** – **(U)** Allometries across tissues of grass leaves. (v) schematic of a grass cross-sectional anatomy; green and brown labels in **(V)** represent cells derived from non-procambium and procambium precursor cells, respectively (unmeasured cells in purple). Each point is one species, $n = 11$ C_3 (eight terrestrial, three aquatics) and $n = 13$ C_4 species. Fitted lines are phylogenetic reduced major axis (PRMA) regressions with statistics on the right and in Table S3.3. Line colors indicate that the relationship was significant across a specific set of grasses, with black lines across all species, red lines across C_3 species, and segmented lines across the terrestrial species either across all

grasses or only C_3 grasses. *b*-values are presented for grasses and eudicots; italics indicate departure from geometric scaling. See Table 3.1 for cell type definitions. *$p < 0.05$, **$p < 0.01$, ***$p < 0.001$.
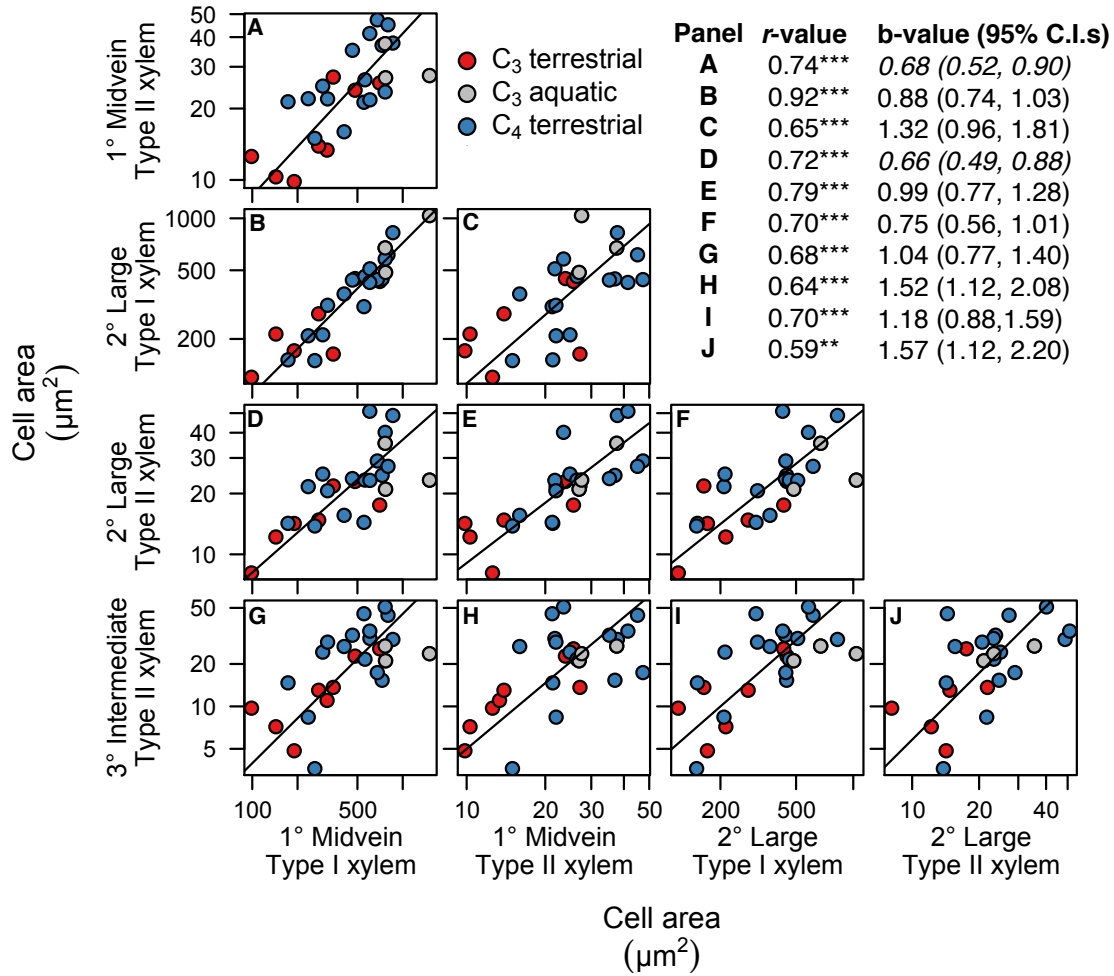
Figure 3.4. Allometries of xylem cells within and across vein orders. Each point is one species, including $n = 11$ C_3 (eight terrestrial) and $n = 16$ C_4 species. Allometries for 4° xylem with cell types of other vein orders were not significant and are omitted (see Table S3.4). Lines were fit with phylogenetic reduced major axis regressions (*PRMA*) and statistics and parameters are found in Table S3.4. Italics indicate departure from geometric scaling. See Table 3.1 for cell type definitions. $*p < 0.05$, $**p < 0.01$, $***p < 0.001$.

Legend entries:
- C₃ terrestrial 3L
- C₃ aquatic 3L
- C₄ terrestrial 3L
- C₄ terrestrial 4L
- All

- C₃ terrestrial
- C₃ aquatic
- C₄ terrestrial
- All
- Terrestrial
- C₃ terrestrial

- All
- C₃
- C₄
- Terrestrial
- C₃ terrestrial 3L
- C₃ terrestrial

- All
- C₃
- C₄
- Terres...
- Terrestrial
- C₃ terrestrial

Panel A: $r = 0.40*$; $b = 0.65\ (0.45, 0.95)$, $0.62\ (0.42, 0.93)$
Panel B: $r = 0.49*$; $b = \mathbf{0.42\ (0.29, 0.61)}$, $\mathbf{0.96\ (0.61, 1.5)}$
Panel C: $r = 0.46*$; $b = 0.49\ (0.35, 0.71)$, $0.73\ (0.44, 1.2)$

Panel D: $r = 0.52**$; $b = 1.5\ (1.1, 2.1)$
Panel E: $r = 0.56*$; $b = 0.97\ (0.66, 1.4)$
Panel F: $r = 0.73*$; $b = 1.2\ (0.66, 2.2)$

Leaf thickness (cm)

Index

Mesophyll | Upper epidermis | Lower epidermis

Leaf width (cm)

Mesophyll | Parenchymatous bundle sheath | Type I xylem

Cell area

Index

Figure 3.5. Allometries of leaf morphological dimensions with leaf cell size as building blocks. (A) – **(P)** Allometries of leaf with leaf cell areas within tissues of grass leaves. Each point is one species, $n = 11$ C₃ (eight terrestrial in red, three aquatic in grey) and $n = 16$ C₄ species in blue. Fitted lines are phylogenetic reduced major axis (PRMA) regressions with statistics above each panel and in Table S3.5. Line colors indicate that the relationship was significant across a specific set of grasses, with black lines across all species, red lines across C₃ species and segmented lines across the terrestrial species either across all grasses or only C₃ grasses. *b*-values are presented for grasses and eudicots for comparisons with leaf thickness and bolded when significantly different. Italics indicate departure from geometric scaling. See Figure 3.3 and Table 3.1 for cell type definitions. *$p < 0.05$, **$p < 0.01$.

Figure 3.6. Allometries of leaf morphological and plant dimensions with leaf cell size for

hydraulic design. (A) – **(P)** Allometries of leaf and plant dimensions with leaf cell areas within

tissues of grass leaves. Each point is one species, $n = 11$ C_3 (eight terrestrial in red, three aquatic

in grey) and $n = 16$ C_4 species in blue. Fitted lines are phylogenetic reduced major axis (PRMA)

regressions with statistics above each panel and in Table S3.5. Line colors indicate that the

relationship was significant across a specific set of grasses, with black lines across all species,

red lines across C_3 species, and segmented lines across the terrestrial species either across all

grasses or only C$_3$ grasses. *b*-values are presented for grasses and eudicots for comparisons with leaf thickness and bolded when significantly different; italics indicate departure from geometric scaling. See Figure 3.3 and Table 3.1 for cell type definitions. *$p < 0.05$, **$p < 0.01$, ***$p < 0.001$.

Figure 3.7. Allometries of mass-based photosynthetic rate with leaf cell size. (A) – (G)

Allometries of light-saturated mass-based leaf photosynthetic rate with leaf cell areas within tissues of grass leaves. Each point is one species, n = 11 C_3 (eight terrestrial in red, three aquatic in grey) and n = 16 C_4 species in blue. Fitted lines are phylogenetic reduced major axis (PRMA) regressions with statistics above each panel and in Table S3.6. Line colors indicate that the relationship was significant across a specific set of grasses, with black lines across all species and the blue line in **(A)** across only C_4 species. See Figure 3.3 and Table 3.1 for cell type definitions. *p < 0.05, **p < 0.01, ***p < 0.001.

73

Appendix 3.1

Relationship of leaf developmental and evolutionary allometries, and insights into development and function

Our study focuses on allometric relationships for leaf cell sizes in mature leaves across grass species. Here I describe how these relationships would arise from, and provide insights into the underlying developmental processes within given leaves, as well as adaptation of the integrated phenotype for function across different species. I here provide a brief theoretical synthesis of (1) the linkage between allometries that emerge among cells within given growing leaves (intraspecific "developmental allometries" ; MacAdam, Volenec & Nelson, 1989; Allard, Nelson & Pallardy, 1991; Rademacher & Nelson, 2001; Taneda & Terashima, 2012) and the allometries that hold across mature leaves of different species (interspecific "evolutionary allometries"; Sack et al., 2012; John, Scoffoni & Sack, 2013; Baird et al., 2021), and (2) how the allometric slopes can provide information on developmental processes and selection.

1.   The relationship of leaf developmental and evolutionary allometries

The pervasiveness of allometric relationships documented across taxonomic and biological scales highlights their importance for organismal function and the constraints they impose on evolution (Poorter & Sack, 2012; Pélabon et al., 2014). Theory to explain allometries, their slopes, and their inter-relationships across scales have identified two types of "origin", i.e., in the *development* of the organism and its organs (Pearsall, 1927; Huxley, 1932; Niklas, 1994; John et al., 2013; Baird et al., 2021); or in *functional optimization* of mature phenotypes based on, e.g., structural, biomechanical, metabolic or transport principles (Murray, 1926; LaBarbera, 1990; Niklas, 1994; West, Brown & Enquist, 1997; Pélabon et al., 2014). Here I draw on this background to synthesize

theory for how the development of cells within and across leaf tissues would determine cell size allometries observed across the mature leaves of different species. Further, I describe how selection would be expected to reinforce or modify these allometries.

Of the numerous types of allometries that can be described across scales of taxonomy, space and time, three in particular have been commonly measured to explain and predict the relationships between structural variables (Gould, 1966; Pélabon et al., 2014; Neiro, 2020). "Ontogenetic" or "developmental" allometries are relationships of traits of a given individual across different developmental stages. "Static" allometries are relationships of traits within a species for individuals at the same developmental stage (e.g., at maturity), in other words, the association of traits that coincide with size variation within a species. "Interspecific evolutionary" allometries are relationships of traits across species, for individuals considered at the same developmental stage (e.g., at maturity). In general, one type of allometry would not necessarily be expected to correspond to another type; a developmental allometry of two traits for a given species may differ in slope and intercept from a static allometry of the two traits across individuals of that species, or the evolutionary allometry across related species (Gould, 1966; Neiro, 2020). Here, I focus on developmental and evolutionary allometries, i.e., relationships within given individuals and across species, and do not focus on the static allometries that would be intermediary in scale, across individuals (of the same or different genotypes) of given species. In our study I average cell sizes for given species across individuals, given insufficient replication to analyze variation in allometries across individuals. Notably, static allometries are a critical avenue for future research, especially, for example, in crop improvement and design of new cultivars, and for plant adaptation (Feldman et al., 2017; Vasseur, Violle, Enquist & Vile, 2023).

It is clearly intuitive that when development processes are conserved across species, as for grass leaves, there is potential for evolutionary allometries to reflect underlying developmental allometries (Hepworth, Caine, Harrison, Sloan & Gray, 2018; Baird et al., 2021). Given that a leaf expands as an organized whole, cells of tissues X and Y that originate from the same precursor cell type would have similar average initiation and maturation times (Gázquez & Beemster, 2017). Further, cells increase proportionally in size due to similar average rates of expansion (Niklas 1994; Gázquez & Beemster, 2017; Baird et al., 2021). Consequently, *geometric scaling* would arise between cell sizes in developing leaves, where cell lengths (L), areas (A) or volumes (V) would scale together as $A \propto A^1$, $L \propto A^{1/2}$, and $A \propto V^{2/3}$ (Sack et al., 2012; John et al., 2013; Baird et al., 2021). On the other hand, for cells that originate from the same or different precursors, and differ in initiation or maturation times or expansion rates, the developmental allometry may depart from geometric. For example, xylem and mestome sheath cells arise from the vein procambium, a dividing tissue that differentiates from lamina cells even after many of those cells have already begun expanding (Sachs, 1975; Nelson & Dengler, 1997; Figure 3.1) and thus xylem or mestome cell sizes may not increase with mesophyll cell sizes strictly proportionally, and thus the allometric slope may differ from the geometric expectation of $b = 1$.

An evolutionary allometry between two traits, for a group of related species, can be considered a consequence of the developmental allometries that hold between the two traits in the development of individuals of the species. For example, if a set of species all show the same developmental scaling of cell sizes in tissues X and Y, then, at leaf maturity, the across-species evolutionary allometry will have the same slope and intercept as the developmental allometry (Figure 3.A1A). However, even given a developmental allometry with a common slope (such as expected from geometric scaling), species may differ in the ratio of the sizes of cells Y relative to

X throughout development, for example due to cell Y having a greater initial size than X, and thereby have parallel developmental allometries with different intercepts (Figure 3.A1B-E). In this case, the evolutionary allometry may differ in slope from the developmental allometry (Gould 1966). If the species vary minimally in their developmental allometries, then the evolutionary slope should be similar to that of the developmental allometry (Figure 3.A1B). On the other hand, if species show great variation in developmental allometries, there would arise different trends for the evolutionary allometry, depending on how intercepts and slopes of the relationships for given species correspond to their final mature cell size. For example, if slopes are similar and intercepts are independent of mature cell size, there may be no significant evolutionary trend (Figure 3.A1C). However, if the intercepts are greater in species with larger mature cells then the evolutionary allometry will have a higher slope than the developmental allometry (Figure 3.A1D), and if the intercepts are lower in species with larger mature cells, then the evolutionary allometry will have a lower slope than the developmental allometry (Figure 3.A1E). Further, if species differ in the slopes of their developmental allometries, this too would influence the strength and parameters of the evolutionary allometry across species.

2. How the allometric slopes can provide information on developmental processes and selection
According to this theory, in many cases in which generalized underlying developmental allometries exist, evolutionary allometries may provide insights into developmental and functional coordination of cell sizes. Thus, when evolutionary allometries are geometric, this would likely reflect a generalized geometric developmental allometry across species, with conservative variation in the intercept, independent of cell size. This geometric scaling across mature leaves of different species that arises from development may further be reinforced for functional adaptation,

for example, when cells would be matched in volume or surface area for coordinated rates of metabolism or transport (Noblin et al., 2008; Marshall et al., 2012; Nobel, 2020). Thus, geometric allometries would arise due to conserved development constraints across species, especially in the case for cell types with similar precursors, and may also arise and/or be reinforced by selection for functional coordinated transport across tissues of different types.

On the other hand, especially in cases in which cells arise from different precursor tissues, or due to selection for specialized function, developmental allometries and evolutionary allometries may depart from geometric scaling. Indeed, the allometric scaling slope b for traits y and x is equivalent to the ratio of the relative growth rates of y and x (Huxley, 1932). Thus, for example, a slope b greater than expected from geometric scaling would arise for the cells of tissue y versus tissue x, if y cells have a greater mean relative expansion rate than x cells. A slope b less than expected from geometric scaling, i.e., a lower increase in the size of y than x cells, should arise if x cells have a greater mean relative expansion rate than y cells. The evolutionary allometry may show a lesser or a stronger difference in b from geometric expectation than the developmental allometry, depending on the variation in species' developmental allometries (as shown in Figure 3.A1), especially when species are selected for adaptive divergence in function. As species evolve differences in cell size, the ratios of cell sizes in different tissues may shift disproportionally with increasing cell sizes. This is analogous to a sapling growing into a tree, and investing more strongly in its trunk than its foliage, such that the mass of the trunk increases disproportionately to mass of foliage ($b > 1$; Poorter et al., 2012). Within a developing leaf, if cells of tissue y provide a support or storage function (analogous to the trunk) that requires disproportionate investment relative to cells of tissue x analogous to the foliage); a disproportional scaling (i.e., greater in slope) of the size of cells y to x would arise (Figure 3.A1d). Indeed, I found that grass epidermal cells increase

disproportionally in size relative to mesophyll cells across species, consistent with larger-celled species adaptating a disproportionately greater investment in upper epidermal cells in storage and, by shrinking with dehydration, enabling leaf rolling (Evert, 2006). In a contrasting scenario, if tissues y and x both contribute to a higher level dimension or function (z), then the relationship of z to the size of y or x cells will show a slope of $b < 1$ (Figure 3.A1e); this might occur, for example, for the relationship of leaf thickness to the size of mesophyll or epidermal cells, as greater numbers of cell layers (i.e., cell numbers in vertical profile) also contribute to leaf thickness. Notably, a b of zero (i.e., y independent of x) may arise if the cells of tissue y and x did not increase together, i.e., if they had separate windows of growth.

Additionally, specialized scaling of vascular tissues for functional optimization would be selected across the leaf blade. Thus, nongeometric scaling of cell sizes would arise between xylem cells of different vein orders, and between xylem cells and other leaf cells, based on optimal transport in branching and distribution systems (McCulloh, Sperry & Adler, 2003; Price, Knox & Brodribb, 2013). Indeed, one may hypothesize that disproportionate scaling should arise between xylem conduit diameters across vein orders in mature leaves, to optimize transport via a matched hydraulic conductance across vein orders. For example, the major vein orders contain type I and type II xylem, whereas $3°$ and higher vein orders only have type II xylem, which are an order of magnitude smaller in cell area (Table S3.1), Across leaves of grass species, the major vein diameters, conduit sizes and conduit numbers tend to increase with leaf size, but major vein density decreases in larger leaves as veins are spaced further apart, and minor vein sizes and density are unrelated to leaf width (Baird et al., 2021). Thus, one may hypothesize that for the major and minor vein systems to maintain a matched transport efficiency across leaves of different sizes, type I xylem conduit sizes would increase disproportionately relative to type II xylem to compensate for

79

the declining vein density of major veins. This hypothesis based on optimizing vein function would thus provide an explanation for the scaling of type II xylem with type I xylem across vein orders with $b < 1$.

Notably, in those cases when evolutionary allometries are not found among cells within a given organ, it would follow that cell size ratios are highly variable across species, independently of cell size. This $b = 0$ situation may be expected when considering cell types arising from different precursors, which can be selected for size independently. Examples include xylem cells arising from the vein procambium, which can achieve sizes independent of those of mesophyll cells arising from non-procambium lamina cells; or stomata, which arise from epidermal meristemoid cells, which originate at different times in leaf development (Torii, 2021). Additionally, the independence of cell sizes across tissues within a leaf would be expected when their functions are not directly linked—or, even if they are linked, when their quantitative association is in relation to a higher level dimension or trait. For example, stomatal size is developmentally independent of mesophyll cell size, based on a guard cell development process that is highly specialized relative to other epidermal and leaf cells (Torii, 2021), and, while stomatal and mesophyll cells have a coordinated function in photosynthetic gas exchange, the linkage would be related to higher level traits mediated by other properties. Thus, mesophyll cell surface area per leaf area (a function of cell size, but also of number of cell layers and arrangement) may be related to stomatal conductance (a function of stomatal size, but also of stomatal density; Sack & Buckley, 2016)
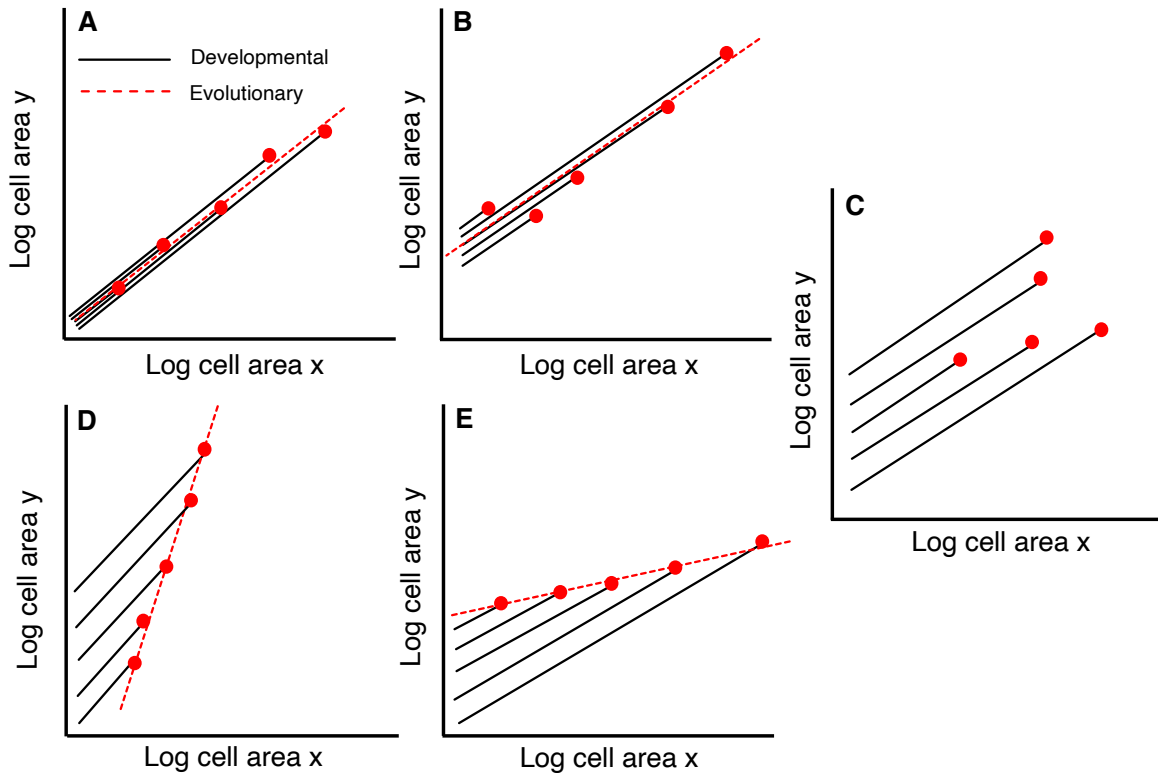
Figure 3.A1. The relationship between generalized developmental allometries arising from geometry (black lines for different species) relating the areas of cell type y with cell type x, and evolutionary allometries across the mature leaves of different species (red dotted lines through red points). Different scenarios visualized: **(A)** negligible differences across species in the intercept (representing the size ratio of cell y to cell x throughout development); **(B)** conservative, or **(C-E)** large differences across species in the intercept, that is **(C)** unrelated to mature leaf cell size or where differences across species in the intercept (representing the size ratio of cell y to cell x) is **(D)** greater or **(E)** smaller in species with larger mature cells. In cases **(A)** and **(B)** the evolutionary allometry would have similar slope to the generalized developmental allometry; in case **(C)**, there would be no significant evolutionary allometry, and in cases **(D)** and **(E)** the evolutionary allometry would differ in slope from the generalized developmental allometry.

Supplementary Materials

Supplementary Data Captions (see attached Excel Workbook)

Table S3.1. Species of grasses (Poaceae) included in the study, subfamily, tribe, C_3/C_4 photosynthetic pathway, BEP/PACMAD clade, 3L/4L i.e., three or four longitudinal vein orders, C_4 subtype, seed source, accession number, seed treatment for germination, terrestrial/aquatic, sun/shade, mean and ± standard errors of anatomical and morphological traits measured. Traits left blank for a given species indicates that this species did not have this trait, e.g. did not have bundle sheath and only had the inner sheath, and did not have the 4° vein. Traits with NA for a given species indicates that I did not ascertain quantifiable data for these species, e.g. 2° vein traits for Lasiacis sorghoidea.

Table S3.2. Parameters and statistics from parametric and nonparametric phylogenetic analyses of variance between C_3 and C_4 species for traits used in this study, and nonphylogenetic analysis of variance testing the influence of species identity versus individual replicate on species' trait values.

Table S3.3. Parameters and statistics for allometries of cell areas across grass leaf tissues. The variables tested, statistical method used, expected scaling exponent b, r- and p- values, scaling exponent b with 95% confidence intervals and the scaling coefficient a are provided, for log transformed data. Tests are provided considering the following groups: 1) all 27 grass species, 2) 24 terrestrial grass species, 3) 11 C_3 grass species, 4) eight terrestrial C_3 grasses and 5) 16 C_4 grass species (all terrestrial). Significant relationships were considered when $p < 0.05$,

and all parameters for a given test are bolded for these. Note: 21 of the 27 species have bundle sheath. Thus, relationships tested that include the bundle sheath are fitted across these 21 species, 18 species for terrestrial grasses, all 11 for the C_3 grasses, all 8 for terrestrial C_3 grasses and 10 for C_4 grasses. †Cell areas for xylem and bundle and/or mestome sheath cells averaged across vein orders. Italicized b-values indicate significant departure from geometric scaling.

Table S3.4. Parameters and statistics for allometries of vascular cell areas across grass leaf vein orders. The variables tested, statistical method used, expected b, r- and p-values, and the scaling exponent b with 95% confidence intervals and the scaling coefficient a are provided, for log-transformed data. Relationships were considered significant when $p < 0.05$, and all parameters given in bold face. Note: 21 of the 27 species have bundle sheath. Thus, relationships tested that include the bundle sheath were fitted across these 21 species. The phylogenetic method implemented was phylogenetic reduced major axis (PRMA). Tests including traits from the 4° small vein implemented non phylogenetic reduced major axis (SMA) as only seven species have this vein order. Italicized b-values indicate significant departure from geometric scaling.

Table S3.5. Parameters and statistics for allometries of cell areas with leaf and plant dimensions. The variables tested, statistical method used, expected scaling exponent b, r- and p-values, and the scaling exponent b with 95% confidence intervals and the scaling coefficient a are provided, for log-transformed data. Relationships were considered significant when $p < 0.05$, and all parameters given in bold face. Note: 21 of the 27 species have bundle sheath. Thus, relationships tested that include the bundle sheath are fitted across these 21 species. The

phylogenetic method implemented was phylogenetic reduced major axis (PRMA). †Cell areas

for xylem and bundle and/or mestome sheath cells averaged across vein orders. Italicized *b*-

values indicate significant departure from geometric scaling.

Table S3.6. Parameters and statistics for allometries of cell areas with leaf functional traits.

The variables tested, statistical method used, *r*- and *p*-values, and the scaling exponent *b* with

95% confidence intervals and the scaling coefficient *a* are provided, for log-transformed data.

Relationships were considered significant when $p < 0.05$, and all parameters given in bold face.

Note: 21 of the 27 species have bundle sheath. Thus, relationships tested that include the bundle

sheath are fitted across these 21 species. The phylogenetic method implemented was

phylogenetic reduced major axis (PRMA). †Cell areas for xylem and bundle and/or mestome

sheath cells averaged across vein orders.
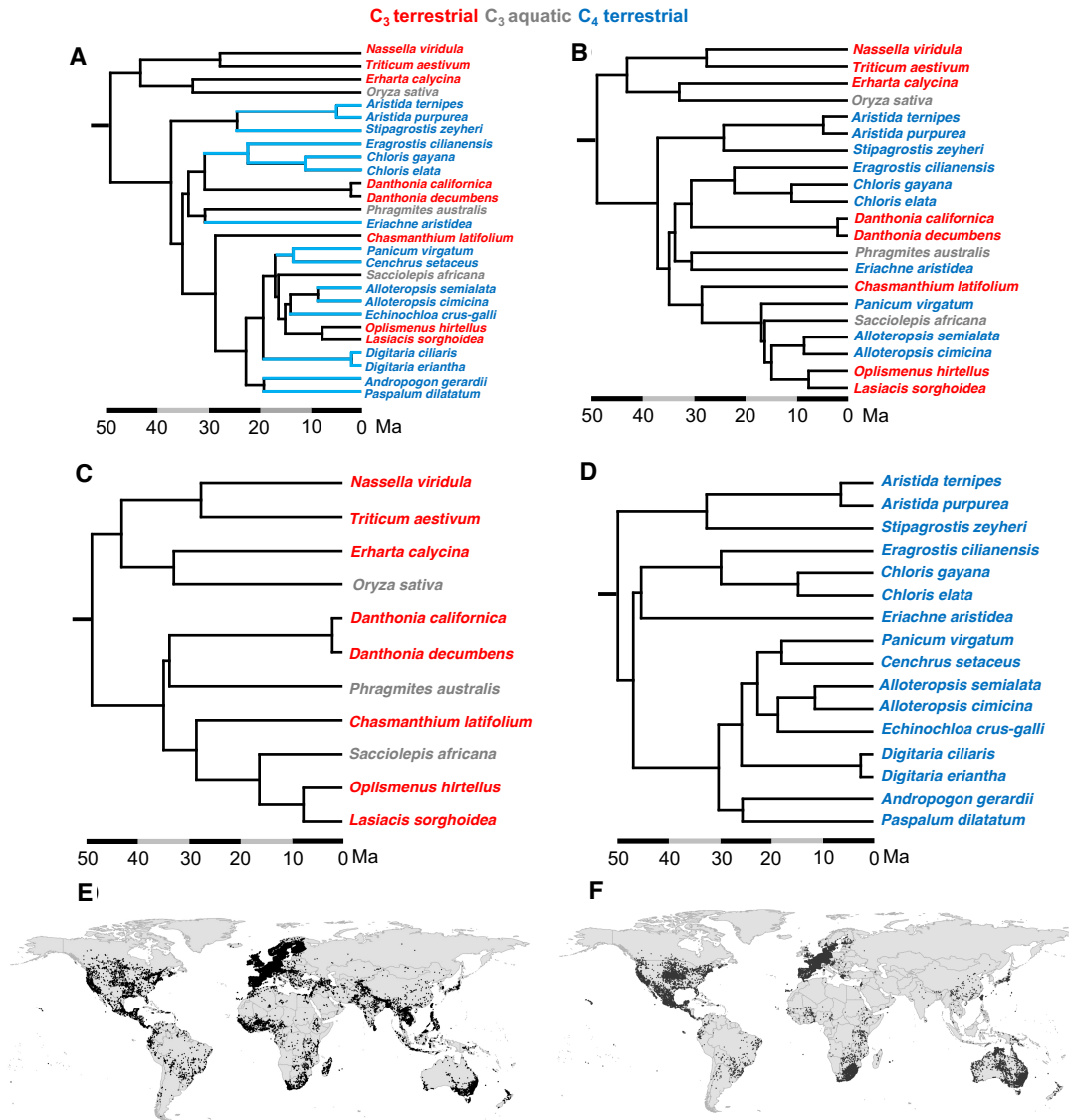
Figure S3.1. Phylogenetic trees used to account for the influence of species relatedness on scaling relationships and species distribution maps. (A) All 27 grass species included in the study. **(B)** 21 grass species that have bundle sheath cells, and used for analyses of tests including bundle sheath traits. **(C)** 11 C_3 species. **(D)** 16 C_4 species. Distributions of **(E)** 11 C_3 grass species and **(F)** 16 C_3 grass species, previously published in Baird et al., (2021). Blue branches in **(A)** indicate a C_4 evolution, including 11 independent evolutions.

85
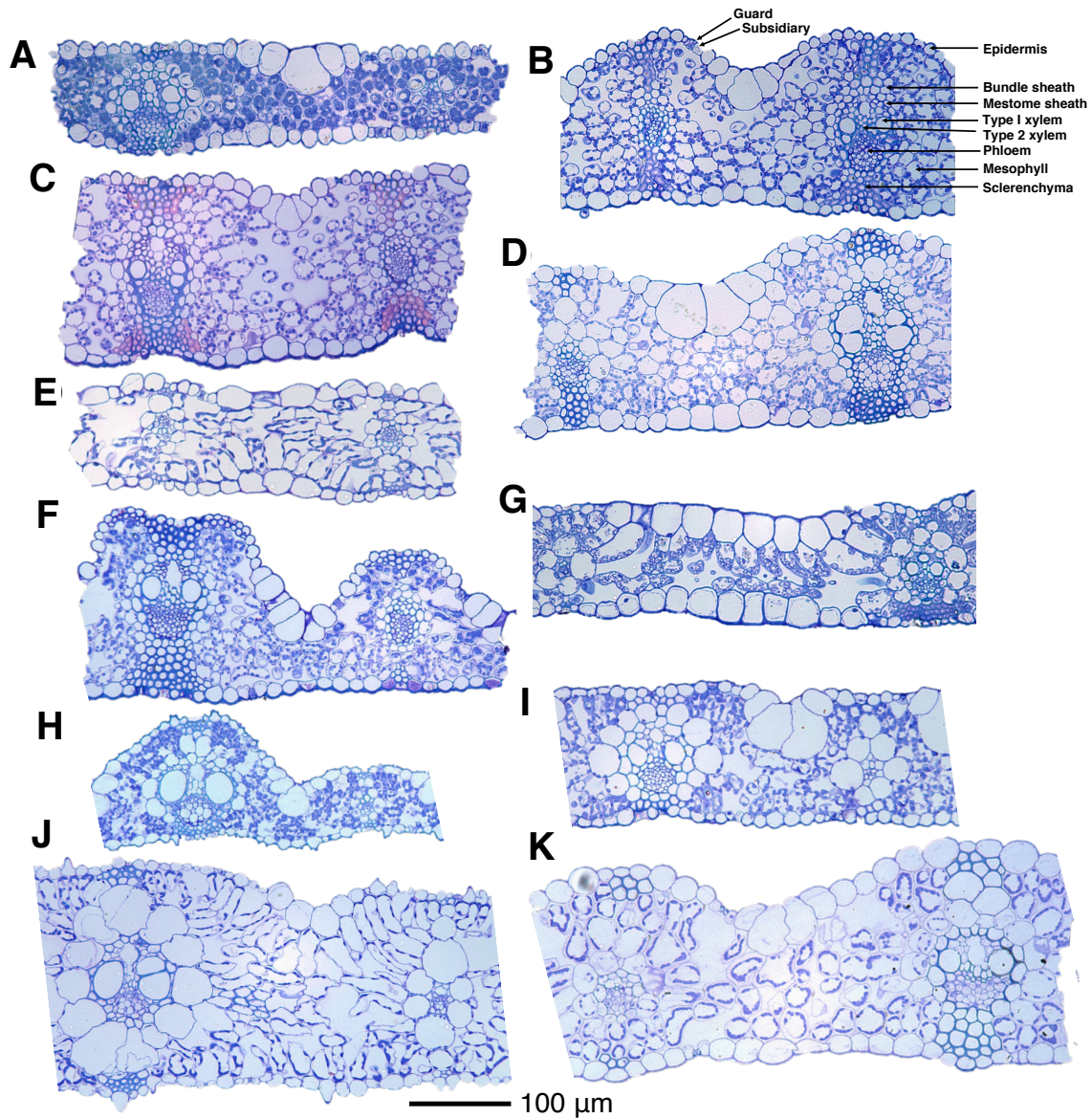
Figure S3.2. Anatomical transverse sections for 11 C₃ grass species included in the study. Images were selected to include one 2° large and one 3° intermediate vein. **(A)** *Chasmanthium latifolium*, **(B)** *Danthonia californica*, **(C)** *Danthonia decumbens*, **(D)** *Ehrharta calycina*, **(E)** *Lasiacis sorghoidea*, **(F)** *Nassella viridula*, **(G)** *Oplismenus hirtellus*, **(H)** *Oryza sativa*, **(I)** *Phragmites australis,* **(J)** *Sacciolepis africana*, **(K)** *Triticum aestivum*.

Labels in panel N: Guard, Subsidiary, Epidermis, Bundle sheath, Mesophyll, Phloem, Sclerenchyma, Mestome sheath, Type 1 xylem, Type 2 xylem
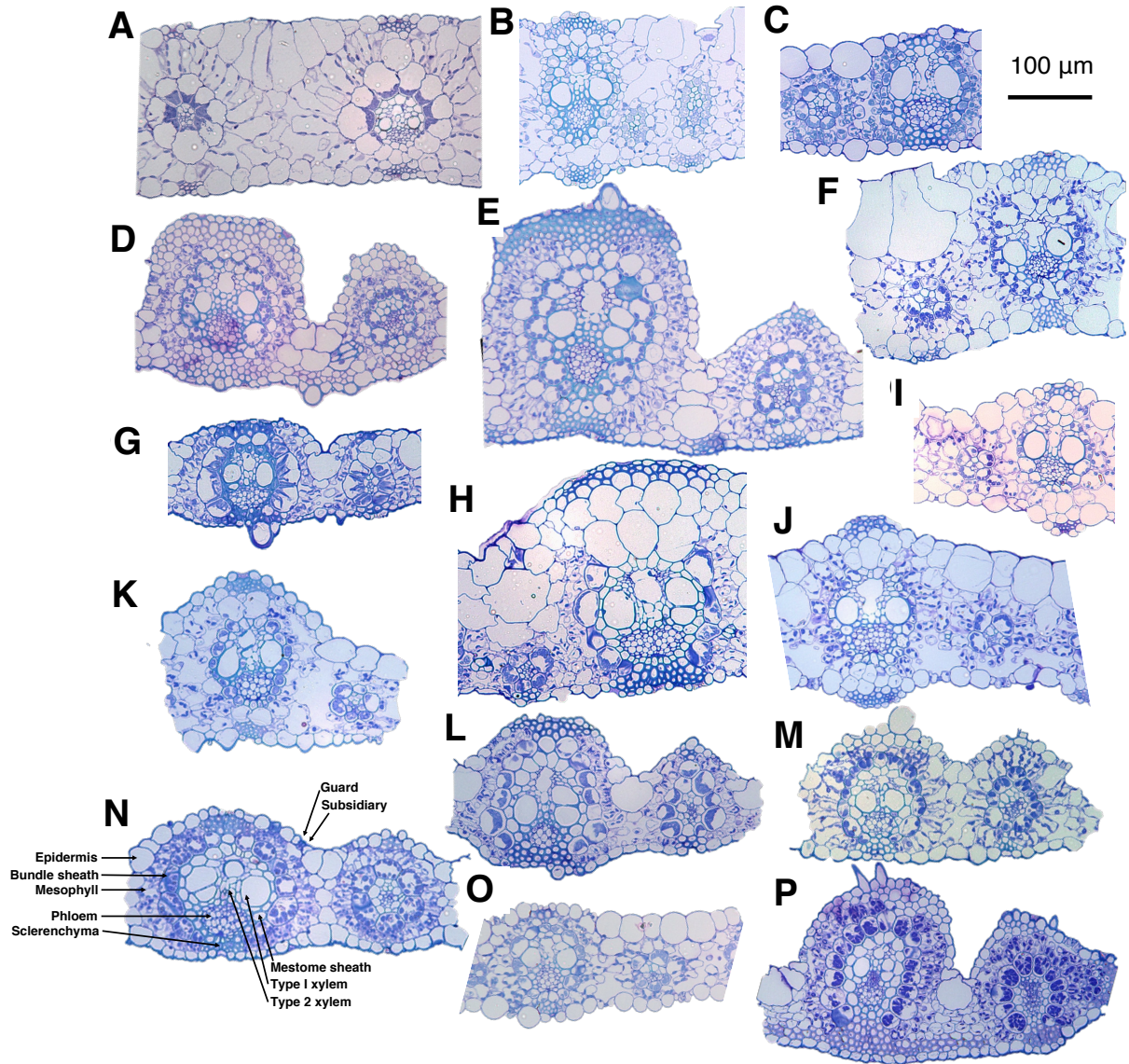
Figure S3.3. Anatomical transverse sections for 16 C$_4$ grass species included in the study.

Images were selected to include one 2° large and one 3° intermediate vein (i.e. C$_{4-3L}$) for **(A)**, **(D)**, **(E)**, **(F)**, **(H)**, **(L)**, **(M)**, **(N)** and **(P)**, or 4° vein (i.e. C$_{4-4L}$) for **(B)**, **(C)**, **(F)**, **(I)**, **(J)**, **(K)** and **(O)**. **(A)** *Alloteropsis cimicina* **(B)** *Alloteropsis semialata*, **(C)** *Andropogon gerardii*, **(D)** *Aristida purpurea*, **(E)** *Aristida ternipes*, **(F)** *Cenchrus setaceus* **(G)** *Chloris elata*, **(H)** *Chloris gayana*,

(I) *Digitaria ciliaris*, **(J)** *Digitaria eriantha,* **(K)** *Echnichloa crus-galli*, **(L)** *Eragrostis cilianensis*, **(M)** *Eriachne aristidea*, **(N)** *Panicum virgatum*, **(O)** *Paspalum dilatatum*, **(P)** *Stipagrostis zeyheri.*
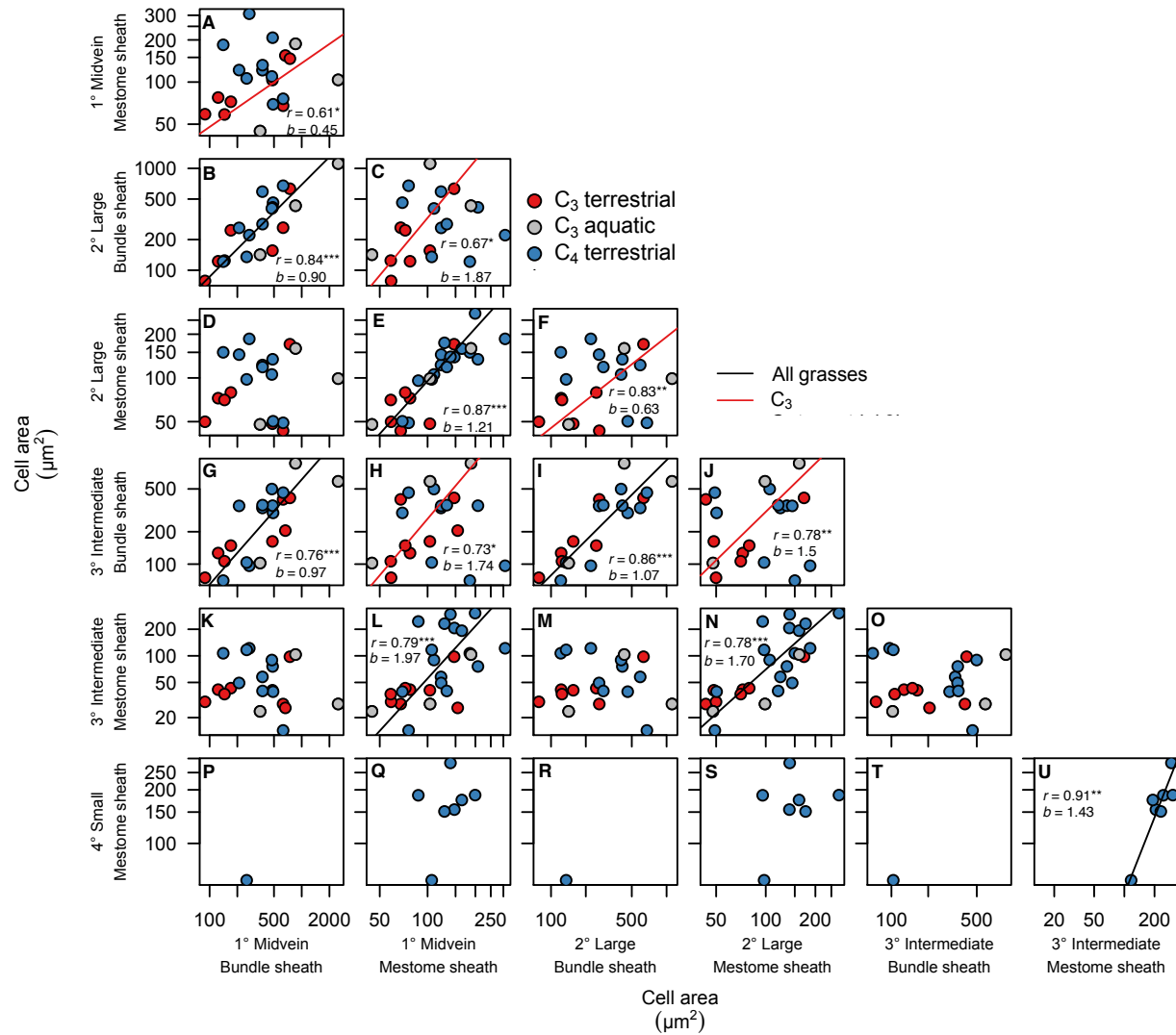
Figure S3.4. Scaling of vein sheath cells across vein orders across 27 grass species grown experimentally Scaling of bundle sheath cells across vein orders, of mestome sheath cells across vein orders, and of the procambial derived mestome sheath with the ground tissue derived bundle sheath across vein orders for C_3 grasses. Each point is one species, $n = 11$ C_3 (eight terrestrial in red, three aquatic in grey) and $n = 16$ C_4 species in blue. Panels **(P)**, **(R)** and **(T)** include only the species *Alloteropsis semialata* as this was the only species with the 4° vein but has both bundle and mestome sheaths. Lines were fit with phylogenetic reduced major axis regressions (PRMA)

and statistics and parameters are found in Table S3.4. Line colors indicate that the relationship was significant across a specific set of grasses, with black lines across all species and red lines across C_3 species. The line in panel **(U)** was fitted with standard major axis (SMA) as there were not > 7 species for a phylogenetic reduced major axis (PRMA) test. *p < 0.05, **p < 0.01, ***p < 0.001.
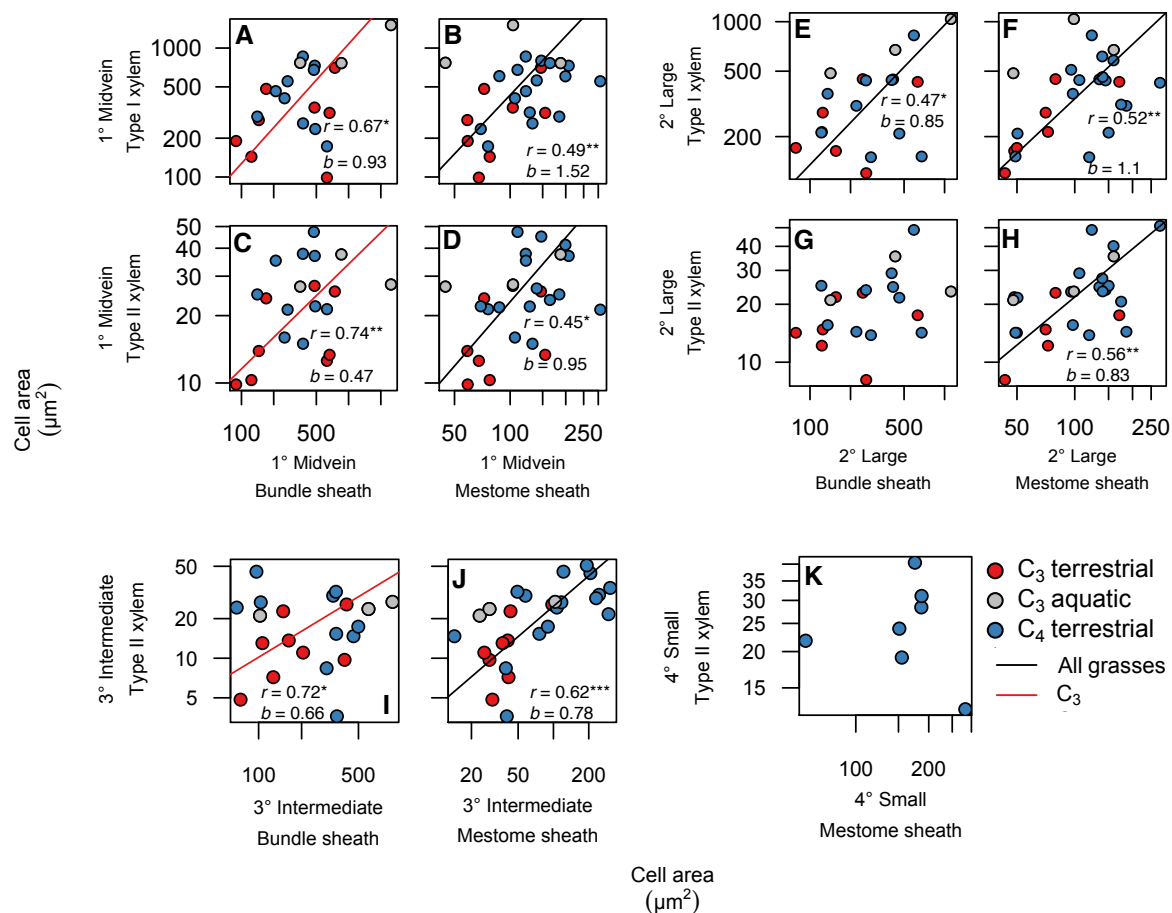
Figure S3.5. Scaling of vein xylem cell sizes with sheath cell types within leaf longitudinal vein orders across 27 grass species grown experimentally. Scaling of mestome sheath cells and xylem within vein orders and of the bundle sheath with xylem within vein orders for C_3 grasses. Each point is one species, $n = 11$ C_3 (eight terrestrial in red, three aquatic in grey) and $n = 16$ C_4 species in blue. Lines were fit with phylogenetic reduced major axis regressions (PRMA) and statistics and parameters are found in Table S3.4. Line colors indicate that the relationship was significant across a specific set of grasses, with black lines across all species and red lines across C_3 species. $*p < 0.05$, $**p < 0.01$, $***p < 0.001$.

91
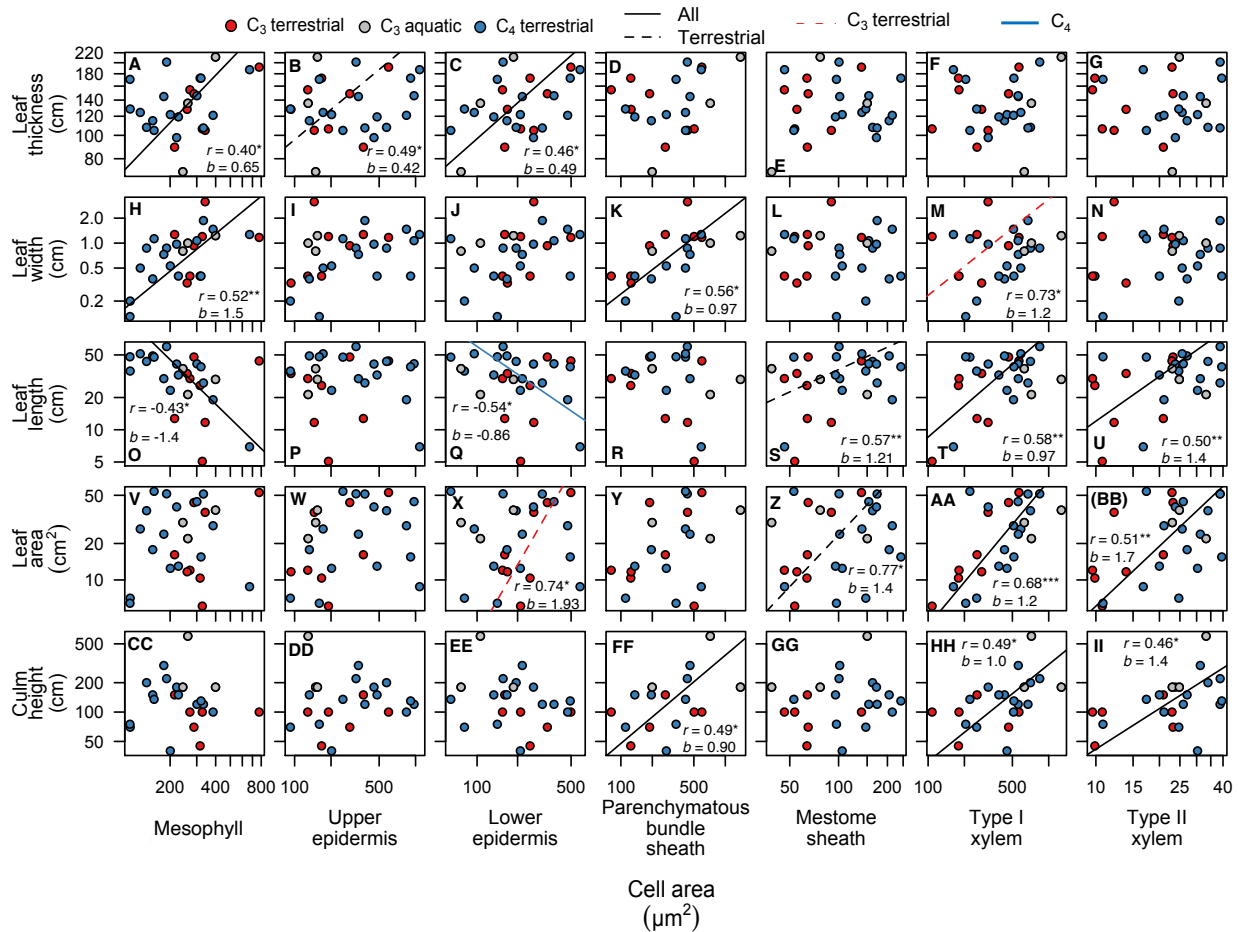
Figure S3.6. Scaling of leaf and plant morphological traits with leaf cell sizes across 27 grass species grown experimentally. Each point is one species, $n = 11$ C$_3$ (eight terrestrial in red, three aquatic in grey) and $n = 16$ C$_4$ species in blue. Lines were fit with phylogenetic reduced major axis regressions (PRMA) and statistics and parameters are found in Table S3.5. Line colors indicate that the relationship was significant across a specific set of grasses, with black lines across all species, red lines across C$_3$ species, and segmented lines across the terrestrial species either across all grasses or only C$_3$ grasses, and blue lines across the C$_4$ species only. *$p < 0.05$, **$p < 0.01$, ***$p < 0.001$.
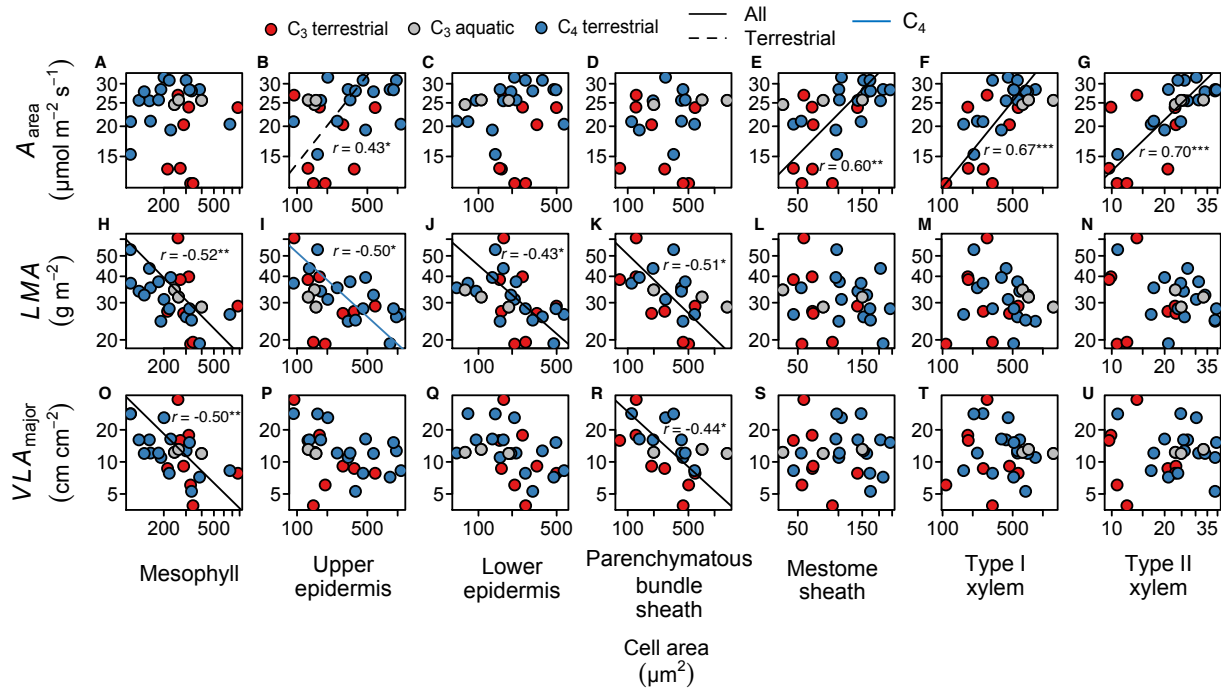
Figure S3.7. Scaling of leaf functional traits with leaf cell sizes across 27 grass species grown experimentally. Each point is one species, $n = 11$ C_3 (eight terrestrial in red, three aquatic in grey) and $n = 16$ C_4 species in blue. Lines were fit with phylogenetic reduced major axis regressions (PRMA) and statistics and parameters are found in Table S3.6. Line colors indicate that the relationship was significant across a specific set of grasses, with black lines across all species, segmented lines across the terrestrial species across all grasses, and blue lines across the C_4 species only. $*p < 0.05$, $**p < 0.01$, $***p < 0.001$.

References

1. Allard, G., C. J. Nelson, and S. G. Pallardy. 1991. Shade Effects on Growth of Tall Fescue: I. Leaf Anatomy and Dry Matter Partitioning. *Crop Science* 31.

2. Baird, A. S., S. H. Taylor, J. Pasquet-Kok, C. Vuong, Y. Zhang, T. Watcharamongkol, C. Scoffoni, et al. 2021. Developmental and biophysical determinants of grass leaf size worldwide. *Nature* 592: 242–247.

3. Beer, C., M. Reichstein, E. Tomelleri, P. Ciais, M. Jung, N. Carvalhais, C. Rödenbeck, et al. 2010. Terrestrial Gross Carbon Dioxide Uptake: Global Distribution and Covariation with Climate. *Science* 329: 834–838.

4. Brodribb, T. J., G. J. Jordan, and R. J. Carpenter. 2013. Unified changes in cell size permit coordinated leaf evolution. *New Phytologist* 199: 559–570.

5. Buckley, T. N., G. P. John, C. Scoffoni, and L. Sack. 2015. How Does Leaf Anatomy Influence Water Transport outside the Xylem? *Plant Physiology* 168: 1616–1635.

6. Cadart, C., and R. Heald. 2022. Scaling of biosynthesis and metabolism with cell size. *Molecular Biology of the Cell* 33: pe5.

7. Charles-Edwards, D. A., J. Charles-Edwards, and F. I. Sant. 1974. Leaf Photosynthetic Activity in Six Temperate Grass Varieties Grown in Contrasting Light and Temperature Environments. *Journal of Experimental Botany* 25: 715–724.

8. Christin, P.-A., C. P. Osborne, D. S. Chatelet, J. T. Columbus, G. Besnard, T. R. Hodkinson, L. M. Garrison, et al. 2013. Anatomical enablers and the evolution of C_4 photosynthesis in grasses. *Proceedings of the National Academy of Sciences* 110: 1381–1386.

9. Clayton, W., M. Vorontsova, K. Harman, and H. Williamson. 2006. RBG Kew: GrassBase - The Online World Grass Flora. Website http://www.kew.org/data/grasses-db.html.

10. Clevering, O. A. 1999. Between- and within-population differences in Phragmites australis. *Oecologia* 121: 447–457.

11. Cutler, J. M., D. W. Rains, and R. S. Loomis. 1977. The Importance of Cell Size in the Water Relations of Plants. *Physiologia Plantarum* 40: 255–260.

12. Danila, F. R., W. P. Quick, R. G. White, R. T. Furbank, and S. von Caemmerer. 2016. The Metabolite Pathway between Bundle Sheath and Mesophyll: Quantification of Plasmodesmata in Leaves of C_3 and C_4 Monocots. *The Plant Cell* 28: 1461–1471.

13. Dannenhoffer, J. M., W. Ebert Jr., and R. F. Evert. 1990. Leaf Vasculature in Barley, *Hordeum Vulgare* (poaceae). *American Journal of Botany* 77: 636–652.

14. Dengler, N. G., R. E. Dengler, and P. W. Hattersley. 1985. Differing Ontogenetic Origins of PCR ('Kranz') Sheaths in Leaf Blades of C_4 Grasses (Poaceae). *American Journal of Botany* 72: 284–302.

15. Eckardt, N. A., E. A. Ainsworth, R. N. Bahuguna, M. R. Broadley, W. Busch, N. C. Carpita, G. Castrillo, et al. 2023. Climate change challenges, plant science solutions. *The Plant Cell* 35: 24–66.

16. Ellis, J. R., and R. M. Leech. 1985. Cell size and chloroplast size in relation to chloroplast replication in light-grown wheat leaves. *Planta* 165: 120–125.

17. Ellis, R. P. 1976. A procedure for standardizing comparative leaf anatomy in the Poaceae. I. The leaf-blade as viewed in transverse section. *Bothalia* 12: 65–109.

18. Ermakova, M., F. R. Danila, R. T. Furbank, and S. von Caemmerer. 2020. On the road to C$_4$ rice: advances and perspectives. *The Plant Journal* 101: 940–950.

19. Evert, R. F. 2006. Esau's Plant Anatomy: Meristems, Cells, and Tissues of the Plant Body: Their Structure, Function, and Development. 3rd ed. John Wiley.

20. Feldman, A. B., H. Leung, M. Baraoidan, A. Elmido-Mabilangan, I. Canicosa, W. P. Quick, J. Sheehy, and E. H. Murchie. 2017. Increasing Leaf Vein Density via Mutagenesis in Rice Results in an Enhanced Rate of Photosynthesis, Smaller Cell Sizes and Can Reduce Interveinal Mesophyll Cell Number. *Frontiers in Plant Science* 8.

21. Fletcher, L. R., H. Cui, H. Callahan, C. Scoffoni, G. P. John, M. K. Bartlett, D. O. Burge, and L. Sack. 2018. Evolution of leaf structure and drought tolerance in species of Californian *Ceanothus*. *American Journal of Botany* 105: 1672–1687.

22. Fournier, C., J. L. Durand, S. Ljutovac, R. Schäufele, F. Gastal, and B. Andrieu. 2005. A functional–structural model of elongation of the grass leaf and its relationships with the phyllochron. *New Phytologist* 166: 881–894.

23. Garland, T., Jr., A. W. Dickerman, C. M. Janis, and J. A. Jones. 1993. Phylogenetic Analysis of Covariance by Computer Simulation. *Systematic Biology* 42: 265–292.

24. Garnier, E., J.-L. Salager, G. Laurent, and L. Sonié. 1999. Relationships between photosynthesis, nitrogen and leaf structure in 14 grass species and their dependence on the basis of expression. *The New Phytologist* 143: 119–129.

25. Gázquez, A., and G. T. S. Beemster. 2017. What determines organ size differences between species? A meta-analysis of the cellular basis. *New Phytologist* 215: 299–308.

26. Gould, S. J. 1966. Allometry and Size in Ontogeny and Phylogeny. *Biological Reviews* 41: 587–638.

27. Granier, C., and F. Tardieu. 2009. Multi-scale phenotyping of leaf expansion in response to environmental changes: the whole is more than the sum of parts. *Plant, Cell & Environment* 32: 1175–1184.

28. Granier, C., and F. Tardieu. 1998. Spatial and Temporal Analyses of Expansion and Cell Cycle in Sunflower Leaves1: A Common Pattern of Development for All Zones of a Leaf and Different Leaves of a Plant. *Plant Physiology* 116: 991–1001.

29. Griffiths, H., G. Weller, L. F. M. Toy, and R. J. Dennis. 2013. You're so vein: bundle sheath physiology, phylogeny and evolution in C_3 and C_4 plants. *Plant, Cell & Environment* 36: 249–261.

30. Hepworth, C., R. S. Caine, E. L. Harrison, J. Sloan, and J. E. Gray. 2018. Stomatal development: focusing on the grasses. *Current Opinion in Plant Biology* 41: 1–7.

31. Hölttä, T., M. Kurppa, and E. Nikinmaa. 2013. Scaling of xylem and phloem transport capacity and resource usage with tree size. *Frontiers in Plant Science* 4.

32. Huxley, J. S. 1932. Problems of relative growth. John Hopkins University Press, Baltimore, Maryland, USA.

33. John, G. P., C. Scoffoni, T. N. Buckley, R. Villar, H. Poorter, and L. Sack. 2017. The anatomical and compositional basis of leaf mass per area. *Ecology Letters* 20: 412–425.

34. John, G. P., C. Scoffoni, and L. Sack. 2013. Allometry of cells and tissues within leaves. *American Journal of Botany* 100: 1936–1948.

35. Kato, Y., and M. Okami. 2010. Root growth dynamics and stomatal behaviour of rice (*Oryza sativa* L.) grown under aerobic and flooded conditions. *Field Crops Research* 117: 9–17.

36. Kemp, C. D. 1960. Methods of Estimating the Leaf Area of Grasses from Linear Measurements. *Annals of Botany* 24: 491–499.

37. Koike, T. 1988. Leaf Structure and Photosynthetic Performance as Related to the Forest Succession of Deciduous Broad-Leaved Trees1. *Plant Species Biology* 3: 77–87.

38. LaBarbera, M. 1990. Principles of Design of Fluid Transport Systems in Zoology. *Science* 249: 992–1000.

39. Lowry, D. B., J. T. Lovell, L. Zhang, J. Bonnette, P. A. Fay, R. B. Mitchell, J. Lloyd-Reilley, et al. 2019. QTL × environment interactions underlie adaptive divergence in switchgrass across a large latitudinal gradient. *Proceedings of the National Academy of Sciences* 116: 12933–12941.

40. MacAdam, J. W., J. J. Volenec, and C. J. Nelson. 1989. Effects of Nitrogen on Mesophyll Cell Division and Epidermal Cell Elongation in Tall Fescue Leaf Blades 1. *Plant Physiology* 89: 549–556.

41. Marshall, W. F., K. D. Young, M. Swaffer, E. Wood, P. Nurse, A. Kimura, J. Frankel, et al. 2012. What determines cell size? *BMC Biology* 10: 101.

42. McCulloh, K. A., J. S. Sperry, and F. R. Adler. 2003. Water transport in plants obeys Murray's law. *Nature* 421: 939–942.

43. McSteen, P., and E. A. Kellogg. 2022. Molecular, cellular, and developmental foundations of grass diversity. *Science* 377: 599–602.

44. Meinzer, F. C., S. A. James, G. Goldstein, and D. Woodruff. 2003. Whole-tree water transport scales with sapwood capacitance in tropical forest canopy trees. *Plant, Cell & Environment* 26: 1147–1155.

45. Murray, C. D. 1926. The Physiological Principle of Minimum Work. *Proceedings of the National Academy of Sciences* 12: 207–214.

46. Neiro, J. S. 2020. Ontogenetic and static allometry of hind femur length in the cricket *Gryllus bimaculatus* (Orthoptera: Gryllidae) with implications for evo-devo of morphological scaling. 2020.03.01.972141.

47. Nelson, T., and N. Dengler. 1997. Leaf Vascular Pattern Formation. *The Plant Cell* 9: 1121–1135.

48. Niinemets, U. 1999. Research Review: Components of Leaf Dry Mass Per Area-Thickness and Density-Alter Leaf Photosynthetic Capacity in Reverse Directions in Woody Plants. *The New Phytologist* 144: 35–47.

49. Niinemets, Ü., A. Díaz-Espejo, J. Flexas, J. Galmés, and C. R. Warren. 2009. Role of mesophyll diffusion conductance in constraining potential photosynthetic productivity in the field. *Journal of Experimental Botany* 60: 2249–2270.

50. Niklas, K. J. 1994. Plant Allometry. University of Chicago Press, Chicago, Illinois.

51. Nobel, P. S. 1976. Photosynthetic Rates of Sun versus Shade Leaves of Hyptis emoryi Torr. 1. *Plant Physiology* 58: 218–223.

52. Nobel, P. S. 2020. Physicochemical and environmental plant physiology. 5th ed. Academic Press, San Diego, CA.

53. Nobel, P. S., L. J. Zaragoza, and W. K. Smith. 1975. Relation between Mesophyll Surface Area, Photosynthetic Rate, and Illumination Level during Development for Leaves of Plectranthus parviflorus Henckel 1. *Plant Physiology* 55: 1067–1070.

54. Noblin, X., L. Mahadevan, I. A. Coomaraswamy, D. A. Weitz, N. M. Holbrook, and M. A. Zwieniecki. 2008. Optimal vein density in artificial and real leaves. *Proceedings of the National Academy of Sciences* 105: 9140–9144.

55. Olson, M. E., D. Soriano, J. A. Rosell, T. Anfodillo, M. J. Donoghue, E. J. Edwards, C. León-Gómez, et al. 2018. Plant height and hydraulic vulnerability to drought and cold. *Proceedings of the National Academy of Sciences* 115: 7551–7556.

56. Pantin, F., T. Simonneau, and B. Muller. 2012. Coming of leaf age: control of growth by hydraulics and metabolics during leaf ontogeny. *New Phytologist* 196: 349–366.

57. Pearsall, W. H. 1927. Growth Studies: VI. On the Relative Sizes of Growing Plant Organs. *Annals of Botany* os-41: 549–556.

58. Pélabon, C., C. Firmat, G. H. Bolstad, K. L. Voje, D. Houle, J. Cassara, A. L. Rouzic, and T. F. Hansen. 2014. Evolution of morphological allometry. *Annals of the New York Academy of Sciences* 1320: 58–75.

59. Poorter, H., K. J. Niklas, P. B. Reich, J. Oleksyn, P. Poot, and L. Mommer. 2012. Biomass allocation to leaves, stems and roots: meta-analyses of interspecific variation and environmental control. *New Phytologist* 193: 30–50.

60. Poorter, H., and L. Sack. 2012. Pitfalls and Possibilities in the Analysis of Biomass Allocation Patterns in Plants. *Frontiers in Plant Science* 3.

61. Price, C. A., S.-J. C. Knox, and T. J. Brodribb. 2013. The Influence of Branch Order on Optimal Leaf Vein Geometries: Murray's Law and Area Preserving Branching. *PLOS ONE* 8: e85420.

62. Rademacher, I. F., and C. J. Nelson. 2001. Nitrogen Effects on Leaf Anatomy within the Intercalary Meristems of Tall Fescue Leaf Blades. *Annals of Botany* 88: 893–903.

63. Revell, L. J. 2012. phytools: an R package for phylogenetic comparative biology (and other things). *Methods in Ecology and Evolution* 3: 217–223.

64. Ronellenfitsch, H., J. Liesche, K. H. Jensen, N. M. Holbrook, A. Schulz, and E. Katifori. 2015. Scaling of phloem structure and optimality of photoassimilate transport in conifer needles. *Proceedings of the Royal Society B: Biological Sciences* 282: 20141863.

65. Russell, S. H., and R. F. Evert. 1985. Leaf vasculature in *Zea mays* L. *Planta* 164: 448–458.

66. Sachs, T. 1975. The Control of the Differentiation of Vascular Networks. *Annals of Botany* 39: 197–204.

67. Sack, L., and T. N. Buckley. 2016. The Developmental Basis of Stomatal Density and Flux. *Plant Physiology* 171: 2358–2363.

68. Sack, L., and C. Scoffoni. 2013. Leaf venation: structure, function, development, evolution, ecology and applications in the past, present and future. *New Phytologist* 198: 983–1000.

69. Sack, L., C. Scoffoni, G. P. John, H. Poorter, C. M. Mason, R. Mendez-Alonzo, and L. A. Donovan. 2013. How do leaf veins influence the worldwide leaf economic spectrum? Review and synthesis. *Journal of Experimental Botany* 64: 4053–4080.

70. Sack, L., C. Scoffoni, A. D. McKown, K. Frole, M. Rawls, J. C. Havran, H. Tran, and T. Tran. 2012. Developmentally based scaling of leaf venation architecture explains global ecological patterns. *Nature Communications* 3: 837.

71. Sage, R. F. 2004. The evolution of C4 photosynthesis. *New Phytologist* 161: 341–370.

72. Salvi, A. M., D. D. Smith, M. A. Adams, K. A. McCulloh, and T. J. Givnish. 2021. Mesophyll photosynthetic sensitivity to leaf water potential in Eucalyptus: a new

dimension of plant adaptation to native moisture supply. *New Phytologist* 230: 1844–1855.

73. Shi, P., M. Liu, D. A. Ratkowsky, J. Gielis, J. Su, X. Yu, P. Wang, et al. 2019. Leaf area–length allometry and its implications in leaf shape evolution. *Trees* 33: 1073–1085.

74. Skinner, R. H., and C. J. Nelson. 1994. Epidermal cell division and the coordination of leaf and tiller development. *Annals of Botany* 74: 9–16.

75. Smith, D. D., and J. S. Sperry. 2014. Coordination between water transport capacity, biomass growth, metabolic scaling and species stature in co-occurring shrub and tree species. *Plant, Cell & Environment* 37: 2679–2690.

76. Sperry, J. S., U. G. Hacke, and J. K. Wheeler. 2005. Comparative analysis of end wall resistivity in xylem conduits. *Plant, Cell & Environment* 28: 456–465.

77. Stickler, F. C., S. Wearden, and A. W. Pauli. 1961. Leaf Area Determination in Grain Sorghum1. *Agronomy Journal* 53: 187–188.

78. Taneda, H., and I. Terashima. 2012. Co-ordinated development of the leaf midrib xylem with the lamina in Nicotiana tabacum. *Annals of Botany* 110: 35–45.

79. Taylor, S. H., S. P. Hulme, M. Rees, B. S. Ripley, F. Ian Woodward, and C. P. Osborne. 2010. Ecophysiological traits in C_3 and C_4 grasses: a phylogenetically controlled screening experiment. *New Phytologist* 185: 780–791.

80. Torii, K. U. 2021. Stomatal development in the context of epidermal tissues. *Annals of Botany* 128: 137–148.

81. VanVolkenburgh, E. 1999. Leaf expansion – an integrating plant behaviour. *Plant, Cell & Environment* 22: 1463–1473.

82. Vasseur, F., C. Violle, B. J. Enquist, and D. Vile. 2023. Genetic variability and plasticity of plant allometry. *Functional Ecology* n/a.

83. Warton, D. I., I. J. Wright, D. S. Falster, and M. Westoby. 2006. Bivariate line-fitting methods for allometry. *Biological Reviews* 81: 259–291.

84. Watcharamongkol, T., P.-A. Christin, and C. P. Osborne. 2018. C_4 photosynthesis evolved in warm climates but promoted migration to cooler ones. *Ecology Letters* 21: 376–383.

85. West, G. B., J. H. Brown, and B. J. Enquist. 1997. A General Model for the Origin of Allometric Scaling Laws in Biology. *Science* 276: 122–126.

86. Wilson, D., and J. P. Cooper. 1967. Assimilation of Lolium in Relation to Leaf Mesophyll. *Nature* 214: 989–992.

87. Wright, I. J., P. B. Reich, M. Westoby, D. D. Ackerly, Z. Baruch, F. Bongers, J. Cavender-Bares, et al. 2004. The worldwide leaf economics spectrum. *Nature* 428: 821–827.

88. Zhong, M., B. E. L. Cerabolini, P. Castro-Díez, J.-P. Puyravaud, and J. H. C. Cornelissen. 2020. Allometric co-variation of xylem and stomata across diverse woody seedlings. *Plant, Cell & Environment* 43: 2301–2310.

Chapter 4: Leaf hydraulic design of C_3 and C_4 grasses

Abstract

The exceptional global distribution and productivity of grasses arises from their diversity, with C_4 species dominating hotter and drier environments with higher photosynthetic rate (A) and higher water use efficiency than C_3 species. A long-standing paradox is the apparent surplus in water transport capacity of C_4 species, given their higher leaf vein density (D_v) and lower stomatal conductance (g_s). Here I clarify C_3 and C_4 grass leaf hydraulic design using experimental data, a compiled database, evolutionary analyses and physiological modeling. Despite their higher D_v, C_4 species have similar hydraulic conductance inside and outside the xylem to C_3 species, and their higher water transport capacity relative to g_s provides a hydraulic hyper-efficiency necessary for their photosynthetic advantage, and representing a key target for novel crop design.

Introduction

The grass family (*Poaceae*) includes 12,000 species from 800 genera that dominate and contribute 31-43% and 33% of the earth's terrestrial surface, respectively, and from which 70% of all crops are derived (Molecular, cellular, and developmental foundations of grass diversity; Terrestrial Gross Carbon Dioxide Uptake: Global Distribution and Covariation with Climate). The C_4 photosynthetic pathway in grasses is of key importance and a model for repeated emergence of a key innovation (Sage, 2004; Gowik & Westhoff, 2011; Marazzi et al*.,* 2012), evolving >20 times in grasses such that >40% of extant species are C_4 (Sage, Christin & Edwards, 2011)*.* C_4 photosynthesis maximizes carbon fixation particularly under hotter, drier conditions and low CO_2 by concentrating CO_2 at rubisco in the bundle sheath around the leaf veins, minimizing photo-respiratory losses and enabling reduced stomatal conductance and higher water-use efficiency (WUE) (Sage 2004). Projected shifts in vegetation under climate change depend crucially on the relative success of C_4 versus C_3 photosynthetic species (Higgins & Scheiter, 2012). In addition, key agricultural crops provide enormous yields due to their C_4 photosynthesis, and a global initiative is underway to engineer novel C_4 crops (e.g., C_4 rice) (Gowik & Westhoff, 2011; Langdale, 2011). However, the hydraulic design of leaves is understudied in grasses, though recognized as critical in determining plant productivity in response to climate (Maherali, Pockman & Jackson, 2004; Blackman, Brodribb & Jordan, 2012; Sack & Scoffoni, 2013; Baird et al*.,* 2021).

Generally across angiosperms, leaves are a hydraulic bottleneck (Sack & Holbrook 2006). Water flows through leaves via the vein network, and then diffuses across the bundle sheath and mesophyll to the sites of evaporation. and hydraulic conductance (K_{leaf}). Thus, K_{leaf} is determined by vein xylem traits such as conduit diameters and numbers, venation density (D_v, i.e. vein length

per leaf area) and vein sheath properties such as sheath perimeter (Figure 1), which influence the conductance of pathways inside (K_x) and outside the xylem (K_{ox}):

$$K_{\text{leaf}} = (K_x^{-1} + K_{ox}^{-1})^{-1} \qquad (1)$$

A high K_{leaf} is necessary for a high stomatal conductance (g_s) and light-saturated photosynthetic rate per unit leaf area (A_{area}) (Sack & Holbrook, 2006; Sack & Scoffoni, 2013) (Table 4.1). C_3 eudicotyledons and grasses exhibit coordination of hydraulics and gas exchange, i.e., K_{leaf}, g_s, photosynthetic rate (A_{area}) and higher D_v (Brodribb, Feild & Sack, 2010; Sack & Scoffoni, 2013; Zhou, Akçay, Edwards & Helliker, 2021; Baird et al., 2021). In turn, a higher K_{leaf} relative to g_s and A_{area} can confer sustained leaf water potential and a higher A_{area} relative to g_s can confer greater leaf water-use efficiency (Scoffoni et al., 2016). All of these can confer drought avoidance capacity, by which species can adapt to arid climates, by mitigating the shorter growing season with more rapid growth in the wet season.

Yet, C_4 grasses may depart from this hydraulic design framework that is general for C_3 species. First, C_4 species possess a specialized "Kranz" anatomy that includes higher D_v (Ueno, Kawano, Wakayama & Takeda, 2006; Liu et al., 2019; Baird et al., 2021; Pan et al., 2022) and enlarged sheath cells in which carbon is concentrated around chloroplasts (Christin et al., 2013) (Box 1), and which allows for a lower g_s and higher operating Ψ_{leaf}. Consequently, C_4 species may not require a high K_{leaf} to enable rapid rates of gas exchange (Zhou, Akçay & Helliker, 2020; Zhou et al., 2021). Indeed, in C_4 eudicots, hydraulic conductance was lower than for closely related C_3 species (Kocacinar & Sage 2003, 2004). Further, studies of specific sets of phylogenetically and functionally diverse C_4 grass species and across sorghum varieties showed higher D_v increased with A_{area} (Pathare, Sonawane, Koteyeva & Cousins, 2020; Pan et al., 2022), or decoupling or negative relationship of K_{leaf} and A_{area} (Ocheltree, Nippert & Prasad, 2016; Pathare et al., 2020;

Zhou et al., 2021) (Table S4.1). The differential coordination of hydraulic, stomatal and photosynthetic traits in C_3 and C_4 species would contribute fundamentally to their contrasting adaptation across environments and to efforts to design climate-forward varieties or novel C_4 plants. I tested hypotheses for the differential physiological design of C_4 relative to C_3 grasses for 11 C_3 and 16 C_4 grass species grown in a common garden, native to diverse habitats and including major crops, and representing 11 independent C_4 origins and C_3 sister clades (Figure S4.1, Table S4.2). I also provide additional evidence for differences between C_3 and C_4 species, and coordination of physiological traits using a larger compiled meta base, including our data and grass data from 35 previously published studies for 328 species (Table S4.3).

Materials and Methods

Plant Material

Plants were grown in a common garden design at the UCLA Plant Growth Center to reduce environmentally-driven plasticity that would occurs across species' distributions in the wild. 27 species were selected to capture large functional and phylogenetic diversity, including 10 and 16 C_3 and C_4 species, respectively, representing 11 independent C_4 origins (Table S4.2). Seeds were acquired from seed banks and commercial sources (Table S4.2), and prior to germination were surface-sterilized with 10% NaClO and 0.1% Triton X-100 detergent, rinsed three times with sterile water, and sown on plates of 0.8% agar sealed with Micropore surgical tape (3M, St. Paul, MN). Seeds were germinated in chambers maintained at 26°C, under moderate intensity cool white fluorescent lighting with a 12 hour photoperiod. When roots ranged from 2-3 cm long, seedlings were transplanted to 3.6 L pots with potting soil (1:1:1.5:1.5:3 of coarse vermiculite: perlite: washed plater sand: sandy loam: peat moss).

Plants were grown at the UCLA Plant Growth Center (minimum, mean and maximum daily values for temperature: 20.1, 23.4 and 34.0°C; for relative humidity: 28, 50 and 65%; and mean and maximum photosynthetically active radiation during daylight period: 107 and 1988 μmol photons m^{-2} s^{-1}; HOBO Micro Station with Smart Sensors; Onset, Bourne, MA). Plants were arranged in six randomized blocks spread over three benches, with one individual per species per block (n = 6 except: *Alloteropsis semialata*, n = 4) and two blocks per bench. Plants were irrigated daily with water containing fertilizer (200-250 ppm of 20:20:20 N:P:K; Scotts Peters Professional water soluble fertilizer; Everris International B.V., Geldermalsen, The Netherlands).

Sample anatomical preparation

Following the establishment of at least 3-4 mature leaves, one leaf from each of three individuals per species was fixed and stored in FAA solution (37% formaldehyde-glacial acidic acid-95% ethanol in deionized water. At the center of the leaf, rectangular samples were cut and under vacuum over the duration of one week, gradually infiltrated with low viscosity acrylic resin (L.R. White; London Resin Co., UK). Infiltrated samples were then set in resin in gelatin capsules to dry at 55 C overnight. From these samples, transverse cross sections of 1 um thickness and of varying width (species dependent) were then prepared using glass knives (LKB 7800 KnifeMaker;LKB Produkter; Bromma, Sweden) in a rotary microtome (Leica Ultracut E, Reichert-Jung California, USA), placed on slides and stained with 0.01% toluidine blue in 1% sodium borate (w/v). Slides were then imaged with a 5×, 20×, and 40× objective using a light microscope (Leica Lietz DMRB; Leica Microsystems) and camera with imaging software (SPOT Imaging Solution; Diagnostic Instruments, Sterling Heights, Michigan USA).

Quantification of leaf hydraulic traits

I measured the leaf hydraulic conductance (K_{leaf}) between 9 Feb and 25 June 2010 using the steady-state evaporative flux method (EFM) (Sack & Scoffoni, 2012). Measurements were typically made for 2-3 leaves per plant from 6 plants, resulting in 6-18 leaves per species. Stems were cut from the plant with a fresh razor blade under water in the growth center, placed in a polythene bag (Whirl-Pak; Nasco, Fort Atkinson, WI, USA), and transported to the lab for measurement. Individual grass leaves were wrapped in parafilm around a plastic rod of appropriate diameter (3-18 mm; McMasterCarr, Elmhurst, IL), re-cut with a fresh razor blade under distilled water and rapidly connected to tubing with a compression fitting (Omnifit A2227 bore adaptor; Omnifit, Cambridge, UK and 18 mm diameter compression coupling Dynamax, Houstin, TX). The tubing contained distilled water that was degassed for at least 8 h with a vacuum pump (GAST Manufacturing, Inc, Michigan, USA), and refiltered 0.2μm; Syringe filter, Cole-Parmer, Vernon Hills, IL) and connected the leaf to a cylinder of water on a balance (Mettler Toledo, XS205 DualRange, ±0.01/0.1 mg), which logged data every 30 s to a computer for the calculation of flow rate into the petiole (*E*). Leaves were held adaxial surface upwards using a wood frame strung with fishing line, which held the leaf horizontal and immobile above a large box fan (Lakewood Engineering & Manufacturing Company, Chicago, Illinois, USA). Leaves were illuminated by a light source (model 73828 1000 W, "UV filter"; Sears, Roebuck, Hoffman Estates, Illinois, USA) suspended above a Pyrex glass container (Corning Incorporated, Corning, New York, USA) filled with water above the leaf producing >1000 μmol m^{-2} s^{-1} PAR at the leaf surface. The leaf temperature was maintained between 23-28°C during the experiment. Leaves were allowed to transpire on the fan apparatus for at least 30 min, until the flow rate stabilized with a coefficient of variation < 5% for at least 5 min. A 30 min period was chosen to ensure that leaves had sufficient

time to acclimate to light, which previous studies have shown to enhance K_{leaf} by several-fold for certain species (Sack, Melcher, Zwieniecki & Holbrook, 2002; Tyree, Nardini, Salleo, Sack & El Omari, 2005; Cochard et al., 2007; Scoffoni, Pou, Aasamaa & Sack, 2008). When flow rate was very low ($< 8\ \mu g\ s^{-1}$) and did not stabilize with that criterion, the measurement was continued until a running average of the last ten flow measurements stabilized with a coefficient of variation <5%. Additionally, flow rate was plotted against time to ensure stability. Measurements were discontinued if the flow suddenly changed, either due to leakage in the system or apparent blockage by particles or air bubbles. Leaf temperature was recorded with a thermocouple thermometer (Cole-Parmer Instrument Company, Vernon Hills, Illinois, USA) and the final 5 min of flow rate were averaged. The leaf was quickly removed from the tubing, the cut end dabbed dry, and the leaf sealed into a Whirlpak bag, which had been exhaled into. Following at least 20 min equilibration, the final leaf water potential (Ψ_f) was measured using a pressure chamber (Plant Moisture Stress, Model 1000, Albany, Oregon, USA). To correct for changes in K_{leaf} induced by the temperature dependence of water viscosity, K_{leaf} values were standardized to 25°C (Weast 1974; Sack, Cowan, Jaikumar & Holbrook 2003). Measurements were made for 2-3 leaves per plant for each of 6 plants (except 9 plants for *A. ternipes*, 4 plants for *A. semialata*, and for *L. sorghoidea* 5 and 8 leaves were measured from two plants); overall 6-18 leaves per species were measured. We removed outliers for each species using Dixon's outlier test (Sokal & Rohlf, 1995); up to 0-3 outliers for 14 of the 28 species; data for 6-18 leaves remained, 12 on average. The values for K_{leaf} with and without removing outliers were highly correlated across species ($r = 0.96$; $P < 0.001$), and all the findings of the study were robust to whether or not outliers were maintained in the dataset.

I initially determined K_{leaf} in three ways. First, I averaged all K_{leaf} measurements for each species. Second, I fitted a line for K_{leaf} versus Ψ_{leaf} and used the y-intercept as an index of maximum K_{leaf} (Brodribb, Feild & Jordan, 2007). Third, I used the fitted line to predict K_{leaf} for a Ψ_{leaf} corresponding to the species mean determined experimentally under glasshouse conditions. Across species, K_{leaf} values quantified using the three methods were inter-correlated (r_s and r_p = 0.63-0.95); data are presented for the mean K_{leaf}.

To estimate hydraulic vulnerability for each species, I fitted lines for K_{leaf} versus leaf water potential (Ψ_{leaf}) during the EFM measurement (using SMATR) (Warton, Duursma, Falster & Taskinen, 2012). I note that species may show variation in the shape of vulnerability curves but that for numerous species including grasses, a straight line approximates the decline at high leaf water potentials (Pasquet-Kok, Creese & Sack, 2010; Holloway-Phillips & Brodribb, 2011; Scoffoni, McKown, Rawls & Sack, 2012). I estimated an index of leaf hydraulic vulnerability for each species, the Ψ_{leaf} at 50% loss of K_{leaf} (P_{50}) as the Ψ_{leaf} at which K_{leaf} had declined to half of the y-intercept value, for the 23 species where a linear regression fitted the data (R^2 = 0.40-0.88; P < 0.001 to 0.019).

I determined hydraulic supply relative to demand in gas exchange with the ratio of leaf hydraulic conductance relative to stomatal conductance (K_{leaf}/g_s).

Using K_x determined based on anatomical measurements (see section *Quantification of vein, xylem and bundle sheath anatomical traits* below), I determined K_{ox} by re-arranging equation (1):

$$K_{ox} = (\frac{1}{K_{Leaf}} - \frac{1}{K_x})^{-1}$$

Quantification of leaf gas exchange

I measured light-saturated rates of gas exchange from 17 Feb to 28 June 2010, between 0900 and 1500 each day, for a mature leaf on each plant for six plants per species. I measured steady state gas exchange (<2% change over 6 minutes) using a LI-6400 XT portable photosynthesis system (LI-COR, Lincoln, Nebraska, USA). The leaf chamber was maintained at 25°C, with reference CO_2 400 ppm, and PPFD 2000 μmol m^{-2} s^{-1}, which was assumed to be saturating irradiance for these species[19]. The relative humidity was 60-80%, leading to vapor pressure deficits (VPD) of 0.80-1.6 kPa (overall mean 1.1 kPa). Measurements were made for 1-2 leaves from each of 6 plants (except from 5 plants for *A. purpurea*, 4 plants for *A. semialata*, 7 plants for *P. australis*, and for *L. sorghoidea* 3 leaves from each of two plants). Overall, 5-9 leaves per species were measured, with 6 on average. Leaf-area normalized values were determined for stomatal conductance (g_s) and net photosynthetic rate per leaf area (A_{area}). The ratio of intercellular to ambient CO_2 (C_i/C_a) was also estimated, since it is negatively related to water use efficiency. Leaves were harvested, scanned for leaf area (Canon Scan Lide 90, Canon USA, Lake Success, NY), dried at 70°C for at least 48h and weighed to determine the leaf dry mass per unit area (LMA) and net CO_2 assimilation rate per unit leaf dry mass (A_{mass}).

Quantification of vein, xylem and bundle sheath anatomical traits

To quantify anatomical traits, I measured and analyzed cross sections of one leaf for each of three individuals per species. Leaf venation traits such as vein density (D_v) and vein diameter (VD) and leaf size traits, were included in a previous study (Baird et al., 2021)

Images of transverse sections measured with a 5× objective were utilized to quantify the densities of all vein orders except 5° transverse veins as these were not visible in transverse

sections. Vein orders were established for each species based on species-specific phylogenetic history (Christin et al., 2013; Lundgren et al., 2019), and by estimations of vein size, presence/absence of enlarged metaxylem, and presence/absence of fibrous tissue above and/or below the vein (Ellis, 1976; Evert, 2006; Baird et al., 2021). I categorized major veins as the 1° vein, i.e., the midvein, the large central vein containing the largest metaxylem and fibrous tissue, and 2°, or "large" veins smaller than the midvein and of similar structure (Evert, 2006; Baird et al., 2021). I categorized minor veins as the 3° or "intermediate", 4° or "small" veins, and 5° or "transverse" veins (Evert, 2006; Baird et al., 2021). For C_3 grasses and most C_4 grasses, the smallest visible longitudinal veins were 3° "intermediate" veins. In NADP-ME C_4 grasses of the subfamily Panicoideae, 4° small veins evolved, which co-opted their mestome sheath for carbon reduction (Christin et al., 2013); these species thus have both 3° "intermediate" and 4° "small" vein orders (*Alloteropsis semialata, Andropogon gerardii, Cenchrus setaceus, Digitaria ciliaris, Digitaria eriantha, Echinochloa crus-galli, Paspalum dilatatum*), whereas Panicoideae species that co-opted the outer bundle sheath for carbon reduction (*Alloteropsis cimicina, Chloris elata, Chloris gayana, Eragrostis cilianensis, Eriachne aristidea, Panicum virgatum*) or non-Panicoideae species that co-opted the inner bundle sheath for carbon reduction (*Aristida purpurea, Aristida ternipes, Stipagrotis zeyheri*) lack 4° "small" vein orders. Due to the parallel formation of longitudinal (1°-4°) veins, vein density (D_v) for each order was quantified as the vein number per leaf width, equivalent to vein length per leaf area, assuming the leaf is approximately rectangular (Baird et al., 2021). Because transverse veins were not quantifiable in the cross-sections, I utilized chemically cleared and stained sections to quantify the densities (vein lengths per area) and diameters of these veins. Vein diameters were measured excluding the bundle and mestome sheath cell layers, averaged from one measure parallel and one measure

perpendicular to the width of the section. For all vein orders, I calculated vein surface area per leaf area (VSA) as $D_v \times \pi \times VD$, vein projected area per leaf area (VPA) as $D_v \times VD$ and vein volume per leaf area (VV) as $D_v \times \pi \times (VD/2)^2$. For the species *Lasiacis sorghoidia,* second-order veins were too few to be counted from transverse sections, and I established vein orders and vein densities and diameters of second order veins using the chemically cleared stained leaves.

Conduit dimensions and numbers were directly measured from one vein per each vein order per species from transverse sections at 20× and 40×, for one leaf per individual for three individuals per species. Xylem conduits were identified by the presence of toluidine blue staining of the highly lignified cell walls (John, Scoffoni & Sack, 2013). As I lacked transverse sections of second-order veins for *L. sorghoidea*, I did not measure its second-order conduit dimensions, and thus was excluded from analyses involving these traits. All xylem conduits were elliptical and the theoretical conductivity (k_t; mmol m s^{-1} MPa^{-1}) was determined from Poiseuille's equation modified for ellipses (Lewis & Boose, 1995; Cochard, Nardini & Coll 2004; Scoffoni et al., 2016),

$$K_t = \frac{\pi}{64\mu} \frac{a^3 b^3}{a^2 + b^2} \tag{2}$$

where μ is the viscosity of water at 25 °C, and *a* and *b* are the major and minor axes of the ellipse, respectively. I measured *a* and *b* for all xylem conduits, and their average, and averaged this estimate of conduit diameter for all conduits within a given vein order for each type. In grass leaves, proto-xylem conduits form early within major vein orders, and are obliterated during leaf

expansion, which results in an empty space termed the proto-xylem lacuna (Evert, 2006). By contrast, meta-xylem conduits differentiate and grow much later during leaf expansion, achieving large diameters in major veins, given their earlier initiation, but much smaller diameters in the minor vein orders (Evert, 2006). I measured the dimensions of the proto-xylem lacunae as this space also transports water (Westermaier, 1884; Strasburger, 1891; Buchholz, 1921; Canny, 2001), wide and narrow metaxylem conduits (Metaxylem I and II, respectively), within major veins and the narrow metaxylem of minor veins (Metaxylem II). The k_t of each vein order was determined as the sum of the k_t of all conduits of all types:

$$1° \, k_t = k_t \, Metaxylem \, I + \, k_t \, Metaxylem \, II + \, k_t \, Protoxylem \, Lacuna \qquad (3)$$

$$2° \, k_t = k_t \, Metaxylem \, I + \, k_t \, Metaxylem \, II + \, k_t \, Protoxylem \, Lacuna \qquad (4)$$

$$3° \, k_t = k_t \, Metaxylem \, II \qquad (5)$$

$$4° \, k_t = k_t \, Metaxylem \, II \qquad (6)$$

where $k_t \, Metaxylem \, I$ is the summed k_t of all type I metaxylem conduits, $k_t \, Metaxylem \, II$ is the summed k_t of all type II metaxylem conduits, and $k_t \, Protoxylem \, Lacuna$ is the k_t of the single protoxylem lacuna.

I calculated whole leaf K_t by summing the k_t values for of each longitudinal vein order:

$$K_t = 1° \, k_t + \, 2° \, k_t + \, 3° \, k_t + \, 4° \, k_t \qquad (7)$$

I calculated a leaf-length and area normalized specific conductivity (K_x, mmol m^{-2} s^{-1} MPa^{-1}) by multiplying the k_t of each vein order by its vein density (D_v, i.e. vein length per leaf

area), which is equivalent to vein number per width for grasses (Baird et al., 2021), and then dividing by half the leaf length (LL) squared. Normalizing by leaf length as well as area is necessary to scale the K_t from a conductivity to an area-specific conductance (Pasquet-Kok et al., 2010); using half the leaf length yields a K_x representing the average vein hydraulic pathway, assuming that longitudinal veins deliver water similarly along their length, on average. K_x determined this way is thus normalized by length- and area-, and thus in the same units as K_{leaf}:

$$K_x = ((1° \, k_t \times 1° \, D_V) + (2° \, k_t \times 2° \, D_V) + (3° \, k_t \times 3° \, D_V) + (4° \, k_t \times 4° \, D_V)) \div)(0.5 \times LL)^2) \tag{8}$$

I also quantified the outer perimeter of the bundle and mestome sheath (P_{bs} and P_{ms}) layers for all vein orders, as an estimate of the surface available for flow out of the vasculature to the mesophyll. For each vein order, I measured the diameter of the major and minor axes of one small, medium and large bundle and/or mestome sheath cell, and averaged the major and minor axis diameters per cell, and then averaged across the cell size classes to obtain an average cell diameter. To estimate the outer perimeter, I divided this average cell diameter (D) by 2 and multiplied by π and by the number of bundle or mestome sheath cells (CN) surrounding the vein of a given order and then averaged this value across all vein orders:

$$P_{bs} = ((1° \, (D_{bs} \div 2) \times \pi \times CN_{bs}) + (2° \, (D_{bs} \div 2) \times \pi \times CN_{bs}) + (3° \, (D_{bs} \div 2) \times \pi \times CN_{bs}) + (4° \, (D_{bs} \div 2) \times \pi \times CN_{bs})) \div 2 \tag{9}$$

$$P_{ms} = ((1° \, (D_{ms} \div 2) \times \pi \times CN_{ms}) + (2° \, (D_{ms} \div 2) \times \pi \times CN_{ms}) + (3° \, (D_{ms} \div 2) \times \pi \times CN_{ms}) + (4° \, (D_{ms} \div 2) \times \pi \times CN_{ms})) \div 2 \tag{10}$$

I also estimated the bundle and mestome sheath surface area per leaf area (*BSSA*, *MSSA*),

projected area per leaf area (*BSPA*, *MSPA*) and volume per leaf area (*BSV*, *MSV*) for each vein

order, and present total *BSSA* and *MSSA*, *BSPA* and *MSPA*, and *BSV* and *MSV* (i.e., sum of all

vein order bundle and mestome sheath surface areas, projected areas, or volumes), major *BSSA*

and *MSSA*, *BSPA* and *MSPA*, and *BSV* and *MSV* (i.e., sum of major vein bundle and mestome

sheath surface areas, projected areas, or volumes) and minor *BSSA* and *MSSA*, *BSPA* and *MSPA*,

and *BSV* and *MSV* (i.e., sum of minor vein bundle and mestome sheath surface areas, projected

areas, or volumes). I estimated the *BSSA* and *MSSA* of each vein order by first multiplying the

average bundle or mestome sheath cell diameter (*D*) (see above) by the D_v of the vein order and

by π and by the number of cells present (*CN*), the *BSPA* and *MSPA* by multiplying the average

bundle or mestome sheath cell diameter (*D*) (see above) by the D_v of the vein order and by the

number of cells present (CN), the *BSV* and *MSV* by multiplying the square of half the average

bundle or mestome sheath cell diameter (*D*) (see above) by the D_v of the vein order and by π and

by the number of cells present (*CN*):

$$BSSA = (1° \ D_{BS} \times \pi \times D_V \times CN_{BS}) + (2° \ D_{BS} \times \pi \times D_V \times CN_{BS}) + (3° \ D_{BS} \times \pi \times$$

$$D_V \times CN_{BS}) \hspace{6cm} (11)$$

$$BSPA = (1° \ D_{BS} \times \ D_V \times CN_{BS}) + (2° \ D_{BS} \times \ VLA \times CN_{BS}) + (3° \ D_{BS} \times \ D_V \times CN_{BS})$$

$$(12)$$

$$BSV = (1° \ (D_{BS} \div 2)^2 \times \ D_V \times CN_{BS}) + (2° \ (D_{BS} \div 2)^2 \times \ D_V \times CN_{BS}) +$$

$$(3° \ (D_{BS} \div 2)^2 \times \ D_V \times CN_{BS}) \hspace{5cm} (13)$$

$$MSSA = (1° D_{MS} \times \pi \times D_V \times CN_{MS}) + (2° D_{MS} \times \pi \times D_V \times CN_{MS}) + (3° D_{BS} \times \pi \times$$

$$D_V \times CN_{MS}) + (4° D_{MS} \times \pi \times D_V \times CN_{MS}) \tag{14}$$

$$MSPA = (1° D_{MS} \times D_V \times CN_{MS}) + (2° D_{MS} \times D_V \times CN_{MS}) + (3° D_{MS} \times D_V \times CN_{MS}) +$$

$$(4° D_{MS} \times \pi \times D_V \times CN_{MS}) \tag{15}$$

$$MSV = (1° (D_{MS} \div 2)^2 \times D_V \times CN_{MS}) + (2° (D_{MS} \div 2)^2 \times D_V \times CN_{MS}) +$$

$$(3° (D_{MS} \div 2)^2 \times D_V \times CN_{MS}) + (4° D_{MS} \times \pi \times D_V \times CN_{MS}) \tag{16}$$

Compilation of grass leaf hydraulic and photosynthetic data

To characterize C_3 and C_4 differences in leaf hydraulic and photosynthetic physiology, as well as their potential contrasts in trait-trait associations, I extracted data from the 34 published studies that included data for the following traits for grasses: light-saturated leaf photosynthetic rate per leaf area (A_{area}), stomatal conductance (g_s), leaf hydraulic conductance (K_{leaf}), leaf xylem hydraulic conductance (K_x), leaf outside-xylem hydraulic conductance (K_{ox}), vein density (D_v), intrinsic leaf water-use efficiency (WUE_i), leaf water potential at turgor loss point (TLP), leaf water potential at 50% loss of leaf hydraulic conductivity (P_{50}), leaf water potential at 80% loss of leaf hydraulic conductivity (P_{80}) and leaf water potential at 88% loss of leaf hydraulic conductivity (P_{88}) (Table S4.3). From each study, I extracted 328 species mean trait values, and when a species was present in multiple studies, the trait was averaged for that species between

studies. I also estimated the ratio of K_{leaf}/g_s for studies that had data for K_{leaf} and g_s at the species level.

Statistical analyses: phylogenetic comparative methods

I utilized a phylogenetic comparative approach to account for the influence of phylogenetic covariance on average C_3 and C_4 trait differences and on trait-trait relationships using the R Language and Environment. For analyses including the 27 species grown in a common garden, I utilized a previously published time-calibrated phylogeny using the same 27 grass species (Baird et al., 2021). For the compiled grass database, I implemented phylogenetic analyses to test differences in traits between C_3 and C_4 species, and to test relationships between traits for all grasses, C_3 grasses only, and C_4 grasses only. As each trait in the larger database had a different sample size, I used numerous different phylogenies depending on the sample size to test for trait differences or trait-trait relationships, each trimmed from a larger global grass phylogeny (Spriggs, Christin & Edwards, 2014).

Our analyses utilized a custom-written code that is available on GitHub (https://github.com/smuel-tylor/grass-leaf-size-). For analyses of the 27 species from the common garden, and for the 328 species from the compiled database, I examined differences in species-level trait means between C_3 and C_4 species using a phylogenetically corrected analysis of variance (ANOVA), both parametric (based on *PGLS*) and nonparametric (Garland, Dickerman, Janis & Jones, 1993) using the phyloANOVA package (Revell, 2012). I also tested for relationships of leaf gas exchange and leaf structure, of climate of species origin and leaf traits, and of leaf hydraulic traits and leaf hydraulic anatomy using phylogenetically corrected regressions, including reduced major axis regressions (*PRMA*) or phylogenetic generalized least-

square regressions (*PGLS*), which incorporate phylogenetic correction as Pagel's λ (Pagel, 1999; Freckleton, Harvey & Pagel, 2002) estimated by maximum likelihood (Nlme - R - W3cubDocs). Thus, for *PRMA* I used the function phyl.RMA (Revell, 2012) and for *PGLS* I used the function corPagel (Revell, 2012) in combination with gls (Nlme - R - W3cubDocs) and optimized (Paradis & Schliep, 2019) to establish maximum likelihood estimates of λ. Utilization of *PRMA* or *PGLS* depended on the two traits being tested. The least squares approach is preferred when a dependent *y*-variable is related to an independent *x*-variable, when (1) there is less error in natural variation and/or measurement error in *x* than *y* and/or in cases when (2) *y* is determined by or to be predicted from *x*, but never *x* from *y* (Poorter & Sack, 2012; Sack et al., 2012; Baird et al., 2021). The reduced major axis approach is preferable in cases in which (1) *x* and *y* have similar error and/or when (2) *x* and *y* are codetermined, or their relationship is due to an underlying functional coordination or could be predicted using each other (Poorter & Sack, 2012; Sack et al., 2012; Baird et al., 2021). I note, however, that only the slope and intercept vary between *PRMA* and *PGLS*, and thus a significant relationship under either *PRMA* or *PGLS* is equally meaningful. I examined trait-trait relationships for both raw and log-transformed data and present both in the supplementary tables.

I implemented both phylogenetic and nonphylogenetic tests for analyses of trait-trait relationships across the 328 species database. The phylogenetic tests resulted in reduced sample size as many of the phylogenies generated for each trait-trait relationship could not account for all of the species in the database, due to species not being present in the larger phylogeny. Thus, I present both phylogenetic and nonphylogenetic analyses, but emphasize the nonphylogenetic analyses for our findings on trait-trait relationships for the 328 species. I used the function

cor.test to test for significant correlations between traits and present the pearson correlation coefficient, r, and p-value.

Modeling of hydraulic-stomatal-photosynthetic function of C₃ and C₄ species during drought under varying vapor pressure deficit and atmospheric CO₂

I modeled the consequences of soil and atmospheric drought, given the experimentally determined variation in hydraulic, stomatal and photosynthetic traits between C₃ and C₄ species. A previously-published model based on reasonable simplifying assumptions (Osborne and Sack, 2012) was used to determine the response of g_s and leaf water potential to declining soil water potential (Ψ_{soil}) and increasing vapor pressure deficit (*VPD*). Then, after adjusting g_s for a response to ambient CO_2 based on published relationships, I modeled the light-saturated net rate of photosynthesis at 25 °C and 35 °C based on well-established models for C₃ and C₄ photosynthesis. The models were run for the mean C₃ and C₄ plant data, and also for a C₃ plant with lower maximum g_s, giving the C₄ advantage in K_{leaf}/g_s, and for a C₄ grass with the mean K_{leaf}/g_s of C₃ species, achieved either by lowering maximum K_{leaf} or by raising maximum g_s, to determine the impacts on g_s and A_{area} under the range of simulated conditions.

The hydraulic-stomatal model determines leaf water potential (Ψ_{leaf}), plant hydraulic conductance (K_{plant}) and g_s at a given Ψ_{soil} and *VPD* based on its decline in response to Ψ_{leaf}. First, Ψ_{leaf} is determined based on steady-state water transport according to the Ohm's Law analogy (Wei et al., 1999; Tyree & Zimmerman, 2002):

$$\Psi_{leaf} = \Psi_{soil} - \frac{(g_s \times VPD)}{K_{plant}} \tag{17}$$

Second, a hydraulic response function modeled the vulnerability of K_{plant} to declining Ψ_{leaf} as a linear function following the approximate fit of the data between full hydration and turgor loss for leaves of grasses and for several other taxa (Holloway-Phillips & Brodribb, 2011; Scoffoni et al., 2012; Brodribb & McAdam, 2011):

$$K_{plant} = K_{max} + a \times \Psi_{leaf} \tag{18}$$

where K_{max} and a were the mean of species' y-intercepts and slopes respectively for K_{leaf} versus Ψ_{leaf} plots. I assumed that K_{plant} showed a similar vulnerability response to leaves (Brodribb & Cochard, 2009; Holloway-Phillips & Brodribb, 2011), calculating $K_{plant} = 80\% \times K_{leaf}$, based on the range shown in previous work on grasses (65% to over 80% of plant resistance in the leaf) (Sack and Holbrook, 2006; Holloway-Phillips & Brodribb, 2011). Changing these assumptions would not affect the comparative findings of our simulations.

Third, a stomatal response function modeled g_s decline with more negative Ψ_{leaf} as a sigmoidal function:

$$g_s = \frac{g^*}{1 + e^{-\frac{-(\Psi_{leaf} - b)}{c}}} \tag{19}$$

where g^* is a constant for a given species and b is the Ψ_{leaf} at 50% stomatal closure; mean P_{50} was used, based on previous work showing the strong similarity in many species, including grasses (Brodribb & Holbrook, 2003; Holloway-Phillips & Brodribb, 2011). The constant c defines

the shape of the sigmoidal curve. For our simulations, g^* was determined by solving eq. S3 using the mean measured g_s and operating Ψ_{leaf} for C_3 and C_4 species.

For given Ψ_{soil} and VPD, eqns 17-19 were solved simultaneously, minimizing the implicit forms by iteration (Microsoft Visual Basic; Microsoft, Redmond, WA, USA).

Using this model, I simulated the response of g to Ψ_{soil} from moist to droughted soil (0 to -2 MPa) and at moderate to high values of VPD (0.5 and 3 kPa), for C_3 and C_4 species, using experimentally determined values as parameters for eqns 17-19 or from the literature as available. I also tested scenarios for a C_3 plant with lower g_s, giving the C_4 advantage in K_{leaf}/g_s, for a C_4 grass with a lower K_{leaf}, giving the K_{leaf}/g_s of C_3 species, and for a C_4 grass with higher g_s, also giving the K_{leaf}/g_s of C_3 species, to determine the impacts on g_s and A_{area} under the range of simulated conditions.

I simulated photosynthetic rate (A_{area}) and its response to CO_2, by first modeling a direct response of g_s to CO_2, and then inputting the adjusted g_s values into equations for C_3 and C_4 photosynthesis.

First, for low and high CO_2 I multiplied the g_s values by a factor corresponding to 20 or 80 Pa (1.72 and 0.58 respectively) based on a previous compilation of responses in C_3 and C_4 grasses (Osborne & Sack, 2012). This multiplicative adjustment of g_s for CO_2 level was applied independently of the g_s response to water status (from which g was determined from eqns 17-19 above) based on the finding that the response of g_s to CO_2 and water status are independent (Morison & Gifford, 1983). Future work must better elucidate the mechanisms and precise optimization by which stomata respond to CO_2 and leaf water status; I modeled these as independent given the current state of understanding.

The g_s, now adjusted for CO_2, was used to predict A_{area} based on the equations for C_3 and C_4 photosynthesis provided by von Caemmerer (2000), using parameters at 20°C from Vico and Porporato (2008), with temperature dependencies according to Vico and Porporato (2008) to allow simulations at 25 °C and 35 °C. I assumed that the impact of Ψ_{leaf} on photosynthesis was mediated by g_s, without any separate, direct impacts on mesophyll conductance or on metabolism itself; these impacts could be added, but without information of differential impacts on C_3 and C_4 species, would not change the outcome of our scenarios (Vico & Porporato, 2008).

Thus, for C_3 species, A_{area} was determined as

$$A_{area} = \min(A_C, A_J) - R_d \tag{20}$$

where A_C is the Rubisco limited rate of photosynthesis, A_J is the rate of RuBP-limited CO_2 assimilation and R_d is the total mitochondrial rate of respiration.

In turn,

$$A_C = V_{c,max} \frac{C_m - \Gamma^*}{C_m + K_c(1 + \frac{o}{K_o})} \tag{21}$$

where $V_{c,max}$ is the maximum catalytic activity of Rubisco at current leaf temperature; C_m is the CO_2 concentration at the site of photosynthesis in the mesophyll cell; Γ^* is the equilibrium CO_2 compensation point for gross photosynthesis; K_c and K_o are the coefficients for CO_2 and O_2 of the Michaelis-Menten kinetics, accounting for competitive inhibition by O_2; and o is the O_2 concentration at the site of photosynthesis.

$$A_J = J_{max} \frac{C_m - \Gamma^*}{4(C_m + 2\Gamma^*)} \tag{22}$$

where J_{max} is the maximum potential rate of electron transport.

To determine A_{area} the equations 21 and 22 were each separately equated with the diffusion equation:

$$A_{area} = (C_a - C_m) \times g_t \qquad (23)$$

where g_t was determined as the conductance to CO_2 from ambient air to the intercellular space (stomatal conductance to CO_2, g_{s,CO_2}) and from the intercellular space to the chloroplast (mesophyll conductance, g_m) in series:

$$g_t = \frac{1}{\frac{1}{g_{s,CO_2}} + \frac{1}{g_m}} \qquad (24)$$

where g_{s,CO_2} was determined as $g_s/1.6$ and g_m as maximum simulated g_s (i.e., at $\Psi_{soil} = 0$ and VPD of 0.5 kPa) $\times \alpha_m$.

In each case (eqn 21 = eqn 23, and eqn 22 = eqn 23) the equations were solved for given g_s and C_a, to determine C_m using the quadratic equation. The values of C_m were inserted into eqs 21 and 22 respectively to determine A_C and A_J, before applying eq. 20 to determine A_{area}.

For the C_4 species, a similar approach was used, but the first step involved determining the PEP carboxylation rate (V_P):

$$V_P = \min\left(\frac{C_m V_{P,max}}{C_m + K_P}, V_{Pr}\right) \qquad (25)$$

where $V_{P,\,max\,is}$ the maximum rate of PEP carboxylation, V_{Pr} is an upper bound PEP regeneration rate, and K_P is the Michaelis-Menten coefficient of PEPC. The C_m was determined by equating eq. 25 with eq. 23 for a given C_a and g_s.

I then used the C_m and V_P to determine the A_{area}, by combining two equations:

$$A_{area} = V_P - L_{bs} - R_d \qquad (26)$$

where L_{bs} is bundle sheath leakage, given by:

$$L_{bs} = g_{bs} (C_{bs} - C_m) \tag{27}$$

and C_{bs} is the CO_2 concentration in the bundle sheath. Substituting eq. 27 into eq. 26, and making this equation equal to each of eqs 21 and 22 separately (substituting C_{bs} for C_m in those equations), allowed solving for C_{bs}, and using eqs 21 and 22 allowed determination of A_C and A_J, and eq. 20 was used to determine A_{area}.

Results and Discussion

The anatomical drivers of grass leaf hydraulic function

The anatomical drivers of K_{leaf} variation in grasses has been paradoxical. As part of their Kranz anatomy enabling carbon fixation to occur in the bundle or mestome sheath, C_4 grasses have higher D_v, which confers greater photosynthetic area (Ueno et al., 2006; Christin et al., 2013; Lundgren et al., 2019; Pathare et al., 2020; Baird et al., 2021) (Figure 4.1, Box 1). However, no clear consensus for the role of this higher D_v on grass leaf hydraulic capacity has emerged (Ogle, 2003; Christin et al., 2013). Whether the higher D_v of C_4 species provides higher K_{leaf} is unclear, as studies of 27 species of grasses of temperate and subtropical habitats found similar K_{leaf} on average for C_3 and C_4 species (Ocheltree, Nippert & Prasad, 2014; Taylor et al., 2018) and for 25 perennial species (Liu et al., 2019), higher K_{leaf} and D_v in 12 C_4 annuals than 5 C_3 annuals of subtropical regions (Liu et al., 2019), and higher K_{leaf} in a C_3 *Panicum* species compared to its C_4 sister taxa (Sonawane, Koteyeva, Johnson & Cousins, 2021). I thus hypothesized that in C_4 grasses the higher D_v associated with Kranz anatomy would not confer a higher K_{leaf} due to high outside-xylem limitation. Previous findings suggest that the evolutionary and ecological role of high D_v for C_4 species is principally for driving carbon concentration that leads to high A_{area} at low g_s and does not result in a higher K_{leaf}. Indeed, some have proposed that the high D_v of C_4 species initially conferred a high K_{leaf} relative to C_3 in early evolved C_4 species, continued selection for low K_{leaf} would drive lower K_{leaf} in lineages in which C_4 more recently evolved (Zhou et al., 2021). I examined the hydraulic role of D_v and xylem anatomy and/or by bundle sheath anatomy in C_4 species, the K_x and K_{ox} of C_3 relative to C_4 and their potential differences for the 27 diverse common garden-grown species (Table 4.1). The higher D_v of C_4 grasses was not associated with higher K_{leaf} (Box 1, Table S4.4). First, K_x did not differ between C_3 and C_4 species, as the higher

minor D_v of C_4 species was counteracted by thinner minor veins containing fewer xylem conduits, and the bulk of K_x is contributed by the major veins, which did not differ between C_3 and C_4 in density or xylem conduit numbers (Figures S4.2-S4.3, Table S4.4). Even more importantly, across grasses, variation in K_{leaf} is most strongly determined by K_{ox} (Box 1E and F, Table S4.4), as has been shown previously across closely related *Viburnum* species and separately across *Arabidopsis* mutants (Caringella et al., 2015; Scoffoni et al., 2016; Scoffoni, Albuquerque, Buckley & Sack). Indeed, C_3 and C_4 grasses exhibited similar >90% hydraulic resistance in the outside-xylem which would lead to the determination of K_{leaf} by K_{ox}, likely from greater anatomical and compositional complexity compared to within veins (Sack & Holbrook, 2006; Scoffoni et al., 2016) (Box 1, Figure S4.3). The low K_{ox} accounting for the dominant bottleneck within K_{leaf} by K_{ox} is consistent with low membrane permeability, which would be adaptative to amplify the response of stomatal closure to leaf dehydration, and to protect the mesophyll from desiccation and the xylem from embolism (Tyree, Fiscus, Wullschleger & Dixon, 1986; Cochard, Ewers & Tyree, 1994; Stiller, Lafitte & Sperry, 2003; Scoffoni et al., 2016, 2017). Across C_3 and C_{4-3L} species, K_{ox} and K_{leaf} were positively associated with the outer perimeter of the bundle and mestome sheaths (Box 1, Figure S4.4, Table S4.4). A greater sheath perimeter could provide greater surface area for transport through sheath cell walls, which are likely highly resistant due to hydrophobic components such as suberin and lignin, and potentially for transport through membrane aquaporins and/or plasmodesmata (*18, 51, 52*). Across all species, K_{ox} and K_{leaf} were independent of other potential correlates of K_{ox}, including D_v, *IVD*, leaf thickness (*LT)* and the minimum distance from veins to stomata (D_m) (Figure S4.5, Table S4.4). Notably, across species, K_{ox} was independent of minor D_v, though a high D_v would be associated with greater bundle sheath surface area and shorter flow pathways outside the xylem (Buckley, John, Scoffoni & Sack, 2015). Overall, on average, C_3

and C_4 grass species did not differ in leaf outside-xylem hydraulic conductance (K_{ox}), though C_3 species had higher leaf xylem hydraulic conductance (K_x), which was largely driven by the three aquatic C_3 species (Figure 4.2, Table S4.2-S4.3).

The decoupling of D_v with K_x and K_{ox} indicates that variation in D_v is less important for the evolution of maximum hydraulic flux in grasses, with a potential role in stress tolerance and for maintained photosynthetic performance. In C_3 species, the higher major D_v of smaller leaves would contribute to stress tolerance during harsh conditions as well as stress avoidance by enabling a higher A that would mitigate shorter growing periods (Baird et al., 2021). The higher minor D_v in C_4 species contributed to C_4 species having on average more than double that of C_3 species for total surface and projected area in the bundle and mestome sheaths, respectively, and two- to six-fold higher total volume per leaf area in the bundle sheath (BS) and mestome sheath (MS), which may contribute to maximized carbon concentration (Figure S4.6).

I partitioned the drivers of leaf xylem hydraulic conductance (K_x). Across the 27 grass species grown in the common garden, K_x increased positively with conduit diameter (*CD)*, but was independent of conduit numbers (*CN*) and D_v (Box 1, Table S4.4). K_x increased positively with the xylem conductance of $1°$ - $3°$ longitudinal vein orders (i.e. $K_{x\text{-vein order}}$, Figure S4.7, Table S4.4), and K_x of each longitudinal vein order (i.e. $K_{x\text{-Midvein}}, K_{x\text{-large}}, K_{x\text{-Intermediate}}, K_{x\text{-Small}}$) scaled positively with the corresponding vein order conduit diameter (Figure S4.7, Table S5). Indeed, the bulk of K_x was driven by the hydraulic conductance of the major vein xylem ($K_{x\text{-major}}$, i.e., $1°$ and $2°$ veins), as $K_{x\text{-major}}/K_x$ was 0.99 and 0.96 for C_3 and C_4 species, respectively (Figure S4.3, Table S4.2). The diameters of the $1°$ and $2°$ veins were strongly associated with the diameters of their type I metaxylem conduits, which contrasts with $3°$ veins whose diameters were driven by changes in conduit numbers (Figure S4.2, Table S4.6). C_4 grasses had 50%

greater minor vein xylem construction costs (CC_{minor}), though similar on average in total K_x/CC, indicating that the reduction in conduit number within these veins results in no change to xylem hydraulic supply relative to costs ($K_{x-minor}/CC_{minor}$), and indicates little constraints on the evolution of high D_v for C_4 carbon concentration (Table S4.2). Such little cost for the evolution of high D_v in C_4 grasses would be similar to the expectation that stems of C_4 eudicots would have reduced costs due to their lower hydraulic conductance (Kocacinar & Sage, 2003, 2004). The similar investment in major vein CC between C_3 and C_4 species is consistent with their similar *LMA* as major vein volume is a main driver of *LMA* variation across species (Sack et al., 2013) (Table S4.2). Across all species the D_v of 5° transverse veins was independent of transverse vein diameters and although the D_v of 5° transverse veins did not differ between C_3 and C_4 grasses, the diameters of these veins were significantly larger for C_3 species, leading to them having larger 5° transverse vein diameters at a given D_v (Figure S4.2, Table S4.2 and S4.6).

Lastly, across the 27 species grown experimentally, a higher A_{area} was related to several vein and bundle sheath size traits, including higher D_v, *VSA*, *VVA*, *MSSA*, *BSVA* and *MSVA*, and lower *IVD*, indicating anatomical drivers of A_{area} (Table 4.1, Figure S4.8, Table S4.7). For C_3 species, the relationships of sheath traits and A_{area} are consistent with the influence of sheath traits, such as P_{bs} and P_{ms} on K_{leaf} and thus coordination mediated by g_s (Table S4.5 and S4.7). Yet, for C_4 species, the higher A_{area} with such traits is consistent with the role of sheath dimensionality on leaf carbon concentration mechanisms, as greater sheath surface area would facilitate higher flow rates between bundle sheath and mesophyll, and greater sheath volume provides more space for sheath compartmentalized carbon reduction. The higher D_v and lower *IVD* would also contribute to maximized photosynthetic productivity by reducing the distance and transport resistance between veins and mesophyll.

130

C₄ hydraulic hyper-efficiency

The hydraulic design associated with photosynthetic divergence in C_3 and C_4 grasses has remained a paradox (Figure 4.1). Among C_3 species, high A_{area} depends on higher D_v and K_{leaf}, but C_4 grasses have higher D_v and lower g_s, presenting an apparent hydraulic surplus (Figure 4.1). I further hypothesized that a high K_{leaf} relative to g_s in C_4 species would provide hydraulic hyper-efficiency. In diversifying diversified across warmer, drier and more open environments, C_4 grasses, benefitted from their greater A_{area} at lower g_s, conferring higher water use efficiency (Osborne & Freckleton, 2009; Edwards & Smith, 2010). Yet, despite their typically lower g_s, associated with their lower stomatal density (Taylor et al., 2012), C_4 photosynthetic rate can decline steeply when CO_2 drawdown occurs within the leaf during stomatal closure (Osborne & Sack, 2012; Israel, Watson-Lazowski, Chen & Ghannoum, 2022). A high K_{leaf}/g_s has been invoked to explain certain species' ability to maintain g_s at high VPD in temperate and tropical tree species (Sack, Tyree & Holbrook, 2005; Brodribb & Jordan, 2008; Scoffoni et al., 2016) and was previously hypothesized to enable evolution of C_4 photosynthesis under drying conditions in a low CO_2 past (Osborne & Sack, 2012). I tested experimentally the hypothesis that unlike C_3 grasses, which would have coordinated A_{area}, g_s and K_{leaf}, in C_4 grasses, A_{area} and g_s would be decoupled from K_{leaf}, such that g_s would be consistently low relative to their K_{leaf} and Ψ_{leaf} remain high during gas exchange (Figure 4.1). Further, I used modeling to test our hypothesis that C_4 plants would benefit from a higher K_{leaf}/g_s, i.e., a "hyper-efficient" water transport system that delivers higher hydraulic supply relative to demand to maintain stomata open, and avoid sensitive decline of A_{area} during transpiration under high evaporative loads or moderate soil drought (Osborne & Sack, 2012). Finally, I hypothesized that this contrasting coordination would be associated with differences between C_3 and C_4 grasses in their adaptation to climatic

131

aridity in species' native environments. Thus, among C_3 grasses, species with higher hydraulic

and photosynthetic rates would dominate the driest climates via an ability to mitigate stressful

periods by growing rapidly when conditions are favorable, whereas among C_4 grasses, the

hydraulic surplus would enable a high A_{area} to be achieved under both moist and dry conditions.

Indeed, a safety-efficiency trade-off in K_{leaf} and hydraulic vulnerability, P_{50}, has been previously

shown across C_4 grasses, and may also contribute varying impacts of C_4 hyper-efficiency on

adaptation to aridity (Ocheltree et al., 2016).

In our database of novel and compiled data C_4 species had higher VLA, K_{leaf}, K_{leaf}/g_s, A_{area}

WUE_i and lower g_s, IVD and P_{80} than C_3 species (phylogenetic ANOVA, Table 4.1, Figure 4.2,

Table S4.3). For the 27 common garden species, as C_3 and C_4 grasses invested similarly in leaf

mass per unit area (LMA), C_4 species had a 36% higher A_{mass} (Figure 4.2, Table S4.2). Further, on

average, C_4 grass species had a twofold higher ratio of hydraulic conductance to stomatal

conductance, K_{leaf}/g_s, arising from C_4 species having 51% lower g_s, and higher K_{leaf} (Figure 4.2,

Table S4.2). C_3 and C_4 species did not differ in hydraulic vulnerability (i.e. P_{50} = Ψ_{leaf} at 50% loss

of K_{leaf}). C_4 species had higher operating Ψ_{leaf} than their C_3 counterparts, and a 48% lower ratio of

intercellular to ambient CO_2 (C_i/C_a), which reflects higher water use efficiency and is consistent

with their higher intrinsic water-use efficiency (WUE_i, i.e., A_{area}/g_s), (Figure 4.2, Table S4.2).

Although K_{leaf} did not differ statistically between C_3 and C_4 species for the 27 common garden

species, the higher K_{leaf} found for the compiled database drives an even higher K_{leaf}/g_s (Figure 4.2,

Table S4.2-S4.3).

Modelling of the integrated photosynthetic, stomatal and hydraulic systems demonstrated

the importance of K_{leaf}/g_s in the C_4 photosynthetic advantage (Martin-StPaul, Delzon & Cochard,

2017). For Ψ_{soil} values representing moist soil and moderate drought, modeled C_4 species

maintained less negative Ψ_{leaf} values than C_3 species and a superior ability to maintain g_s and A_{area} (Figure 4.3). At moderate leaf temperature (25 °C) and vapor pressure deficit (VPD) (0.5 kPa), and at higher temperature (35 °C), the C_4 photosynthetic advantage occurred at Ψ_{soil} above -0.5 MPa, and was maintained over a broader range of Ψ_{soil}, respectively (Figure 4.3, Figures S4.9-S4.10). At higher VPD (3 kPa), C_4 assimilation advantages were maintained at all Ψ_{soil} and were reproduced at current CO_2 levels, at the low CO_2 levels representing the atmospheric conditions when C_4 evolved in many lineages (Edwards & Smith, 2010) and at double current CO_2 levels expected in future climates (Figure 4.3, Figures S4.9-S4.10). When I simulated a C_4 grass with the lower K_{leaf}/g_s observed in C_3 grasses, by maintaining g_s while reducing K_{leaf}, this C_4 grass failed in all conditions, with a low g_s and A_{area} in moist soil that declined steeply with reduction of Ψ_{soil} (Figure 4.3, Figures S4.9-S4.10). I also simulated a C_4 grass with the lower K_{leaf}/g_s observed in C_3 grasses, but maintaining K_{leaf} while increasing maximum g_s, this C_4 grass with high g_s showed a strong advantage in A_{area} at low VPD, but failed hydraulically at high VPD, resulting in strong depression of Ψ_{leaf}, g_s, and A_{area} (Figure 4.3, Figures S4.9-S4.10). I tested the impact of increasing K_{leaf}/g_s in a C_3 plant to that observed in C_4 species, by lowering maximum g_s. This manipulation led to a C_4-like ability to maintain g_s during drought, but exacted a considerable penalty in A_{area} for the C_3 species (Figure 4.3, Figures S4.9-S4.10).

The disproportionally higher K_{leaf}/g_s, i.e. hyper-efficiency, in C_4 grasses is a required adaptation for their higher maximum photosynthetic rates and provides a physiological basis for the repeated evolution of C_4 species and their subsequent radiation in dry environments (Sage, 2004; Edwards & Smith, 2010; Sage et al., 2011; Osborne & Sack, 2012). Our simulations show that the advantage of high K_{leaf}/g_s is as important an adaptation as C_4 biochemistry in contributing to the photosynthetic advantage of C_4 over C_3 grasses in moist soil and moderate drought, and thus

contributes to their domination of open, lower rainfall environments in the tropics (Edwards & Smith, 2010). While rising global CO_2 levels favor C_3 plants by reducing their photorespiration (Higgins & Scheiter, 2012), our models incorporating hydraulic adaptation indicated that C_4 grasses would sustain their physiological advantage in dry environments, whereas a reduction of K_{leaf} in concert with maximum g_s would have limited A_{area} even for C_4 species under low VPD. Conversely, even with reduced maximum g_s, a high K_{leaf}/g_s would drive an advantage in A_{area} for C_4 photosynthetic species at high VPD, especially under the low CO_2 atmosphere experienced during the proliferation of the C_4 grass lineages in the Miocene (Edwards et al., 2010). Hyper-efficient water transport provides a hydraulic-basis for the higher A_{area} in C_4 grasses, and would arise repeatedly given that a low g_s and its anatomical basis in low stomatal density, and a high K_{leaf} given its anatomical basis in vein sheath properties, and D_v, would be selected in C_3 species of dry and sunny environments, along with the evolution of large bundle sheath cells (Sage, 2004; Taylor et al., 2012; Osborne & Sack, 2012; Christin et al., 2013). Thus, a high K_{leaf}/g_s may have evolved simultaneously with C_4 biochemistry, or even as a precursor adaptation (Marazzi et al., 2012), indicating that a high K_{leaf}/g_s would be a necessary target in engineering novel C_4 crop species, with emphasis on a high K_{leaf}.

Contrasting evolution of leaf hydraulics and gas exchange with climate in C_3 and C_4 grasses

Hyper-efficient water transport also explains the contrasting coordination of leaf hydraulics and gas exchange traits among C_3 and C_4 grasses and their adaptation to climate (Figure S4.11, Table S4.7-S4.9). Across our database, C_3 and C_4 species exhibited contrasting coordination of hydraulics and gas exchange, reflecting differential adaptation to the environment as modulated by climate (Brodribb & Jordan, 2008; Scoffoni et al., 2016) (Fig. 2, fig. S11, Table S4.7-S4.8).

Among the terrestrial C_3 grasses of the 27 species in the common garden, A_{area} and g_s scaled with K_{leaf}, indicating investment in a hydraulic system to match the demand (Sack & Holbrook, 2006), and is consistent with previous work on C_3 grasses, and in the compiled database (Zhou et al., 2021) (Figure 4.2, Figure S4.11, Table S4.7-S4.8). Further, consistent with the hypothesis that a disproportionate hydraulic supply to similar demand could lead to their decoupling, the C_4 grasses showed no correlation among gas exchange or hydraulics traits, having low g_s relative to C_3 species, and moderate to high A_{area} across the range of K_{leaf} (Figure 4.2, Figure S4.11, Table S4.7-S4.8). C_4 grasses in the common garden also exhibited a trade off in hydraulic safety vs. efficiency, as has been previously shown across nine C_4 grasses, though this was not found in the compiled database (Ocheltree et al., 2016) (Figure S4.12, Table S4.8). Consistent with other studies and for species in the compiled database, for our 27 species the coordination of A_{area} and g_s differed strongly between C_3 and C_4 species (Downes, 1969; Osborne & Sack, 2012; Zhou et al., 2021), as A_{area} for C_3 species saturated at high g_s, signifying increasing limitations on CO_2 diffusion and assimilation (von Caemmerer & Evans, 2010), whereas C_4 species showed a steeper relationship, shifted towards higher A_{area} at a given g_s (Figure 4.2, Figure S4.11), implying a consistent limitation of A_{area} by g_s due to the greater intercellular CO_2 drawdown (Bjorkman, 1971).

Coordination of hydraulics and gas exchange for C_3 grasses would contribute to C_3 species with higher physiological rates being associated in drier and colder climates, whereas the hydraulic specialization of C_4 grasses would be associated with environments that are dryer and have greater evaporative demand. Such associations would arise from C_3 and C_4 avoidance of drought, compensating with rapid growth during the shorter duration of high moisture enabling distribution across climates (Baird et al., 2021). Indeed, across the 27 common garden grasses,

C_3 species of warmer and drier areas (lower mean annual precipitation; MAP and higher mean annual temperature; MAT) exhibited higher K_{leaf}, g_s and A_{area} (Figure 4.3, Figure S4.13, Table S4.9), consistent with stress avoidance, as such plants would capitalize on short rainfall pulses and growing seasons, and compensate for reduced performance during dry and cold periods (Grubb, 1998). However, for C_4 grasses, K_{leaf}, g_s and A_{area} were decoupled from MAP, which suggests an alternate mechanism for drought avoidance (Table S4.9). Indeed, C_4 grass species with higher K_{leaf}/g_s and K_{leaf}/A_{area} were associated with environments with higher potential evapotranspiration (*PET*, Figure 4.3, Table S4.9), and as our simulations showed, a high K_{leaf}/g_s would provide advantages under resource plentiful and dry conditions, and thus contributes to maximized growth for C_4 species contributing to their ability to avoid drought (Figure 4.1). Across all grasses, those with higher WUE_i were found in environments with greater evaporative demand and drier environments overall (potential evapotranspiration, PET, mm day^{-1}; aridity index, AI, Figure 4.3, Table S4.9). Lastly, three aquatic C_3 grass species showed higher gas exchange rates at a given K_{leaf} than terrestrial C_3 species, consistent with adaptation to higher Ψ_{soil}, which would reduce the hydraulic conductance required to obtain a given water supply to stomata (Sack et al., 2005; Feild et al., 2011) (Figure 4.2, Figure S4.12).

Table

Table 4.1. Variables quantified to resolve the paradoxes of C$_4$ grass ecology and vasculature. Note that many of these traits can be partitioned between vein orders and/or partitioned into total, major, or minor vein categories.

Trait	Symbol	Unit
Leaf hydraulic physiology		
Leaf hydraulic conductance	K_{leaf}	mmol m^{-2} s^{-1} MPa^{-1}
Leaf xylem hydraulic conductance	K_x	mmol m^{-2} s^{-1} MPa^{-1}
Leaf outside-xylem hydraulic conductance	K_{ox}	mmol m^{-2} s^{-1} MPa^{-1}
Leaf water potential	Ψ_{leaf}	-MPa
Leaf water potential at 50% loss of hydraulic conductance	P_{50}	-MPa
Leaf gas exchange physiology		
Light-saturated leaf photosynthetic rate per leaf area	A_{area}	μmol m^{-2} s^{-1}
Light-saturated leaf photosynthetic rate per leaf mass	A_{mass}	μmol g^{-1} s^{-1}
Light-saturated leaf stomatal conductance per leaf area	g_s	mol m^{-2} s^{-1}
Ratio of photosynthetic rate to stomatal conductance, i.e. intrinsic leaf water-use efficiency	A_{area}/g_s or WUE_i	μmol mol^{-1}
Ratio of leaf hydraulic conductance to stomatal conductance	K_{leaf}/g_s	mmol MPa^{-1} mol^{-1}
Ratio of leaf hydraulic conductance to photosynthetic rate	K_{leaf}/A_{area}	mmol MPa^{-1} μmol^{-1}
Light-saturated leaf intrinsic water-use efficiency per leaf area	WUE_i	μmol mol^{-1}
Leaf venation and structure		
Vein density, i.e. vein length per leaf area	D_v	cm cm^{-2}
Vein diameter	VD	mm
Vein surface area per leaf area	VSA	unitless
Vein projected area per leaf area	VPA	unitless
Vein volume per leaf area	VVA	mm
Conduit diameter		
Type I xylem conduit diameter	CD_{meta1}	μm
Type II xylem conduit diameter	CD_{meta2}	μm
Type I xylem conduit number	CN_{meta1}	#
Type II xylem conduit number	CN_{meta2}	#
Vein xylem construction cost	CC	unitless
Ratio of xylem hydraulic conductance to xylem construction cost	K_x/CC	mmol m^{-2} s^{-1} MPa^{-1}
Interveinal distance	IVD	μm
Vein to epidermal distance	D_m	μm
Leaf thickness	LT	μm
Leaf mass per area	LMA	g m^{-2}
Vein sheath		
Bundle sheath surface area per leaf area	$BSSA$	unitless
Mestome sheath surface area per leaf area	$MSSA$	unitless
Bundle sheath projected area per leaf area	$BSPA$	unitless
Mestome sheath projected area per leaf area	$MSPA$	unitless
Bundle sheath volume per leaf area	BSV	mm^3 mm^{-2}
Mestome sheath volume per leaf area	MSV	mm^3 mm^{-2}
Bundle sheath perimeter	P_{bs}	μm
Mestome sheath perimeter	P_{ms}	μm

Box

A **C₃**

3° 2° 3° 3° 1° 3° 3° 2° 3°

2° H_2O CO_2 3° 3°

Bundle sheath cell
Mestome sheath cell
Type I xylem conduit
Type II xylem conduit
Phloem cell
Sclerenchyma cell

Epidermal cell
Mesophyll cell
Guard cell
Subsidiary cell

H_2O CO_2

B **C₄₋₃ₗ**

2° H_2O CO_2 3° 3° 3°

H_2O CO_2

C **C₄**

D

| Vein xylem pathways | Vein density (D_v) | Outside-xylem pathways |

K_x K_{ox}

K_{leaf}

C₃ terrestrial 3L C₄ terrestrial 3L
C₃ aquatic 3L C₄ terrestrial 4L

E   F $r = 0.98^{***}$

K_{leaf} (mmol m⁻² s⁻¹ MPa⁻¹)

K_x (mmol m⁻² s⁻¹ MPa⁻¹) K_{ox} (mmol m⁻² s⁻¹ MPa⁻¹)

0 200 400   0 10 20 30

G   H $r = 0.45^*$ I

K_x (mmol m⁻² s⁻¹ MPa⁻¹)

D_v (cm cm⁻²) CD (µm) CN (#)

40 80 120   10 15 20   2 4 6 8 10

J   K   L $r = 0.65^{**}$

D_v (cm cm⁻²) P (µm) P_{ms} (µm)

40 80 120   300 500 700   200 300 400

138

Box 4.1. Leaf hydraulic anatomy and physiology of C_3 and C_4 grasses. Grasses have linearized leaves with up to four orders of parallel longitudinal veins, including the 1° midvein and large 2° major veins, intermediate 3° minor veins and, in C_4 NADP-ME species of the subfamily Panicoideae, small 4° veins, all connected by 5° transverse veins. Water flows through xylem conduits within veins and radially across sheaths, which often have hydrophobic cell walls due to suberization and/or lignification, and grasses have a mestome sheath interior to their bundle sheath (Sade, Shatil-Cohen & Moshelion, 2015; Caringella, Bongers & Sack, 2015; Ohtsuka, Sack & Taneda, 2018) and through the outside-xylem mesophyll pathways before evaporating and diffusing out of the leaf. Three longitudinal vein orders occur in **(A)** C_3 and **(B)** most C_4 species (i.e., C_{4-3L}) although **(C)** most C_4 species of the subfamily Panicoideae evolved an additional 4th vein order, in which the mestome sheath is the only sheath type (i.e., C_{4-4L}). Carbon reduction reactions occur in mesophyll of C_3 species **(A)** and bundle sheath in C_{4-3L} species **(B)** and in the mestome sheath in C_{4-4L} species **(C)**. **(D)** Leaf hydraulic conductance (K_{leaf}) can be partitioned into two components, i.e., the hydraulic conductance of the vein xylem pathways (K_x), which depends on xylem conduit conductivities and vein density (D_v), and the hydraulic conductance of the outside-xylem pathways (K_{ox}), which depends on biochemical and dimensional properties of the living tissues outside the xylem. Images from left to right: *Triticum aestivum* midrib cross-section (bar, 0.1 mm), micrograph of a chemically cleared and stained leaf, and lamina cross-section (bar, 0.1mm). C_4 grasses have higher minor D_v, higher bundle and mestome sheath diameters (Christin et al., 2013), and lower stomatal densities (Taylor et al., 2012). Across 27 C_3 and C_4 grass species grown in a common garden, **(E)** K_{leaf} and leaf xylem hydraulic conductance (K_x) were independent, and **(F)** K_{leaf} is determined by leaf outside-xylem hydraulic conductance (K_{ox}). Relationships of K_x and **(G)** vein density (D_v), **(H)** vein conduit

diameter (*CD*) and **(I)** vein conduit number *(CN)*, and of K_{ox} and **(J)** D_v, **(K)** the outer perimeter of the bundle sheath tissue (P_{bs}) and **(L)** the outer perimeter of the mestome sheath (P_{ms}). Barplots in panels **(G)** and **(H)** show the difference in total D_v, and type II *CN* averaged across vein orders, respectively, between C_3 and C_4 species. Only terrestrial species with three longitudinal vein orders were included for relationships in **(K)** and **(L).**

Figures
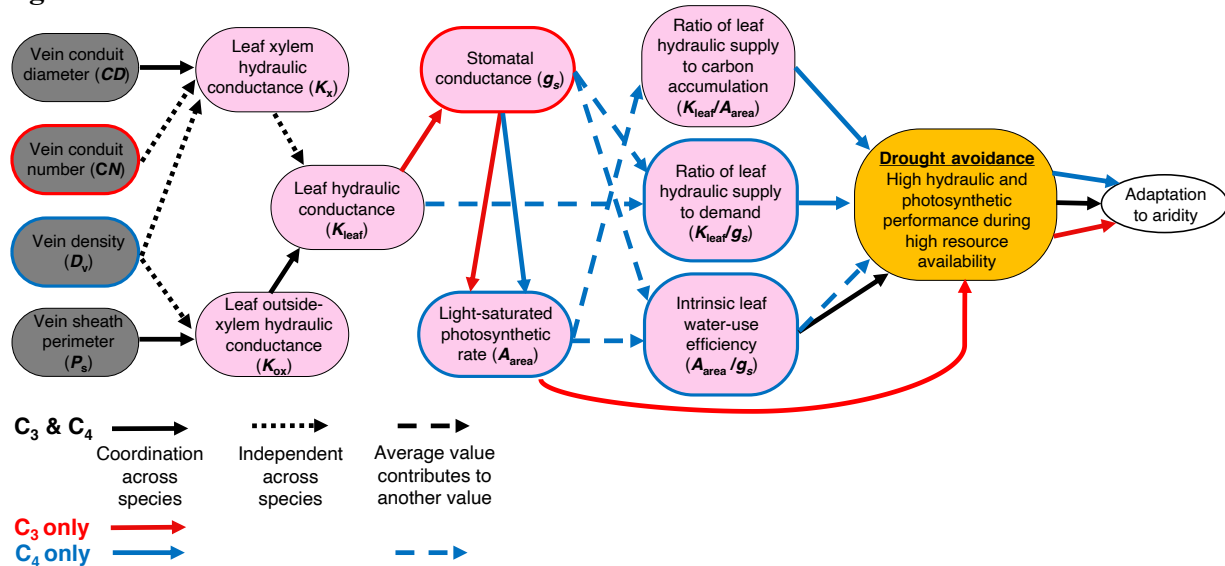
Figure 4.1. Conceptual diagram depicting linkages of leaf anatomy and leaf hydraulics, leaf hydraulics and leaf gas exchange, and their coordinated influence that scales to influence leaf drought tolerance and adaptation to climatic aridity. Solid black, red or blue lines indicates a significant relationship across all, C_3 only or C_4 only species, respectively. Dotted black, red or blue lines indicates a hypothesized relationship but was independent across all, C_3 only or C_4 only species, respectively. Dashed red or blue lines indicate that averages for a trait for C_3 or C_4 species, respectively, contributes to another trait value that leads to differential adaptation to climate between C_3 and C_4 species. Boxes with thickened borders indicate a significant difference in average C_3 and C_4 traits, with colors representing which group had the higher value. Across all species, variation in P_s drives variation in K_{ox}, and variation in CD drives variation in K_x, with variation in K_{ox} ultimately determining K_{leaf}. Only C_3 grasses exhibit coordination of K_{leaf}, g_s and A_{area}, and C_4 grasses exhibit coordination of only g_s and A_{area}. This leads to both C_3 and C_4 grass species exhibiting greater drought avoidance via divergent mechanisms, as C_3 grasses with highest K_{leaf}, g_s and A_{area} would maximize growth under favorable conditions. The disproportionately high

141

K_{leaf} relative to consistent low g_s in C_4 grasses leads to a decoupling of K_{leaf} and g_s, though the high K_{leaf}/g_s contributes to drought avoidance as the high K_{leaf}/g_s allows for maintained water potential and higher photosynthetic rate, leading to them also maximizing growth under favorable conditions and tolerance of dry conditions. Across all grasses, higher leaf water-use efficiency also contributes to drought avoidance, as a high leaf water-use efficiency would lead to reduced water loss relative to carbon gain and allow for continued growth under resource-rich conditions. Yet, the average higher WUE_i of C_4 grasses would further contribute to their greater ability to avoid drought compared to C_3 grasses. Grey and pink boxes reflect structural and physiological traits, respectively, whereas the orange box reflects the mechanism of adaptation to drought.
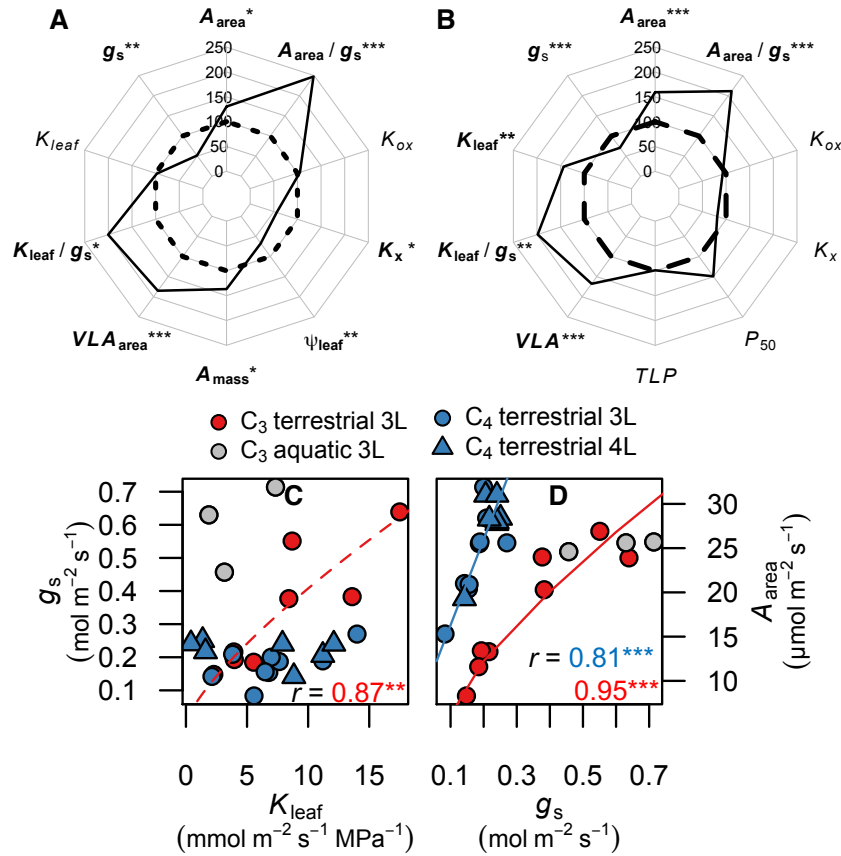
Figure 4.2. Differences and contrasting coordination in hydraulic and photosynthetic physiology for C$_3$ and C$_4$ grasses.

Radar graphs for leaf hydraulic and photosynthetic traits for **(A)** 27 common garden grown grasses and **(B)** 328 grasses from the compiled database, where C$_3$ species means were fixed arbitrarily as the 100% reference value (dark dashed line), and the black solid line indicates the percent difference between the C$_3$ and C$_4$ species. Bolded traits indicate a significant difference by phylogenetic analysis of variance. Relationships of **(C)** stomatal conductance (g_s) and leaf hydraulic conductance (K_{leaf}) and of **(D)** light-saturated leaf photosynthetic rate per leaf area (A_{area}) and g_s. Power laws were fitted using phylogenetic reduced major axis regressions (*PRMA*) for all relationships, except for C$_4$ species in **(D)** in which a linear model better characterized this

relationship. Red and blue lines indicate that the relationship was significant across C_3 or C_4 species only, respectively, or C_3 and C_4 species with varying slopes, as in **(D)**. Only terrestrial species were included for relationships of C_3 species in **(C)**. Significance: *$P < 0.05$; **$P < 0.01$; ***$P < 0.001$. $N = 11$ C_3, 16 C_4 species in **(C)** and **(D)**. Statistics and parameters are found in Tables S4.2-S4.3, S4.7-S4.8. See Table 4.1 for trait definitions and units.
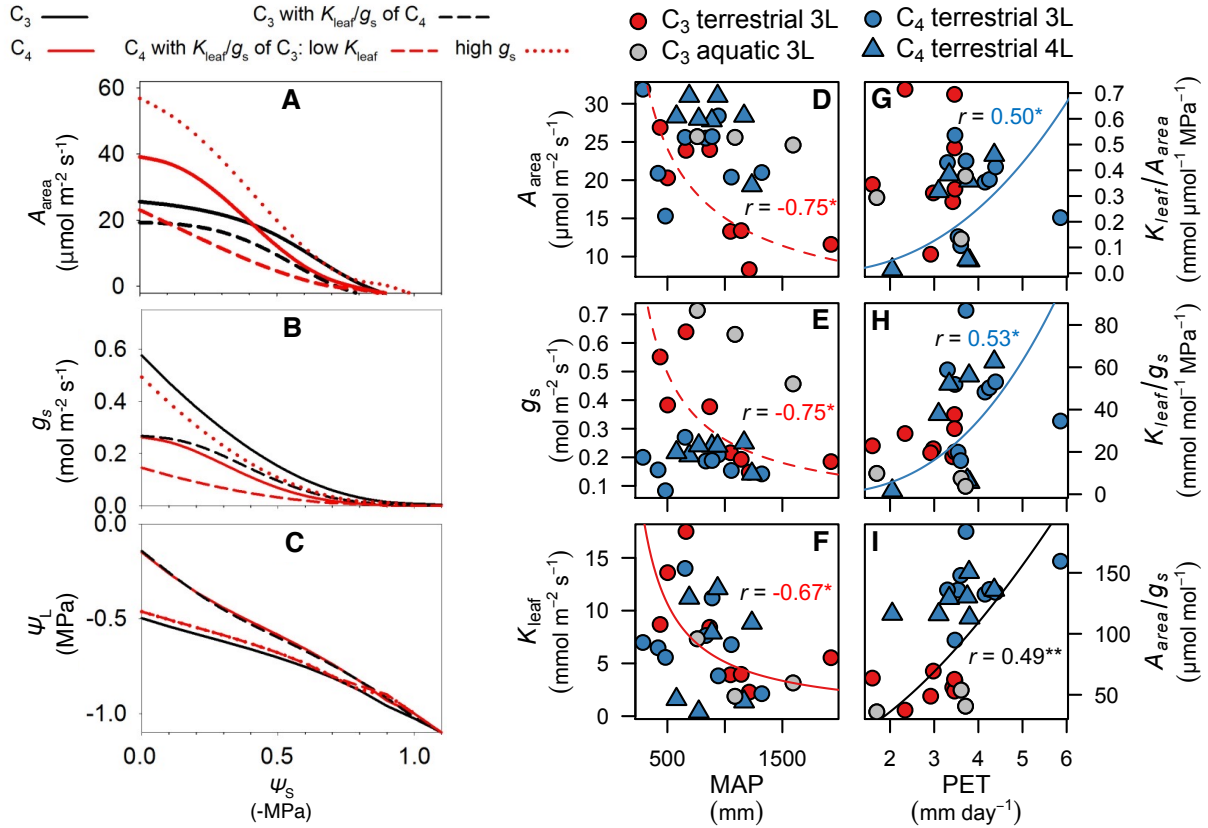
Figure 4.3. Contrasting physiological adaptation to aridity in C₃ and C₄ grasses. The responses of **(A)** A_{area} **(B)** g_s and **(C)** K_{leaf} to declining Ψ_{soil} at vapor pressure deficit (VPD) of 0.5 kPA and at CO_2 of 40 Pa (at 3 kPA VPD in figs. S9-S10). Simulations were run at 25 °C (at 35°C in fig. S10). Relationships of **(D)** A_{area}, **(E)** g_s and **(F)** K_{leaf} with mean annual precipitation (MAP) for only terrestrial C₃ plants in **(D)** and **(E)** and all C₃ in **(F)**, and of **(G)** the ratio of leaf hydraulic conductance to photosynthetic rate (K_{leaf}/A_{area}) and **(H)** of the ratio of leaf hydraulic conductance to stomatal conductance (K_{leaf}/g_s) to potential evapotranspiration (*PET*) for C₄ grasses, and **(I)** of the ratio of photosynthetic rate to stomatal conductance (A_{area}/g_s, i.e. *WUE*ᵢ) with PET across all species. Significance: *$P < 0.05$; **$P < 0.01$. $N = 11$ C₃, 16 C₄ species in **(D)** – **(I).** Statistics and parameters are found in Table S4.9. See Table 4.1 for trait definitions and units.

Supplementary Materials

Supplementary Data Captions (see attached Excel Workbook)

Table S4.1. Published studies for grasses on the relationships of photosynthetic rate, stomatal conductance, leaf hydraulic conductance and leaf hydraulic anatomical traits. For each study, I report the species numbers and taxonomic information; growing conditions; and confirmation of trends supported across species, as presented in the study or by our analyses of their data. Legend is provided below Table. References ordered from most recent to oldest.

Table S4.2. Species of grasses (Poaceae) included in the common garden study, subfamily, tribe, C₃/C₄ photosynthetic pathway, C₄ subtype, seed source, accession number, seed treatment for germination, terrestrial/aquatic, sun/shade, and means of anatomical and morphological traits measured and climate data, and statistics from phylogenetic analysis of variance below trait means. Traits left blank for a given species indicates that this species did not have this trait, e.g. did not have bundle sheath and only had the inner sheath, and did not have the 4° vein. Traits with NA for a given species indicates that I did not ascertain quantifiable data for these species, e.g. 2° vein traits for *Lasiacis sorghoidea*.

Table S4.3. Hydraulic, photosynthetic and anatomical data for 328 grass species from published studies and used to test relationships of leaf gas exchange and hydraulics across species, and to test average differences between C₃ and C₄ species. I present the reference, species, C₃/C₄ photosynthetic pathway for the species, method used to measure leaf hydraulic conductance (K_{leaf}), and values from all studies **(A)** for the traits: K_{leaf}, K_x, K_{ox}, g_s, A_{area}, WUE_i,

146

TLP, P_{50}, P_{80}, P_{88}, *VLA*, and *IVD* or **(B)** averaged to the species level across all studies, including

this study. Average C$_3$ and C$_4$ differences and statistics from phylogenetic analysis of variance

are found below table **(B)**

**Table S4.4. Statistics and parameters for associations of leaf hydraulic traits with leaf
hydraulic, photosynthetic and anatomical traits across all species, terrestrial species only,
C$_3$ species only, C$_3$ terrestrial species only and C$_4$ species only.** I present the leaf hydraulic
traits and leaf structural traits as *y*- and *x*- variables, respectively, the *r*- and *p*- values, *a*- and *b*-
values which correspond to the intercept and slope, respectively, for significant relationships.
Relationships using log-transformed data are presented first, and those with raw data are found
directly beneath.

**Table S4.5. Statistics and parameters for associations of leaf xylem hydraulic conductance
per vein order with leaf hydraulic anatomy across all species.** I present the leaf hydraulic
traits and leaf structural traits as *y*- and *x*- variables, respectively, the *r*- and *p*- values, *a*- and *b*-
values which correspond to the intercept and slope, respectively, for significant relationships.
Relationships using log-transformed data are presented first, and those with raw data are found
directly beneath.

**Table S4.6. Statistics and parameters for coordination or trade-offs of leaf structural traits
across all species.** I present leaf structural traits as both *y*- and *x*- variables, the *r*- and *p*- values,
a- and *b*- values which correspond to the intercept and slope, respectively, for significant

relationships. Relationships using log-transformed data are presented first, and those with raw data are found to the right.

Table S4.7. Statistics and parameters for associations of leaf photosynthetic traits with leaf hydraulic and anatomical traits across all species, terrestrial species only, C_3 species only, C_3 terrestrial species only and C_4 species only. I present the photosynthetic traits and leaf traits as y- and x- variables, respectively, the r- and p- values, a- and b- values which correspond to the intercept and slope, respectively, for significant relationships. Relationships using log-transformed data are presented first, and those with raw data are found directly beneath.

Table S4.8. Correlation matrices for trait-trait relationships for the compiled grass database. I present pairwise tests for all traits, tested across all species, or C_3 or C_4 species alone. R- values are provided with p- values in parentheses. The upper and lower diagonals include analyses on log-transformed and raw data, respectively. Matrices are presented for nonphylogenetic and phylogenetic tests. NA indicates that the relationship was not tested due to sample size $n < 4$ for at least one of the traits. Significant relationships are highlighted in yellow at $p < 0.05$.

Table S4.9. Statistics and parameters for associations of climate with leaf hydraulic, photosynthetic and anatomical traits across all species, terrestrial species only, C_3 species only, C_3 terrestrial species only and C_4 species only. I present the climate variables and leaf traits as y- and x- variables, respectively, the r- and p- values, a- and b- values which correspond

to the intercept and slope, respectively, for significant relationships. Relationships using log-transformed data are presented first, and those with raw data are found directly beneath.

Supplementary Figures
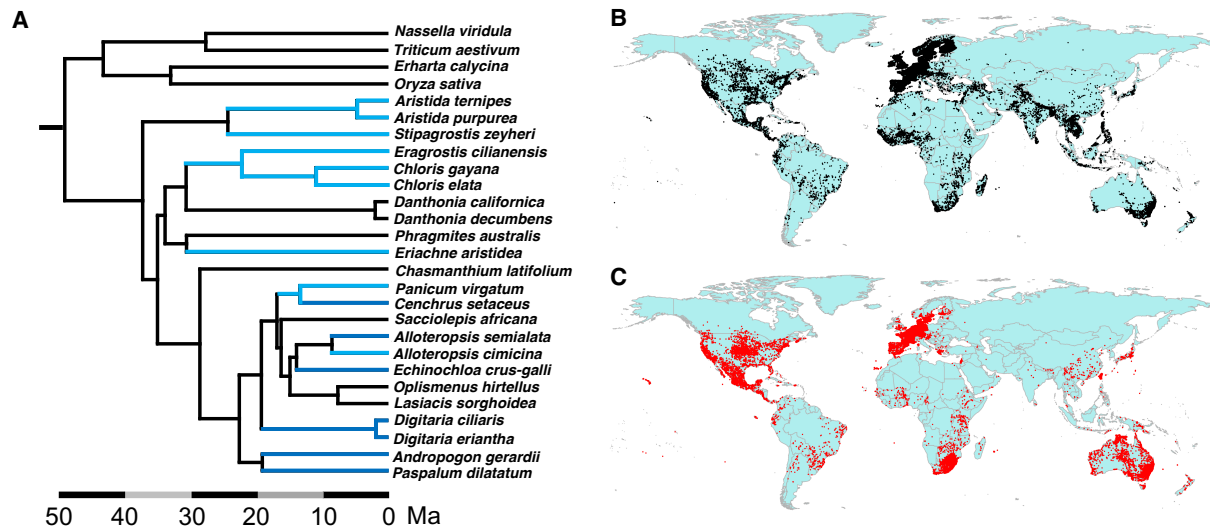
Figure S4.1. Phylogenetic tree and biogeographic distributions of 27 grass species grown in a common garden and sampled for hydraulic and anatomical traits. (A) black branches, 11 C_3 species; light blue branches, 9 C_{4-3} species; dark blue branches, 7 C_{4-4L} species (Baird et al. 2021). Map of the distributions of **(B)** 11 C_3 and **(C)** 16 C_4 species (Baird et al., 2021).
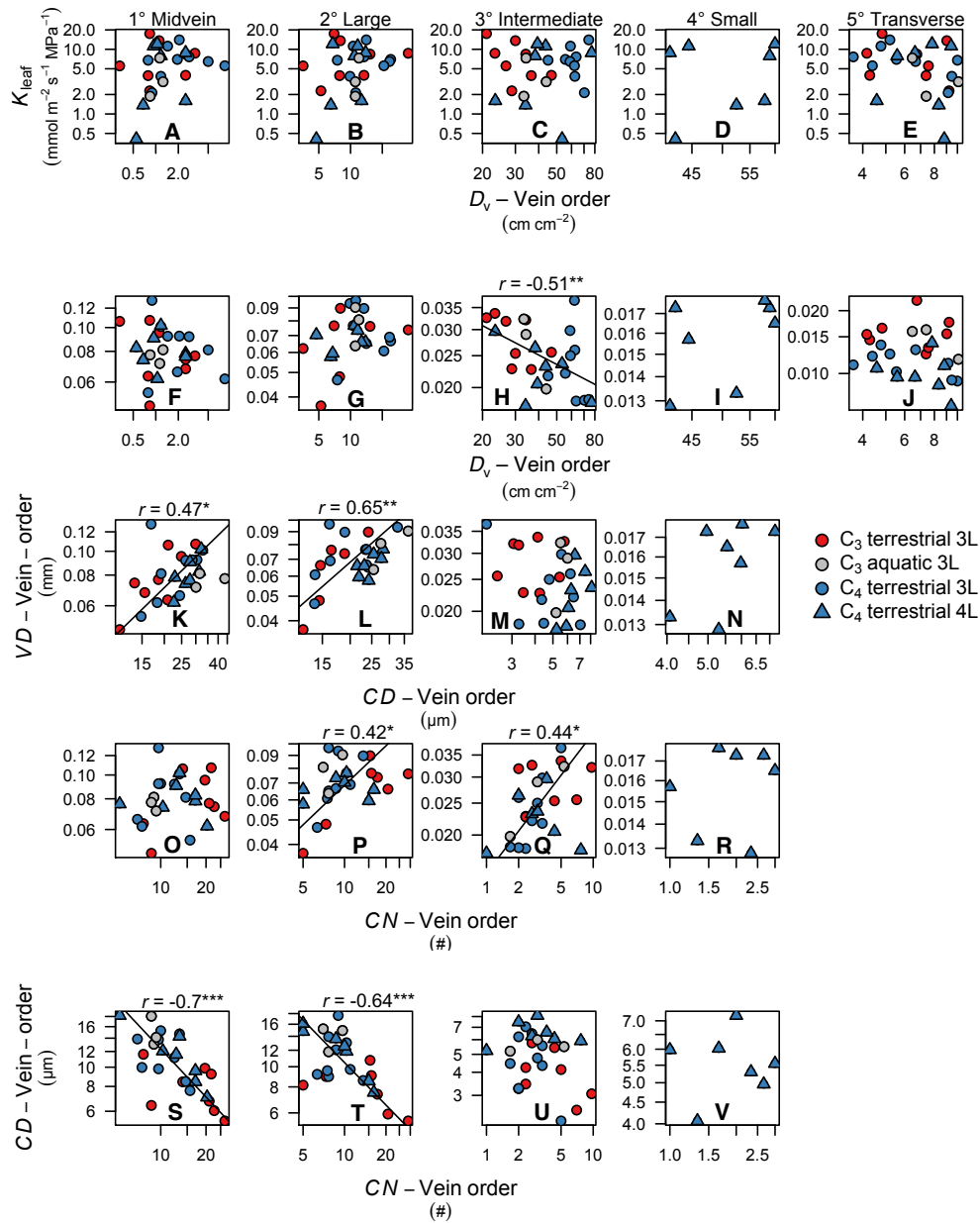
Figure S4.2. Counteracting the influence of higher vein density (D_v) in C$_4$ grasses.

Independence of leaf hydraulic conductance (K_{leaf}) with vein density (D_v) of **(A)** 1°, **(B)** 2°, **(C)** 3°, **(D)** 4° and **(E)** 5° veins. Relationships of leaf vein order specific diameter (VD) with D_v of **(F)** 1°, **(G)** 2°, **(H)** 3°, **(I)** 4° and **(J)** 5° veins, with leaf vein specific conduit diameter (CD) of **(K)** 1°, **(L)** 2°, **(M)** 3° and **(N)** 4° veins, and with leaf vein specific conduit number (CN)

of **(O)** $1°$, **(P)** $2°$, **(Q)** $3°$ and **(R)** $4°$ veins. Relationships of leaf vein order specific *CD* with leaf vein specific *CN* of **(S)** $1°$, **(T)** $2°$, **(U)** $3°$ and **(V)** $4°$ veins. Lines were fitted with phylogenetic reduced major axis regressions (PRMA) and drawn when significant: $*P < 0.05$; $**P < 0.01$; $***P < 0.001$. $N = 11$ C$_3$, 16 C$_4$.
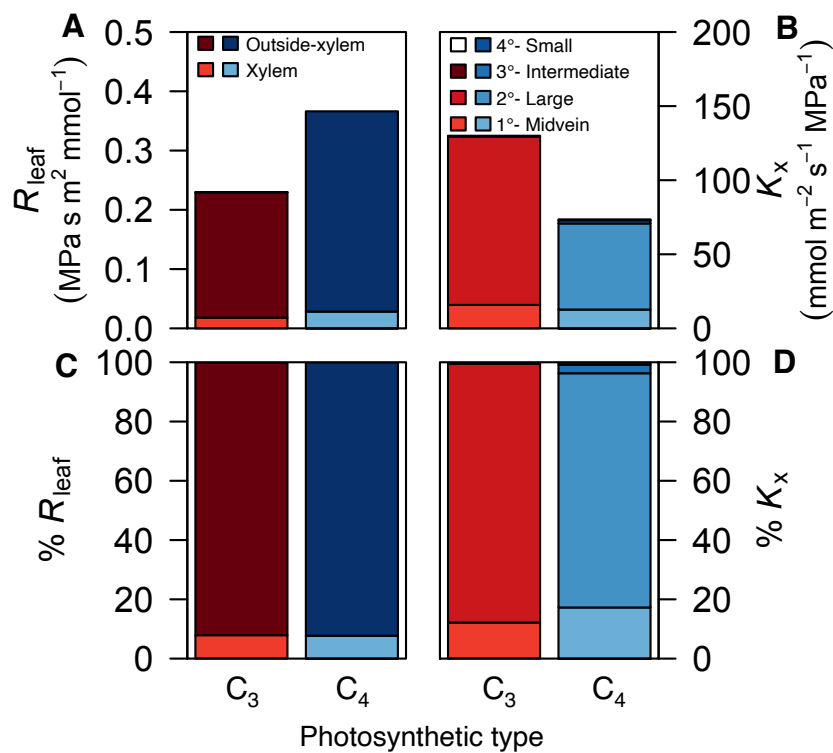
Figure S4.3. Partitioning of the leaf hydraulic resistance and leaf xylem conductance across vein orders (A) Leaf hydraulic resistance (R_{leaf}) of the outside-xylem and xylem pathways, **(B)** Leaf xylem hydraulic conductance (K_x) of each longitudinal vein order, **(C)** Percentage of R_{leaf} of the outside-xylem and xylem pathways **(D)** Percentage of K_x of each longitudinal vein order. $N = 10$ C$_3$, 11 C$_4$.
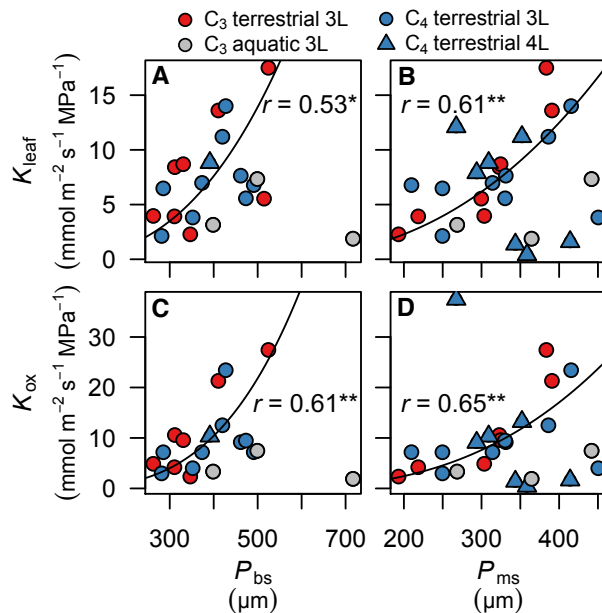
Figure S4.4. Determinants of leaf hydraulic conductance (K_{leaf}) and leaf outside-xylem hydraulic conductance (K_{ox}), for 27 grasses, grown in a common garden. Relationships of **(A)** K_{leaf} and **(C)** K_{ox} with the perimeter of the bundle sheath (P_{bs}), and of **(B)** K_{leaf} and **(D)** K_{ox} with the perimeter of the mestome sheath (P_{ms}). Lines drawn through 17 terrestrial species with 3 longitudinal vein orders (C_3, 7 species; C_4, 10 species). Lines were fit with phylogenetic reduced major axis regressions (PRMA) and drawn when significant: *$P < 0.05$; **$P < 0.01$; ***$P < 0.001$.
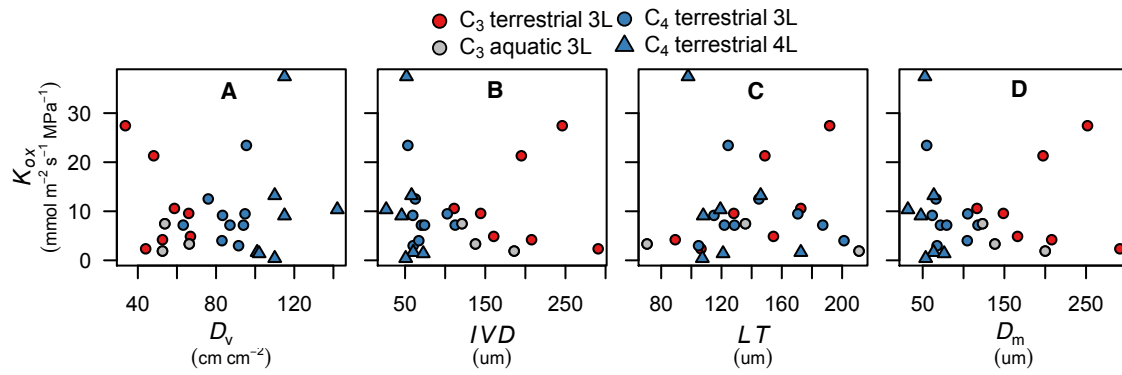
Figure S4.5. Potential drivers of leaf outside-xylem hydraulic conductance. Independence of leaf outside-xylem hydraulic conductance (K_{ox}) with **(A)** vein density (D_v), **(B)** inter-veinal distance (*IVD*), **(C)** leaf thickness (*LT*) and **(D)** maximum distance from vein to stomata (D_m). N = 10 C_3, 16 C_4.
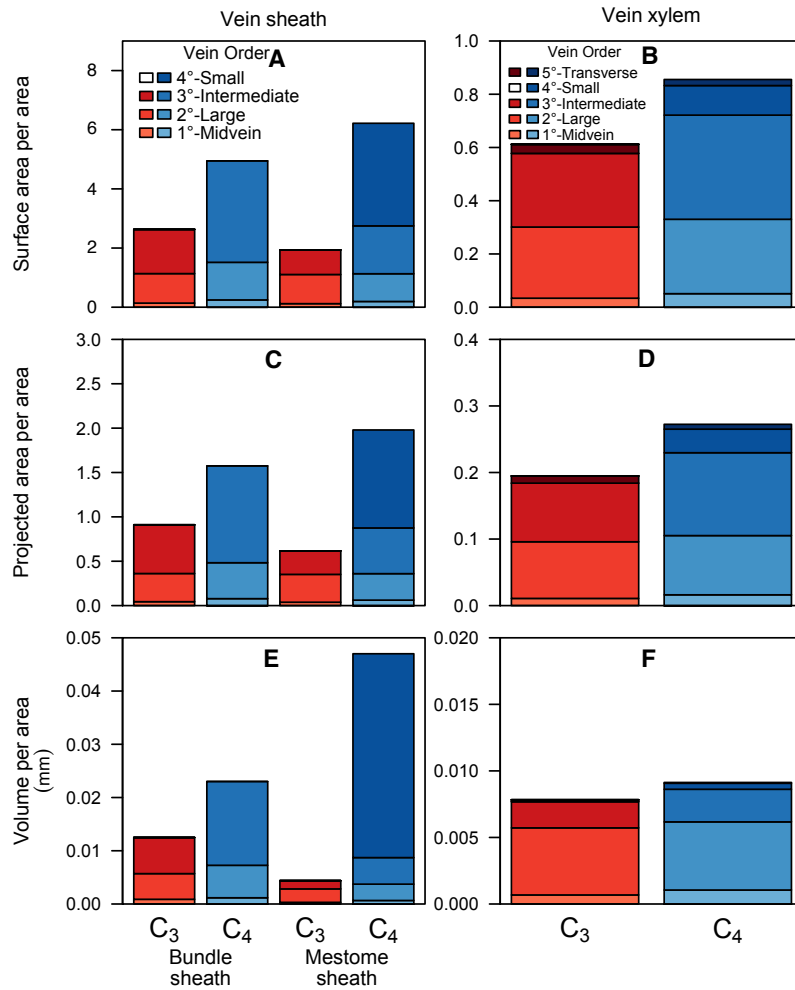
Figure S4.6. Partitioning of the total surface area, projected area and volume of leaf vein sheaths and leaf vein xylem, and volume for C_3 and C_4 grass species and by vein order. (A) Leaf vein bundle and mestome sheath surface area per area (*SA*), (C) projected area per area (*PA*) and (E) volume per area (*VA*). (B) Leaf vein xylem *SA*, (D) *PA* and (F) *VA*. Average C_3 and C_4 differences found in Table S4.2. $N = 11$ C_3, 16 C_4.
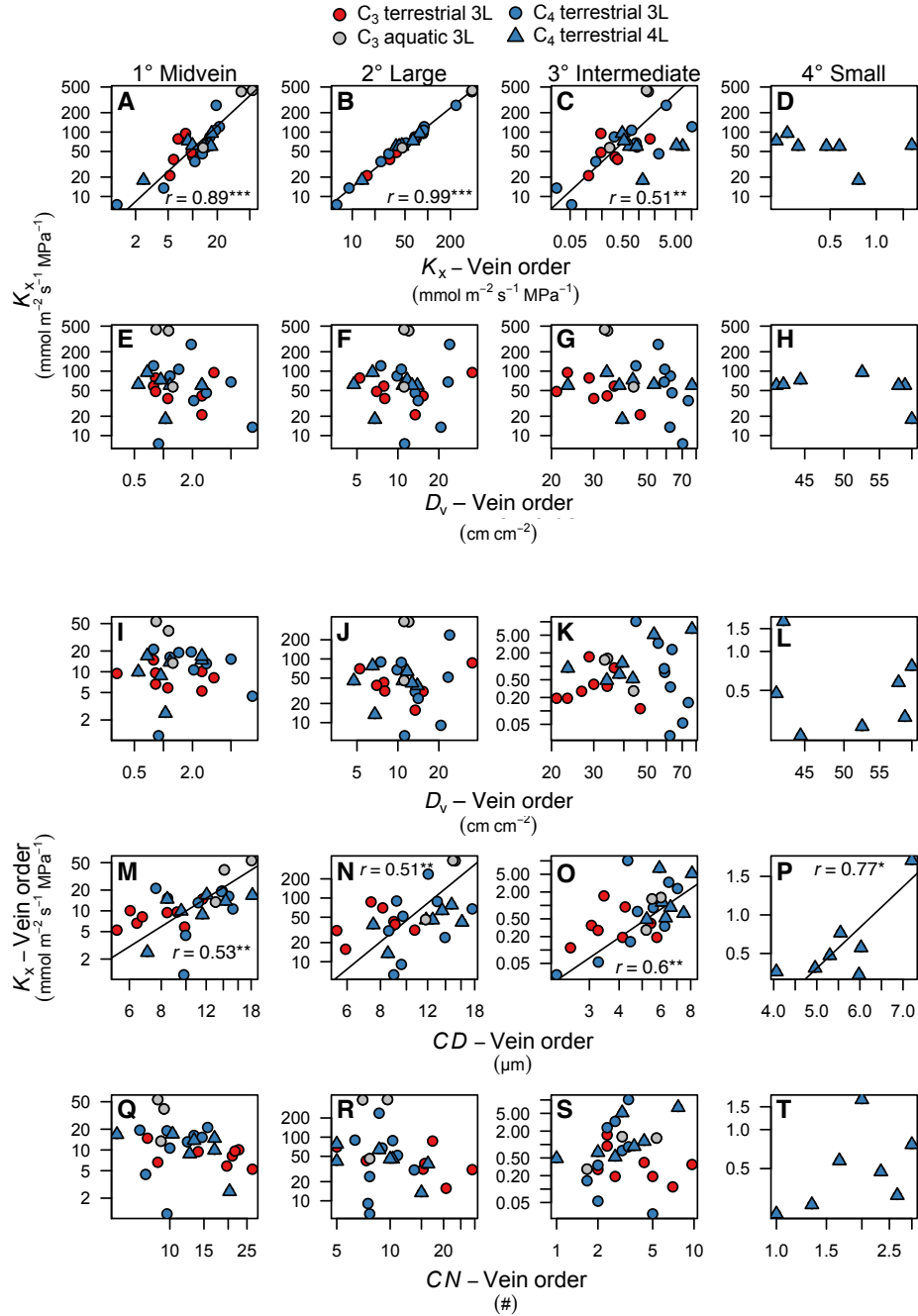
Figure S4.7. Determinants of leaf xylem hydraulic conductance (Kx). Relationships of whole leaf xylem hydraulic conductance (K_x) with **(A)** midvein xylem hydraulic conductance ($K_{x\text{-midvein}}$), **(B)** second order xylem hydraulic conductance ($K_{x\text{-large}}$), **(C)** third order xylem hydraulic conductance ($K_{x\text{-intermediate}}$) and **(D)** fourth order xylem hydraulic conductance ($K_{x\text{-small}}$).

Independence of K_x with **(E)** midvein vein density ($D_{v\text{-midvein}}$), **(F)** second order vein density ($D_{v\text{-large}}$), **(G)** third order vein density ($D_{v\text{-intermediate}}$) and **(H)** fourth order vein density ($D_{v\text{-small}}$). Relationships of vein order specific K_x with **(I)** $D_{v\text{-midvein}}$ **(J)** $D_{v\text{- large}}$, **(K)** $D_{v\text{-intermediate}}$ and **(L)** $D_{v\text{-small}}$, with vein order specific conduit diameter (CD) for **(M)** first order midvein ($CD_{midvein}$), **(N)** second order large veins (CD_{large}), **(O)** third order intermediate veins ($CD_{intermediate}$) and **(P)** fourth order small veins (CD_{small}), with vein order specific conduit number (CN) for **(Q)** midvein conduit number ($CN_{midvein}$), **(R)** second order conduit number (CN_{large}), **(S)** third order conduit number ($CN_{intermediate}$) and **(T)** fourth order conduit number (CN_{small}). Lines were fit with phylogenetic reduced major axis regressions (PRMA) and drawn when significant: $*P < 0.05$; $**P < 0.01$; $***P < 0.001$. $N = 10$ C$_3$, 16 C$_4$ species.
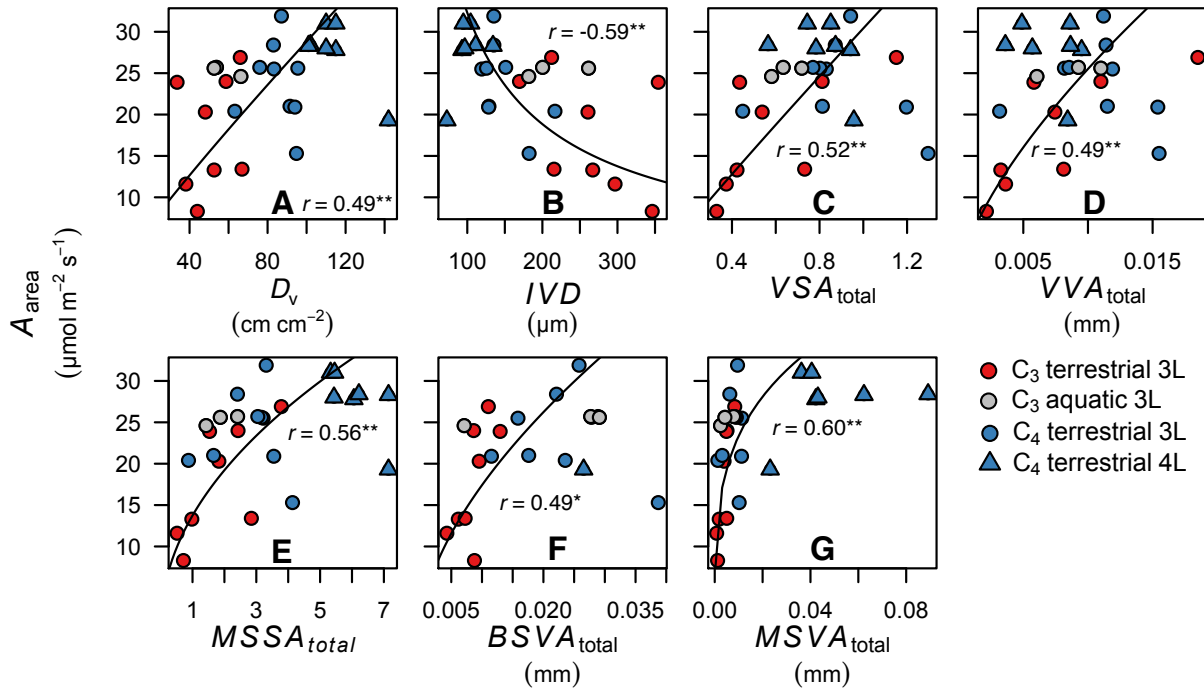
Figure S4.8. Coordination of leaf photosynthetic rate with leaf hydraulic anatomy.

Relationships of leaf photosynthetic rate (A_{area}) with **(A)** total vein density (D_v) **(B)** interveinal-distance (IVD), **(C)** total vein surface area per area (VSA), **(D)** total vein volume per area (VVA), **(E)** total bundle sheath surface area per area ($BSSA$), **(F)** total mestome sheath surface area per area ($MSSA$), **(G)** total bundle sheath volume per area ($BSVA$) and **(H)**, total mestome sheath volume per area ($MSVA$). Lines were fit with phylogenetic reduced major axis regressions (PRMA) and drawn when significant: $*P < 0.05$; $**P < 0.01$; $***P < 0.001$. $N = 11$ C$_3$, 16 C$_4$ species.
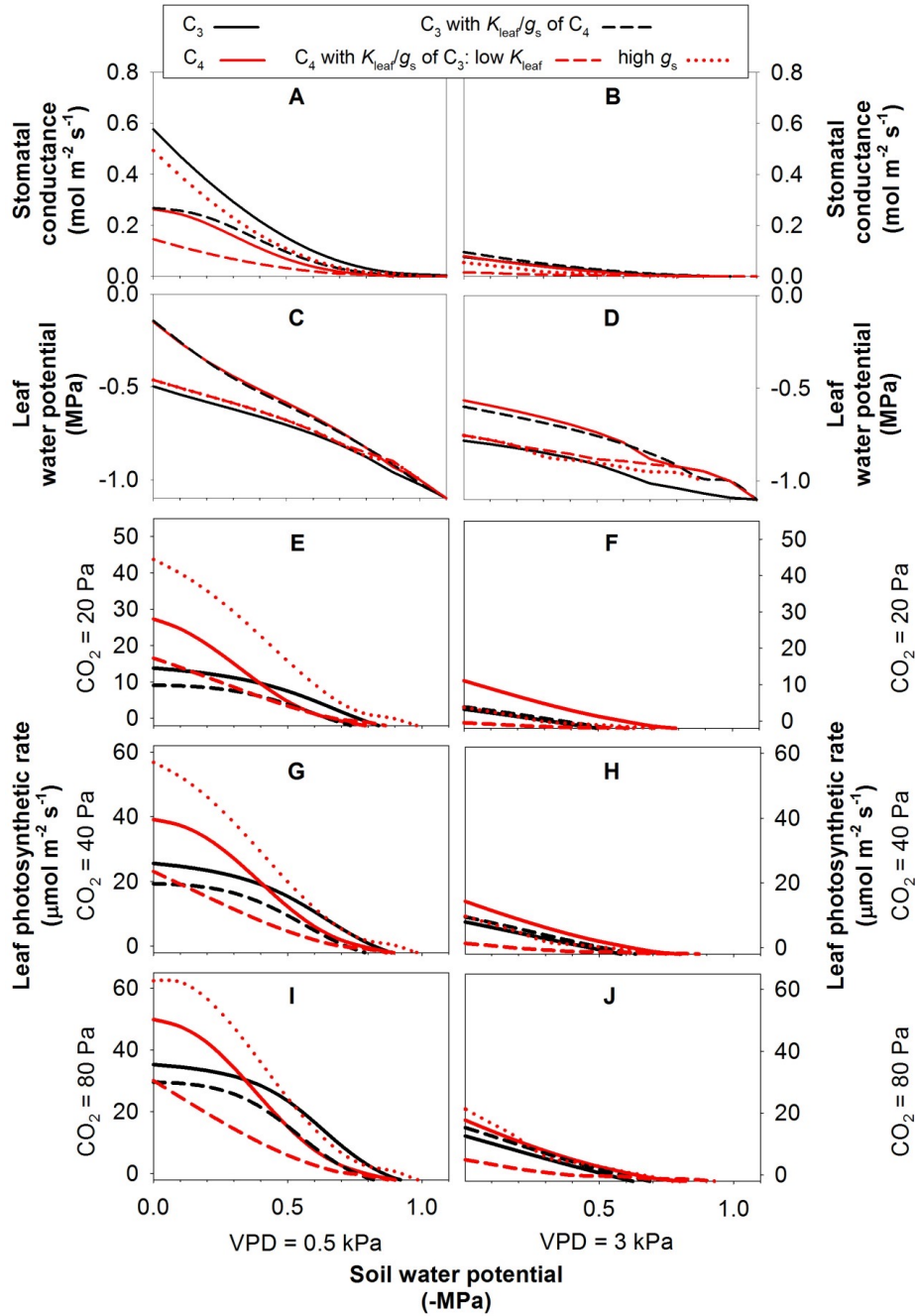
Figure S4.9. Results of simulation modeling of the hydraulic-stomatal-photosynthetic system of C₃ and C₄ grasses. The responses of **(A and B)** stomatal conductance (g_s), **(C and D)** leaf water potential and **(E-J)** light-saturated leaf net photosynthetic rate (A_{area}) to declining soil water

potential (Ψ_{soil}) at low and high vapor pressure deficit (VPD) and at low, current and high CO_2. Simulations were run at 25°C (at 35°C in Figure S4.10).
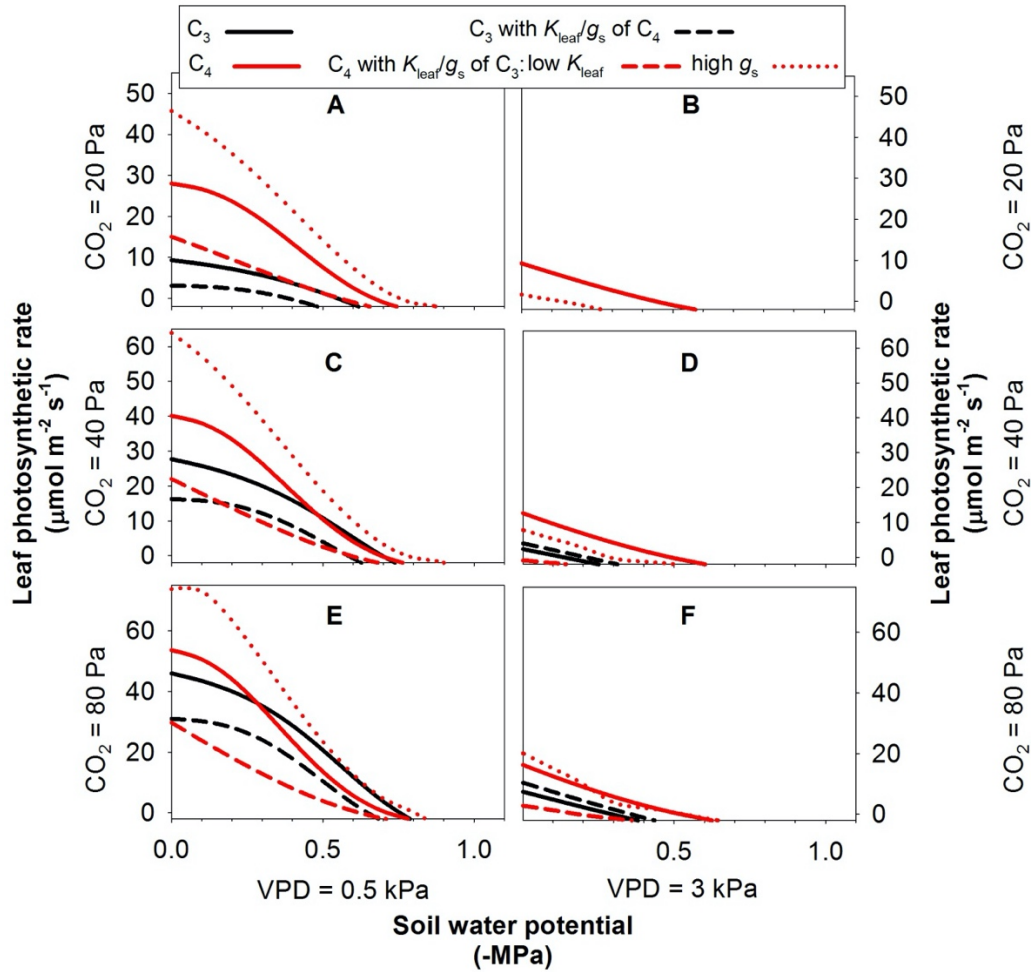
Figure S4.10. Results of simulation modeling of the hydraulic-stomatal-photosynthetic system of C₃ and C₄ grasses, showing the increasing photosynthetic advantage of C₄ grasses at higher temperature (35ºC, by contrast with 25ºC in Figure S4.9), in well-watered conditions as well as drought, due to the importance of hydraulic hyper-efficiency in C₄ grasses. The response of light-saturated leaf net photosynthetic rate (A_{area}) to declining soil water potential at low and high vapor pressure deficit (VPD) i.e., 0.5 kPa **(A, C, E)** and 3 kPa **(B, D, F)**, and additionally, the response of A_{area} was simulated at low, current and high CO_2, i.e., 20 Pa **(A and B)**, 40 Pa **(C and D)** and 80 Pa **(E and F)**. The model was based on measured hydraulic and gas exchange parameters for C₃ and C₄ species (see Methods). Additionally simulations were run

for a modeled species with all parameters as for the C_3 species, but with the maximum g_s value of C_4 species, such that the ratio of leaf hydraulic conductance to g_s (K_{leaf}/g_s) was equivalent to that of the C_4 species, and for a modeled species with all parameters as for the C_4 species, but with the K_{leaf}/g_s equivalent to that of the C_3 species, achieved either by lowering K_{leaf} or by raising maximum g_s.
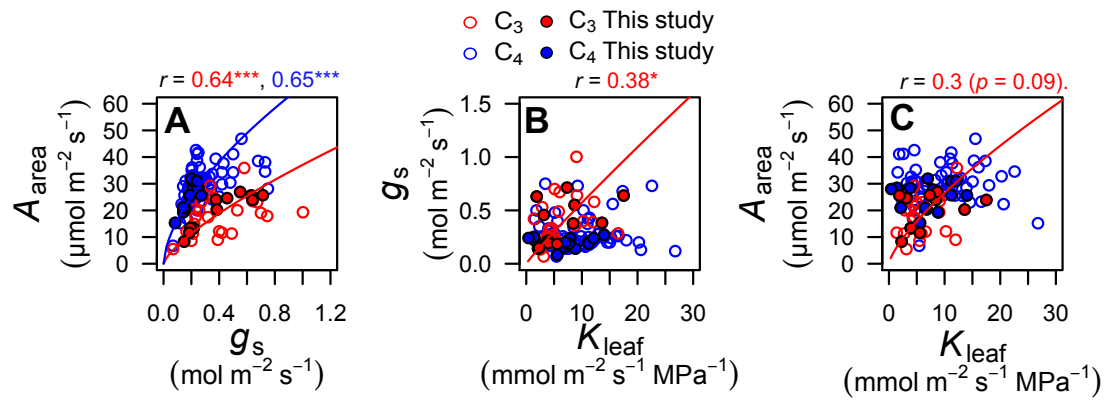
Figure S4.11. Results of leaf physiological coordination across grasses, compiled from published studies (Tables S4.3 and S4.8). Relationships of **(A)** leaf photosynthetic rate (A_{area}) with stomatal conductance (g_s), **(B)** stomatal conductance with leaf hydraulic conductance (K_{leaf}) and **(C)** A_{area} with K_{leaf}. Lines were fit with standard major axis regressions (SMA) and drawn when significant: $*P < 0.05$; $**P < 0.01$; $***P < 0.001$. Values were averaged per species across studies, and analyses include data from this study, represented by filled circles in the plots. Statistics and parameters for both nonphylogenetic and phylogenetic regressions for all pairwise combinations of traits are found in Table S4.8.
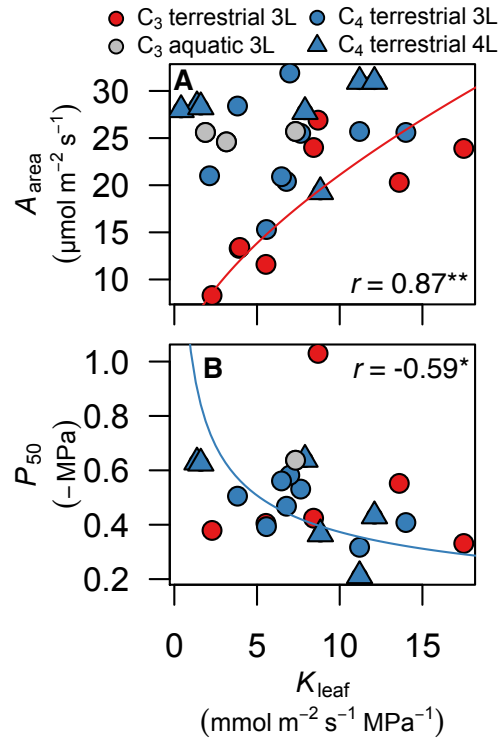
Figure S4.12. Contrasting coordination of hydraulics and gas exchange traits for 27 C$_3$ and C$_4$ grasses, grown in a common garden. Relationships of **(A)** leaf photosynthetic rate (A_{area}), and **(B)** leaf water potential at 50% loss of leaf hydraulic conductivity (P_{50}) with leaf hydraulic conductance (K_{leaf}), across C$_3$ or C$_4$ species, respectively. Lines were fit with phylogenetic reduced major axis regressions (PRMA) and drawn when significant: *$P < 0.05$; **$P < 0.01$; ***$P < 0.001$. Line parameters are provided in Table S4.4. $N = 11$ C$_3$, 16 C$_4$.
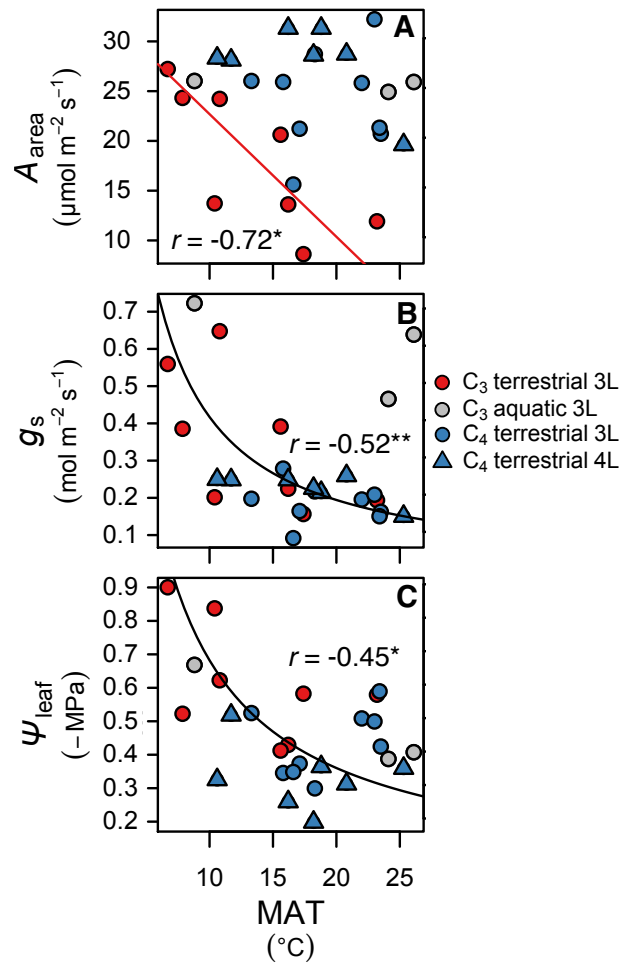
Figure S4.13. Relationships of leaf physiological traits with mean annual temperature for 27 grasses, grown in a common garden. (A) Leaf photosynthetic rate (A_{area}), **(B)** stomatal conductance (g_s) and **(C)** operating leaf water potential (Ψ_L), with mean annual temperature (MAT, °C), across C_3 terrestrial species in panel **(A)** and all species in **(B)** and **(C)**. Lines were fit with phylogenetic reduced major axis regressions (PRMA) and drawn when significant: *$P <$ 0.05; **$P < 0.01$; ***$P < 0.001$. Line parameters are provided in Table S4.5. $N = 11$ C_3, 16 C_4.

References

1. Baird, A. S., S. H. Taylor, J. Pasquet-Kok, C. Vuong, Y. Zhang, T. Watcharamongkol, C. Scoffoni, et al. 2021. Developmental and biophysical determinants of grass leaf size worldwide. *Nature* 592: 242–247.

2. Beer C., M., Reichstein, E., Tomelleri., P., Ciais., M., Jung., N., Carvalhais. 2010. Terrestrial Gross Carbon Dioxide Uptake: Global Distribution and Covariation with Climate. *Science* 329: 834-837

3. Bjorkman, O. 1971. Interaction between the effects of oxygen and CO_2 concentration on quantum yield and light saturated rate of photosynthesis in the leaves of Atriplex patula, ssp. spicata. 70: 520–526.

4. Blackman, C. J., T. J. Brodribb, and G. J. Jordan. 2012. Leaf hydraulic vulnerability influences species' bioclimatic limits in a diverse group of woody angiosperms. *Oecologia* 168: 1–10.

5. Brodribb, T. J. & Holbrook, N. M. 2003. Stomatal closure during leaf dehydration, correlation with other leaf physiological traits. *Plant Physiology* 132: 2166-2173.

6. Brodribb, T. J. & Cochard, H. 2009. Hydraulic failure defines the recovery and point of death in water stressed conifers. *Plant Physiology* 149: 575-584.

7. Brodribb, T. J. & McAdam, S. A. M. 2011 Passive origins of stomatal control in vascular plants *Science* 331: 582-585.

8. Brodribb, T. J., T. S. Feild, and G. J. Jordan. 2007. Leaf Maximum Photosynthetic Rate and Venation Are Linked by Hydraulics. *Plant Physiology* 144: 1890–1898.

9. Brodribb, T. J., T. S. Feild, and L. Sack. 2010. Viewing leaf structure and evolution from a hydraulic perspective. *Functional Plant Biology* 37: 488–498.

10. Brodribb, T. J., and G. J. Jordan. 2008. Internal coordination between hydraulics and stomatal control in leaves. *Plant, Cell & Environment* 31: 1557–1564.

11. Buchholz, M. 1921. Über die Wasserleitungsbahnen in den interkalaren Wachstumszonen monokotyler Sprosse. 114: 119–186.

12. Buckley, T. N., G. P. John, C. Scoffoni, and L. Sack. 2015. How Does Leaf Anatomy Influence Water Transport outside the Xylem? *Plant Physiology* 168: 1616–1635.

13. von Caemmerer, S., and J. R. Evans. 2010. Enhancing C_3 Photosynthesis. *Plant Physiology* 154: 589–592.

14. Canny, M. J. 2001. Embolisms and refilling in the maize leaf lamina, and the role of the protoxylem lacuna. *American Journal of Botany* 88: 47–51.

15. Caringella, M. A., F. J. Bongers, and L. Sack. 2015. Leaf hydraulic conductance varies with vein anatomy across *Arabidopsis thaliana* wild-type and leaf vein mutants: Leaf hydraulics of *Arabidopsis* venation mutants. *Plant, Cell & Environment* 38: 2735–2746.

16. Christin, P.-A., C. P. Osborne, D. S. Chatelet, J. T. Columbus, G. Besnard, T. R. Hodkinson, L. M. Garrison, et al. 2013. Anatomical enablers and the evolution of C_4 photosynthesis in grasses. *Proceedings of the National Academy of Sciences* 110: 1381–1386.

17. Cochard, H., F. W. Ewers, and M. T. Tyree. 1994. Water relations of a tropical vine-like bamboo (*Rhipidocladum racemiflorum*): root pressures, vulnerability to cavitation and seasonal changes in embolism. *Journal of Experimental Botany* 45: 1085–1089.

18. Cochard, H., A. Nardini, and L. Coll. 2004. Hydraulic architecture of leaf blades: where is the main resistance? *Plant, Cell and Environment* 27: 1257–1267.

19. Cochard, H., J.-S. Venisse, T. S. Barigah, N. Brunel, S. Herbette, A. Guilliot, M. T. Tyree, and S. Sakr. 2007. Putative Role of Aquaporins in Variable Hydraulic Conductance of Leaves in Response to Light. *Plant Physiology* 143: 122–133.

20. Downes, R. W. 1969. Differences in Transpiration Rates between Tropical and Temperate Grasses under Controlled Conditions. *Planta* 88: 261–273.

21. Edwards, E. J., C. P. Osborne, C. A. E. Strömberg, S. A. Smith, C_4 GRASSES CONSORTIUM, W. J. Bond, P.-A. Christin, et al. 2010. The Origins of C_4 Grasslands: Integrating Evolutionary and Ecosystem Science. *Science* 328: 587–591.

22. Edwards, E. J., and S. A. Smith. 2010. Phylogenetic analyses reveal the shady history of C_4 grasses. *Proceedings of the National Academy of Sciences* 107: 2532–2537.

23. Ellis, R. P. 1976. A procedure for standardizing comparative leaf anatomy in the Poaceae. I. The leaf-blade as viewed in transverse section. *Bothalia* 12: 65–109.

24. Evert, R. F. 2006. Esau's Plant Anatomy: Meristems, Cells, and Tissues of the Plant Body: Their Structure, Function, and Development. 3rd ed. John Wiley.

25. Feild, T. S., T. J. Brodribb, A. Iglesias, D. S. Chatelet, A. Baresch, G. R. Upchurch, B. Gomez, et al. 2011. Fossil evidence for Cretaceous escalation in angiosperm leaf vein evolution. *Proceedings of the National Academy of Sciences* 108: 8363–8366.

26. Freckleton, R. P., P. H. Harvey, and M. Pagel. 2002. Phylogenetic Analysis and Comparative Data: A Test and Review of Evidence. *The American Naturalist* 160: 712–726.

27. Garland, T., Jr., A. W. Dickerman, C. M. Janis, and J. A. Jones. 1993. Phylogenetic Analysis of Covariance by Computer Simulation. *Systematic Biology* 42: 265–292.

28. Gowik, U., and P. Westhoff. 2011. The Path from C_3 to C_4 Photosynthesis. *Plant Physiology* 155: 56–63.

29. Grubb, P. J. 1998. A reassessment of the strategies of plants which cope with shortages of resources. *Perspectives in Plant Ecology, Evolution and Systematics* 1: 3–31.

30. Higgins, S. I., and S. Scheiter. 2012. Atmospheric CO_2 forces abrupt vegetation shifts locally, but not globally. *Nature* 488: 209–212.

31. Holloway-Phillips, M.-M., and T. J. Brodribb. 2011. Minimum hydraulic safety leads to maximum water-use efficiency in a forage grass. *Plant, Cell & Environment* 34: 302–313.

32. Ii, G. P. W. G. 2012. New grass phylogeny resolves deep evolutionary relationships and discovers C_4 origins. *New Phytologist* 193: 304–312.

33. Israel, W. K., A. Watson-Lazowski, Z.-H. Chen, and O. Ghannoum. 2022. High intrinsic water use efficiency is underpinned by high stomatal aperture and guard cell potassium flux in C_3 and C_4 grasses grown at glacial CO_2 and low light. *Journal of Experimental Botany* 73: 1546–1565.

34. John, G. P., C. Scoffoni, and L. Sack. 2013. Allometry of cells and tissues within leaves. *American Journal of Botany* 100: 1936–1948.

35. Kocacinar, F., and R. F. Sage. 2004. Photosynthetic pathway alters hydraulic structure and function in woody plants. *Oecologia* 139: 214–223.

36. Kocacinar, F., and R. F. Sage. 2003. Photosynthetic pathway alters xylem structure and hydraulic function in herbaceous plants. *Plant, Cell & Environment* 26: 2015–2026.

37. Langdale, J. A. 2011. C_4 cycles: past, present, and future research on C_4 photosynthesis. *The Plant Cell* 23: 3879–3892.

38. Lewis, A. M., and E. R. Boose. 1995. Estimating volume flow rates through xylem conduits. *American Journal of Botany* 82: 1112–1116.

39. Liu, H., S. H. Taylor, Q. Xu, Y. Lin, H. Hou, G. Wu, and Q. Ye. 2019. Life history is a key factor explaining functional trait diversity among subtropical grasses, and its influence differs between C_3 and C_4 species. *Journal of Experimental Botany* 70: 1567–1580.

40. Lundgren, M. R., L. T. Dunning, J. K. Olofsson, J. J. Moreno-Villena, J. W. Bouvier, T. L. Sage, R. Khoshravesh, et al. 2019. C_4 anatomy can evolve via a single developmental change. *Ecology Letters* 22: 302–312.

41. Maherali, H., W. T. Pockman, and R. B. Jackson. 2004. Adaptive variation in the vulnerability of woody plants to xylem cavitation. *Ecology* 85: 2184–2199.

42. Marazzi, B., C. Ané, M. F. Simon, A. Delgado-Salinas, M. Luckow, and M. J. Sanderson. 2012. Locating Evolutionary Precursors on a Phylogenetic Tree. *Evolution* 66: 3918–3930.

43. Martin-StPaul, N., S. Delzon, and H. Cochard. 2017. Plant resistance to drought depends on timely stomatal closure. *Ecology Letters* 20: 1437–1447.

44. McSteen, P., Kellog, E.A. 2022. Molecular, cellular, and developmental foundations of grass diversity. *Science* 377: 599-602.

45. Morison, J. I. L. & Gifford, R. M. 2983. Stomatal sensitivity to carbon dioxide and humidity: a comparison of two C_3 and two C_4 grass species. *Plant Physiology* 71: 789-796.

46. Ocheltree, T. W., J. B. Nippert, and P. V. V. Prasad. 2016. A safety vs efficiency trade-off identified in the hydraulic pathway of grass leaves is decoupled from photosynthesis, stomatal conductance and precipitation. *New Phytologist* 210: 97–107.

47. Ocheltree, T. W., J. B. Nippert, and P. V. V. Prasad. 2014. Stomatal responses to changes in vapor pressure deficit reflect tissue-specific differences in hydraulic conductance. *Plant, Cell & Environment* 37: 132–139.

48. Ogle, K. 2003. Implications of interveinal distance for quantum yield in C_4 grasses: a modeling and meta-analysis. *Oecologia* 136: 532–542.

49. Ohtsuka, A., Sack, L., & Taneda H. 2018. Bundle sheath lignification mediates the linkage of leaf hydraulics and venation. *Plant, Cell & Environment* 41: 342–353.

50. Osborne, C. P., and R. P. Freckleton. 2009. Ecological selection pressures for C_4 photosynthesis in the grasses. *Proceedings of the Royal Society B: Biological Sciences* 276: 1753–1760.

51. Osborne, C. P., and L. Sack. 2012. Evolution of C_4 plants: a new hypothesis for an interaction of CO2 and water relations mediated by plant hydraulics. *Philosophical Transactions of the Royal Society B: Biological Sciences* 367: 583–600.

52. Pagel, M. 1999. Inferring the historical patterns of biological evolution. *Nature* 401: 877–884.

53. Pan, L., B. George-Jaeggli, A. Borrell, D. Jordan, F. Koller, Y. Al-Salman, O. Ghannoum, and F. J. Cano. 2022. Coordination of stomata and vein patterns with leaf width underpins water-use efficiency in a C_4 crop. *Plant, Cell & Environment* 45: 1612–1630.

54. Paradis, E., and K. Schliep. 2019. ape 5.0: an environment for modern phylogenetics and evolutionary analyses in R. *Bioinformatics* 35: 526–528.

55. Pasquet-Kok, J., C. Creese, and L. Sack. 2010. Turning over a new 'leaf': multiple functional significances of leaves versus phyllodes in Hawaiian Acacia koa. *Plant, Cell & Environment* 33: 2084–2100.

56. Pathare, V. S., B. V. Sonawane, N. Koteyeva, and A. B. Cousins. 2020. C4 grasses adapted to low precipitation habitats show traits related to greater mesophyll conductance and lower leaf hydraulic conductance. *Plant, Cell & Environment* 43: 1897–1910.

57. Poorter, H., and L. Sack. 2012. Pitfalls and Possibilities in the Analysis of Biomass Allocation Patterns in Plants. *Frontiers in Plant Science* 3.

58. Revell, L. J. 2012. phytools: an R package for phylogenetic comparative biology (and other things). *Methods in Ecology and Evolution* 3: 217–223.

59. Sack, L., P. D. Cowan, N. Jaikumar, and N. M. Holbrook. 2003. The 'hydrology' of leaves: co-ordination of structure and function in temperate woody species. *Plant, Cell & Environment* 26: 1343–1356.

60. Sack, L., and N. M. Holbrook. 2006. Leaf Hydraulics. *Annual Review of Plant Biology* 57: 361–381.

61. Sack, L., P. J. Melcher, M. A. Zwieniecki, and N. M. Holbrook. 2002. The hydraulic conductance of the angiosperm leaf lamina: a comparison of three measurement methods. *Journal of Experimental Botany* 53: 2177–2184.

62. Sack, L., and C. Scoffoni. 2013. Leaf venation: structure, function, development, evolution, ecology and applications in the past, present and future. *New Phytologist* 198: 983–1000.

63. Sack, L., and C. Scoffoni. 2012. Measurement of Leaf Hydraulic Conductance and Stomatal Conductance and Their Responses to Irradiance and Dehydration Using the Evaporative Flux Method (EFM). *Journal of Visualized Experiments : JoVE*: 4179.

64. Sack, L., C. Scoffoni, G. P. John, H. Poorter, C. M. Mason, R. Mendez-Alonzo, and L. A. Donovan. 2013. How do leaf veins influence the worldwide leaf economic spectrum? Review and synthesis. *Journal of Experimental Botany* 64: 4053–4080.

65. Sack, L., C. Scoffoni, A. D. McKown, K. Frole, M. Rawls, J. C. Havran, H. Tran, and T. Tran. 2012. Developmentally based scaling of leaf venation architecture explains global ecological patterns. *Nature Communications* 3: 837.

66. Sack, L., M. T. Tyree, and N. M. Holbrook. 2005. Leaf hydraulic architecture correlates with regeneration irradiance in tropical rainforest trees. *New Phytologist* 167: 403–413.

67. Sade, N., A. Shatil-Cohen, and M. Moshelion. 2015. Bundle-sheath aquaporins play a role in controlling Arabidopsis leaf hydraulic conductivity. *Plant Signaling & Behavior* 10: e1017177.

68. Sage, R. F. 2004. The evolution of C_4 photosynthesis. *New Phytologist* 161: 341–370.

69. Sage, R. F., P.-A. Christin, and E. J. Edwards. 2011. The C_4 plant lineages of planet Earth. *Journal of Experimental Botany* 62: 3155–3169.

70. Scoffoni, C., C. Albuquerque, C. R. Brodersen, S. V. Townes, G. P. John, M. K. Bartlett, T. N. Buckley, et al. 2017. Outside-Xylem Vulnerability, Not Xylem Embolism, Controls Leaf Hydraulic Decline during Dehydration. *Plant Physiology* 173: 1197–1210.

71. Scoffoni, C., C. Albuquerque, T. N. Buckley, and L. Sack. The dynamic multi-functionality of leaf water transport outside the xylem. *New Phytologist* n/a.

72. Scoffoni, C., D. S. Chatelet, J. Pasquet-kok, M. Rawls, M. J. Donoghue, E. J. Edwards, and L. Sack. 2016. Hydraulic basis for the evolution of photosynthetic productivity. *Nature Plants* 2: 1–8.

73. Scoffoni, C., A. D. McKown, M. Rawls, and L. Sack. 2012. Dynamics of leaf hydraulic conductance with water status: quantification and analysis of species differences under steady state. *Journal of Experimental Botany* 63: 643–658.

74. Scoffoni, C., A. Pou, K. Aasamaa, and L. Sack. 2008. The rapid light response of leaf hydraulic conductance: new evidence from two experimental methods. *Plant, Cell & Environment* 31: 1803–1812.

75. Sokal, R. R., and F. J. Rohlf. 1995. Biometry. W.H. Freeman.

76. Sonawane, B. V., N. K. Koteyeva, D. M. Johnson, and A. B. Cousins. 2021. Differences in leaf anatomy determines temperature response of leaf hydraulic and mesophyll CO_2 conductance in phylogenetically related C_4 and C_3 grass species. *New Phytologist* 230: 1802–1814.

77. Spriggs, E. L., P.-A. Christin, and E. J. Edwards. 2014. C_4 Photosynthesis Promoted Species Diversification during the Miocene Grassland Expansion. *PLOS ONE* 9: e97722.

78. Stiller, V., H. R. Lafitte, and J. S. Sperry. 2003. Hydraulic Properties of Rice and the Response of Gas Exchange to Water Stress. *Plant Physiology* 132: 1698–1706.

79. Strasburger, E. 1891. Über den Bau und die Verrichtungen der Leitungsbahnen in den Pflanzen.

80. Taylor, S. H., M. J. Aspinwall, C. J. Blackman, B. Choat, D. T. Tissue, and O. Ghannoum. 2018. CO_2 availability influences hydraulic function of C_3 and C_4 grass leaves. *Journal of Experimental Botany* 69: 2731–2741.

81. Taylor, S. H., P. J. Franks, S. P. Hulme, E. Spriggs, P. A. Christin, E. J. Edwards, F. I. Woodward, and C. P. Osborne. 2012. Photosynthetic pathway and ecological adaptation explain stomatal trait diversity amongst grasses. *New Phytologist* 193: 387–396.

82. Tyree, M. T., E. L. Fiscus, S. D. Wullschleger, and M. A. Dixon. 1986. Detection of Xylem Cavitation in Corn under Field Conditions 1. *Plant Physiology* 82: 597–599.

83. Tyree, M. T., & Zimmermann, M. H. *Xylem structure and the ascent of sap.* (Springer, 2002).

84. Tyree, M. T., A. Nardini, S. Salleo, L. Sack, and B. El Omari. 2005. The dependence of leaf hydraulic conductance on irradiance during HPFM measurements: any role for stomatal response? *Journal of Experimental Botany* 56: 737–744.

85. Ueno O., Kawano Y., Wakayama M. & Takeda T. 2006. Leaf Vascular Systems in C_3 and C_4 Grasses: A Two-dimensional Analysis. *Annals of Botany* 97: 611–621.

86. Vico, G., & Porporato, A. 2008. Modelling C_3 and C_4 photosynthesis under water-stressed conditions. *Plant Soil* 313: 187-203.

87. Von Caemmerer S. 2002. Biochemical Models of Leaf Photosynthesis. Collingwood, Aust: CSIRO.

88. Warton, D. I., R. A. Duursma, D. S. Falster, and S. Taskinen. 2012. smatr 3 - an R package for estimation and inference about allometric lines: *The smatr 3 - an R package*. *Methods in Ecology and Evolution* 3: 257–259.

89. Weast, R. C. 1974. Handbook of Chemistry and Physics. 54th ed. CRC Press.

90. Wei, C. F., Tyree, M. T. & Steudle, E. 1999. Direct measurement of xylem pressure in leaves of intact maize plants. A test of the cohesion-tension theory taking hydraulic architecture into consideration. *Plant Physiology* 121: 1191-1205.

91. Westermaier, M. 1884. Untersuchungen über die Bedeutung todter Röhren und lebender Zellen für die Wasserbewegung in der Pflanze. 1105–1117.

92. Zhou, H., E. Akçay, E. Edwards, and B. Helliker. 2021. The legacy of C_4 evolution in the hydraulics of C_3 and C_4 grasses. BioRxiv. 2020.05.14.097030.

93. Zhou, H., E. Akçay, and B. Helliker. 2022. Optimal reorganization of photosynthesis after the evolution of C_4. *Plant, Cell & Environment* 46: 796-811

Chapter 5: Disentangling the developmental associations of leaf trichome and stomatal densities across diverse angiosperm species

Abstract

Trichome density (D_t, i.e., no. trichomes/leaf area) contributes to acclimation and adaptation to the environment. Studies of model species indicated a trade-off between D_t and stomatal density (D_s) due to shared cell precursors in development, but studies across closely-related or diverse species have not supported a trade-off. I aimed to answer the question of how a developmental trade-off may be overcome, and under what conditions this would be likely to occur. I compiled studies ($n = 18$) that examined D_t-D_s relationships within and across species to determine the commonness of trade-offs vs. positive coordination vs. independence. In a novel dataset for 78 trichomous species of California ecosystems I disentangled the developmental origin of the relationship across diverse species by deriving mathematical expressions for D_t and D_s as functions of anatomical variables proximal to development, i.e, trichome and stomatal initiation rates (i_t and i_s), and the mature sizes of epidermal pavement cells (e), trichome bases (t) and stomata (s). In studies comparing patterns within species, a D_t-D_s trade-off was found in 4/16 studies, positive coordination in 12/16 studies and independence of D_t and D_s in 5/16 studies. Positive coordination was found in both previous studies testing patterns across diverses species, and in our novel analysis of California species, in which a high D_t arose on average 86% due to high i_t and 10% to low e, whereas a high D_s arose due 51% to high i_s and 41% to low e, and a positive D_t-D_s coordination arose principally due to i_t-i_s coordination, with lesser role of e. Across and within diverse species, a positive D_t-D_s coordination is common. The trade-off reported within certain model species, associated with a developmental antagonism of shared

trichome and stomatal precursor cells, is evidently overcome in many species that have evolved a greater number of precursor cells, and thus higher i_t and i_s and, in addition, smaller e, and thereby higher D_t and D_s, providing an adaptive advantage in multiple scenarios. These findings indicate the power of developmental mechanisms in determining patterns of trait diversity and coordination within and across diverse species.

Introduction

Trichomes, plant hairs, occur in the majority of plant species (Evert, 2006) and their diversity in number, shape, size and adaptive functions have fascinated biologists for centuries (Figure 1; Haberlandt, 1914; Werker, 2000; Evert, 2006). Trichomes can be uni- or multi-cellular, with straight, spiral, star, hooked or branched morphology, and can be glandular (Werker, 2000; Li et al., 2023). Diversity in trichome morphology and number arises between organs on the same plant, between surfaces of the same organ, in plastic responses to environmental stress, and in adaptive differences among species (Bickford, 2016; Wang et al., 2021). An emerging key functional trait is leaf trichome density (D_t, Table 5.1), i.e., the number of trichomes per leaf area, which can influence plant survival and performance in crop and wild ecosystems, depending on trichome properties and their environmental context (Doughty et al., 2011; Snyder and Antonious, 2011; Bickford, 2016; Huchelmann et al., 2017; Sack and Buckley, 2020; Gupt et al., 2021; Vinod et al., 2023). A high D_t reduces light absorbance, including UV (Ehleringer *et al.*, 1976; Ehleringer and Björkman, 1978), and thereby can lessen leaf overheating and photochemical damage. This protection from light and heat enables gain in carbon accumulation at lower transpiration rates, as does the contribution of trichomes to a greater boundary layer thickness, and these effects further improve water-use efficiency, which is advantageous in hot and arid environments (Ehleringer and Mooney, 1978; Ripley et al., 1999; Bickford, 2016). A high D_t may also reduce surface wettability during rainy conditions (Brewer et al., 1991), and/or improve water uptake (Fernández et al., 2014; Kim et al.,, 2017; Schwerbrock and Leuschner, 2017; Schreel et al., 2020; Pan et al., 2021; Li et al., 2023). In many species trichomes are important for sequestering and detoxifying metals (Choi et al., 2001; Azmat et al., 2009; Li et al., 2023). Lastly, higher D_t may increase resistance to herbivores and pathogens by providing a

physical barrier and/or influencing secondary metabolite production (Agren and Schemske, 1993; Mauricio, 1998; Valverde et al., 2001; Hare and Elle, 2002; Handley et al., 2005; Agrawal et al., 2009).

The many functions of a high D_t would contribute to leaf survival and function under multiple environmental factors, including high irradiance and potentially short growing seasons, and thus might especially benefit species with a high stomatal density (D_s), which would contribute to a high maximum rate of gas exchange (Wong et al., 1979; Hetherington and Woodward, 2003; Franks and Beerling, 2009; Lin et al., 2015). However, detailed research in model species has suggested a developmentally constrained trade-off between D_t and D_s (Glover et al., 1998; Yan et al., 2014; Adrian et al., 2015; Torii, 2021). Trichomes are initiated early in leaf development as protodermal precursors divide and successively undergo cell fate determination, specification and morphogenesis (Figure 5.1; Larkin et al., 1997; Glover, 2000; Fambrini & Pugliesi, 2019; Torii, 2021). Protodermal cell divisions meristemoid mother cells (MMCs), which can either develop into trichomes themselves, or can give rise to stomatal cell lineages, by dividing and differentiating into stomatal meristemoid cells, which in turn divide and give rise to guard mother cells, and finally guard cells (Figure 5.1; Torii, 2021). In Arabidopsis, the molecular mechanisms overlap between stomatal and trichome formation (Adrian et al., 2015). Thus, a high expression of SPEECHLESS (SPCH) proteins in MMCs drives the initiation of the stomatal cell lineage pathway (Torii, 2021), and upregulates the expression of TOO MANY MOUTHS (TMM), which drives a negative feedback loop that ensures one-cell-spacing between stomata, and also reduces trichome numbers via an unknown mechanism (Yan et al., 2014). Yet, several studies have shown that SPCH also upregulates the expression of the genes that drive trichome initiation, indicating that its direct role in trichome

and stomatal development is still uncertain (Adrian et al., 2015; Torii, 2021). These molecular mechanisms may result in mutual inhibition between stomatal versus trichome formation during cell fate specification and development (Torii, 2021), resulting in a trade-off between D_s and D_t (Glover et al., 1998).

However, in apparent contrast with the suggestion of a developmentally-determined D_s-D_t trade-off, a number of studies across species have indicated a positive relationship between D_s and D_t (Skelton et al., 2012; Pan et al., 2021).

I aimed to clarify how a developmental trade-off may be overcome, and under what conditions this would be likely to occur. I compiled studies of D_t-D_s relationships within and across species to determine the commonness of trade-offs vs positive coordination vs independence. Further, for 78 trichomous species of California ecosystems I disentangled the developmental origin of the relationship by deriving mathematical expressions for D_t and D_s as functions of anatomical variables of mature leaves that reflect their development, i.e, trichome and stomatal initiation rates (i_t and i_s), and the area of epidermal pavement cells (e), trichome bases (t) and stomata (s) (Table 5.1).

Our approach extends that of a previous study of stomatal variables as functions of developmental traits including stomatal initiation rate (i_s, the number of stomata per number of total epidermal cells), e and s (Sack and Buckley, 2016). In that study of glabrous-leafed species, species tended to achieve higher D_s through both higher i_s and lower e—that is, by initiating more stomata as well as by reducing spacing between them with smaller epidermal pavement cells (Sack and Buckley, 2016). The achievement of higher D_s through higher i_s has been referred to as 'active initiation' and that through smaller e as 'passive dilution' for plants of given species grown under different light or vapor pressure deficits (Carins Murphy et al., 2012,

2014, 2017b, a). Indeed, the ability to disentangle the effect of i_s on D_s from that of e, i.e., the effect of stomatal numbers independent of cell and leaf size, dates to Salisbury (Salisbury, 1927), and i_s has become a major trait used to quantify stomatal development and its influence on D_s independently of epidermal cell size, with application in studies of stomatal evolution and paleobiology (Royer, 2001; Konrad et al., 2021; Muir et al., 2022). In this study, I introduce the analogous variable i_t, which similarly resolves the contribution of increased trichome numbers to D_t, independently of cell and leaf size.

I applied our equations for D_t and D_s to resolve these traits' developmental drivers, and the origin of their relationship across 78 angiosperm species of California ecosystems. I hypothesized that a positive D_s vs D_t coordination would arise if developmental antagonism can be overcome by evolving greater number of precursor cells, which would enable development of both higher i_t and i_s, or through smaller e, which would reduce cell spacing and increase both D_t and D_s. I thus tested the commonness of D_t-D_s relationships and the developmental basis for D_t, D_s and their relationship.

Materials and Methods

Meta-analysis of the relationship between leaf trichome and stomatal densities

I compiled studies that included analyses of the relations between leaf trichome density and stomatal density for individuals, genotypes or populations of a species, or for distinct species, from published literature via searches using GoogleScholar, Web of Science, and references from articles (Table 5.2). I searched for studies using the keywords 'leaf trichome density', 'leaf stomatal density' combined with 'coordination', 'association', and 'relationship'.

Plant material

To quantify the basis of D_t and D_s across diverse species, I sampled 157 common angiosperm species at seven sites (19 to 41 species, depending on site) representative of ecosystems within the California Floristic Province (Table S5.1; alpine, chaparral, coastal sage scrub, desert, mixed conifer-broadleaf forest, mixed riparian woodland and montane wet forest). From each of five individuals per species I sampled fresh fully expanded, mature leaves. For 78 of the 157 species, representative of 29 families, trichomes were apparent on leaf surfaces, and all epidermal cell types could be resolved and traits quantified using our methods (Table S5.1; *Quantification of anatomical traits*).

Sample anatomical preparation

Sampled leaves were fixed in formalin-acetic-acid (FAA) solution. I quantified epidermal traits from micrographs taken from nail varnish impressions of the abaxial and adaxial leaf surfaces (Medeiros et al., 2019) for one leaf for each of the five individuals per species, imaged with a light microscope (40× objective; Leica Lietz DMRB; Leica Microsystems) and a camera with imaging software (SPOT Imaging Solution, Diagnostic Instruments).

Quantification of anatomical traits

From the leaf micrographs, I measured the areas of individual trichome bases (t), stomata (s; one guard cell pair) and epidermal pavement cells (e), and trichome, stomatal and epidermal densities (D_t, D_s and D_e; number of cells or stomata per mm^2) for both abaxial and adaxial surfaces (Medeiros et al., 2019). For each image, I distinguished quadrants by drawing central vertical and horizontal lines, and measured the area of four stomata, two epidermal pavement cells, and

one to four trichome bases from distinct quadrants as centrally as possible, given visibility. Traits were quantified using the software ImageJ (https://imagej.nih.gov/ij/index.html). I traced stomatal and pavement cell outlines to measure s and e, and estimated t by measuring the major and minor axes (a and b respectively) of the trichome cell base and calculating the area of an ellipse, as, area $= \pi \times a \times b$. Trichome and stomatal cell densities (D_t and D_s) were estimated by counting the number of trichomes and stomata and dividing these values by the area of the image. For epidermal cell density (D_e), I counted the number of epidermal cells for two of the four quadrants, divided these numbers by the areas of the respective quadrants, and then averaged these two values. D_e was assessed for images for three to five of the individuals per species, i.e., when the image quality assured accurate cell counts. As our measures of cell densities were sometimes from different individuals per species, I calculated mean trichome and stomatal indices (i_t and i_s) at the species level using species mean values of numbers of trichomes and stomata respectively per total number of trichomes, stomata and epidermal pavement cells (Salisbury, 1927; Sack and Buckley, 2016).

Our method for measurement of epidermal traits was successful for most leaves, for trichome densities up to 360 mm^{-2}, though not for very densely hairy leaves, for which D_t and other epidermal traits cannot be resolved from impressions. I acknowledge and emphasize the need for further studies of D_t for the hairiest leaves; scanning electron microscopy of shaved leaves (Hoof et al., 2008) can work in some cases but not others. Further, for some leaves, epidermal irregularities prevented assessment of epidermal pavement cell numbers or sizes. For 78 species, measurements could be made of all traits for one or both leaf surfaces; for 37 of the 78 species, both surfaces could be measured, but for 26 species, only the adaxial surface, and for 15 species only the abaxial (Table S5.1). For species in which measurements could only be made

for one surface and not the other, this difficulty was typically due to inability to assure accuracy in epidermal pavement cell number or trichome base diameters. Thus, for analyzing the developmental basis of trichome density, I present data for all 78 species, but for species for which all variables were quantifiable for only one surface, I present data only for that surface (Table S5.1). For 24 amphistomatous and for 13 hypostomatous species I had complete data for both surfaces. For 46 of the 78 species, I could also determine from our micrograph images the trichome types present, i.e. simple, pilate/capitate, peltate or stellate, and glandular or non-glandular (Table S5.1). Trichomes of the simple type are single-stalked, without a distinct secretory cell tip, and either unicellular or multicellular uniseriate (Werker, 2000). Pilate and capitate trichomes are single stalked, with a secretory cell tip; pilate trichomes have elongated stalks, though this was not discernible in our images (Werker, 2000). Peltate trichomes are also single stalked, with multicellular secretory cells at the head of the stalk (Werker, 2000). Stellate trichomes are star-shaped with several elongated arms attached to a common base (Werker, 2000). Lastly, glandular trichomes possess a secretory cell at the tip of the trichome, capable of secreting specialized metabolites (Werker, 2000).

Derivation of leaf trichome density and stomatal density on the basis of developmental traits
I derived a novel equation for leaf trichome density (D_t) on the basis of developmental traits i_t and i_s, and anatomical traits t, s and e, to enable calculation of how quantitative changes in size and initiation of epidermal cell types influence D_t. I derived a similar equation for the D_s of trichomous species, as the original study that derived D_s as a function of developmental parameters focused on glabrous-leafed species, and thus did not include i_t or t (Sack and Buckley, 2016).

Statistical and comparative analyses

For the six species that were sampled in two sites (Table S5.1), I averaged traits across individuals within each site, and then averaged the two species values for each site.

To validate the correctness of our mathematical derivation of the developmental basis of leaf trichome density, I tested relationships of measured D_t with that estimated from eqn 4 for the abaxial and adaxial surfaces using ordinary least squares (OLS) regressions with a fixed zero intercept using the SMATR package (Warton et al., 2012). Similarly, I implemented the same analysis to validate the correctness of our mathematical derivation of leaf stomatal density (D_s). Validation of the mathematical derivations were indicated by a high R^2 and if the 1:1 line falls within the 95% prediction intervals of the tested relationships (Sack and Buckley, 2016). Analyses were performed using the R Language and Environment (R Core Team, 2021).

I tested for potential trade-offs or positive coordination in trichome and stomatal densities (D_t and D_s), and in trichome and stomatal initiation rates (i_t and i_s) using standard major axes (SMA) (Warton *et al.*, 2012). Of the 78 total species, I tested these relationships across the subset of 39 and 52 species for the adaxial and abaxial surfaces, respectively, for which I had complete data (Table S5.1).

I tested the quantitative impact of the variables that determine leaf D_t using two causal analyses. First, I tested the "intrinsic sensitivity" of D_t to each input variable from eqn 6, i.e., how D_t varied when each variable was changed from -100% to 200% of its mean across species, maintaining all other variables constant at their mean value (John *et al.*, 2017). Second, I tested the "realized sensitivity" of D_t and D_s to each input variable by partitioning the causal contribution of each input variable to the differences in D_t or D_s for each pairwise species combination, and then calculating the median contribution across all pairwise species

combinations (Buckley and Diaz-Espejo, 2015; John et al., 2017). A higher positive %

contribution indicates that variable plays a stronger causal role in determining D_t or D_s across the

species set. By contrast, a variable with negative % causal contribution indicates that for a

species with higher D_t or D_s, that variable differed across species in the direction that would have

caused a lower D_t or D_s, and this negative effect is overcome by positive effects of the other

variables. Notably, the causal contributions of underlying variables in a realized sensitivity

analysis depends on the variation of all variables and thus on the species-set (John et al., 2017).

To enable robust comparisons of the realized sensitivity of D_t and D_s to input variables on both

leaf surfaces, this analysis focused on the 37 species for which data were available for D_t and D_s

for both surfaces, separately considering the 24 amphistomatous species, i.e., with $D_s > 0$ on both

surfaces, and the 13 hypostomatous species, i.e., with D_s and s of 0 on the adaxial surface.

Results

Meta-analysis of the relationship of D_t and D_s

Our meta-analysis resulted in a compilation of 17 studies that leaf trichome and stomatal

densities across diverse species, or across populations or genotypes of given species, or for plants

of given species grown under different experimental treatments (Table 5.2). 14 of 18 (78%)

studies supported positive D_t-D_s coordination, 3/18 (27%) a trade-off, and 7/18 (39%)

independence (Table 5.2). Notably, 6/18 (33%) studies showed mixed results, depending on

specific comparison sets (i.e., abaxial vs adaxial, or comparisons between populations or

genotypes within species of given studies). These studies typically provided greater support for

positive D_t-D_s coordination or independence than for a trade-off (Table 5.2).

Derivation and validation of an expression of the basis for D_t in developmental traits

I derived equations for trichome density (D_t, no. trichomes/leaf area mm^2) and stomatal density (D_t, no. stomata/leaf area mm^2) as functions of underlying epidermal anatomical traits with proximal relationship to development, i.e., trichome and stomatal initiation rates (i_t and i_s, respectively), and the areas of trichome cell bases (t), stomata (s) and epidermal pavement cells (e) (Table 5.1). The i_t is analogous to the i_s introduced by Salisbury (Salisbury, 1927) as a means to correct D_t for the effect of larger epidermal cells in spacing stomata apart; these indices correspond to the number of trichomes (n_t) or stomata (n_s) divided by the sum of n_t, n_s and the number of epidermal pavement cells (n_e). Thus, the i_t and i_s are related to n_t, n_s, n_e, t, s and e as:

$$i_t = \frac{n_t}{n_t+n_s+n_e} \qquad i_s = \frac{n_s}{n_s+n_t+n_e} \tag{1}$$

D_t is related to n_t, n_s, n_e, t, s and e as:

$$D_t = \frac{n_t}{\text{total area}} = \frac{n_t}{n_t t+n_s s+n_e e} = \frac{1}{t+\frac{n_s}{n_t}s+\frac{n_e}{n_t}e} = \frac{1}{t+\frac{n_s}{n_t}s+\frac{n_e n_s}{n_s n_t}e} \tag{2}$$

where total area is that of the entire leaf surface with trichomes and/or stomata (mm^2). Noting that $n_e/n_s = i_e/i_s$, and $n_s/n_t = i_s/i_t$, equation 2 can be rearranged as:

$$D_t = \frac{1}{t+\frac{i_s}{i_t}s+\frac{i_e i_s}{i_s i_t}e} \tag{3}$$

Applying $i_e = 1 - (i_s + i_t)$ to equation 3 gives:

$$D_t = \frac{i_t}{i_t t+i_s s+(1-i_t-i_s)e} \tag{4}$$

An equation for D_s for trichomous species can be derived by swapping i_s for i_t, and s for t in Equation 4:

$$D_s = \frac{i_s}{i_s s+i_t t+(1-i_s-i_t)e} \tag{5}$$

I validated eqns 4 and 5 using data for the 78 diverse angiosperm California species, for which D_t varied from 4.51 mm^{-2} for *Adenostoma fasciculatum* to 310 mm^{-2} for *Antennaria media* on the abaxial surface, and from 5.09 mm^{-2} for *Cercocarpus betuloides* to 418 mm^{-2} for *Eriogonum douglasii* on the adaxial surface (Figure 5.2; Table S5.1). For both D_t and D_s, observed D_t and D_s values versus values estimated from eqns 4 and 5 were closely related, and lines fitted through the origin across abaxial and adaxial surfaces had 95% prediction intervals that included the 1:1 line (Figure 5.2; Table S5.1; R^2 = 0.98-0.99, slope b = 0.91-0.94).

Intrinsic sensitivity of D_t and D_s to its developmental drivers

Equations 4 and 5 enables analyses of the developmental determinants of differences in D_t and D_s. In an intrinsic sensitivity analysis, i.e., shifting each driver of D_t and D_s in trichomous leaves from their mean values, holding other drivers at their mean values, i_t and e most strongly influence D_t and i_s and e most strongly influence D_s, a finding, for D_s, congruous with that shown for non-trichomous leaves previously (Sack and Buckley, 2016). Notably, while i_t positively influences D_t and i_s positively influences D_s, e has a negative influence on both, as larger e spaces specialized cell types further apart (Figure 5.3; Table S5.2-S5.5). The other variables have much lower intrinsic impacts on D_t. The influence of i_s is positive for D_t, because differentiating more epidermal cells with generally small stomata, would result in trichomes spaced more closely together, and similarly the influence of i_t is also positive for D_s. The intrinsic influences of t and s are negative on both D_t and D_s, as larger cells space trichomes and stomata further apart (Figure 5.3; Table S5.2-S5.3).

Causal partitioning of D_t and D_s with respect to developmental traits in California angiosperm

species

The 78 California species were diverse in trichomes i.e., simple, pilate/capitate, peltate or

stellate, and glandular or non-glandular (Table 5.1). The variation in D_t and D_s across a set of

species is driven by the simultaneous differences in all input variables of equations 4 and 5. For a

subset of 24 amphi- and 13 hypostomatous California angiosperm species for which I had data

for all input variables, I analyzed the realized drivers of shifts in D_t and D_s against the

background of true trait variation (Figure 5.4). I found the determination of D_t was similar for

both surfaces, and for amphi- and hypostomatous leaves, whereas that of D_s differed depending

on the surface and stomatal distribution (Table S5.6). On average for the two surfaces of

amphistomatous species and the abaxial surface of hypostomatous species, i_t accounted for the

bulk (72-88%) of variation in D_t across species, and e for a substantial minority of variation (7.7-

20%), and i_s, s and t contributed negligibly on average (Table S5.6). For D_s, for amphistomatous

species i_s accounted for the majority of variation (66%) on the adaxial surface, and e for a

substantial minority of variation (29%), whereas on the abaxial surface, e accounted for the

majority (55%) of variation in D_s across species and i_s a minority (36%); in all cases, on average,

t and s contributed negligibly to variation in D_s across species (Figure 5.4; Table S5.6). Similar

determinants of D_s were observed for the abaxial surface of hypostomatous species, except that

variation in s accounted for 6% of across species variation in D_s (Table S5.6).

Positive coordination of D_t and D_s, and its developmental basis in California angiosperm species

Across the dataset for California angiosperm species, D_t and D_s were positively related on the adaxial and abaxial surfaces (Figure 5.5; ($n = 39$ and 52, respectively; $r = 0.51\text{-}0.62$, $p < 0.001$). In both cases, this positive coordination was driven both by the association between i_t and i_s across species, which were major causal drivers of, respectively, D_t and D_s (Figure 5.5; $r = 0.33\text{-}0.4$, $p < 0.05$), and by the influence of small e as a minor causal driver of high D_t and substantial causal driver of D_s across species (Figure 5.4).

Discussion

I found that despite the developmental conflict between D_t and D_s identified in the model species *Nicotiana tabacum* (Glover et al., 1998), in the meta-analysis, a positive coordination of D_t and D_s was the most general pattern (Table 5.2). Our derivation of a novel equation for leaf trichome density (D_t) and D_s on the basis of developmental traits i_t and i_s, and anatomical traits e, s and t, enables calculation of how quantitative shifts in size and initiation of epidermal cell types influence D_t. These equations enabled deeper causal analysis for California species of the drivers of D_t and D_s and their coordination and showed that the coordination was achieved by both 'active' and 'passive' developmental determinants, i.e. i and e.

In the meta-analysis I found much more support for positive D_t-D_s coordination than for their trade-off or independence. Notably, trade-offs and independence in D_t and D_s arose particularly in studies focusing within species, including *Arabidopsis helleri*, *Artemisia tridentata*, *Capsicum annuum*, *Digitaria insularis*, *Nicotiana tabacum*, *Quercus brantii*, *Solanum lycopersicum*, *Solanum melongena*, *Tillandsia streptophylla* and *Trichosanthes cucumerina*

(Table 5.2). The variation in D_t-D_s relationships across studies indicates a lack of strict developmental constraint on this relationship, and thus, the possibility for species to adapt a wide range of combinations, and for different sets of genotypes or of species to vary in the D_t-D_s association depending on adaptive context. Thus, the trade-offs in D_t and D_s may reflect responses to environments wherein a high D_t coupled with low D_s, or low D_t coupled with high D_s would provide advantages or be too costly in certain environments, depending on the numerous functions of trichomes. For example, a high D_t if coupled with a low D_s may impose fitness costs, e.g. in the absence of herbivores, as was proposed for *Arabidopsis halleri* (Simon et al., 2020). Similarly, a low D_t and high D_s may be advantageous in resource-rich environments if herbivory is not a driving selective pressure, as a high D_s would drive rapid carbon accumulation and growth. Indeed, plants in resource-rich environments may experience more herbivory than those in temperate environments, and have evolved other defenses beyond trichomes (Coley, 1998). By contrast, a high D_t and low D_s has been proposed to contribute to adaptation to dry and/or salty environments (Glover et al., 1998), by increasing light reflectance and leaf overheating, coupled with reduced water loss to transpiration (Ehleringer and Mooney, 1978; Weiglin and Winter, 1991). In the meta-analysis the independence of D_t and D_s did not arise across species, but within species of varying populations or genotypes. This may reflect plasticity to the microenvironment or local adaptation in populations and genotypes of species, as decoupling of D_t and D_s would allow for a wide range of D_t and D_s. By contrast, the positive coordination of D_t and D_s is much more general, arising across many taxonomic scales, including across species of different plant families (Figure 5.5), across species within a family, e.g. Proteaceae, across species within a genus, e.g. *Dendrobium*, between isolated populations for several species, between genotypes of several crop species, and between individuals grown under

experimental treatments such as salt or water stress, and for both adaxial and abaxial leaf surfaces (Table 5.2; Downs and Black, 1999; Zsögön, 2011; Adebooye et al., 2012; Skelton et al., 2012; Barroso et al., 2015; Cach-Pérez et al., 2016; Mediavilla et al., 2019; Mirzaie et al., 2020; Pan et al., 2021; Patel et al., 2021; Aryane do Nascimento Accioly et al., 2022; Soheili et al., 2023; Zhu *et al.*, 2023).

Our sensitivity analysis of the developmental drivers of D_t and D_s with respect to equations 4 and 5 showed their determination from different factors. All else being equal, a high D_t is principally achieved by increasing i_t, due to the initiation of a higher proportion of trichomes from epidermal precursors, with an additional lesser role of small epidermal pavement cell size decreasing the spacing between trichomes (Figure 5.3), as previously described for stomata in glabrous-leafed species (Salisbury, 1927; Sack and Buckley, 2016). Our analysis of D_s for the California angiosperms found that high D_s is principally achieved with high i_s and small e. Yet, our causal analysis, which clarifies the true drivers of variation in D_t and D_s against the background of variation in all input variables, indicated contrasting developmental drivers for the two leaf surfaces for the California angiosperms, with adaxial D_s being more strongly driven by i_s, followed by e, and abaxial D_s more strongly driven by e, followed by i_s, consistent with previous studies showing independent molecular controls on development and anatomy of adaxial and abaxial leaf surfaces (Figure 5.4; Kidner & Timmermans, 2010; Yamaguchi et al., 2012). Notably, the "passive dilution" effect of larger e in reducing D_s, would also drive coordinated changes in trichomes, stomata as well as vein density (Brodribb et al., 2013; Carins Murphy et al., 2016). Although trichome cell fate determination occurs early during development in Arabidopsis, our finding that D_t was more strongly determined by i_t and less by e, whereas D_s was less strongly determined by i_s and more by e, may indicate that for other plant species,

trichome initiation might continue for longer than stomatal initiation, and even as epidermal cells are still expanding. Additionally, shedding of trichomes between early development and leaf maturation (Choinski and Wise, 1999; Fernández et al., 2014) may also contribute to the lesser impact of e on D_t, as shedding of trichomes would be represented in the i_t, and may be an alternate mechanism to shift D_t independently of changes in e.

Notably, some previous studies within species, especially of genetic TMM mutants in *Arabidopsis*, found negative relationships between D_t with D_s, attributed to an allocation trade-off of epidermal precursor cells, driven by mutual inhibition in the development of trichomes vs stomata (Yan et al., 2014; Simon *et al*., 2020). Our finding of a positive relationship between i_t and i_s across a set of diverse species indicates that during diversification any allocation trade-off between trichome and stomata precursors was superseded by a positive coordination in trichome and stomatal initiation rates. In theory, such positive coordination may arise from increasing total precursor number and from loss of mutual inhibition of trichomes vs. stomata.

The positive relationship of D_t and D_s across a set of diverse California angiosperm species, as for that reported in other studies within and across species (Table 5.2), is consistent with coordinated trait evolution and/or plasticity in response to the environment. For the California angiosperm species in our study, this positive relationship arose from the coordination of i_t and i_s, and from the contribution of small e to high D_t and D_s. Multiple explanations may underlie this coordination. First, under higher irradiance, where greater D_s would promote higher maximum rates of gas exchange, a higher D_t may be beneficial to reflect excess irradiance, maintain lower leaf temperatures, and improve water use efficiency (Camargo and Marenco, 2011). Second, a high D_s to achieve higher maximum gas exchange rates can contribute to 'drought avoidance', i.e., rapid growth in shorter growing periods when water is available

(Grubb, 1998; Hetherington and Woodward, 2003; Sack and Buckley, 2016). When trichomes benefit water relations, through improved foliar surface water uptake, or enabling more rapid leaf drying after rainfall due to repellency (Brewer *et al*., 1991), this too would benefit adaptation to arid climates by allowing for maintained gas exchange. Third, faster growing plants may show higher D_s and may be especially benefitted by hairs as a specialized defense to resist insect damage, given their generally higher leaf nutrient concentrations (Grubb, 1992, 1998). Finally, as plants with high D_s have greater likelihood of disease susceptibility through entering the stomata (Gudesblat et al., 2009), a high D_t may entrap spores and prevent their contact with the epidermis (Gupt et al., 2021). Indeed, the advantages of such coordination would be especially important for more vulnerable, young, developing leaves when the numerous functions of trichomes are even more important (Karabourniotis and Fasseas, 1996; Choinski and Wise, 1999), and given the higher cost of developing a leaf with high D_s (Franks and Beerling, 2009). Despite the evidence for positive coordination in trichome and stomatal densities from the meta-analysis and as I show here, it is evident that some species can have high D_t but low D_s, or vice versa (Figure 5.5; Table 5.2), indicating that their coupling may not be advantageous and/or potentially too costly, in certain environments.

Disentangling the molecular and genetic drivers across diverse species underlying the coordination or decoupling of D_t and D_s is a critical avenue for future studies, given the importance of both traits on wild and agricultural species. The coordination of D_t and D_s has implications and applications in agriculture. Indeed, several studies in the meta-analysis found positive coordination in D_t and D_s on comparisons of crop varieties. Engineering and breeding of traits that enhance biotic resistance into crops is a promising alternative to harmful chemical agents (Dong and Ronald, 2019). Indeed, a high D_t is a trait that has been bred for higher

herbivore deterrence and disease resistance (Pillemer and Tingey, 1976; Snyder and Antonious, 2011), and a high D_s would allow for maximized gas exchange. Yet, the carbon cost of plant defenses, including high D_t, has raised concern due to the allocation of resources away from growth or reproduction (Strauss and Agrawal, 1999). However, a high D_t coupled with high D_s may result in herbivory resistance without reducing growth or reproductive yield, which is consistent with several studies testing the growth-defense trade-off of trichomes (Agren and Schemske, 1993; Kaplan et al., 2009). Consistent with this, a high D_s has been shown to drive higher yield (Lu et al., 1998; Roche, 2015). A high D_t has also been suggested for increasing albedo of crops, and influencing regional temperatures (Doughty et al., 2011), although much work is needed on the impact of trichome density across greater scales. As increasing global food production is essential for global food security (Searchinger et al., 2019), future studies should resolve the combined impacts of high D_t and D_s on crop productivity and yield, and stress tolerance.

Tables

Table 5.1. Definitions of anatomical and developmental traits influencing leaf trichome density (D_t).

Trait	Symbol	Unit	Definition
Trichome density	D_t	no. mm^{-2}	The number of trichomes per leaf area.
Stomatal density	D_s	no. mm^{-2}	The number of stomata per leaf area.
Epidermal pavement cell initiation rate/index	i_e	unitless	The number of pavement epidermal cells relative to the total number of epidermal cell types ($n_e \div (n_s + n_t + n_e)$).
Stomatal initiation rate/index	i_s	unitless	The number of stomata relative to the total number of epidermal cell types ($n_s \div (n_s + n_t + n_e)$).
Trichome initiation rate/index	i_t	unitless	The number of trichomes relative to the total number of epidermal cell types ($n_t \div (n_s + n_t + n_e)$).
Epidermal area	e	mm^2	The projected area of an epidermal pavement cell.
Stomatal area	s	mm^2	The projected area of an epidermal stoma.
Trichome area	t	mm^2	The projected area of an epidermal trichome cell.
Stomatal number	n_s	no.	The total number of stomata.
Trichome number	n_t	no.	The total number of trichome cells.
Epidermal number	n_e	no.	The total number of epidermal pavement cells.

Table 5.2. Published studies showing variation in the association of leaf trichome and stomatal densities within and across species. For each study, I report whether or not the study supported evidence of a trade-off (i.e, decreasing trend), positive coordination (i.e,. increasing trend) or independence (i.e., no trend) in trichome and stomatal densities, sampled species and family, scale at which the comparison was made, growing conditions, leaf surface tested, and the reference. References ordered by their support for a trade-off, positive coordination or independence. For the leaf surface, NA indicates information about the leaf surface tested was not provided in the study.

Relationship of trichome density vs. stomatal density (Trade-off = TO; Positive Coordination = PC; I = Independent)	Species	Family	Scale	Growing conditions	Leaf surface (Ad = adaxial; Ab = abaxial)	Reference	
TO	*Arabidopsis halleri*	Brassicaceae	Between two populations	Field sites	Ad	1.	Simon et al., 2020
TO	*Nicotiana tabacum*	Solanaceae	Between wild and transgenic individuals	Not reported	Ad; Ab	2.	Glover et al., 1998
PC	*Artemisia tridentata*	Asteraceae	Between two populations	Common garden	NA	3.	Downs and Black, 1999
PC	*Cenostigma microphyllum*	Fabaceae	Across 15 populations	Field sites	Ab	4.	Accioly et al., 2022
PC	*Cymbopogon citratus*	Poaceae	Between individuals within water-deficit treatments	Experimental water-deficit and arbuscular mycorrhizal fungi	NA	5.	Mirzaie et al., 2020
PC	*Dendrobium bellatulum, D. cariniferum, D. draconis, D. longicornu, D. trigonopus, D. williamsonii*	Orchidaceae	Across six species	Common garden	Ab	6.	Pan et al., 2021
PC	*Leucadendron* spp., *Leucospermum* spp., *Protea* spp.	Proteaceae	Across 18 species and within *Leucadendron conocarpodendron*	Common garden	Ad	7.	Skelton et al., 2012
PC	*Quercis faginea, Q. suber* and *Q. ilex*	Fagaceae	Within each species	Field sites	Ab	8.	Mediavilla et al., 2019
PC	*Quercus variabilis*	Fagaceae	Across 44 natural and 15 common garden populations	44 natural and 15 common garden populations	NA	9.	Zhu et al., 2023
PC	*Solanum pennellii*	Solanaceae	For two genotypes between well watered and water-deficit experiments	Experimental water-deficit	Ad; Ab	10.	Zsögön, 2011
I	*Capsicum annuum*	Solanaceae	Across 7 varieties	Common garden	Ad; Ab	11.	Serrano-Mejía *et al.* 2022
I	*Solanum lycopersicum*	Solanaceae	Between four varieties	Experimental water-deficit	Ad	12.	Galdon-Armero et al., 2018
I (Ad for both varieties); PC (Ab, one variety); I (Ab, one variety)	*Trichosanthes cucumerina* L.	Cucurbitaceae	Across experimental salt-stress treatments for two varieties	Experimental salt-stress	Ad; Ab	13.	Adebooye et al., 2012
I (Ad); PC (Ab)	*Digitaria insularis*	Poaceae	Between three vegetative stages and for two varieties	Experimental glyphosate	Ad; Ab	14.	Barroso et al., 2015
I (Ad); PC (Ab)	*Lens* spp.	Fabaceae	Across 12 varieties	Growth chamber	Ad; Ab	15.	Patel et al., 2021
I (Ad); PC (Ab)	*Solanum melongena*	Solanaceae	Between experimental water-deficit treatments	Experimental water-deficit		16.	Fu et al., 2013
TO; PC; I (population specific)	*Quercus brantii*	Fagaceae	Within populations	Field sites	NA	17.	Soheili et al., 2023
PC; PC; TO; PC (species specific)	*Tillandsia balbisiana, T. juncea, T. streptophylla* and *T. utriculata*	Bromeliaceae	Within individuals of each species	Field sites	Ab	18.	Cach-Pérez et al., 2016

Figures
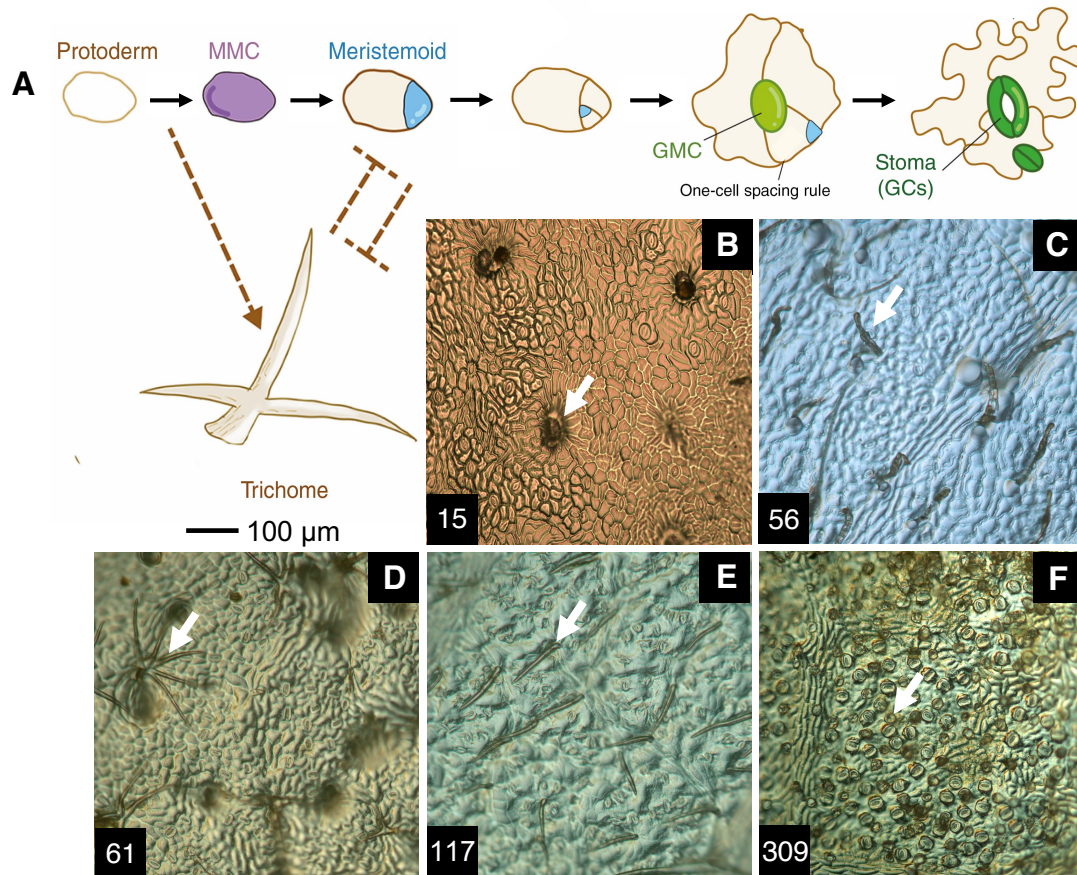
Figure 5.1. The developmental sequence of leaf trichome and stomata formation, and diversity of leaf trichomes of California species. (A) The developmental sequence of trichome and stomatal formation (modified from figures 2 and 3 of Torii, 2021). In eudicots, trichomes are initiated by protodermal cells or meristemoid mother cells (MMC), i.e., prior to stomatal meristemoid formation. Asymmetric cell divisions of the MMC result in meristemoid precursors that divide further and then differentiate into guard mother cells (GMC) which divide and differentiate into stomatal guard cells (GC). High activity of SPEECHLESS (SPCH) proteins in the protoderm and MMCs drives stomatal formation. SPCH activity is also high in meristemoid cells, and drives upregulation of TOO MANY MOUTHS (*TMM*), which contributes to ensuring

one-cell spacing and also reduces trichome numbers via an unknown mechanism. SPCH activity

also leads to the upregulation of genes that drive trichome formation. Both trichome and stomatal

precursors may exclude each other's development from protodermal precursors. Abaxial

trichomes visualized from nail varnish peels of leaf surfaces for **(B)** *Ericameria cuneata*, **(C)**

Encelia californica, **(D)** *Quercus garryana*, **(E)** *Ceanothus cordulatus* and **(F)** *Chrysolepis*

sempervirens. The white arrow in panels **(B)** – **(F)** indicates a trichome and the number in the

bottom left indicates the abaxial trichome density (D_t) for that species, ordered from lowest to

highest.
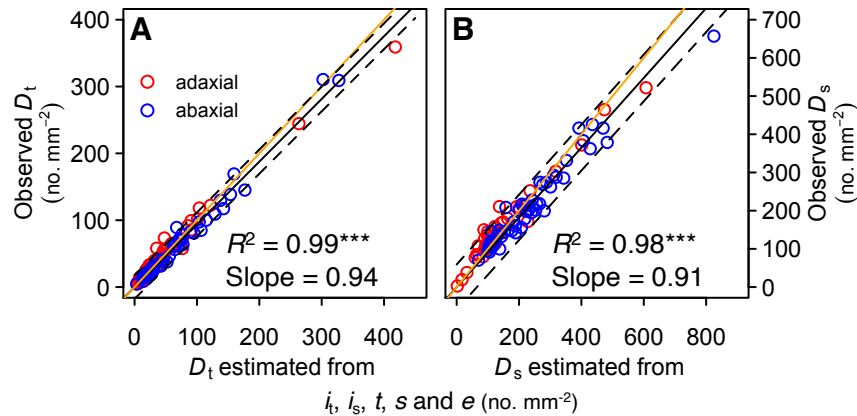
Figure 5.2. Validating the developmental basis for leaf trichome density and analyzing the contributions of anatomical and developmental traits to leaf trichome density for diverse California species. Estimation of adaxial and abaxial **(A)** leaf trichome density (D_t), and **(B)** leaf stomatal density (D_s) as functions of the trichome index (i_t), stomatal index (i_s), trichome cell area (t), stomatal cell area (s) and epidermal pavement cell area (e), plotted against measured values of D_t and D_s. ***$p < 0.001$. Black solid lines in both panels are ordinary least square regressions (OLS) fitted to the data with a fixed zero intercept, with the 1:1 line in orange and 95% prediction intervals as segmented black lines. $N = 63$ and 54 in **(A)** and $N = 39$ and 51 in **(B)**, corresponding to adaxial and abaxial surfaces, in red and blue, respectively. The total species number represented by both surfaces for both traits was 78.
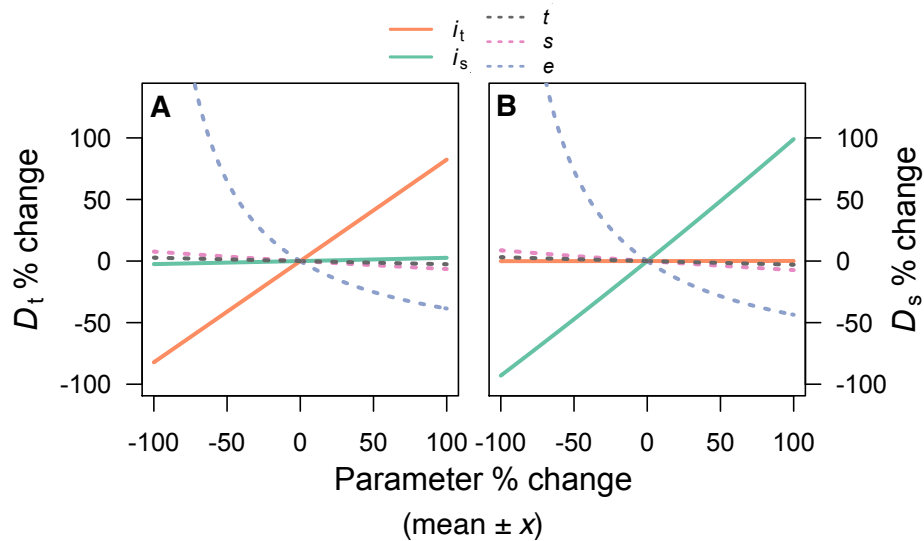
Figure 5.3. The intrinsic sensitivity of leaf trichome and stomatal densities to underlying developmental parameters. Panels **(A)** and **(B)** show the intrinsic sensitivity of D_t and D_s, respectively, for the abaxial surface (Tables S5.2-S5.3). The intrinsic sensitivity for the adaxial surface was similar with that of abaxial surface (Table S5.4-S5.5). The intrinsic sensitivity signifies the impact on D_t or D_s of shifting one parameter in equations 4 and 5, respectively, while holding all others constant.
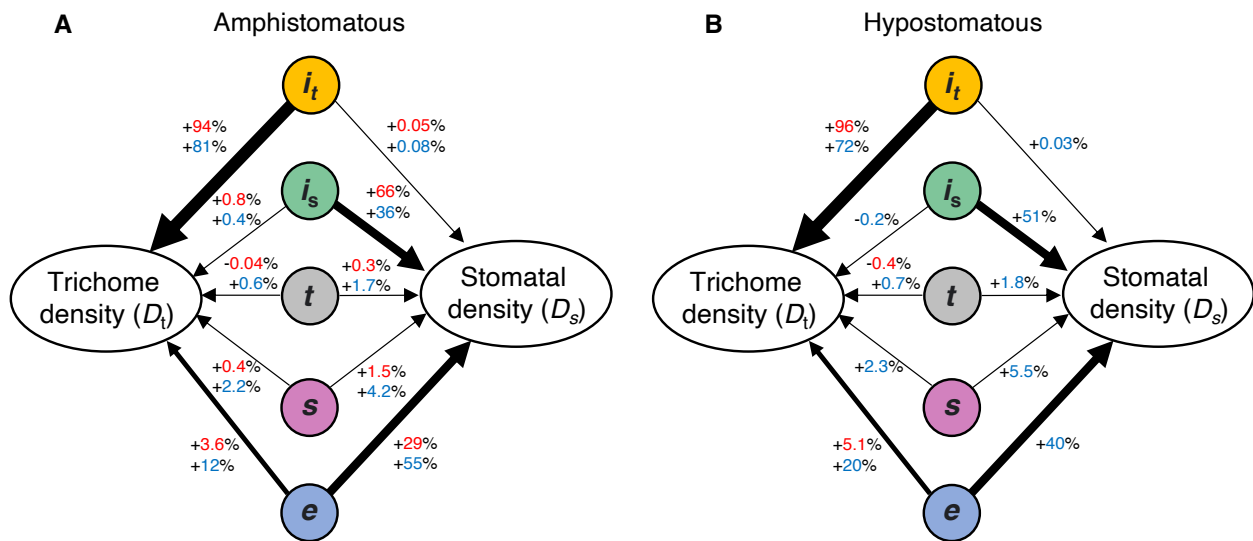
Figure 5.4. Contributions of anatomical and developmental traits to leaf trichome density for diverse California species. The realized sensitivity of D_t and D_s to underlying developmental parameters for **(A)** amphistomatous and **(B)** hypostomatous leaves. Causal influences are presented as percentages adjacent to arrows, with the upper red value for the adaxial surface and lower blue value for the abaxial surface; the thickness of the arrows reflect relative causal influences (Table S5.6).
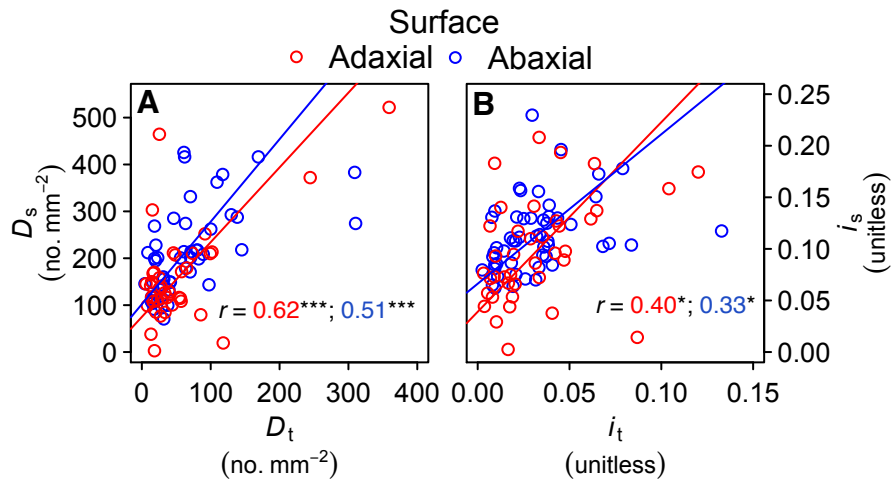
Figure 5.5. Testing the association of leaf trichome density (D_t) with stomatal density (D_s), and trichome initiation rates (i_t) with stomatal initiation rates (i_s) across diverse California species. Relationships of **(A)** trichome density (D_t) with stomatal density (D_s) and **(B)** leaf trichome initiation rate (i_t) and stomatal initiation rate (i_s), for the adaxial and abaxial leaf surfaces, in red and blue points, respectively. $N = 39$ and 52 in both panels, corresponding to adaxial and abaxial surfaces, in red and blue, respectively. Lines are standard major axes (SMA) regressions. *$p < 0.05$, ***$p < 0.001$.

Supplementary Materials

Supplementary Table Captions (see attached excel workbook)

Table S5.1. Species of diverse California angiosperm species included in the study, site(s) sampled, site latitude and longitude, site vegetation type, family, trichome morphology, trichome glandular/non-glandular, measurements able to quantify per surface and used for analyses, mean and ± standard errors of leaf epidermal traits measured. Traits left blank for a given species indicates that data could not be collected for the abaxial or adaxial surface for these species.

Table S5.2. The intrinsic sensitivity of leaf abaxial trichome density (D_t) to developmental parameters: i_s, i_t, t, s and e. I present calculations for changing mean estimated D_t across a range of increasing and decreasing parameter values from 0 - 100 %, for each developmental parameter. Thus, I estimated D_t by inputting mean values for the parameters listed, and then increased and decreased each parameter from 0 - 100%, holding all other parameters constant. I then calculated the % change in D_t across the range of increasing and decreasing parameter values relative to the mean estimated D_t of 69.6. I then normalized this value to reflect actual % change values from the mean D_t, in columns I and P.

Table S5.3. The intrinsic sensitivity of leaf abaxial stomatal density (D_s) to developmental parameters: i_s, i_t, t, s and e. I present calculations for changing mean estimated D_s across a range of increasing and decreasing parameter values from 0 - 100 %, for each developmental parameter. Thus, I estimated D_s by inputting mean values for the parameters listed, and then

increased and decreased each parameter from 0 - 100%, holding all other parameters constant. I then calculated the % change in D_s across the range of increasing and decreasing parameter values relative to the mean estimated D_s of 215.2. I then normalized this value to reflect actual % change values from the mean D_s, in columns I and P.

Table S5.4. The intrinsic sensitivity of leaf adaxial trichome density (D_t) to developmental parameters: i_s, i_t, t, s and e. I present calculations for changing mean estimated D_t across a range of increasing and decreasing parameter values from 0 - 100 %, for each developmental parameter. Thus, I estimated D_t by inputting mean values for the parameters listed, and then increased and decreased each parameter from 0 - 100%, holding all other parameters constant. I then calculated the % change in D_t across the range of increasing and decreasing parameter values relative to the mean estimated D_t of 44.3. I then normalized this value to reflect actual % change values from the mean D_t, in columns I and P.

Table S5.5. The intrinsic sensitivity of leaf adaxial stomatal density (D_s) to developmental parameters: i_s, i_t, t, s and e. I present calculations for changing mean estimated D_s across a range of increasing and decreasing parameter values from 0 - 100 %, for each developmental parameter. Thus, I estimated D_s by inputting mean values for the parameters listed, and then increased and decreased each parameter from 0 - 100%, holding all other parameters constant. I then calculated the % change in D_s across the range of increasing and decreasing parameter values relative to the mean estimated D_s of 144.5. I then normalized this value to reflect actual % change values from the mean D_s, in columns I and P.

Table S6.6. The realized sensitivity of leaf trichome density (D_t) and leaf stomatal density (D_s) to developmental parameters: i_s, i_t, t, s and e. To enable robust comparisons of the realized sensitivity of D_t and D_s to input variables on both leaf surfaces, this analysis focused on the 37 species for which data were available for D_t and D_s for both surfaces, separately considering the 24 amphistomatous species, i.e., with $D_s > 0$ on both surfaces, and the 13 hypostomatous species, i.e., with D_s and s of 0 on the adaxial surface. Values in bold indicate contribution > 5%.

References

1. Adebooye, O. C., M. Hunsche, G. Noga, and C. Lankes. 2012. Morphology and density of trichomes and stomata of *Trichosanthes cucumerina* (Cucurbitaceae) as affected by leaf age and salinity. *Turkish Journal of Botany* 36: 328-335.

2. Adrian, J., J. Chang, C. E. Ballenger, B. O. R. Bargmann, J. Alassimone, K. A. Davies, O. S. Lau, et al. 2015. Transcriptome dynamics of the stomatal lineage: birth, amplification and termination of a self-renewing population. *Developmental cell* 33: 107–118.

3. Agrawal, A. A., M., Fishbein, R., Jetter, J., Salminen, J. B., Goldstein, A. E., Freitag, and J. P., Sparks. 2009. Phylogenetic ecology of leaf surface traits in the milkweeds (*Asclepias* spp.): chemistry, ecophysiology, and insect behavior. *New Phytologist* 183: 848–867.

4. Agren, J., and D. W. Schemske. 1993. The Cost of Defense Against Herbivores: An Experimental Study of Trichome Production in *Brassica rapa*. *The American Naturalist* 141: 338–350.

5. do Nascimento Accioly, A., N., Corte-Real, R., de Paiva Farias, and E.C., Pereira de Arruda. 2022. Phenotypic plasticity of trichomes and stomatal density in *Cenostigma microphyllum* (Mart. ex G. Don) E. Gagnon and G. P. Lewis (Fabaceae) in a seasonally dry tropical forest, Brazil. *Revista brasileira de botânica* 45: 645–650.

6. Azmat, R., S. Haider, H. Nasreen, F. Aziz, and M. Riaz. 2009. A viable alternative mechanism in adapting the plants to heavy metal environment. *Pakistan Journal of Botany* 41: 2729–2738.

7. Barroso, A. A. M., E. Galeano, A. J. P. Albrecht, F. C. dos Reis, and R. V. Filho. 2015. Does Sourgrass leaf anatomy influence glyphosate resistance? *Comunicata Scientiae* 6: 445–453.

8. Bickford, C. P. 2016. Ecophysiology of leaf trichomes. *Functional plant biology* 43: 807–814.

9. Brewer, C. A., W. K. Smith, and T. C. Vogelmann. 1991. Functional interaction between leaf trichomes, leaf wettability and the optical properties of water droplets. *Plant, Cell & Environment* 14: 955–962.

10. Brodribb, T. J., G. J. Jordan, and R. J. Carpenter. 2013. Unified changes in cell size permit coordinated leaf evolution. *New Phytologist* 199: 559–570.

11. Buckley, T. N., and A. Diaz-Espejo. 2015. Partitioning changes in photosynthetic rate into contributions from different variables. *Plant, Cell & Environment* 38: 1200–1211.

12. Cach-Pérez, M. J., J. L. Andrade, W. Cetzal-Ix, and C. Reyes-García. 2016. Environmental influence on the inter- and intraspecific variation in the density and morphology of stomata and trichomes of epiphytic bromeliads of the Yucatan Peninsula. *Botanical Journal of the Linnean Society* 181: 441–458.

13. Camargo, M. A. B., and R. A. Marenco. 2011. Density, size and distribution of stomata in 35 rainforest tree species in Central Amazonia. *Acta Amazonica* 41: 205–212.

14. Carins Murphy, M. R., G. J. Dow, G. J. Jordan, and T. J. Brodribb. 2017a. Vein density is independent of epidermal cell size in Arabidopsis mutants. *Functional Plant Biology* 44: 410–418.

15. Carins Murphy, M. R., G. J. Jordan, and T. J. Brodribb. 2017b. Ferns are less dependent on passive dilution by cell expansion to coordinate leaf vein and stomatal spacing than angiosperms. *PLOS ONE* 12: e0185648.

16. Carins Murphy, M. R., G. J. Jordan, and T. J. Brodribb. 2014. Acclimation to humidity modifies the link between leaf size and the density of veins and stomata. *Plant, Cell & Environment* 37: 124–131.

17. Carins Murphy, M. R., G. J. Jordan, and T. J. Brodribb. 2016. Cell expansion not cell differentiation predominantly co-ordinates veins and stomata within and among herbs and woody angiosperms grown under sun and shade. *Annals of Botany* 118: 1127–1138.

18. Carins Murphy, M. R., G. J. Jordan, and T. J. Brodribb. 2012. Differential leaf expansion can enable hydraulic acclimation to sun and shade. *Plant, Cell & Environment* 35: 1407–1418.

19. Choi, Y.-E., E. Harada, M. Wada, H. Tsuboi, Y. Morita, T. Kusano, and H. Sano. 2001. Detoxification of cadmium in tobacco plants: formation and active excretion of crystals containing cadmium and calcium through trichomes. *Planta* 213: 45–50.

20. Choinski, J. S., and R. R. Wise. 1999. Leaf Growth Development in Relation to Gas Exchange in *Quercus marilandica* Muenchh. *Journal of Plant Physiology* 154: 302–309.

21. Coley, P. D. 1998. Possible Effects of Climate Change on Plant/Herbivore Interactions in Moist Tropical Forests. *Climatic Change* 39: 455–472.

22. Dong, O. X., and P. C. Ronald. 2019. Genetic Engineering for Disease Resistance in Plants: Recent Progress and Future Perspectives. *Plant Physiology* 180: 26–38.

23. Doughty, C. E., C. B. Field, and A. M. S. McMillan. 2011. Can crop albedo be increased through the modification of leaf trichomes, and could this cool regional climate? *Climatic Change* 104: 379–387.

24. Downs, J. L., and R. A. Black. 1999. Leaf surface characteristics and gas exchange in Artemisia tridentata subspecies wyomingensis and tridentata. *USDA Forest Service Proceedings*.

25. Ehleringer, J., O. Björkman, and H. A. Mooney. 1976. Leaf Pubescence: Effects on Absorptance and Photosynthesis in a Desert Shrub. *Science* 192: 376–377.

26. Ehleringer, J. R., and O. Björkman. 1978. Pubescence and leaf spectral characteristics in a desert shrub, *Encelia farinosa*. *Oecologia* 36: 151–162.

27. Ehleringer, J. R., and H. A. Mooney. 1978. Leaf hairs: Effects on physiological activity and adaptive value to a desert shrub. *Oecologia* 37: 183–200.

28. Evert, R. F. 2006. Esau's Plant Anatomy: Meristems, Cells, and Tissues of the Plant Body: Their Structure, Function, and Development. 3rd ed. John Wiley.

29. Fambrini, M., and C. Pugliesi. 2019. The Dynamic Genetic-Hormonal Regulatory Network Controlling the Trichome Development in Leaves. *Plants (Basel, Switzerland)* 8: 253.

30. Fernández, V., D. Sancho-Knapik, P. Guzmán, J. J. Peguero-Pina, L. Gil, G. Karabourniotis, M. Khayet, et al. 2014. Wettability, Polarity, and Water Absorption of Holm Oak Leaves: Effect of Leaf Side and Age. *Plant Physiology* 166: 168–180.

31. Franks, P. J., and D. J. Beerling. 2009. Maximum leaf conductance driven by CO_2 effects on stomatal size and density over geologic time. *Proceedings of the National Academy of Sciences* 106: 10343–10347.

32. Glover, B. J. 2000. Differentiation in plant epidermal cells. *Journal of Experimental Botany* 51: 497–505.

33. Glover, B. J., M., Perez-Rodriguez, and C., Martin. 1998. Development of several epidermal cell types can be specified by the same MYB-related plant transcription factor. *Development* 125: 3497–3508.

34. Grubb, P. J. 1998. A reassessment of the strategies of plants which cope with shortages of resources. *Perspectives in Plant Ecology, Evolution and Systematics* 1: 3–31.

35. Grubb, P. J. 1992. Presidential Address: A Positive Distrust in Simplicity - Lessons From Plant Defences and From Competition Among Plants and Among Animals. *Journal of Ecology* 80: 585–610.

36. Gudesblat, G. E., P. S. Torres, and A. A. Vojnov. 2009. Stomata and pathogens. *Plant Signaling & Behavior* 4: 1114–1116.

37. Gupt, S. K., R. Chand, V. K. Mishra, R. N. Ahirwar, M. Bhatta, and A. K. Joshi. 2021. Spot blotch disease of wheat as influenced by foliar trichome and stomata density. *Journal of Agriculture and Food Research* 6: 100227.

38. Haberlandt, G. 1914. Physiological plant anatomy. 4th ed. MacMillan, London, UK.

39. Handley, R., B. Ekbom, and J. Ågren. 2005. Variation in trichome density and resistance against a specialist insect herbivore in natural populations of Arabidopsis thaliana. *Ecological Entomology* 30: 284–292.

40. Hare, J. D., and E. Elle. 2002. Variable Impact of Diverse Insect Herbivores on Dimorphic *Datura wrightii*. *Ecology* 83: 2711–2720.

41. Hetherington, A. M., and F. I. Woodward. 2003. The role of stomata in sensing and driving environmental change. *Nature* 424: 901–908.

42. Hoof, J., L. Sack, D. T. Webb, and E. T. Nilsen. 2008. Contrasting Structure and Function of Pubescent and Glabrous Varieties of Hawaiian *Metrosideros polymorpha* (Myrtaceae) at High Elevation. *Biotropica* 40: 113–118.

43. John, G. P., C. Scoffoni, T. N. Buckley, R. Villar, H. Poorter, and L. Sack. 2017. The anatomical and compositional basis of leaf mass per area. *Ecology Letters* 20: 412–425.

44. Kaplan, I., G. P. Dively, and R. F. Denno. 2009. The costs of anti-herbivore defense traits in agricultural crop plants: a case study involving leafhoppers and trichomes. *Ecological Applications* 19: 864–872.

45. Karabourniotis, G., and C. Fasseas. 1996. The dense indumentum with its polyphenol content may replace the protective role of the epidermis in some young xeromorphic leaves. *Canadian Journal of Botany* 74: 347–351.

46. Kidner, C. A., and M. C. P. Timmermans. 2010. Signaling sides adaxial-abaxial patterning in leaves. *Current Topics in Developmental Biology* 91: 141–168.

47. Kim, K., H. Kim, S. Ho Park, and S. Joon Lee. 2017. Hydraulic Strategy of Cactus Trichome for Absorption and Storage of Water under Arid Environment. *Frontiers in Plant Science* 8.

48. Konrad, W., D. L. Royer, P. J. Franks, and A. Roth-Nebelsick. 2021. Quantitative critique of leaf-based paleo-CO_2 proxies: Consequences for their reliability and applicability. *Geological Journal* 56: 886–902.

49. Larkin, J. C., M. D. Marks, J. Nadeau, and F. Sack. 1997. Epidermal cell fate and patterning in leaves. *The Plant Cell* 9: 1109–1120.

50. Li, C., Y. Mo, N. Wang, L. Xing, Y. Qu, Y. Chen, Z. Yuan, et al. 2023. The overlooked functions of trichomes: Water absorption and metal detoxication. *Plant, Cell & Environment* 46: 669–687.

51. Lin, Y.-S., B. E. Medlyn, R. A. Duursma, I. C. Prentice, H. Wang, S. Baig, D. Eamus, et al. 2015. Optimal stomatal behaviour around the world. *Nature Climate Change* 5: 459–464.

52. Lu, Z., R. G. Percy, C. O. Qualset, and E. Zeiger. 1998. Stomatal conductance predicts yields in irrigated Pima cotton and bread wheat grown at high temperatures. *Journal of Experimental Botany* 49: 453–460.

53. Mauricio, R. 1998. Costs of Resistance to Natural Enemies in Field Populations of the Annual Plant *Arabidopsis thaliana*. *The American Naturalist* 151: 20–28.

54. Medeiros, C. D., C. Scoffoni, G. P. John, M. K. Bartlett, F. Inman-Narahari, R. Ostertag, S. Cordell, et al. 2019. An extensive suite of functional traits distinguishes Hawaiian wet and dry forests and enables prediction of species vital rates. *Functional Ecology* 33: 712–734.

55. Mediavilla, S., I. Martín, J. Babiano, and A. Escudero. 2019. Foliar plasticity related to gradients of heat and drought stress across crown orientations in three Mediterranean *Quercus* species. *PLoS ONE* 14: e0224462.

56. Mirzaie, M., A. R. Ladanmoghadam, L. Hakimi, and E. Danaee. 2020. Water Stress Modifies Essential Oil Yield and Composition, Glandular Trichomes and Stomatal Features of Lemongrass (*Cymbopogon citratus*) Inoculated with Arbuscular Mycorrhizal Fungi. *Journal of Agricultural Science and Technology* 22: 1575–1585.

57. Muir, C. D., M. À. Conesa, J. Galmés, V. Pathare, P. Rivera, R. L. Rodríguez, T. Terrazas, and D. Xiong. 2022. How important are functional and developmental constraints on phenotypic evolution? An empirical test with the stomatal anatomy of flowering plants. *The American Naturalist*.

58. Pan, Z.-L., W. Guo, Y.-J. Zhang, J. D. M. Schreel, J.-Y. Gao, Y.-P. Li, and S.-J. Yang. 2021. Leaf trichomes of *Dendrobium* species (epiphytic orchids) in relation to foliar water uptake, leaf surface wettability, and water balance. *Environmental and Experimental Botany* 190: 104568.

59. Patel, I., L. Y. Gorim, K. Tanino, and A. Vandenberg. 2021. Diversity in Surface Microstructures of Trichomes, Epidermal Cells, and Stomata in Lentil Germplasm. *Frontiers in Plant Science* 12.

60. Pillemer, E. A., and W. M. Tingey. 1976. Hooked Trichomes: A Physical Plant Barrier to a Major Agricultural Pest. *Science* 193: 482–484.

61. Ripley, B. S., N. W. Pammenter, and V. R. Smith. 1999. Function of Leaf Hairs Revisited: The Hair Layer on Leaves *Arctotheca populifolia* Reduces Photoinhibition, but Leads to Higher Leaf Temperatures Caused by Lower Transpiration Rates. *Journal of Plant Physiology* 155: 78–85.

62. Roche, D. 2015. Stomatal Conductance Is Essential for Higher Yield Potential of C_3 Crops. *Critical Reviews in Plant Sciences* 34: 429–453.

63. Royer, D. L. 2001. Stomatal density and stomatal index as indicators of paleoatmospheric CO_2 concentration. *Review of Palaeobotany and Palynology* 114: 1–28.

64. Sack, L., and T. N. Buckley. 2016. The Developmental Basis of Stomatal Density and Flux. *Plant Physiology* 171: 2358–2363.

65. Sack, L., and T. N. Buckley. 2020. Trait Multi-Functionality in Plant Stress Response. *Integrative and Comparative Biology* 60: 98–112.

66. Salisbury, E. 1927. I. On the causes and ecological significance of stomatal frequency, with special reference to the woodland flora. *Philosophical Transactions of the Royal Society B: Biological Sciences* 216: 1–65.

67. Schreel, J. D. M., O. Leroux, W. Goossens, C. Brodersen, A. Rubinstein, and K. Steppe. 2020. Identifying the pathways for foliar water uptake in beech (*Fagus sylvatica* L.): a major role for trichomes. *The Plant Journal* 103: 769–780.

68. Schwerbrock, R., and C. Leuschner. 2017. Foliar water uptake, a widespread phenomenon in temperate woodland ferns? *Plant Ecology* 218: 555–563.

69. Searchinger, T., R. Waite, C. Hanson, J. Ranganathan, and E. Matthews. 2019. Creating a Sustainable Food Future.

70. Simon, N. M. L., J. Sugisaka, M. N. Honjo, S. A. Tunstad, G. Tunna, H. Kudoh, and A. N. Dodd. 2020. Altered stomatal patterning accompanies a trichome dimorphism in a natural population of *Arabidopsis*. *Plant Direct* 4: e00262.

71. Skelton, R. P., J. J. Midgley, J. M. Nyaga, S. D. Johnson, M. D. Cramer, R. P. Skelton, J. J. Midgley, et al. 2012. Is leaf pubescence of Cape Proteaceae a xeromorphic or radiation-protective trait? *Australian Journal of Botany* 60: 104–113.

72. Snyder, J. C., and G. F. Antonious. 2011. Trichomes - importance in plant defence and plant breeding. *CABI Reviews* 2009: 1–16.

73. Soheili, F., M. Heydari, S. Woodward, and H. R. Naji. 2023. Adaptive mechanism in *Quercus brantii* Lindl. leaves under climatic differentiation: morphological and anatomical traits. *Scientific Reports* 13: 3580.

74. Strauss, S. Y., and A. A. Agrawal. 1999. The ecology and evolution of plant tolerance to herbivory. *Trends in Ecology & Evolution* 14: 179–185.

75. Torii, K. U. 2021. Stomatal development in the context of epidermal tissues. *Annals of Botany* 128: 137–148.

76. Valverde, P. L., J. Fornoni, and J. NÚÑez-Farfán. 2001. Defensive role of leaf trichomes in resistance to herbivorous insects in *Datura stramonium*. *Journal of Evolutionary Biology* 14: 424–432.

77. Vinod, N., M. Slot, I. R. McGregor, E. M. Ordway, M. N. Smith, T. C. Taylor, L. Sack, et al. 2023. Thermal sensitivity across forest vertical profiles: patterns, mechanisms, and ecological implications. *New Phytologist* 237: 22–47.

78. Wang, X., C. Shen, P. Meng, G. Tan, and L. Lv. 2021. Analysis and review of trichomes in plants. *BMC Plant Biology* 21: 70.

79. Warton, D. I., R. A. Duursma, D. S. Falster, and S. Taskinen. 2012. smatr 3 - an R package for estimation and inference about allometric lines: *The smatr 3 - an R package Methods in Ecology and Evolution* 3: 257–259.

80. Weiglin, C., and E. Winter. 1991. Leaf Structures of Xerohalophytes from an East Jordanian Salt Pan. *Flora* 185: 405–424.

81. Werker, E. 2000. Trichome diversity and development. Advances in Botanical Research, 1–35. Elsevier.

82. Wong, S. C., I. R. Cowan, and G. D. Farquhar. 1979. Stomatal conductance correlates with photosynthetic capacity. *Nature* 282: 424–426.

83. Yamaguchi, T., A. Nukazuka, and H. Tsukaya. 2012. Leaf adaxial–abaxial polarity specification and lamina outgrowth: evolution and development. *Plant and Cell Physiology* 53: 1180–1194.

84. Yan, L., X. Cheng, R. Jia, Q. Qin, L. Guan, H. Du, and S. Hou. 2014. New phenotypic characteristics of three tmm alleles in *Arabidopsis thaliana*. *Plant Cell Reports* 33: 719–731.

85. Zhu, Y., J. Zheng, H. Kang, N. Hui, S. Yin, Z. Chen, B. Du, and C. Liu. 2023. Spatial variations in leaf trichomes and their coordination with stomata in *Quercus variabilis* across Eastern Asia. Preprints.

86. Zsögön, A. 2011. Identification and characterization of a tomato introgression line with reduced wilting under drought.

Chapter 6: Integrating leaf expansion kinematics into the leaf economics spectrum: a meta-analysis across species

Abstract

Leaf traits, including those related to size and economics importantly influence species'
adaptation, resource-acquisition and productivity. While leaf size confers adaptation to climate
and microclimate, leaf economics spectrum (LES) traits underlie growth "strategy" according to
the "fast vs. slow" axis of trait variation, such that, on average, species with higher rates of
photosynthesis and respiration per unit leaf mass (A_{mass} and R_{mass}) have lower leaf mass per area
(LMA), higher foliar nitrogen per mass (N_{mass}), and shorter leaf lifespans (LL). Although mature
leaf size is typically weakly related to LES traits, I hypothesized that the "fast vs slow"
developmental rates and durations underlying leaf area would be associated within the LES,
through metabolism and ecological adaptation. To address previous debates on whether leaf
expansion rate or duration tends to be the strongest drivers of mature leaf area (LA_m), I applied a
novel approach to extracting leaf expansion kinematics parameters from the sigmoidal dynamics
of leaf expansion with time, i.e., primordium size (LA_p), leaf maximum expansion rate (R) and
expansion duration (T) and to determining their causal influences on LA_m. I extracted these
parameters for a compiled database for 38 diverse angiosperm species including all published
leaf expansion trajectories, and further estimated parameters for the 118 additional species for
which leaf size and expansion time were available, and tested relationships with LES traits.
Higher LA_p and R and lower T were associated across species with high A_{mass}, R_{mass} and N_{mass} and
low LMA and LL. Yet, a strong general trade-off between R and T constrains LA_m across species,
and thus, the bulk of across species variation in LA_m is determined by LA_p rather than R or T.

Despite such constraint, higher LA_m was positively associated with both mass- and area- based LES traits, excluding LMA, and LL was negatively related to LA_m. Our findings resolve developmental trait causality of LA_m across diverse species and their relationship with the LES, with key implications species' productivity, stress tolerance and biogeographical distributions.

Introduction

Leaf traits influence plant species performance, productivity, adaptation and biogeography in past and present ecosystems worldwide (Osborne et al., 2004; Violle et al., 2007; Wright et al., 2017; Baird et al., 2021). The mature leaf area (LA_m) varies > 100,000-fold across species, affecting leaf energy balance, stress tolerance and carbon accumulation (Wright et al., 2017; Baird et al., 2021). Yet, its determination by underlying developmental processes, i.e. leaf expansion rate vs. duration, across diverse species is poorly understood (Gázquez & Beemster, 2017; Wright et al., 2017; Baird et al., 2021). Further, the potential association of leaf developmental traits with other leaf traits has remained unexamined. By contrast, a strong understanding of associations among other key leaf traits has arisen in recent decades (Wright et al., 2004). The leaf economic spectrum (LES) represents a unified axis of leaf trait variation across species globally, in which traits are associated that confer fast-growth and resource acquisition or, conversely slow growth and resource retentiveness (Wright et al., 2004; Reich, 2014). Thus, species with lower leaf mass per area (LMA) also have lower leaf lifespan (LL), higher photosynthetic rate per mass (A_{mass}), dark respiration rate per mass (R_{mass}), and foliar nitrogen and phosphorus contents per mass (N_{mass} and P_{mass}) (Wright et al., 2004). This generalization is mechanistically based, as higher A_{mass}, N_{mass}, P_{mass} and R_{mass} arise from greater allocation to photosynthetic machinery and associated metabolic reactions relative to structural components that would contribute to higher LMA and longer leaf longevity, and higher A_{mass} and lower LMA (or higher specific leaf area) contribute to rapid plant relative growth rate (Poorter, 1990; Poorter & Van Der Werk, 1998; Poorter & Garnier, 2007). The aim of this study was to resolve the control of final leaf size by leaf expansion rate and duration and test their associations with LES traits, with implications and applications across biological scales.

223

Although the regulation of leaf growth has been extensively studied at the molecular, cellular, and genetic scale, mainly in model organisms, we still lack a clear understanding of how leaf developmental processes determine final leaf size across diverse species (Van Volkenburgh, 1999; Granier et al., 2000; Granier & Tardieu, 2009; Gonzalez et al., 2010, 2012; Kalve et al., 2014; Ma, Buckley & Sack *in prep.*). Species differences in final leaf size are driven by variation in the rate of leaf expansion and/or its duration (Moles & Westoby, 2000; Sun et al., 2006; Granier & Tardieu, 2009; Ma, Buckley & Sack *in prep.*). The few comparative studies of the developmental determinants of LA_m have alternatively suggested that across species, larger leaves arise from longer durations of leaf expansion (Moles & Westoby, 2000), or more rapid rates leaf expansion, or both (Sun et al., 2006; Gázquez & Beemster, 2017). Previous approaches to resolve the developmental traits underlying LA_m faced several challenges. First, the parameters of leaf expansion have typically been estimated from functions fitted to time series, but there has not been a clear approach to independently resolving separate initial (primordium) leaf size from expansion rate and duration. Second, the causal role of developmental traits in driving leaf size has been inferred by comparing the strength of their correlations with LA_m, although this approach cannot provide robust evidence for causation, especially when variables are inter-correlated (Granier et al., 2000; Moles & Westoby, 2000; Sun et al., 2006; Voorend et al., 2014; Gázquez & Beemster, 2017; John et al., 2017). I aimed to resolve the developmental controls of leaf size across species, resolving primordium leaf size, and leaf expansion rate and duration independently and their separate causal influences on LA_m, and to provide insight into the underlying drivers of diversity in leaf size and their potential relationship with other ecologically important traits across species.

Studies of the relationship of LA_m with other LES traits have typically shown weak relationships across diverse species. Thus, a study across 1943 species found larger leaves tended to have higher LMA, representing a weak tendency for larger leaves to require increasing allocation to structural support resulting in "diminishing returns" in photosynthetic mass per leaf area (Niklas et al., 2007). By contrast, tests of the relationship of LA_m to LMA on smaller diverse species sets, whether closely related within lineages, or across lineages, tended to show an opposite trend, with smaller leaves tending to have higher LMA, apparently driven by independent trait adaptation to dry or higher irradiance conditions, within lineages or across communities (Grubb, 1998; Osada, 2020). Other studies within communities or across species have found no associations (Scoffoni et al., 2011; John et al., 2018; Medeiros et al., 2019). Yet, while several studies have shown that rapidly growing species tend to have rapid rates of canopy leaf area expansion (Lambers et al., 1998; Poorter & Van Der Werk, 1998), no studies to our knowledge have directly considered potential relationships of developmental traits underlying LA_m with LES traits. I hypothesized that leaf expansion rate and duration may be linked with LES traits due to multiple mechanisms, based on developmental or metabolic or ecological processes. First, leaf developmental traits may be linked with LES traits due to developmental coordination. High LMA leaves may take longer to expand in size due to the need to transport and assimilate more materials to construct the leaf with larger thick-walled cells, and with more tissue layers (John et al., 2017). Second, leaf expansion rate may be linked with higher metabolic rates (Green et al., 1971; Cleland, 1981; Nielsen & Veierskov, 1990), and thus with greater A_{mass} and R_{mass}, and higher nutrient concentrations that underlie these rates. Indeed, a higher source leaf photosynthetic activity might enable greater rates of sugar export, and thus, a higher relative sink strength in growing leaves, and thus more rapid rates of leaf expansion (Marcelis, 1996;

White et al., 2016). Third, the linkage may arise from coordinated selection for rapid growth, resource-acquisition and competition under high resource supplies, and slow growth, resource retention and stress resistance under low nutrient supplies (Grubb, 1998). Such impacts would be consistent with a high A_{mass} driving rapid leaf flush and expansion, with high leaf turnover of less-protected leaves due to self-shading, herbivory, mechanical damage and senescence (Ackerly & Bazzaz, 1995). By contrast, selection may favor greater structural tissue allocation under low resources, i.e., high LMA, and LL, which are associated with lower A_{mass} and N_{mass}, leading to lower allocation to rapid leaf expansion and longer expansion times. Finally, adaptive responses of both leaf expansion processes and metabolism to environmental factors such as temperature may also contribute to their coordination (Morison & Morecroft, 2006). Indeed, the covariation in area-based LES traits is typically much weaker than mass-based traits in large data sets (Wright et al., 2004), however linkages of area-based LES traits with leaf size and leaf expansion traits may arise across angiosperms, though indirectly due to variation in height and/or diversification across light environments (Price et al., 2014; Scoffoni et al., 2016). LA_m is often associated with climate (Wright et al., 2017; Baird et al., 2021), and its developmental determinants would potentially also be related to climate as shifts in LA_m would necessitate shifts in its underlying developmental processes (Gray & Brady, 2016). Yet, LES traits tend to exhibit weak relationships with climate overall, as there is typically large variation in LES traits within communities under similar climates, with trait variation reflecting functional diversity that contributes to partitioning of niches (Wright et al., 2004, 2005).

I tested the hypothesis of general determination of species differences in LA_m by specific underlying developmental traits, and that these would be linked with LES traits and climate. I developed our approach expanding on a previous study of the causal basis of LA_m in epidermal

cell developmental traits within and across 12 eudicotyledonous species (Ma, Buckley and Sack *in prep.*). That study found that LA_m was determined most strongly by leaf primordium cell number, and the rate of cell proliferation during leaf expansion, and resolved multiple trade-offs among parameters, including between primordium cell size and overall cell expansion, between primordium cell number and cell overall proliferation, between the rate and duration of cell proliferation, and between the rate and duration of cell expansion (Ma, Buckley & Sack *in prep.*). Here I developed an analogous approach for whole leaf expansion, enabling analyses of many more available data, and tests of developmental trait relationships with LES traits. I compiled available data for time series of leaf expansion and measurements of leaf expansion durations, for a total of 140 widely distributed angiosperm species, representing 53 families, grown in controlled and natural conditions, and extracted developmental parameters for the determinants of leaf size, including primordium size (LA_p) and absolute growth (G), and further analyzed G as a function of maximum relative rate of leaf expansion (R) and the duration of leaf expansion (T). I extracted LES trait data from the TRY global trait network database (Kattge et al., 2020). I then tested the hypothesis that leaf expansion developmental parameters are linked with LES traits, such that R would be positively coordinated with LES traits related to fast-growth and resource acquisition (i.e., high A_{mass}, R_{mass}, N_{mass} and P_{mass}) and negatively with traits associated with slow growth and resource retention (i.e., high LMA and LL). I also tested the hypotheses that trade-offs reported at the leaf cell level would scale up to whole leaf development, i.e., between LA_p and G and between R and T.

Materials and Methods

Compilation of leaf expansion datasets

I compiled a database of time-series data for leaf expansion growth for 38 wild and crop eudicot species, representative of 34 genera in 23 families, grown under controlled and natural conditions from published literature via searches using GoogleScholar, Web of Science, and references from articles (Table S6.1-S6.2; Figure 6.1). Our selection included species for which at least six data points were available for leaf area growth as a function of time (Table S6.2). I also compiled a second database for 140 diverse species, representative of 108 genera in 53 families, from studies that included measurements of final leaf area and leaf expansion duration, also including the species from the first database, for which I could also estimate R (see equation 10 below). I searched for studies for both databases using the keywords 'leaf expansion, 'leaf growth', 'leaf area' or 'leaf expansion' combined with 'rate', 'duration', 'time' and 'during'. For some of the studies for which I compiled data for dataset two, some species were sampled from multiple sites, thus I averaged LA_m and T_{99} values between sites per species.

Extraction of leaf economics data from TRY

For the 140 diverse species, I extracted leaf mass per area excluding the petiole, leaf lifespan, leaf photosynthetic rate per area and per mass, leaf dark respiration rate per area and per mass, leaf nitrogen per area and per mass and leaf phosphorus per area and per mass, and averaged values for each trait per species (Table S6.1). Prior to averaging per species, I excluded mis-entered values of *Lonicera maackii* for A_{area} which were 154 umol m^{-2} s^{-1}, a value orders of magnitude higher than the typical A_{area}. Further, for *Arabidopsis thaliana*, I excluded values from Blonder et al., 2015 as many of the values were extremely low compared to other studies,

entered numerous times in the database, measured from mutants and the conditions upon

measuring were not provided, i.e. uncertainty if at light-saturation.

Data Analysis

For species in the first database of 38 species, for which species had at least six data points for

leaf area growth with time, I fitted a statistical model capturing the sigmoidal process of leaf

expansion with time (Ma, Buckley & Sack *in prep.*):

$$LA(t) = \frac{LA_m}{1+e^{-R(T-T_{50})}} \tag{1}$$

where $LA(t)$ is the instantaneous value of leaf area at time t, LA_m is the maximum value of LA, R

is the maximum growth rate of leaf area, T is time, and T_{50} is the time at which y reaches 50% of

its maximum value. I fitted this equation to each species using the R programming language and

extracted LA_m, R, and T_{50}. Our aim was to determine traits influencing the expansion of final leaf

size reflecting the in principle independent roles of primordium size, expansion rate and

duration. Thus, I extracted primordium size (LA_p) and leaf absolute growth (G; the proportional

increase, i.e., LA_m / LA_p), and partitioned G as a function of maximum relative growth rate and

growth duration. Mature leaf size is causally partitioned as:

$$LA_m = LA_p G \tag{2}$$

where LA_p and G are primordium size (cm^2) and its absolute growth increase, respectively. Thus,

for each species, I calculated the primordium size, i.e., the initial value at $t = 0$ from equation 1,

and using the inputs from the extracted values of LA_m, R, and T_{50} as:

$$LA_p = y_0 = \frac{LA_m}{1+e^{RT_{50}}} \tag{3}$$

The absolute growth of the primordium to mature leaf area is:

229

$$G = \frac{(1+0.01e^{RT})}{1.01} \tag{4}$$

where R is the maximum growth rate of LA_m and T is the duration of leaf expansion. I calculated the time at which y, i.e., leaf area, reaches 99% of its mature value as:

$$0.99LA_m = \frac{LA_m}{1+e^{-R(T_{99}-T_{50})}} \tag{5}$$

Equation 5 can be re-arranged as:

$$T_{99} = T_{50} - \frac{\ln(0.01)}{R} \tag{6}$$

Equation 3 can be re-arranged as:

$$LA_m = LA_p(1 + e^{RT_{50}}) \tag{7}$$

Solving for T_{50} in equation 6, and applying this to equation 7, and then to equation 1 gives:

$$y(t) = LA_p \frac{(1+0.01e^{RT_{99}})}{1+0.01e^{(-R(T-T_{99}))}} \tag{8}$$

Equation 8 represents the growth in leaf area as functions of primordium size (y_p) and growth durations (t_y). Thus, a mature leaf, i.e. at leaf expansion of 99% leaf area, can be expressed by replacing t with the total durations of growth (i.e. cell proliferation and expansion) in the denominator of equation 8, to give:

$$LA_m = LA_p \frac{(1+0.01e^{RT_{99}})}{1.01} \tag{9}$$

This equation 9 is the same as equation 2, but with the drivers of G explicitly considered, and thus allows for causal partitioning of LA_m by LA_p, R and T_{99}. Lastly, solving for R in equation 9 gives:

$$R = \frac{\ln \frac{\frac{LA_m}{LA_p 1.01}-1}{0.01}}{T_{99}} \tag{10}$$

230

Equation 9 represents the causal determination of mature leaf area by primordium size and growth, i.e. the rates and durations of cell proliferation and expansion. Further, Equation 10 allows for estimation of r from values of LA_m, LA_p and T_{99}. I acknowledge uncertainty in our LA_p values, for several reasons. First, the criteria for selecting $T = 0$ in each compiled study was not clear, i.e. how the emerging primordium was first distinguished from the shoot apical meristem, and secondly, studies varied in the time points at which leaf areas were quantified, with some studies using as $t = 0$ the time of certain processes, e.g. seed sowing, seed germinating, etc. Thus, for species in which the first time point was $t > 5$ and $LA_m < 1$ cm^2, I standardized t by setting the first time point as $t = 0$ with the corresponding initial LA_m, and each following t value was the difference of the two next data points, such that increasing LA_m corresponded to the differences in t. In other cases, some species first time points were $1 < t < 5$, and $1 < LA_m < 5$, and for these I added a $t = 0$, and $LA_m = 0$ as the first time point. Thus, $t = 0$, and $LA_m = 0$ were not added as the first time point when a species first LA_m was < 1 cm^2, as this first value was considered close to 0.

For species in the larger second database of, for which measurements were made only for final leaf area and the total duration of leaf expansion, I estimated R based on eqn 8 using different scenarios for assumed LA_p values. First, because in the first dataset, LA_p and LA_m were related ($\log_{10}(LA_p) = 0.879 \times \log_{10}(LA_m) -1.9$; $r^2 = 0.16$; $P = 0.011$), I estimated LA_p based on LA_m. To validate this method for estimating R, for the first dataset, I compared R values estimated from the sigmoidal trajectory with R values estimated this way. Values did not significantly differ in the two methods of determination (Figure S6.1; 0.43 ± 0.05 vs. 0.42 ± 0.03; $P = 0.74$; paired t-test), and were correlated (Figure S6.1; $r = 0.86$; $P < 0.001$). For

subsequent analyses of the larger dataset I focused on R values for the larger dataset estimated using the correlation of LA_p and LA_m.

I also causally partitioned the realized drivers of leaf expansion on mature leaf size in two ways. First, I conducted a hierarchical causal partitioning analysis that partitioned the impacts of LA_p and G on LA_m, and then I partitioned the impacts of R and T on G, i.e., using Equations 2 and 4. Second, I determined the overall impacts of LA_p, R and T on LA_m, i.e. equation 9, by multiplying the impact of G on LA_m by the impact of R on G, and of T_{99} on G. For the causal partitioning analyses, I utilized the species from dataset one, i.e. including the 38 species from which I had leaf area growth with time data, using equation 1 to extract R, equation 3 to extract LA_p and equation 6 to extract T_{99}. Such causal analyses partition the causal contribution of each input variable to the differences in mature leaf size for each pairwise species combination, and then calculating the median contribution across all pairwise combinations (Buckley & Diaz-Espejo, 2015; John et al., 2017; Ma, Buckley & Sack *in prep.*). Thus, a higher positive % contribution indicates that the variable has a strong causal role in determining mature leaf size, whereas a negative % contribution indicates that for species with higher mature leaf size, the variable differed across species in the direction that would reduce leaf size, and this negative impact is overcome by the positive impacts of the other variables. Notably, the realized causal contributions depend on the variation of all variables, and thus on the species-set of the analysis.

To elucidate potential associations of leaf traits with developmental processes, I tested correlations. First, I tested for a trade-off in R and T_{99}, across the 140 species from the larger second database. I also tested for correlations of mature leaf area and leaf economic spectrum (LES) area- and mass-based traits with LA_p, R and T_{99}, using ordinary least square (OLS) regressions. Further, I also re-confirmed the tight covariation in mass-based LES traits for our

species, using standard major axis (SMA) regressions (Figure S6.2). Data were log-transformed prior to correlation analyses. In all figures, datasets one and two are presented as solid black and grey points, respectively. Analyses were performed using the R Programming Language (R Core Team 2023).

Results

Variation in leaf expansion parameters

I found large variation in developmental traits for the 38 species for which full time series for leaf expansion was available, and the sigmoidal function was fitted (Figure 6.1). Across these 38 species, LA_m varied from 1.55-331 cm^2, LA_p from 2,600 μm^2 to 6.86 cm^2, R from 0.09-1.75 cm^2 day^{-1}, and T_{99} from 9.8 to 94 days. I also found large variation across the 140 species for which T was measured, and I estimated R (Table S6.1); LA_m varied from 0.027-331 cm^2, R from 0.048-1.14 day^{-1} and T_{99} from 8.4-201 days (Table S6.1).

Causal drivers of leaf size across species and trade-offs among developmental traits

Our causal partitioning analysis showed that across the 38 species for which full time series for leaf expansion was available, LA_p and G determined 93% and 7% of LA variation, respectively (Figure 6.2; Table S6.3). In turn, on average, G was causally determined entirely by R, and T_{99} had a negative causal impact on G (Figure 6.2; Table S6.3). Thus, on average, a species with a higher G than another achieved this with higher R, and it also tended to have a shorter T (thus a negative causal influence of T). Our analysis of the ultimate developmental drivers of LA_m, i.e., of the influences of LA_p, R and T, showed that LA_m was positively determined 93% by LA_p and 9% by R, and -2% by T_{99} (Figure 6.2; Table S6.3). The causal partitioning analysis differed in

some respects from the findings of correlation analyses across species. The critical importance of LA_p in determining LA_m across species was supported by the their positive association, and, additionally, the robustness of this trend, despite the extraction of LA_p from fitted curves was supported by the association of LA_m with the first measured leaf area for each species, and the first measured leaf area was related to LA_p (Figure S6.3-S6.4). Further, LA_m was not associated with G and T_{99}. However, across species, LA_m was positively correlated with R (Figure S6.3; Table 2), despite this relationship being nonreflective of causality.

I resolved strong trade-offs across species between the developmental traits. Across the 38 species, I found strong trade-offs between LA_p and G and between T and R (standard major axis; $P < 0.001$; Figure 6.2; Table S6.4). The trade-off in T and R was supported for both the 38 species with full time series and the 140 species for which T was measured and I estimated R (standard major axis; $P < 0.001$; Figure 6.2; Table S6.4).

Coordination in leaf expansion parameters and leaf economic spectrum traits

I found novel relationships of leaf economic spectrum traits with leaf expansion developmental traits across species (Figure 6.3). For the 38 species with full time series I tested relationships of LES traits with LA_p, G, R and T_{99}. Across species, leaf mass per area (*LMA*) was negatively associated with LA_p (ordinary least squares, $P < 0.05$; Figure 6.3; Table 6.2) and positively with T_{99} (ordinary least squares, $P < 0.05$; Figure 6.3; Table 6.2). Photosynthetic and respiration rates per mass (A_{mass} and R_{mass}), and nitrogen and phosphorus per mass (N_{mass} and P_{mass}) were positively associated with R and negatively associated with T_{99} ($P < 0.001$; Figure 6.3, Table 6.2). Indeed, photosynthetic rate per area (A_{area}) was also positively associated with R ($P < 0.001$; Figure 6.2, Table 6.2). All *LES* traits were independent of G for the 38 species (Figure S6.5). For

the 140 species for which T was measured and I estimated G and R, I found broadly similar

relationships with LES traits, with additional resolution, given the greater power arising in the

larger dataset. *LMA* and *LL* were negatively related to R and positively related to T_{99}, and

independent of G ($P < 0.05$; Figure 6.3; Table 2; Figure S6.5), and A_{mass}, R_{mass}, N_{mass} and P_{mass}

increased positively with R, and negatively with T_{99}, and A_{mass}, N_{mass} and P_{mass} were positively

related to higher G ($P < 0.001$; Figure 6.3; Table 2; Figure S6.5). R_{area} and P_{area} also increased

positively with R, and negatively with T_{99}, and N_{area} declined with increasing R and increased

with higher T_{99} ($P < 0.001$; Figure 6.3; Table 2).

Discussion

Our meta-analyses linking leaf expansion processes with leaf economic spectrum (LES) traits

provides a novel understanding of the drivers and importance of leaf structure and function

across scales. First, I confirmed a critical role of primordium size (LA_p) and the maximum

growth rate (R) as main determinants of across species variation in mature leaf size (LA_m), rather

than T_{99} as has been previously proposed. Second, I provide strong evidence for two important

trade-offs, in the primordium size (LA_p) and absolute growth of the primordium to final leaf size

(G), and in the determinants of G, i.e. the maximum rate (R) versus duration (T_{99}) of leaf

expansion. These trade-offs both provide insight into how the determinants of LA_m arise, and

how such determinants would be linked with LES traits. Third, I demonstrate important linkages

of LES traits with leaf expansion processes that would arise for several reasons, which I discuss

below.

Our study resolves the higher level developmental traits driving differences in mature leaf

size across species. Our results indicate a critical role of the leaf primordium size in determining

LA_m. This finding is consistent with higher primordium cell number driving increasing LA in a previous analysis of cell-level determinants of LA_p (Ma, Buckley & Sack *in prep.*). This finding indicates a very early canalization of leaf size variation even in the shoot apical meristem, as larger leaf primordia would recruit more cells from the apical meristem during leaf initiation (Autran et al., 2002; Gonzalez et al., 2012; Schnablová et al., 2017). Thus, larger apical meristems arise from greater cell numbers, which in turn leads to larger leaf primordium with greater cell numbers (Schnablová et al., 2017). Our finding that the leaf primordium size contributes strongly to the determination of mature leaf size across species may extend the overall pattern of size-coordination among plant organs known as Corner's Rules, by which stems/branches of trees with greater cross sectional area support leaves with higher LA_m, whereas trees with thinner but more numerous branches will support leaves with lower LA_m (Corner, 1949; Lauri, 2019).

The trade-offs resolved among leaf area expansion traits are consistent with those determined at the cell scale (Ma, Buckley & Sack *in prep.*), i.e., those between LA_p and G, and R vs. T reflect at a higher level those previously shown to hold between primordium cell number and size and their increases in leaf development, and between the rates and durations of cell proliferation and cell expansion. Several mechanisms have been proposed to explain the cell level trade-offs, and such mechanisms can also explain the higher level trade-offs shown here, including mechanical and biochemical constraints, fitness advantages, and/or constrained selection for optimal range of leaf sizes across species (Brown et al., 2004; Savage et al., 2007; Pantin et al., 2012; Niklas & Cobb, 2017; Trinh et al., 2021; Ma, Buckley & Sack *in prep.*). Thus, larger primordia, with more numerous or larger cells may be constrained in expansion capacity by their lower surface area-to-volume ratio (Savage et al., 2007; Trinh et al., 2021).

Biochemically, processes occurring at greater rates typically cannot be sustained because of greater resource depletion and/or the accumulation of waste-products (Brown et al., 2004; Pantin et al., 2012), which has been proposed to explain and is also consistent with high A_{mass} being coupled with low LMA and LL (Wright et al., 2004). The trade-offs may also arise from fitness advantages that would occur from selection on one of the variables , e.g. selection to reduce duration but increase expansion rate to acclimate to herbivory or other abiotic stresses (Moles & Westoby, 2000; Baird et al., 2021). Lastly, the trade-offs would arise extrinsically if LA_m was selected for an optimal range of values, and thus the trade-offs would then constrain the range of LA_m (Ma, Buckley & Sack *in prep.*). Notably, the trade-off in LA_p and G indicates that species with lower LA_p have higher growth from LA_p to LA_m, however this higher growth is not high enough to drive higher LA_m.

I found that LA_m was also causally determined by variation in R and not T, as has been proposed from some correlation analyses in studies for which we re-analyzed data as part of our compiled dataset (Sun et al., 2006; Gázquez & Beemster, 2017); but see (Moles & Westoby, 2000). Indeed, I found that species with higher LA_m do not generally arise from higher T, but in fact, species with higher LA_m actually would have lower T. While a high LA_m could intrinsically arise from either a high R or T, or both, the trade-off in R and T leads to species with higher R having lower T, and explains the negative causal impact of T on LA_m. That species with higher LA_m have higher R but lower T is consistent with species with lower T having higher shoot hydraulic conductance, as a higher shoot hydraulic conductance would provide greater water availability to expanding leaves (Nardini, 2002) , and potentially increasing R. Notably, R and T values are partially interdependent mathematically; R and T_{50} are extracted from the same curves, and T is calculated based on T_{50} and R (Methods, equation 6). Thus, the trade-off between R and

T would correspond to conservative variation in T_{50} relative to R (see Brett, 2004). The conservation of T_{50} is consistent with adaptation to reduce the period of leaf vulnerability early in development (Ma, Buckley & Sack *in prep.*), during which leaves would be vulnerable to herbivory or dehydration (Moles & Westoby, 2000; Barton et al., 2019; Kane et al., 2020). Our resolution of the higher level developmental traits underlying species variation in LA_m provides insight into previously proposed ecological patterns. Previous hypotheses that a lower T would result in a lower LA_m, and thus a lower T would be adaptive to reduce the susceptibility to herbivory (Moles & Westoby, 2000), yet our findings suggest that T_{50} is conserved, and that overall a higher LA_m would arise from higher R, and not generally from higher T.

The linkages between leaf expansion developmental traits and LES traits would arise for numerous non-exclusive reasons and highlight the linkages of leaf growth with leaf functional traits. First, high LMA species also arose from meristems that developed smaller $LA_\mathrm{p,}$ (Figure 6.3), though LMA was not related to LA_m in spite of its relationship with its principal driver. I hypothesize that small primordia may be selected for stress tolerance, similarly to low LMA, given the strong vulnerability of the early expanded leaf. Second, the positive coordination of LMA and LL with T indicates that the anatomical and compositional components underlying high LMA, i.e. larger cells, thicker cell walls, denser cells and more cell layers (John et al., 2017; Onoda et al., 2017), may require greater leaf expansion durations. Third, a greater mass and N allocation to cell walls arises from increases in wall thickness, which also reduces mesophyll conductance, and reduces A_mass (Onoda et al., 2017). Indeed, this is one of several ways in which R may be linked with metabolic rates (Green et al., 1971; Cleland, 1981; Nielsen & Veierskov, 1990), which would lead to the positive coordination in R with A_mass, R_mass, N_mass and P_mass. A linkage of R with metabolism would also potentially arise from complex source-sink processes

as greater source activity arising from high A_{mass} would drive higher export rates, and therefore enabling higher relative sink strength in growing leaves, and contributing to greater R. Such a proposition would be consistent with source-sink feedback and regulation, i.e. reduced utilization of photosynthetic products through reduced sink activity or reduced export reduces photosynthetic activity (Moorby, 1977; Paul & Foyer, 2001; Ainsworth & Bush, 2011). Finally, the linkages of developmental traits with LES traits may arise from co-selection for rapid growth, resource-acquisition and competition under high resource supplies versus slow growth, resource retention and stress resistance under low nutrient supplies (Grubb, 1998). Indeed, selection for rapid growth may favor greater allocation to properties underlying high photosynthetic rate and thus, higher A_{mass} and N_{mass}, as well as more rapid expansion and shorter duration to achieve mature leaves faster. This would be consistent with more rapid leaf expansion leading to quicker source maturation, self-shading, and whole plant growth, as mediated by impacts of high A_{mass}, R_{mass}, N_{mass} and P_{mass}, and causing positive-feedback (Ackerly & Bazzaz, 1995).

The developmental traits underlying leaf size expansion can also provide mechanistic detail to clarify trends observed across mature leaves of diverse species. Thus, the higher R in larger leaves can also explain the scaling across eudicots globally of greater major vein diameters and lower major vein densities with higher LA_m, a pattern proposed to constrain the global distribution of leaf size and climate (Sack et al., 2012). Those traits would be achieved by the greater rate of tissue expansion of major veins, enabling their larger diameters at maturity, and of the lamina between veins, contributing to their lower major vein density at maturity. Future studies should explore the linkages of climate adaptation with leaf expansion developmental parameters.

Our study highlights the important developmental traits that underlie diversity in LA_m, and will provide greater resolution in future research on the evolution of leaf size variation within and across lineages. Further, leaf expansion developmental traits may be more proximally related to genetics and evolution than LA_m, with applications in global ecology and agriculture. The relationship of developmental traits to LES traits provides further potential applications. In particular, crop yield is highly influenced by source limitations (White et al., 2016), and species with higher leaf expansion rates have higher yields (Cross, 1991; van den Boogaard et al., 1996). Thus, the potential role of R in increasing LA_m and its coordination with fast-growing LES traits such as A_{mass} suggests that R may be a promising target for increasing yield, though potentially at the expense of reduced LMA and LL, and stress tolerance (Richards, 2000). Indeed, as the genetic and molecular drivers underlying LA_m are being increasingly dissected, our study provides an additional functional linkage of the resulting structural and functional components that would be coupled with genetic and molecular transformation, and also would allow for more precise bioengineering. Furthermore, elucidating the higher level processes driving leaf expansion and their linkage with the LES across species provides a foundational basis of leaf functional ecology and points to further pursuits of LA_m variation, including the developmental drivers of leaf size within single plants and species and those developmental drivers underpinning leaf size adaptation to sun vs. shade, low vs. high soil nutrients and aridity,

Tables

Table 6.1. Definitions of developmental variables and leaf traits involved in the link between leaf size and the leaf economic spectrum (LES).

Trait, variable or feature	Symbol	Unit	N
Leaf area and leaf expansion traits			
Maximum leaf area at maturity	LA_m	cm^2	140
Primordium size	LA_p	cm^2	38
Absolute leaf growth, i.e., estimated from equation 8	G	unitless	
Obtained two ways,			
Estimated with R_1 and T_{99}	G_1	unitless	38
Estimated with R_2 and T_{99}	G_2	unitless	140
Maximum absolute rate of rapid leaf expansion	R	cm^2 day	
• Obtained two ways,			
1. Extracted as model parameter from equation 1 for leaf expansion and time data	R_1	cm^2 day	38
	R_2		
Estimated from equation 10 with observed LA_m and t_{99}, and estimated LA_p.		cm^2 day	140
Duration of leaf expansion at 99% final leaf area	T_{99}	days	140
Duration of leaf expansion at 50% final leaf area	T_{50}	days	38
Leaf economics traits			
Leaf mass per area	LMA	$mg\ m^{-2}$	75
Leaf lifespan	LL	months	34
Photosynthetic rate per leaf mass and per leaf area	A_{mass} and A_{area}	$\mu mol\ g^{-1}\ s^{-2}$ and $\mu mol\ m^{-2}\ s^{-2}$	50
Dark respiration rate per leaf mass and per leaf area	R_{mass} and R_{area}	$\mu mol\ g^{-1}\ s^{-2}$ and $\mu mol\ m^{-2}\ s^{-2}$	28
Leaf nitrogen per leaf mass and per leaf area	N_{mass} and N_{area}	$mg\ g^{-1}$ and $mg\ mm^{-2}$	82
Leaf phosphorus per leaf mass or per leaf area	P_{mass} and P_{area}	$mg\ g^{-1}$ and $mg\ mm^{-2}$	75

Table 6.2. Bivariate relationships between leaf expansion parameters with leaf area and mass-based leaf economics traits. Ordinary least square regressions were used to test relationships of leaf expansion traits (x-variables) with leaf area and leaf economics spectrum traits (y-variables). R^2 and P-values are provided for all tests, and slopes, including 95% confidence intervals when significant at $P < 0.05$. R_1 and R_2, correspond to the expansion traits extracted from model fits for the 38 species with leaf area growth with time data (equation 1), and for 140 species for which we estimated LA_p from a relationship of LA_m and LA_p across the 38 species, which was then used to estimate R_2 (equation 10). Tests with T_{99} were performed across all 140 species. Parameters in bold indicate significant relationships.

| X	Y	Raw		Log	
		R^2 (P)	Slope (95 C.I.s)	R^2 (P)	Slope (95 C.I.s)
LA_p	LA	0.10 (0.055)		**0.16 (0.011)**	0.187 (0.045, 0.330)
	LMA	**0.29 (0.045)**	-0.018 (-0.035, -0.00045)	0.27 (0.059)	
	LL	0.083 (0.42)		0.00018 (0.97)	
	A_{mass}	0.13 (0.12)		0.0066 (0.73)	
	A_{area}	0.037 (0.41)		0.0082 (0.69)	
	R_{mass}	0.38 (0.057)		0.0035 (0.87)	
	R_{area}	0.36 (0.051)		0.36 (0.050)	
	N_{mass}	0.025 (0.52)		0.085 (0.23)	
	N_{area}	0.071 (0.24)		0.0043 (0.78)	
	P_{mass}	0.23 (0.07)		0.019 (0.62)	
	P_{area}	0.054 (0.52)		0.28 (0.12)	
R_1; R_2	LA	**0.19 (0.007)**; **0.08 (0.001)**	132 (39.23, 224.0); 89.6 (36.7, 142)	0.04 (0.224); **0.06 (0.01)**	0.636 (0.193, 1.08)
	LMA	0.01 (0.75); **0.16 (0.0004)**	-0.07 (-0.10, -0.03)	2.1e-06 (0.99); **0.30 (3.57e^{-7})**	-0.384 (-0.521, -0.248)
	LL	**0.50 (0.03)**; **0.21 (0.006)**	-25.2 (-47.9, -2.51); -17.3 (-29.2, -5.32)	0.35 (0.096); **0.33 (0.0003)**	-0.532 (-0.797, -0.266)
	A_{mass}	0.14 (0.11); **0.18 (0.002)**	0.330 (0.125, 0.534)	**0.38 (0.005)**; **0.34 (7.55e^{-6})**	0.83 (0.28, 1.37); 0.630 (0.377, 0.882)
	A_{area}	**0.22 (0.03)**; 0.014 (0.37)		0.11 (0.15); 0.011 (0.42)	
	R_{mass}	**0.75 (0.003)**; **0.53 (1.16e^{-5})**	0.10 (0.05, 1.5); 0.052 (0.032, 0.072)	**0.60 (0.014)**; **0.57 (3.01e^{-6})**	0.98 (0.27, 1.69); 0.741 (0.484, 0.998)
	R_{area}	0.34 (0.075); **0.24 (0.0061)**		0.12 (0.32); **0.17 (0.02)**	
	N_{mass}	**0.43 (0.003)**; **0.14 (0.0005)**	51.7 (20.3, 83.1); 15.1 (6.80, 24.4)	**0.41 (0.004)**; **0.30 (1.10e^{-7})**	0.54 (0.19, 0.89); 0.342 (0.225, 0.458)
	N_{area}	0.052 (0.33); **0.051 (0.041)**		0.13 (0.12); **0.08 (0.0088)**	
	P_{mass}	0.20 (0.11); **0.21 (3.58e^{-5})**	3.02 (1.65, 4.38)	0.24 (0.072); **0.45 (4.32e^{-11})**	0.814 (0.604, 1.02)
	P_{area}	0.021 (0.71); **0.23 (4.86e^{-5})**		0.11 (0.39); **0.26 (1.23e-5)**	
T_{99}	LA	0.02 (0.07)		**0.04 (0.018)**	-0.545 (-0.995, -0.095)
	LMA	**0.33 (6.10e^{-8})**	0.0006 (0.0004, 0.0008)	**0.30 (3.66e^{-7})**	0.387 (0.249, 0.525)
	LL	**0.21 (0.005)**	0.09 (0.03, 0.16)	**0.33 (0.0003)**	0.531 (0.263, 0.798)
	A_{mass}	**0.20 (0.001)**	-0.002 (-0.003, -0.0008)	**0.33 (1.17e^{-5})**	-0.623 (-0.879, -0.367)
	A_{area}	0.061 (0.062)		0.011 (0.44)	
	R_{mass}	**0.21 (0.014)**	-1.54e^{-4} (-2.73e^{-4}, -3.42e^{-5})	**0.56 (4.07e^{-6})**	-0.734 (-0.994, -0.474)
	R_{area}	**0.18 (0.018)**		**0.17 (0.021)**	
	N_{mass}	**0.18 (6.90e^{-5})**	-0.1 (-0.15, -0.05)	**0.29 (1.94e^{-7})**	-0.338 (-0.456, -0.220)
	N_{area}	**0.058 (0.029)**		**0.083 (0.0087)**	
	P_{mass}	**0.20 (4.76e^{-5})**	-0.017 (-0.025, -0.010)	**0.43 (1.34e^{-10})**	-0.803 (-1.02, -0.589)
	P_{area}	**0.19 (0.0002)**		**0.24 (2.29e-5)**	

Figures
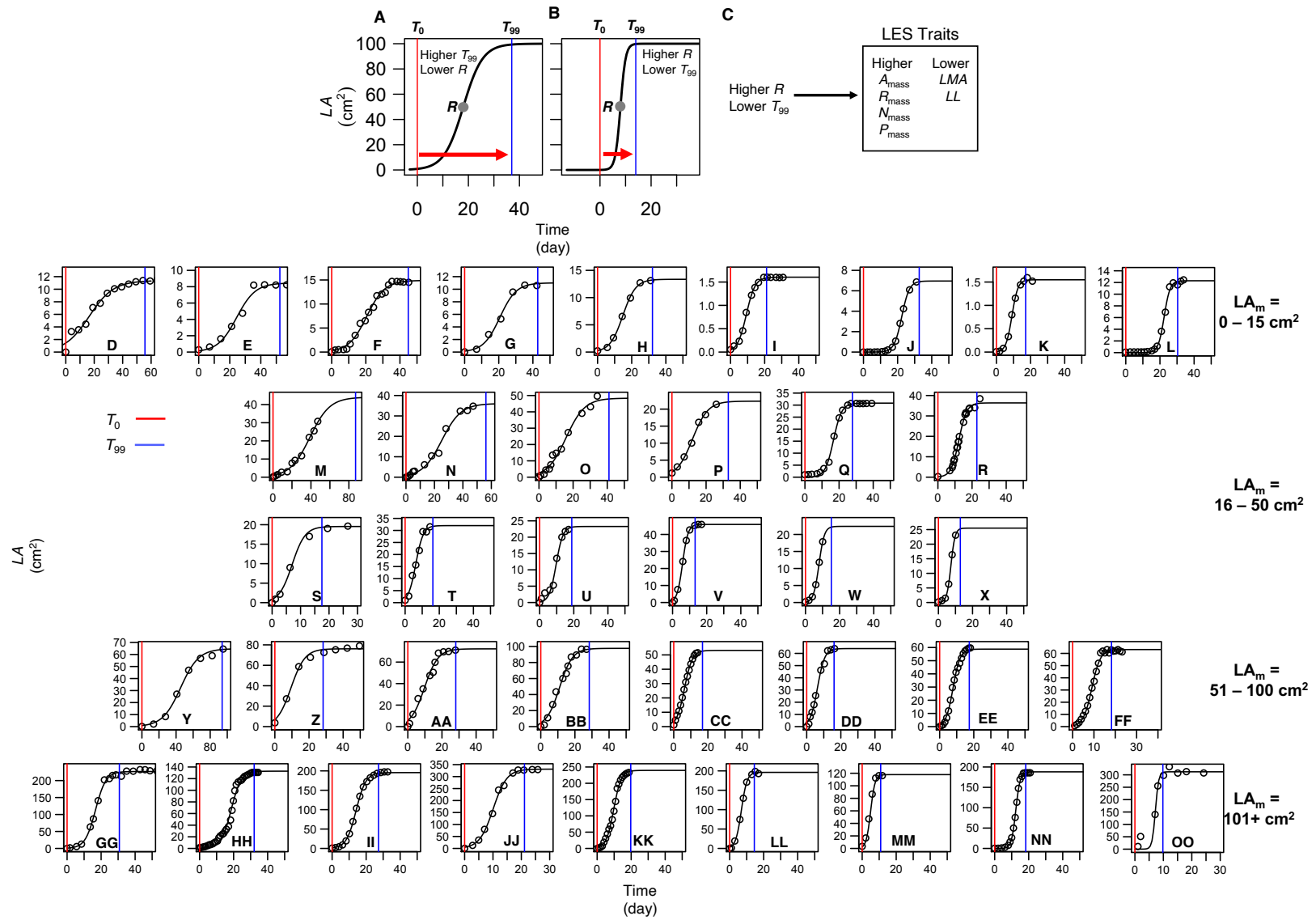
Figure 6.1. Schematics of leaf expansion with time and the influence of developmental traits on LES traits, and leaf expansion growth with time for 38 diverse species from published studies. (A) and **(B)** The process of leaf expansion is sigmoidal with time, reflecting rapid increases in cell proliferation and expansion. In theory, species that have a higher R, i.e. the maximum rate of increase of the sigmoidal curve, also evolve a lower T_{99}, i.e., the time at 99 % of leaf expansion. **(C)** The trade-off in these developmental processes would be coordinated with the spectrum of LES trait variation, as a higher R represents more rapid expansion growth, which would be coupled with quick resource acquisition and investment and thus higher A_{mass}, R_{mass}, N_{mass} and P_{mass}, but lower LMA and LL given the lower T_{99}. Leaf expansion curves from **(D)** – **(OO),** binned by LA_m, i.e. **(D)** – **(L),** 0-15 cm^2, **(M)** – **(R),** 16-50 cm^2, **(S)** – **(X)**, 51-100 cm^2, and **(GG)** – **(OO)**, 101+ cm^2. Within each bin, species are presented from low to high R to demonstrate that species with higher T_{99} have less steep curves, i.e. the distance between the red and blue lines decreases from left to right, as shown in the schematics in **(A)** and **(B)**. **(D)** *Arbutus unedo*, **(E)** *Rhamnus alaternus*, **(F)** *Lithrea brasiliensis***, (G)** *Quercus ilex*, **(H)** *Ochna pulchra*, **(I)** *Myrciaria cuspidata*, **(J)** *Trifolium repens*, **(K)** *Arabidopsis thaliana*, **(L)** *Pisum sativum*, **(M)** *Lonicera maackii***, (N)** *Syringa oblata*, **(O)** *Prunus yedoensis*, **(P)** *Lupinus albus*, **(Q)** *Erythroxylum argentinum*, **(R)** *Nicotiana tabacum*, **(S)** *Capsicum annuum*, **(T)** *Phaseolus vulgaris*, **(U)** *Populus alba*, **(V)** *Populus nigra*, **(W)** *Tarenaya hassleriana*, **(X)** *Gynandropsis gynandra*, **(Y)** *Eucalyptus regnans*, **(Z)** *Pelargonium zonale*, **(AA)** *Litsea pierrei*, **(BB)** *Litsea dilleniifolia*, **(CC)** *Fragaria virginiana*, **(DD)** *Cucurbita pepo*, **(EE)** *Lactuca sativa*, **(FF)** *Quercus rubra*, **(GG)** *Solanum tuberosum*, **(HH)** *Myrsine umbellata*, **(II)** *Manihot esculenta*, **(JJ)** *Actinidia deliciosa*, **(KK)** *Cucumis sativus*, **(LL)** *Populus euramericana*, **(MM)** *Glycine max*, **(NN)** *Helianthus annus*, **(OO)** *Anthocephalus chihensis*. Notably, although R and T differ

dramatically in panels **(A)** versus **(B)**, the maximum leaf size is the same, and thus leaves of similar sizes may in theory achieve such sizes via higher R or T, however a trade-off in R and T would constrain which of these drives higher LA_m and LES traits. The LA_p in **(A)** and **(B)** were 0.0017 and 5.18 cm^2, respectively.
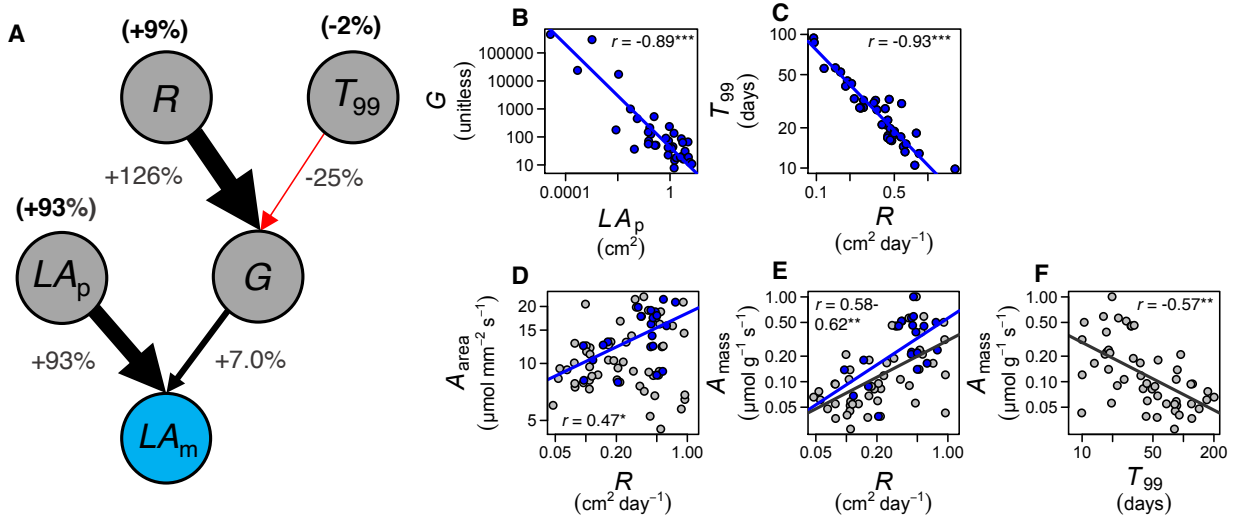
Figure 6.2. Causal determinants of maximum leaf size (LA$_m$), trade-offs in leaf expansion developmental traits, and coordination of leaf expansion developmental traits with area- and mass-based photosynthetic rate. Causal partitioning of LA_m for the 38 species for which we had leaf area growth with time data, with causal influences presented as percentages adjacent to arrows. LA_m is a function of primordium size (LA_p) and the total growth from the primordium to the mature leaf (G), which is a function of the maximum rate (R) and duration of growth (T_{99}). Grey numbers indicate causal influences based on the hierarchical causal partitioning, whereas black numbers indicate causal influences without hierarchical causal partitioning, i.e. LA_m causally determined by the three ultimate traits. Black and red arrows indicate a positive or negative causal influence, with arrows scaled in size to the magnitude of the causal influence. A negative causal role, as for T_{99} indicates that larger LA was associated with lower t_{99} that would ultimately reduce LA, but this was compensated for by higher R, given the trade-off in R and T_{99} shown in **(C)**. Across species, trade-offs in **(B)** leaf expansion absolute growth (G) and primordium size (LA_p) and in **(C)** leaf expansion duration (T_{99}) and maximum growth rate (R).

Across species, coordination of **(D)** photosynthetic rate per leaf area (A_{area}) and **(E)** photosynthetic rate per leaf mass (A_{mass}) with R, and a trade-off of **(F)** A_{mass} with T_{99}. Lines in panels **(B)** and **(C)** were fitted with standard major axis (SMA) regressions on log-transformed data across the 38 species with LA growth with time. Lines in panels **(D)** – **(F)** were fitted with ordinary least square (OLS) regressions on log-transformed data, across the 38 species with LA growth with time shown in blue, and across the larger dataset of 140 species for which I additionally estimated R, shown in grey. As the 38 species from data set one are also included in data set two, the black line is fitted against all points in **(E)**.
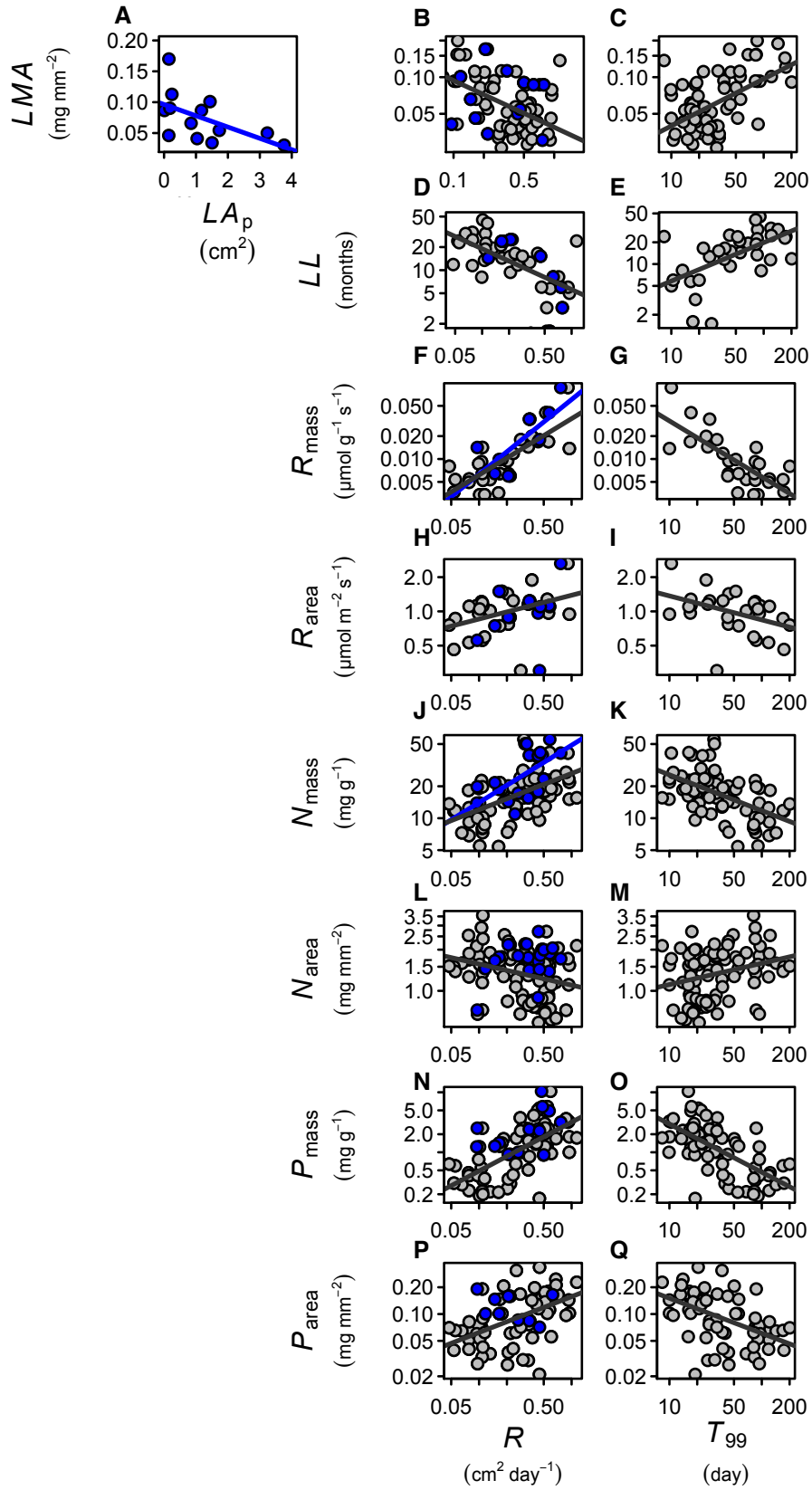
Figure 6.3. Integration of leaf expansion kinematics with the leaf economic spectrum.

Negative associations of leaf mass per area (*LMA*) with **(A)** leaf primordium size (LA_p), **(B)** maximum absolute leaf expansion rate (*R*), and a positive association with **(C)** the duration of leaf expansion (T_{99}). Leaf lifespan (*LL*) exhibited similar negative and positive associations with **(D)** *R* and **(E)** T_{99}. By contrast, **(F)** – **(P)**, dark-respiration rate per mass (R_mass), dark-respiration rate per area (R_area), nitrogen content per mass (N_mass), phosphorus content per mass (P_mass) and phosphorus content per area (P_area) were positively coordinated with *R* and negatively related to T_{99}. By contrast, **(L)** – **(M)** nitrogen content per area (N_area) was negatively related to *R* and positively coordinated with T_{99}. Trait definitions, and statistics and slopes are found in Tables 6.1 and 6.2, respectively. Plotted lines are ordinary least square (OLS) regressions on log-transformed data. Blue and grey points correspond to datasets one and two, respectively.

Supplementary Materials

Supplementary Data Captions (see attached Excel Workbook)

Table S6.1. Species included in the study, the reference from which leaf expansion with time, or final leaf expansion and leaf expansion duration were extracted, leaf expansion traits, and leaf economics traits extracted from the TRY global plant trait database.

Table S6.2. Leaf expansion with time data extracted from published studies. The data used to fit equation 1 per species are in columns E and F.

Table S6.3. Causal partitioning of leaf area (LA) to developmental traits: primordium size (LA_p) and growth (G), and of (G) partitioned by leaf expansion rate (R) and duration (T_{99}), or, non-hierarchical partitioning of LA, partitioned by LA_p, R and T_{99}.

Table S6.4. Correlation matrix of the associations between leaf expansion traits

Supplementary Figures
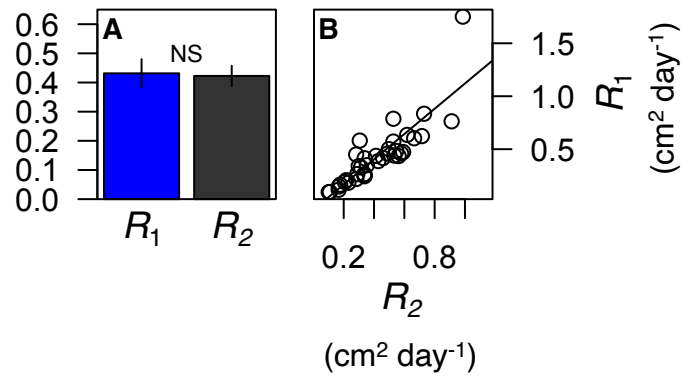
Figure S6.1. Comparison of leaf expansion rates (R). (A) Barplot showing the average R_1, extracted from equation 1, and R_2, estimated from equation 10, for the 38 species from dataset one. **(B)** Correlation between R_1 and R_2. Averages in **(A)** were compared and not statistically significant by t-test, and the relationship in **(B)** was significant, at $P < 0.05$.

Figure S6.2. Covariation in leaf economics traits for the species in dataset 2. Confirmation of the covariation in mass-based leaf economics traits, extracted from TRY. All relationships are significant at $P < 0.05$. Trait definitions are found in Tables 6.1
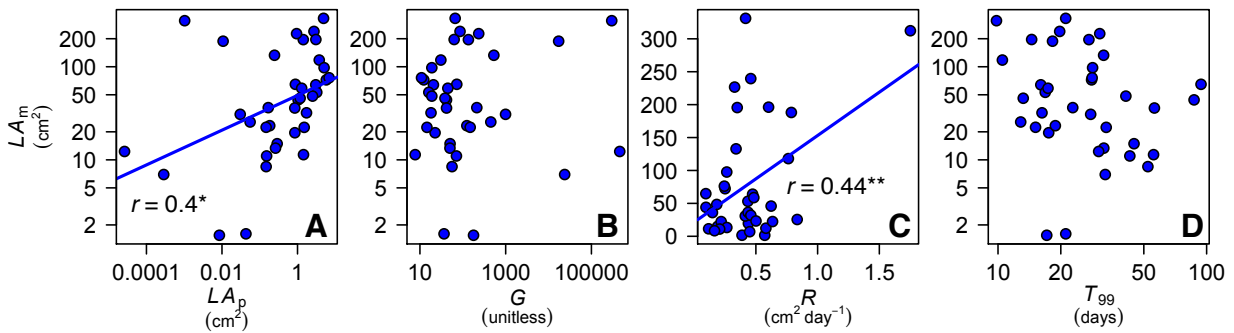
Figure S6.3. Correlations of the drivers of mature leaf size (LA_m) across species. LA_m with **(A)** primordium size (LA_p), **(B)** growth (G), **(C)** expansion rate (R)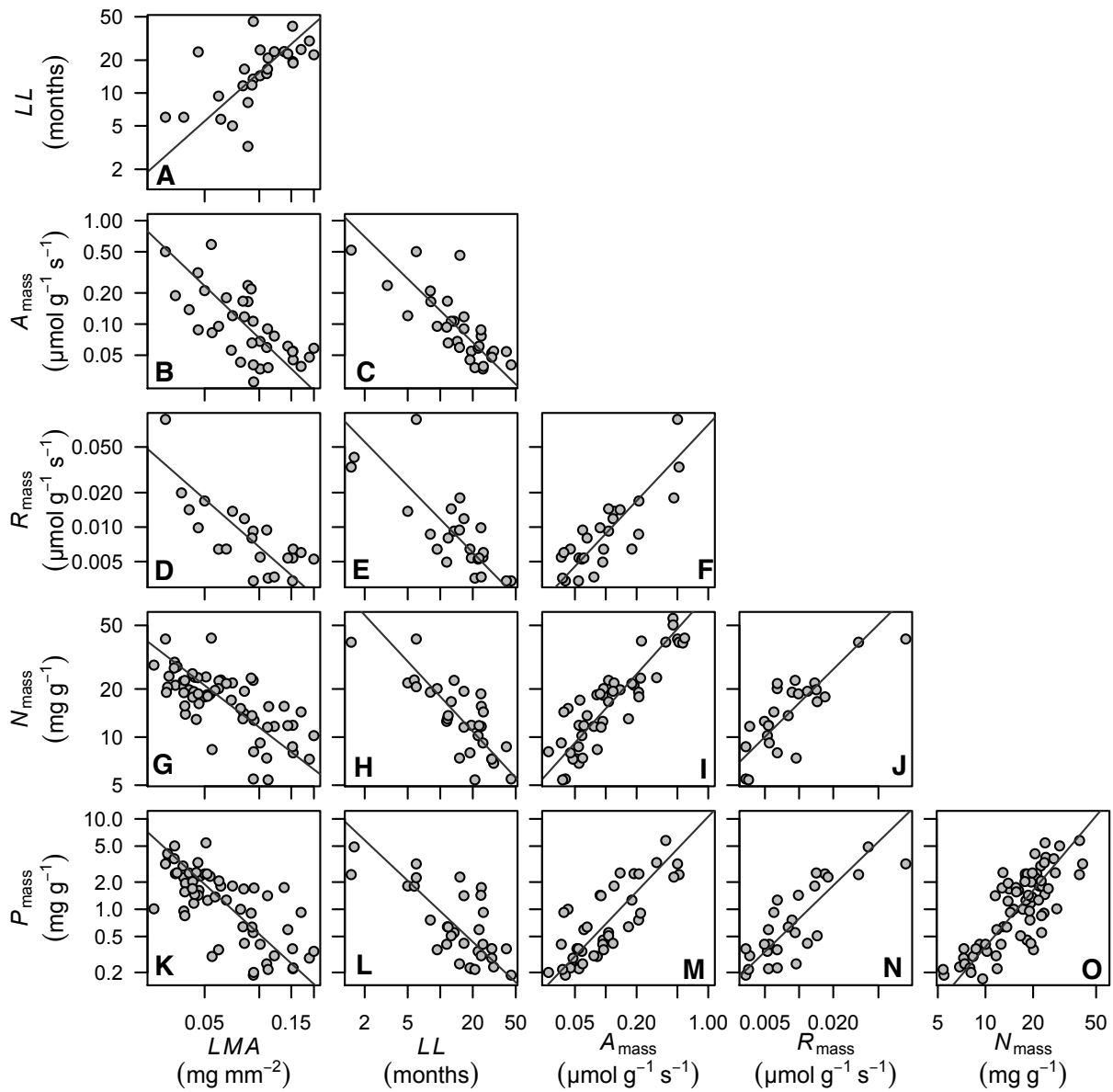 and **(D)** expansion duration (T_{99}), across the same 38 species used for causal analyses. Lines in panels **(A) – (D)** are ordinary least square (OLS) regressions on log-transformed data in all excluding **(C)** for which only the analysis on raw data was significant. Although LA_m was independent from T_{99} across the 38 species here, there was a negative association between the two traits across the 140 species (Table 6.2). Trait definitions, and statistics and slopes are found in Tables 6.1 and 6.2, respectively.
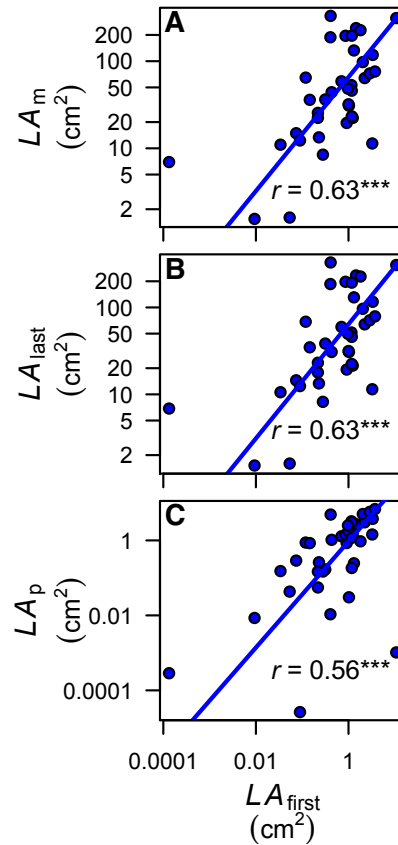
Figure S6.4. Additional support for the critical role of primordium size (LA_p) on final leaf size (LA_m). Associations of **(A)** maximum leaf size at maturity (LA_m), **(B)** the last LA value of each of the 38 species LA with time data (LA_{last}), and **(C)** primordium size (LA_p) with the first LA value of each of the 38 species LA with time data (LA_{first}). Lines were fitted with standard major axis (SMA) regression on log-transformed data.
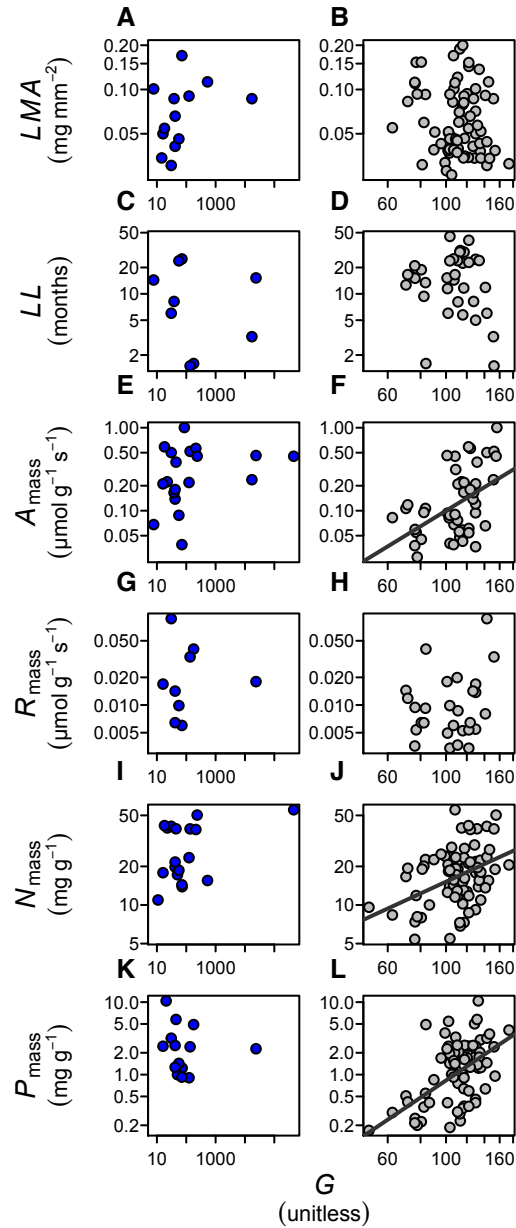
Figure S6.5. Integration of leaf economic spectrum (LES) traits with leaf expansion growth (*G*). (A) – (D), (G) – (H) Independence of leaf mass per area (*LMA*), leaf lifespan (*LL*), and dark respiration rate per mass (R_{mass}) with absolute leaf expansion growth (*G*), and **(F), (J)** and **(L)** coordination of light-saturated photosynthetic rate per mass (A_{mass}), nitrogen content per mass (N_{mass}) and phosphorus content per mass (P_{mass}) with *G*. Trait definitions are found in Table 6.1.

Plotted lines are ordinary least square (OLS) regressions on log-transformed data. Black and grey points correspond to datasets one and two, respectively, and are plotted separately due to varying ranges in G.

References

1. Ackerly, D.D. & F.A., Bazzaz 1995. Leaf dynamics, self-shading and carbon gain in seedlings of a tropical pioneer tree. *Oecologia* 101: 289–298.

2. Alves, A.C. & T.L., Setter 2004. Response of Cassava Leaf Area Expansion to Water Deficit: Cell Proliferation, Cell Expansion. and Delayed Development. *Annals of Botany* 94: 605-613.

3. Ainsworth, E.A. & D.R., Bush 2011. Carbohydrate Export from the Leaf: A Highly Regulated Process and Target to Enhance Photosynthesis and Productivity. *Plant Physiology* 155: 64–69.

4. Amer, F.A. & W.T., Williams 1957. Leaf-area growth in *Pelargonium zonale*. *Annals of Botany* 21: 339-342.

5. Autran, D., C., Jonak, K., Belcram, G.T.S., Beemster, J., Kronenberger, O., Grandjean, O., et al., 2002. Cell numbers and leaf development in *Arabidopsis*: a functional analysis of the STRUWWELPETER gene. *EMBO J* 21: 6036–6049.

6. Baird, A.S., S.H., Taylor, J., Pasquet-Kok, C., Vuong, Y., Zhang, T., Watcharamongkol, T., et al., 2021. Developmental and biophysical determinants of grass leaf size worldwide. *Nature* 592: 242–247.

7. Barton, K.E., K.F., Edwards, & J., Koricheva, 2019. Shifts in woody plant defence syndromes during leaf development. *Funct Ecol*, 33, 2095–2104.

8. Blonder, B., F., Vasseur, C., Violle, B., Shipley, B.J., Enquist, D., Vile. 2015. Testing models for the leaf economics spectrum with leaf and whole-plant traits in *Arabidopsis thaliana*. *AoB Plants* 7.

9. van den Boogaard, R., E. J. Veneklaas, J. M. Peacock, and H. Lambers. 1996. Yield and water use of wheat (*Triticum aestivum*) in a Mediterranean environment: Cultivar differences and sowing density effects. *Plant and Soil* 181: 251–262.

10. Brett, M. T. 2004. When is a correlation between non-independent variables "spurious"? *Oikos* 105: 647–656.

11. Brown, J. H., J. F. Gillooly, A. P. Allen, V. M. Savage, and G. B. West. 2004. Toward a Metabolic Theory of Ecology. *Ecology* 85: 1771–1789.

12. Buckley, T. N., and A. Diaz-Espejo. 2015. Partitioning changes in photosynthetic rate into contributions from different variables. *Plant, Cell & Environment* 38: 1200–1211.

13. Cai, Z.Q., M., Slot, Z.-X., Fan. 2005. Leaf development and photosynthetic properties of three tropical tree species with delayed greening. *Photosynthetica* 43: 91-98.

14. Cleland, R. E. 1981. Wall Extensibility: Hormones and Wall Extension. *In* W. Tanner, and F. A. Loewus [eds.], Plant Carbohydrates II: Extracellular Carbohydrates, Encyclopedia of Plant Physiology, 255–273. Springer, Berlin, Heidelberg.

15. Cookson, S.J., M., van Lijsebettens, C., Granier. 2005. Correlation between leaf growth variables suggest intrinsic and early controls of leaf size in *Arabidopsis thaliana*. *Plant, Cell & Environment* 21: 1355-1366.

16. Corner, E. J. H. 1949. The Durian Theory or the Origin of the Modern Tree. *Annals of Botany* 13: 367–414.

17. Cross, H. Z. 1991. Leaf Expansion Rate Effects on Yield and Yield Components in Early-Maturing Maize. *Crop Science* 31: cropsci1991.0011183X003100030006x.

18. Denne, P.M. (1966) Leaf development in *Trifolium repens*. *Botanical Gazette* 127: 202-210.

19. Ding, Y., Q.-S., Zheng, Y., Zhang, C., He, B., Xie. 2014. Observation of Apparently Unchanging Mesophyll Cell Diameters Throughout Leaf Ontogeny in Woody Species. *Journal of Plant Growth Regulation* 33: 150-159.

20. England, J.R., P.M., Attiwill. 2008. Patterns of growth and nutrient accumulation in expanding leaves of *Eucalyptus regnans* (Myrtaceae). *Australian Journal of Botany* 56, 44-50

21. Ferris, M., G., Taylor. 2001. Leaf area is stimulated in *Populus* by free air CO_2 enrichment (POPFACE), through increased cell expansion and production. *Plant, Cell & Environment*. 24: 305-315

22. Gázquez, A., and G. T. S. Beemster. 2017. What determines organ size differences between species? A meta-analysis of the cellular basis. *New Phytologist* 215: 299–308.

23. Gonzalez, N., S. De Bodt, R. Sulpice, Y. Jikumaru, E. Chae, S. Dhondt, T. Van Daele, et al. 2010. Increased Leaf Size: Different Means to an End. *Plant Physiology* 153: 1261–1279.

24. Gonzalez, N., H. Vanhaeren, and D. Inzé. 2012. Leaf size control: complex coordination of cell division and expansion. *Trends in Plant Science* 17: 332–340.

25. Granier, C., and F. Tardieu. 2009. Multi-scale phenotyping of leaf expansion in response to environmental changes: the whole is more than the sum of parts. *Plant, Cell & Environment* 32: 1175–1184.

26. Granier, C., O. Turc, and F. Tardieu. 2000. Co-Ordination of Cell Division and Tissue Expansion in Sunflower, Tobacco, and Pea Leaves: Dependence or Independence of Both Processes? *Journal of Plant Growth Regulation* 19: 45–54.

27. Gratani, L., A., Bonito. 2009. Leaf traits variation during leaf expansion in *Quercus ilex* L. *Photosynthetica*. 47: 323-330.

28. Gratani, L., E., Ghia. 2002. Changes in morphological and physiological traits during leaf expansion of *Arbutus unedo*. *Environmental and Experimental Botany* 48: 51-60.

29. Gray, S. B., and S. M. Brady. 2016. Plant developmental responses to climate change. *Developmental Biology* 419: 64–77.

30. Green, P. B., R. O. Erickson, and J. Buggy. 1971. Metabolic and Physical Control of Cell Elongation Rate. *Plant Physiology* 47: 423–430.

31. Gregory, F. G. 1921. Studies in the Energy Relations of Plants. *Annals of Botany*. 35: 93-123.

32. Grubb, P. J. 1998. A reassessment of the strategies of plants which cope with shortages of resources. *Perspectives in Plant Ecology, Evolution and Systematics* 1: 3–31.

33. Jing, J., K. Li, Z Liu. 2016. Effects of varying temperature on leaf phenology and herbivory of dominant tree species in subtropical evergreen broad-leaves forest in eastern China. *Polish Journal of Plant Ecology* 64: 53-69.

34. John, G. P., C. Henry, and L. Sack. 2018. Leaf rehydration capacity: Associations with other indices of drought tolerance and environment. *Plant, Cell & Environment* 41: 2638–2653.

35. John, G. P., C. Scoffoni, T. N. Buckley, R. Villar, H. Poorter, and L. Sack. 2017. The anatomical and compositional basis of leaf mass per area. *Ecology Letters* 20: 412–425.

36. Jurik, T. W., B.F. Chabot. 1986. Leaf dynamics and profitability in wild strawberries. *Oecologia*. 69: 296-304

37. Kalve, S., D. De Vos, and G. T. S. Beemster. 2014. Leaf development: a cellular perspective. *Frontiers in Plant Science* 5.

38. Kane, C. N., G. J. Jordan, S. Jansen, and S. A. M. McAdam. 2020. A Permeable Cuticle, Not Open Stomata, Is the Primary Source of Water Loss From Expanding Leaves. *Frontiers in Plant Science* 11.

39. Kattge, J., G. Bönisch, S. Díaz, S. Lavorel, I. C. Prentice, P. Leadley, S. Tautenhahn, et al. 2020. TRY plant trait database – enhanced coverage and open access. *Global Change Biology* 26: 119–188.

40. Külahoglu, C., A.K. Denton, M. Sommer, J. Mab, S. Schliesky, T.J. Wrobel, et al. 2014. Comparative transcriptome atlases reveal altered gene expression modules between two Cleomaceae C_3 and C_4 plant species. *Plant Cell*

41. Lambers, H., H. Poorter, and M. M. I. Van Vuuren. 1998. Inherent Variation in Plant Growth. Backhuys Publishers, Leiden, The Netherlands.

42. Lauri, P.-É. 2019. Corner's rules as a framework for plant morphology, architecture and functioning – issues and steps forward. *New Phytologist* 221: 1679–1684.

43. Ludlow, A.E. 1991. *Ochna pulcha* Hook: Leaf growth and development related to photosynthetic activity. *Annals of Botany* 68: 527-540.

44. Marcelis, L. F. M. 1996. Sink strength as a determinant of dry matter partitioning in the whole plant. *Journal of Experimental Botany* 47: 1281–1291.

45. Medeiros, C. D., C. Scoffoni, G. P. John, M. K. Bartlett, F. Inman-Narahari, R. Ostertag, S. Cordell, et al. 2019. An extensive suite of functional traits distinguishes Hawaiian wet and dry forests and enables prediction of species vital rates. *Functional Ecology* 33: 712–734.

46. Moles, A. T., and M. Westoby. 2000. Do Small Leaves Expand Faster Than Large Leaves, and Do Shorter Expansion Times Reduce Herbivore Damage? *Oikos* 90: 517–524.

47. Moorby, J. 1977. Integration and regulation of translocation within the whole plant. *Symposia of the Society for Experimental Biology* 31: 425–454.

48. Morison, J. I. L., and M. D. Morecroft eds. . 2006. Plant growth and climate change. Blackwell Pub, Oxford ; Ames, Iowa.

49. Nardini, A. 2002. Relations between efficiency of water transport and duration of leaf growth in some deciduous and evergreen trees. *Trees* 16: 417–422.

50. Nielsen, T. H., and B. Veierskov. 1990. Regulation of Carbon Partitioning in Source and Sink Leaf Parts in Sweet Pepper (Capsicum annuum L.) Plants 1. *Plant Physiology* 93: 637–641.

51. Niklas, K. J., and E. D. Cobb. 2017. Size-dependent variation in plant form. *Current Biology* 27: R900–R905.

52. Niklas, K. J., E. D. Cobb, Ü. Niinemets, P. B. Reich, A. Sellin, B. Shipley, and I. J. Wright. 2007. "Diminishing returns" in the scaling of functional leaf traits across and within species groups. *Proceedings of the National Academy of Sciences of the United States of America* 104: 8891–8896.

53. Onoda, Y., I. J. Wright, J. R. Evans, K. Hikosaka, K. Kitajima, Ü. Niinemets, H. Poorter, et al. 2017. Physiological and structural tradeoffs underlying the leaf economics spectrum. *New Phytologist* 214: 1447–1463.

54. Osada, N. 2020. Intraspecific variation in spring leaf phenology and duration of leaf expansion in relation to leaf habit and leaf size of temperate tree species. *Plant Ecology* 221: 939–950.

55. Osborne, C. P., D. J. Beerling, B. H. Lomax, and W. G. Chaloner. 2004. Biophysical constraints on the origin of leaves inferred from the fossil record. *Proceedings of the National Academy of Sciences* 101: 10360–10362.

56. Pantin, F., T. Simonneau, and B. Muller. 2012. Coming of leaf age: control of growth by hydraulics and metabolics during leaf ontogeny. *New Phytologist* 196: 349–366.

57. Paul, M. J., and C. H. Foyer. 2001. Sink regulation of photosynthesis. *Journal of Experimental Botany* 52: 1383–1400.

58. Poorter, H. 1990. Interspecific Variation in Relative Growth Rate: On Ecological Causes and Physiological Consequences. Causes and consequences of variation in growth rate and productivity of higher plants, 45–68. The Hague: SPB Academic Publishing.

59. Poorter, H., and E. Garnier. 2007. Ecological Significance of Inherent Variation in Relative Growth Rate and Its Components. Functional Plant Ecology, CRC Press.

60. Poorter, H., and A. Van Der Werk. 1998. Is Inherent Variation in RGR Determined by LAR at Low Irradiance and by NAR at High Irradiance? A review of Herbaceous Species. Physiological Mechanisms and Ecological Consequences, Backhuys Publishers, Leiden, The Netherlands.

61. Price, C. A., I. J. Wright, D. D. Ackerly, Ü. Niinemets, P. B. Reich, and E. J. Veneklaas. 2014. Are leaf functional traits 'invariant' with plant size and what is 'invariance' anyway? *Functional Ecology* 28: 1330–1343.

62. Reich, P. B. 2014. The world-wide 'fast-slow' plant economics spectrum: a traits manifesto H. Cornelissen [ed.],. *Journal of Ecology* 102: 275–301.

63. Richards, R. A. 2000. Selectable traits to increase crop photosynthesis and yield of grain crops. *Journal of Experimental Botany* 51: 447–458.

64. Ron'zhina E.S. 2003. Cytokinin-regulated mesophyll cell division and expansion during development of *Cucurbita pepo* leaves. *Russian Journal of Plant Physiology* 50: 646-655.

65. Sack, L., C. Scoffoni, A. D. McKown, K. Frole, M. Rawls, J. C. Havran, H. Tran, and T. Tran. 2012. Developmentally based scaling of leaf venation architecture explains global ecological patterns. *Nature Communications* 3: 837.

66. Savage, V. M., A. P. Allen, J. H. Brown, J. F. Gillooly, A. B. Herman, W. H. Woodruff, and G. B. West. 2007. Scaling of number, size, and metabolic rate of cells with body size in mammals. *Proceedings of the National Academy of Sciences* 104: 4718–4723.

67. Schlindwein C.C.D., A.G. Fett-Neto, and L.R. Dillenburg. Chemical and mechanical changes during leaf expansion of four woody species of a dry resting woodland. *Plant Biology* 8: 430-438.

68. Schnablová, R., T. Herben, and J. Klimešová. 2017. Shoot apical meristem and plant body organization: a cross-species comparative study. *Annals of Botany* 120: 833–843.

69. Scoffoni, C., D. S. Chatelet, J. Pasquet-kok, M. Rawls, M. J. Donoghue, E. J. Edwards, and L. Sack. 2016. Hydraulic basis for the evolution of photosynthetic productivity. *Nature Plants* 2: 1–8.

70. Scoffoni, C., M. Rawls, A. McKown, H. Cochard, and L. Sack. 2011. Decline of Leaf Hydraulic Conductance with Dehydration: Relationship to Leaf Size and Venation Architecture. *Plant Physiology* 156: 832–843.

71. Seleznyova A.N., D.H. Greer. 2001. Effects of temperature and leaf position on leaf area expansion of kiwifruit (*Actinidia deliciosa*) shoots: development of a modelling framework. *Annals of Botany* 88: 605-615.

72. Sui, Z.L., S.L Mao., L.H. Wang., B.X., Zhang., Z.X. Zhang. 2012. Effect of low light on the characteristics of photosynthesis and chlorophyll a fluorescence during leaf development of sweet pepper. *Journal of Integrative Agriculture*. 11: 1633-1643.

73. Sun, S., D. Jin, and R. Li. 2006. Leaf emergence in relation to leaf traits in temperate woody species in East-Chinese Quercus fabri forests. *Acta Oecologica* 30: 212–222.

74. Taneda, H., I. Terashima. 2012. Co-ordinated development of the leaf midrib xylem with the lamina in *Nicotiana tabacum*. *Annals of Botany* 110: 35-45.

75. Trinh, D.-C., J. Alonso-Serra, M. Asaoka, L. Colin, M. Cortes, A. Malivert, S. Takatani, et al. 2021. How Mechanical Forces Shape Plant Organs. *Current Biology* 31: R143–R159.

76. Van Volkenburgh, E. 1999. Leaf expansion – an integrating plant behaviour. *Plant, Cell & Environment* 22: 1463–1473.

77. Varone, L., L. Gratani. 2009. Leaf expansion in *Rhamnus alaternus* L. by leaf morphological, anatomical and physiological analysis. *Trees* 23: 1255-1262.

78. Violle, C., M.-L. Navas, D. Vile, E. Kazakou, C. Fortunel, I. Hummel, and E. Garnier. 2007. Let the concept of trait be functional! *Oikos* 116: 882–892.

79. Voorend, W., P. Lootens, H. Nelissen, I. Roldán-Ruiz, D. Inzé, and H. Muylle. 2014. LEAF-E: a tool to analyze grass leaf growth using function fitting. *Plant Methods* 10: 37.

80. Vos, K., and H. Biemond. 1992. Effects of nitrogen on the development and growth of the potato plant. 1. Leaf appearance, expansion growth, life span of leaves and stem branching. *Annals of Botany*. 70: 27-35.

81. Wargent J, J., J.P. Moore, A.R. Ennos, N.D. Paul. 2009. Ultraviolet radiation as a limiting factor in leaf expansion and development. *Photochemistry and photobiology*. 85: 279-286.

82. White, A. C., A. Rogers, M. Rees, and C. P. Osborne. 2016. How can we make plants grow faster? A source–sink perspective on growth rate. *Journal of Experimental Botany* 67: 31–45.

83. Wilson, G. L., and M.M. Ludlow. 1968. Bean leaf expansion in relation to temperature. *Journal of Experimental Botany* 19: 309-321.

84. Wright, I. J., N. Dong, V. Maire, I. C. Prentice, M. Westoby, S. Díaz, R. V. Gallagher, et al. 2017. Global climatic drivers of leaf size. *Science* 357: 917–921.

85. Wright, I. J., P. B. Reich, J. H. C. Cornelissen, D. S. Falster, P. K. Groom, K. Hikosaka, W. Lee, et al. 2005. Modulation of leaf economic traits and trait relationships by climate. *Global Ecology and Biogeography* 14: 411–421.

86. Wright, I. J., P. B. Reich, M. Westoby, D. D. Ackerly, Z. Baruch, F. Bongers, J. Cavender-Bares, et al. 2004. The worldwide leaf economics spectrum. *Nature* 428: 821–827

Chapter 7: Conclusions and Future Directions

The integration of leaf hydraulics with developmental processes is a key avenue to understand the evolutionary basis for structural and functional diversity. The emergence and expansion of leaf hydraulics throughout the past few decades has vastly increased our understanding of leaf and whole plant function (Sack & Holbrook 2006; Sack & Scoffoni 2013; Scoffoni & Sack 2017). Historically, many in the field of plant water relations have focused on water transport through stems or roots, as the pathways for water transport through leaves are much more complex, though this complexity has been increasingly embraced and disentangled for eudicotyledonous angiosperms and other more basal lineages (Sack & Holbrook 2006). Indeed, the leaf has been of key focus for researchers focusing on plant growth and/or development for many decades beyond that of leaf hydraulics (Van Volkenburgh 1999; Granier & Tardieu 2009; Pantin, Simonneau & Muller 2012; Kalve, De Vos & Beemster 2014). My dissertation work aimed to integrate leaf developmental and growth processes with leaf hydraulic structure and function, and also to increase our understanding of leaf level adaptations and leaf hydraulic function in the grasses, an ecologically and agriculturally vital lineage within the monocotyledons.

In Chapter 2 I established a global relationship of leaf size and climate for the grasses (Poaceae) and provided experimental and modeling evidence for the biophysical and developmental processes driving such relationship. Indeed, associations of leaf size variation with climate have been noted since classical times by Theophrastus (Hort 1948), who noted the occurrence of larger leaves in warm and wet environments, and smaller leaves in cold and dryer climates. Consistent with what has been shown for eudicotyledons globally (Wright et al., 2017), narrower and shorter grass leaves are found in colder and dryer climates worldwide, though the

mechanisms differed for such patterns. This study highlighted how processes during development can constrain trait evolution, i.e. small leaves are developmentally constrained to have vein traits that provide tolerance of cold and aridity. This work thus demonstrates how biophysical and developmental processes can drive convergence across major lineages, and highlights the importance of leaf size and venation architecture for grass performance.

In Chapter 3 I aimed to further understand the evolution of grass leaf design. Anatomical allometries across grass leaves shown theoretically and empirically in this chapter highlight the critical role of developmental processes in driving allometries across species, and should be explored in future studies focused at the level of cell development within and across species, e.g. identifying the genetic regulators of differences in cell size within the model grass *Brachypodium*. The strong allometric patterns demonstrated show how leaf construction emerges from differences at the level of cells that cascade upwards to tissues, organs, and through linkages with photosynthetic efficiency, potentially to whole plant form and function. Future studies should resolve whether allometric scaling patterns determined here are generalizable across further diversity in the grass family by sampling additional C_3 and C_4 lineages across the grass phylogeny (e.g. C_3 Pooid, PCK C_4, bamboos), and other monocots.

In chapter 4 I coupled experimental data for 27 common garden grown grass species with data compiled from the literature for 328 grass species and examined the anatomical drivers of leaf hydraulic function for C_3 and C_4 grasses. This study highlighted the critical role of grass leaf structure and hydraulic function for grass leaf photosynthetic physiology, with implications for grass evolution, ecology and bio-geography. The contrasting evolutionary diversification in the coordination of leaf hydraulics and gas exchange suggests different mechanisms for adaptation to climate. A high vein density (D_v) in C_4 species contributes to greater potential photosynthetic

rate (A_{area}), but not to leaf hydraulic conductance (K_{leaf},) and given their lower stomatal conductance (g_s), the higher K_{leaf}/g_s ratio enables this potential to be realized. Whereas C_3 grasses with the highest A_{area}, K_{leaf} and g_s can persist in stressful climates, by avoiding harsh conditions via dormancy and maximizing growth under high resource conditions, among C_4 grasses, those with the greatest K_{leaf}/g_s ratios that enables their higher A_{area}. Our findings also have applications in agriculture, as a high K_{leaf}/g_s would be a necessary target in engineering novel C_4 crop species, with emphasis on a high K_{leaf} that would arise from increasing leaf outside-xylem hydraulic condutance (K_{ox}). The critical importance of C_4 hyper-efficiency will inform both evolutionary ecologists and agricultural breeders on the anatomical and physiological mechanisms by which C_4 photosynthesis evolves and can be engineered into crops.

In Chapter 5 I utilized developmental processes to disentangle the potential association or independence of two critical leaf functional traits, i.e. leaf trichome and stomatal densities. Such findings emphasize the power of analyzing a functional trait in terms of its underlying developmental traits, resolving the role of multiple developmental factors that underlie variation in leaf trichome density (D_t), and that account for its contrasting associations with leaf stomatal density (D_s) in different contexts. Thus, future studies should examine the relationships of these developmental drivers that underlie D_t and D_s in relation to environmental controls. The higher resolution of developmental causation of important functional traits provides new avenues to examine trait evolution, and toward breeding climate-forward variants in crop species.

In Chapter 6 I returned to focus on leaf size and its underlying determinants for diverse eudicotyledonous species. My study highlights the important developmental traits that underlie diversity in mature maximum leaf size (LA_m), and will provide greater resolution in future research on the evolution of leaf size variation within and across lineages. Further, leaf

expansion developmental traits may be more proximally related to genetics and evolution than LA_m, with applications in global ecology and agriculture. The relationship of developmental traits to the leaf economics spectrum (LES) traits provides further potential applications. In particular, crop yield is highly influenced by source limitations (White, Rogers, Rees & Osborne 2016), and species with higher leaf expansion rates have higher yields (Cross 1991; van den Boogaard, Veneklaas, Peacock & Lambers 1996). Thus, the potential role of expansion rate (R) in increasing LA_m and its coordination with fast-growing LES traits such as photosynthetic rate per leaf mass (A_{mass}) suggests that R may be a promising target for increasing yield, though potentially at the expense of reduced leaf mass per area (*LMA*) and leaf lifespan (*LL*), and stress tolerance (Richards 2000). Indeed, as the genetic and molecular drivers underlying LA_m are being increasingly dissected, our study provides an additional functional linkage of the resulting structural and functional components that would be coupled with genetic and molecular transformation, and also would allow for more precise bioengineering. Furthermore, elucidating the higher level processes driving leaf expansion and their linkage with the LES across species provides a new foundational basis for leaf functional ecology to consider the developmental drivers of leaf size within single plants and species and those developmental drivers underpinning leaf size adaptation to sun vs. shade, low vs. high soil nutrients and aridity.

Overall, my dissertation provides evidence for the power of integrating quantitative developmental processes with leaf structure and function to increase our understanding of leaf adaptive design and function. My first three chapters add to a body of literature that was lacking in studies focusing on leaf level adaptation for the grasses, i.e. the bulk of leaf ecophysiological studies focus on eudicotyledons, despite the importance of the grasses and other monocotyledonous lineages. Such foundational work presented here will provide fundamental

implications for grass ecology and applications for agricultural breeding. Indeed, my studies focusing on the grasses focused on highly diverse grasses across the phylogeny, and thus future studies should examine the generality of the findings presented here within closer related lineages within the grasses, and also with respect to the evolution of the specific C_4 subtypes. My fifth chapter took a novel approach to assess whether or not the molecular processes underlying leaf trichome and stomatal formation in model species also translate across diverse species. The quantification of developmental traits and assessing their roles in driving variation in trichome and stomatal densities allowed for this examination. Thus, future studies should aim to link molecular processes in model species with trait diversity across species as mediated by development, which will provide greater resolution on whether or not findings in model species occur for non-model species. My last chapter was also novel by linking leaf growth kinematics with leaf global ecology across species. This study also highlighted the importance of quantifying developmental traits and linking them to leaf functional traits. Future studies should assess the generality of my findings across different scales, e.g. within individuals and between early-forming and late-forming leaves, across individuals within a species, and across species within a genera. Overall, this dissertation highlights the power of taking a broadly integrative approach to understanding leaf design and function.

References

1. van den Boogaard, R., E.J. Veneklaas, J.M. Peacock, and H. Lambers. 1996. Yield and water use of wheat (*Triticum aestivum*) in a Mediterranean environment: Cultivar differences and sowing density effects. *Plant and Soil* 181: 251–262.

2. Cross, H.Z. 1991. Leaf Expansion Rate Effects on Yield and Yield Components in Early-Maturing Maize. *Crop Science* 31, cropsci1991.0011183X003100030006x.

3. Granier, C. and F. Tardieu. 2009. Multi-scale phenotyping of leaf expansion in response to environmental changes: the whole is more than the sum of parts. *Plant, Cell & Environment* 32: 1175–1184.

4. Hort, A. 1948. *Enquiry into Plants by Theophrastus*. Harvard University Press.

5. Kalve, S., D. De Vos, and G.T.S. Beemster. 2014. Leaf development: a cellular perspective. *Frontiers in Plant Science* 5.

6. Pantin, F., T., Simonneau, and B. Muller. 2012. Coming of leaf age: control of growth by hydraulics and metabolics during leaf ontogeny. *New Phytologist* 196: 349–366.

7. Richards, R.A. 2000. Selectable traits to increase crop photosynthesis and yield of grain crops. *Journal of Experimental Botany* 51: 447–458.

8. Sack, L., and N.M. Holbrook. 2006. Leaf Hydraulics. *Annual Review of Plant Biology* 57, 361–381.

9. Sack, L., and C. Scoffoni. 2013. Leaf venation: structure, function, development, evolution, ecology and applications in the past, present and future. *New Phytologist* 198: 983–1000.

10. Scoffoni, C., and L. Sack. 2017. The causes and consequences of leaf hydraulic decline with dehydration. *Journal of Experimental Botany* 68: 4479–4496.

11. Van Volkenburgh, E. 1999. Leaf expansion – an integrating plant behaviour. *Plant, Cell & Environment* 22: 1463–1473.

12. White, A.C., A. Rogers, M. Rees, and C.P. Osborne. 2016. How can we make plants grow faster? A source–sink perspective on growth rate. *Journal of Experimental Botany* 67: 31–45.

13. Wright, I.J., N. Dong, V. Maire, I.C. Prentice, M. Westoby, S. Díaz, et al. (2017) Global climatic drivers of leaf size. *Science* 357: 917–921.